

Towards understanding the impacts of land management on productivity in the Daly River

Barbara J. Robson¹, Julia Schult², Jodie Smith³, Ian Webster², Michele Burford⁴, Andy Revill⁵, Simon Townsend⁶, Ralf Haese³ and Daniel Holdsworth⁶

November, 2010



¹ CSIRO Land and Water

² NRETAS, N.T. Government

³ Geoscience Australia

⁴ Griffith University

⁵ CSIRO Marine and Atmospheric Research

⁶ Charles Darwin University



Australian Government

Department of Sustainability, Environment,
Water, Population and Communities

National Water Commission

Fisheries Research and
Development Corporation

Disclaimer

TRaCK has published the information contained in this publication to assist public knowledge and discussion and to help improve the sustainable management of Australia's tropical rivers and coasts. Where technical information has been prepared by or contributed by authors external to TRaCK, readers should contact the author(s), and conduct their own enquiries, before making use of that information. No person should act on the contents of this publication whether as to matters of fact or opinion or other content, without first obtaining specific independent professional advice which confirms the information contained within this publication.

While all reasonable efforts have been made to ensure that the information in this publication is correct, matters covered by the publication are subject to change. Charles Darwin University does not assume and hereby disclaims any express or implied liability whatsoever to any party for any loss or damage caused by errors or omissions, whether these errors or omissions result from negligence, accident or any other cause.

Copyright

This publication is copyright. Apart from any fair dealing for the purpose of private study, research, criticism or review as permitted under the Copyright Act, no part may be reproduced, by any process, without written permission from the publisher. Enquiries should be made to the publisher, Charles Darwin University, c/- TRaCK, Casuarina Campus, Building Red 1 Level 3, Darwin NT 0909.

TRaCK brings together leading tropical river researchers and managers from Charles Darwin University, Griffith University, the University of Western Australia, CSIRO, James Cook University, the Australian National University, Geoscience Australia, the Environmental Research Institute of the Supervising Scientist, the Australian Institute of Marine Science, the North Australia Indigenous Land and Sea Management Alliance, and the Governments of Queensland, the Northern Territory and Western Australia.

TRaCK receives major funding for its research through the Australian Government's Commonwealth Environment Research Facilities initiative; the Australian Government's Raising National Water Standards Program; Land and Water Australia; the Fisheries Research and Development Corporation and the Queensland Government's Smart State Innovation Fund.

Robson, B.J., Schult, J., Smith, J., Webster, I., Burford, M., Revill, A., Townsend, S., Haese, R. and Holdsworth, D. (2010). Towards understanding the impacts of land management on productivity in the Daly River. Charles Darwin University, Darwin.

For further information about this publication:

Barbara Robson, CSIRO
Email: Barbara.robson@csiro.au

Or to find out more about TRaCK

Visit: <http://www.track.gov.au/>
Email: track@cdu.edu.au
Phone: 08 8946 7444

ISBN: 978-1-921576-29-4
Published by: Charles Darwin University
Printed by: CSIRO Land and Water

Contents

Executive Summary.....	5
Acknowledgements.....	7
I. Introduction	8
1.1. What is known about sediments, nutrients and ecology in tropical rivers?.....	8
1.2. The Daly River	9
1.3. Contents of this report	11
2. Nutrient and sediment loads	13
2.1. Introduction	13
2.2. Methods	13
2.2.1. Wet Season Sampling	13
2.2.2. Dry Season Sampling.....	19
2.2.3. Calculation of approximate whole-system budgets	20
2.3. Results and Discussion.....	21
2.3.1. Flow	21
2.3.2. Wet Season loads	21
2.3.3. Dry Season Loads	29
2.3.4. Approximate Total Nitrogen, Phosphorus and Total Suspended Sediments budgets	33
2.4. Conclusion.....	39
3. Composition of sediments and organic matter.....	41
3.1. Introduction	41
3.1.1. Physical properties and geochemical composition	41
3.1.2. Sources of organic matter	42
3.1.3. Lipid biomarkers.....	43
3.2. Methods	44
3.2.1. Sample Collection.....	44
3.2.2. Physical properties	45
3.2.3. Geochemical analysis.....	45

3.2.4. Biomarker analysis.....	46
3.3. Results and Discussion.....	47
3.3.1. Bulk Grainsize Composition.....	47
3.3.2. Habitat Extents.....	52
3.3.3. Fine Sediment Deposition Over the Dry Season	53
3.3.4. Fine Sediment Composition.....	54
3.3.5. Porewater Nutrient Profiles.....	58
3.3.6. Do fine sediments support algal growth?.....	61
3.3.7. Biomarker analyses.....	62
3.4. Conclusions	66
4. Primary Producers: biomass, standing crop and nutrient limitation of aquatic plants and algae.....	68
4.1. Introduction	68
4.2. Methods	68
4.2.1. Characteristics of study reach	68
4.2.2. Water Quality	69
4.2.3. Biomass survey	69
4.2.4. Nutrient limitation.....	72
4.2.5. Carbon fixation and photosynthesis-irradiance responses	72
4.3. Results and Discussion.....	73
4.3.1. Study reach characteristics and water quality	73
4.3.2. Biomass of primary producers	76
4.3.3. Nutrient limitation of benthic algae and phytoplankton	83
4.3.4. Carbon fixation and photosynthesis–irradiance response	86
4.4. Conclusion.....	87
5. Whole-system photosynthesis and respiration	89
5.1. Introduction	89
5.2. Methods	89
5.2.1. Deployment of Hydrolab dataloggers.....	89

5.2.2.	Analysis of diurnal oxygen curves.....	89
5.2.3.	Photosynthesis modelling	93
5.3.	Results	100
5.3.1.	Diurnal oxygen analysis.....	100
5.3.2.	Temporal trends	102
5.3.3.	Error estimates	104
5.4.	Discussion	108
5.5.	Conclusions	109
6.	Hydraulic modelling	111
6.1.	Introduction	111
6.2.	Channel shape and dimensions.....	111
6.3.	Application of hydraulic model.....	115
6.3.1.	Specification of bed roughness	115
6.3.2.	Low flow simulations	117
6.4.	Conclusions	119
7.	A dynamic model of primary production and plant coverage in the Daly River	121
7.1.	Introduction	121
7.2.	Methods	121
7.2.1.	Model overview	121
7.2.2.	Growth rates.....	122
7.2.3.	2D hydrodynamic model.....	124
7.2.4.	Depth and velocity as a function of flow	125
7.2.5.	Friction velocity as a function of flow	125
7.2.6.	Physical habitat categories	127
7.2.7.	Light.....	128
7.2.8.	Nitrogen and phosphorus requirements of plants	131
7.2.9.	Nitrogen and phosphorus transfer and uptake rates.....	133
7.2.10.	Nitrogen and phosphorus concentrations.....	133
7.2.11.	Boundary layer transfers	136

7.2.12.	Sloughing	138
7.2.13.	Substrate.....	139
7.2.14.	Self-shading and competition for substrate.....	140
7.2.15.	Grazing and mortality	141
7.2.16.	Time-steps and initialisation	142
7.3.	Results	142
7.3.1.	Photosynthesis and primary production.....	145
7.3.2.	Nitrogen and phosphorus stores.....	146
7.4.	Scenarios	147
7.4.1.	Scenario descriptions	147
7.4.2.	Results.....	148
7.4.3.	Limitations	153
7.5.	Conclusions	153
8.	Summary and Concluding Remarks.....	155
References		158
Appendix 1: Details of sediment sampling.....		163

Executive Summary

“At a time of increasing awareness of the value of water across Australia, it is vital that public debate, policy and management decisions about our tropical rivers and estuaries are informed by sound science.

[TRaCK (Tropical Rivers and Coastal Knowledge) is] providing the science and knowledge that governments, communities and industries need for the sustainable use and management of Australia’s tropical rivers and estuaries.” [From the TRaCK website]

This document is the final report for the Daly River component of TRaCK Project 4.3, “Towards understanding the impacts of land management on productivity in the Daly and Flinders Rivers”. The project was designed to improve our understanding of materials fluxes, nutrient and sediment processes and primary production in tropical rivers like the Daly River, Northern Territory, and to build the knowledge and models needed to answer the question, “How will changes in land and water management affect the productivity of the Daly River?”

The project has combined water quality monitoring at a number of sites in the river throughout the wet and dry seasons of 2008 with intensive fieldwork campaigns to measure and assess the properties of sediments, organic material, plants and algae in the river, and modelling to simulate key processes and provide a basis for predicting how the river is likely to respond to changes in flow, nutrient or sediment loads.

The results suggest the following conceptual picture for nutrients cycling, sediments and primary production in the Daly River:

Wet season (December to March)

High flow volumes during the wet season bring >95% of total annual sediment, nitrogen and phosphorus loads reaching the Daly River. High shear stresses associated with high flows scour the bed, removing most benthic plant biomass, though in lower-flow years, some *Vallisneria* beds survive. Turbidity is high during the wet season and water residence time is low, so primary production in the main channel is accordingly low.

Early Dry Season (April to June)

At the end of the wet season, sediments settle out of the water column and benthic substrate stabilises into alternating stretches of dynamic sand ripples, stable gravel beds and slightly deeper pools. The water clears and benthic microalgae (in periphyton) and fast-growing macroalgae (*Spirogyra*) establish rapidly, storing nutrients from the water column and keeping them within the system. Most benthic production occurs in gravel runs and along the edges of pools, with little production in sand ripples. Phytoplankton contribute little to total primary production in current conditions.

Total primary production is limited not by light, but by nitrogen and phosphorus concentrations and transfer of these nutrients across a benthic boundary layer.

Late Dry Season (July to November)

In the late dry season, flow is sustained entirely by groundwater inflows and hydrological breaks (i.e. small waterfalls) play an important role in controlling flow and water depth.

Primary production remains limited by nitrogen and phosphorus and much of the measured photosynthesis does not contribute to production of plant biomass.

With little additional nutrient input from the catchment, the system in the late dry season depends on nutrients recycled within the benthic community. *Spirogyra* biomass drops as lower flows cause a decline in transfer-limited nutrient uptake rates.

Release of nutrients from sediment muds does not appear to contribute significantly to the supply of nutrients in the system during the dry season: rather, nutrients released from decaying *Spirogyra* and periphyton or otherwise recycled within the biotic community drive the growth of slower-growing benthic algae (*Chara* or *Nitella*) and aquatic plants (*Vallisneria*). Sand ripples may play an important role in remineralisation of detrital organic matter.

Outputs from this project include a one-dimensional hydraulic model and a preliminary model to simulate changes in biomass of five key groups of plant and algae, presented in Chapter 7. The latter has been applied to two simple scenarios, exploring the possible effects of increased nutrient concentrations and reduced flows.

The results suggest that the Daly River is likely to be particularly sensitive to any increase in nutrient loads that may result from changes in catchment management or land use.

Significant knowledge gaps remain, and are discussed in Chapter 8.

Further work is needed to test the models presented here and to assess the impacts of land use on catchment runoff, sediment and nutrient loads, the impact of grazing on primary production in the river and the likely effects of climate change.

Acknowledgements

This work was funded by the Tropical Rivers and Coastal Knowledge (TRaCK) research hub, with in-kind support from CSIRO, NRETAS, Geoscience Australia, Griffith University and Charles Darwin University. TRaCK receives major funding for its research through the Australian Government's Commonwealth Environment Research Facilities initiative; the Australian Government's Raising National Water Standards Program; Land and Water Australia; the Fisheries Research and Development Corporation and the Queensland Government's Smart State Innovation Fund.

Thanks are due to NRETAS for provision of flow monitoring data for the Daly River and its tributaries, Markus Billarbeck (formally CSIRO, now at the University of Queensland), who contributed to field-work, Sandeep Patil (formerly CDU) for provision of 2D hydrodynamic modelling output, and Cheuk Yu Lee (CSIRO Land and Water) for assistance in converting that output into a suitable format for our models.

We would also like to thank Joye Madison and the Wangamaty Landcare Group, Peter O'Brien from the Douglas-Daly Research Farm and staff from the Katherine Water Assessment Branch for collecting many water samples for this project. Without their support, high intensity sampling during the wet season would not have been possible.

Thanks also to Paul Rustomji (CSIRO Land and Water and TRaCK), whose detailed review of an earlier draft has improved this report substantially.

I. Introduction

The Tropical Rivers and Coastal Knowledge research hub (TRaCK) aims to provide the science and knowledge that governments, communities and industries need for the sustainable use and management of Australia's tropical rivers and estuaries. TRaCK Theme 4 (Materials Budgets) was designed to develop the knowledge and models required to predict and monitor the effects of current and future changes (including developments in land use and climate change) on the sources, amounts and movement of water, carbon, sediment, and major nutrients (nitrogen and phosphorus). This project, Project 4.3, focuses on in-stream sediments and nutrients in tropical rivers, processing of sediments and nutrients within river systems and their impact on primary production (the growth of algae and other aquatic plants) and river metabolism. In so doing, the project is an essential link between the TRaCK projects studying river flows, carbon, nutrient and sediment inputs and other projects studying food-webs and patterns of biodiversity.

A common result of human activity in catchments is an increase in the amount of sediment and nutrients found in rivers (Smith 2003). Extra nutrients in rivers can feed plant growth in the form of algae and aquatic plants (known as primary production). On the other hand, fine sediments suspended in the water column can restrict the amount of light necessary for growth. So how do tropical rivers respond to these increased inputs?

Project 4.3 focuses on two case studies, the Daly River in the Northern Territory, and Flinders River in Queensland. This report describes the outcomes of work in the Daly River.

This report aims to contribute to:

- Improved understanding of the origin, transport and fate of carbon, nutrients and fine sediments in the Daly River and similar tropical rivers in Australia.
- Improved capacity to predict the consequences of land use and water resource changes on primary production in the Daly rivers
- Improved understanding on the linkage between flows and the transport and fate of nutrients and fine sediments

This (predictive) capability is key to assessing impacts of land-use change on ecological condition in tropical rivers, an essential step for effective management of river catchments.

1.1. *What is known about sediments, nutrients and ecology in tropical rivers?*

Hamilton and Gehrke (2005) review knowledge of Australia's tropical river systems, and conclude that they are poorly understood and existing knowledge is insufficient to support policy and planning decisions. This echoes the findings of the Australian tropical rivers data audit (Australia 2004). Most of the available research regarding

Australian tropical rivers has been published since these reports, in the second half of the present decade. Hamilton and Gehrke (2005) identify a need for research aimed at “improved quantification of available water resources, hydrological, biogeochemical and ecological linkages at system scales, understanding and valuing ecosystem processes and services, and projecting the effects of long-term climate change.” Stable isotope studies “suggest that algae, which are usually inconspicuous as a source of organic matter compared to vascular plants, are disproportionately important in supporting food webs in tropical streams, floodplains and estuaries. We therefore need to better understand controls on algal production.”

Brodie and Mitchell (2005), writing of Australian tropical rivers in general argue that “historical conditions in these rivers were probably characterised by low-moderate SS [suspended sediment] concentrations and low concentrations of dissolved inorganic nitrogen and phosphorus in flow events.” They argue that grazing has probably increased suspended sediment and particulate nutrient loads during flow events, while areas of fertilised agriculture have probably increased dissolved nutrient loads. “The restricted period of... highly energetic flows means that little trapping of materials occurs,” and “processes such as denitrification and in-channel sedimentation may be of limited importance”.

During the dry season, by contrast, residence times in water holes are long, and in-channel processes such as denitrification are much more likely to be important, at least to the dry-season nutrient budget.

On the basis of work on biodiversity in the Flinders and Nicholson catchments, Leigh and Sheldon (2008) (2008) propose that “[flow permanence and regularity; flow variability and absence and wet-dry seasonality] are the key hydrological drivers of biodiversity and ecological function in the floodplain rivers of Australia’s north”. Water resource development is expected to change inter-annual flow variability and adversely impact biodiversity and ecological function in such rivers.

Bunn et al. (Bunn, Thoms *et al.* 2006), considering flow variability in dryland tropical rivers in general, discuss mechanisms by which flow variability may affect food webs. Flood pulses in dryland rivers bring nutrients and carbon, and “are responsible for a boom of production on inundated floodplains and in [terminal] wetlands”.

Waterholes can persist for up to two years without flow, despite an absence of groundwater inputs, and flows, when they come, although necessary for the long-term existence of the waterholes, “may lead to food limitation and stress for populations of fish and other consumers”. Benthic algal production in these rivers is high. (several g C/m²/d), and littoral zone benthic algal production is important to the food web.

Water resource developments tend to increase the frequency and duration of small flow pulses (but reduce the frequency and magnitude of larger flood pulses), which can lead to a suppression of algal production during flows, and subsequent ecological decline in the longer term.

1.2. The Daly River

The Daly River flows through outback country in the Northern Territory, through approximately 300 km before reaching the coast west of Darwin. It is one of the better monitored rivers in Australia’s tropical North, and has been the subject of previous studies of *Spirogyra* growth (Townsend and Padovan 2009), environmental flow

requirements for *Vallisneria* (Rea, Postine *et al.* 2002) and photosynthesis (Webster, Rea *et al.* 2005). It is one of the few tropical rivers in Australia to flow all year around, as a consequence of groundwater inputs from two limestone aquifers in its catchment (CSIRO 2009). The Daly River has been chosen as a focus site for the TRaCK research hub, with a number of projects from Themes 2, 4 and 5 exploring various aspects of the biophysical and ecological function of the river and its cultural and economic values.

1.3. *Contents of this report*

The project has combined water quality monitoring at a number of sites in the river throughout the wet and dry seasons of 2008 with intensive fieldwork campaigns to measure and assess the properties of sediments, organic material, plants and algae in the river, and modelling to simulate key processes and provide a basis for predicting how the river is likely to respond to changes in flow, nutrient or sediment loads.

First, by monitoring nutrient and sediment concentrations, turbidity and other aspects of water quality throughout the 2008 wet and dry season, the project has built up a database and calculated loads and budgets of sediments, nitrogen and phosphorus in the river, working out how much sediment and nutrient material passes through different parts of the system and when, and how the form of these nutrients changes through the year as nutrients are brought in with sediments during rain events, pass through the system in flood, and are subsequently transformed within the river during the longer dry season. These results are presented in Chapter 2.

Second, sampling of suspended sediment material and sediment cores has provided insight into the properties of sediments in the system and how these vary in different habitats within the river and over the course of the dry season. These properties include particle sizes, organic matter and nutrient content, helping to provide a picture of how important sediments are as a source of carbon and nutrients to drive production.

A study of organic matter associated with these sediments, measuring lipids, carbon and nitrogen isotopes has provided information on where organic matter in the river comes from, and what is driving production. The results of sediment and organic matter analyses are presented in Chapter 3.

In Chapter 4, we present our findings from measurements of the biomass, coverage and nutrient content of each of the main plant types in the river, which have helped to build knowledge of where these plants grow, how much nitrogen and phosphorus they store, and how their relative coverage changes over the course of a season. Alongside these measurements, a study of the controls on primary production in the river has helped us to assess how fast algae in the river grow and how they respond to changes in light, nitrogen and phosphorus concentrations.

Chapter 5 presents calculations of total system metabolism (photosynthesis and respiration) from diurnal oxygen curves.

Chapters 6 and 7 present numerical models that have been developed as a tool to integrate this knowledge. This includes a one-dimensional model of river hydraulics as well as a dynamic simulation model of the growth and biomass of five key plant groups in the river.

The primary production model has been applied to some preliminary scenarios to demonstrate and how plant biomass and productivity in the Daly River might change in response to changes in flow, turbidity and nutrient concentrations.

Because of the number of assumptions that have been made in the development of the model, the results of scenario predictions must be considered speculative rather than

conclusive; they do, however provide hypotheses that can be tested with further well-targeted process studies.

The final chapter of the report presents a summary of our findings, conceptual model of nutrients, sediments and primary production in the Daly River, and recommendations for future work.

2. Nutrient and sediment loads

2.1. *Introduction*

A first step towards understanding sediments and nutrients in the Daly River is to determine the quantity of sediments, nitrogen and phosphorus that is associated with this flow in different parts of the catchment. With this information, we can begin to understand where sediments and nutrients in the Daly River come from, and what happens to them as they are transported through the river and transformed by physical and biogeochemical processes within the river.

In this chapter nutrient and sediment loads are determined for four sites during the 2007/08 wet season, and the 2008 dry season in the Daly River catchment.

2.2. *Methods*

2.2.1. *Wet Season Sampling*

Four sites were selected for intensive water quality sampling during the wet season (Figure 1). These were Fenton Creek (A, Figure 1), Douglas River Bridge (B), the lower Daly River (C) and the Katherine River bridge in the township of Katherine (D). These sites were selected for location and accessibility, and represent different sub-catchment types.

The Katherine River site sub-catchment represents a large area of the upper catchment of the Daly which contains 8640 km² of largely undeveloped land much of which lies within the sandstone escarpment of Kakadu and Nitmiluk National Parks and Western Arnhem Land. Part of the township of Katherine is included in the sub-catchment but the main areas of town and major point-sources of pollution (e.g. the Katherine sewage plant) are downstream of the site. Samples at this site were collected manually from the water's edge by NRETAS staff using a sampling rod.

Fenton Creek is a small seasonal creek in the upper catchment of the Douglas River. Its total catchment area is approximately 20 km² of largely uncleared land with some cattle grazing activity. Samples were collected at a NRETAS gauge station by an automatic sampler at pre-determined stage heights. These heights varied and were adjusted remotely according to the amount of rainfall and flow. Samples were collected from the gauge station weekly.

The Douglas River Bridge sub-catchment contains mostly native vegetation but also part of one of the major agricultural areas in the region with some land-clearing for grazing, forestry and horticulture. The size of the sub-catchment is 832 km². The Douglas River is the last major perennial tributary to the Daly before its estuary. The sampling site is located in the middle reaches of the river, near the Oolloo Road bridge, approximately 25 km upstream of its confluence with the Daly River. Samples were collected manually by NRETAS staff.

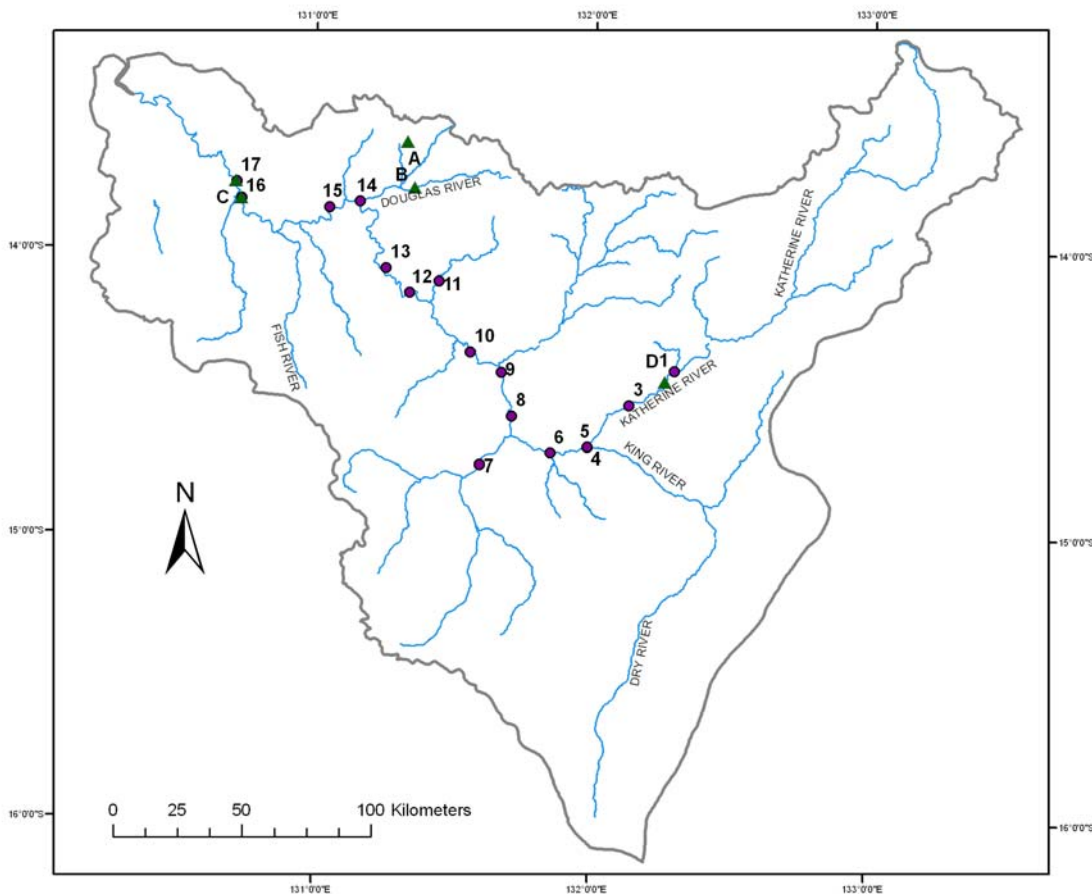


Figure 1 The Daly River and major tributaries. Dry season water quality sample sites are indicated with numbers 1-17 (round dots), wet season sample sites with letters A-D (triangles).

The site on the lower Daly River with a catchment size of 47,000 km² represents the entire Daly River catchment upstream of the estuary. Samples were collected approximately daily by community members and NRETAS staff near the Daly River community. A sampling pole was used to avoid sampling close to the edge.

To ensure this sampling technique provided representative data, a comparison of edge and mid-channel samples was conducted during the 2008/09 wet season, where samples were collected simultaneously from both areas. Preliminary results of this comparison are presented below.

A summary of catchment characteristics and total sample numbers for each site is provided in Table 1.

Table 1. Overview of sub-catchment characteristics and sample numbers collected at intensive wet season sampling sites.

Site	Size (km ²)	Main catchment land uses (from NRETAS land use mapping data 2008)	Nearest gauge station	Distance from site (km)	No. of samples collected (Nov – April)
Fenton Creek	20	Production from relatively natural environments	G8140169	0	168
Douglas River	830	Production from relatively natural environments Dryland and irrigated agriculture and plantations Conservation & Natural Environments	G8140063	2	61
Katherine River	8600	Conservation / Natural Environments	G8140001	0	76
Daly River	47000	Conservation / Natural Environments Production from relatively natural environments	G8140040	10	154

Flow data for all sites were obtained from the nearest NRETAS gauging stations. Routine, automated monitoring of stage height, which can be converted to flow with an accuracy of $\pm 5\%$ (Allan Russ, NRETAS, *pers. comm.*), is conducted by NRETAS at a number of sites within the Daly River catchment. Gauge station sites used in this report are listed in Table 2.

Table 2. Gauge station locations.

Site	Site Name	Zone	Easting	Northing
G8140001	Katherine River at Railway Bridge	53	204328	8399285
G8140040	Daly River at Mt Nancar	52	687474	8470184
G8140063	Douglas River Downstream Old Douglas Homestead	52	752880	8473461
G8140169	Fenton Creek	52	751789	8492339

Water samples were analysed for total nitrogen (TN), total phosphorus (TP), total suspended solids (TSS) and volatile suspended solids (VSS). Where appropriate, grab samples were filtered on site and frozen until analysis for nitrate (NO₃), nitrite (NO₂), ammonia (NH₃) and filterable reactive phosphorus (FRP) according to APHA (1998) standard methods (Table 3).

Table 3. Analytical methods and APHA standard method numbers

Parameter	Method	APHA(1998) number
NO ₃	Automated cadmium reduction method	4500-NO ₃ -F
NO ₂	Automated cadmium reduction method	4500-NO ₃ F
NH ₃	Automated Phenate method	4500-NH ₃ F
Total N	Persulfate method	4500-N C
Filterable reactive P	Flow injection analysis for orthophosphate	4500-P F (B1)
Total Phosphorus	Flow injection analysis for orthophosphate	4500-P F (B3)
Total Suspended Solids	Total Suspended Solids dried at 103-105°C method	2540 D
Volatile Suspended Solids	Fixed and volatile Solids ignited at 550 °C	2540 E
Dissolved Organic Carbon	High-temperature combustion method	5310 B + filtration 0.45 µm

Additional measurements of temperature, pH, dissolved oxygen, conductivity and turbidity were made on site or on return to the laboratory (conductivity and turbidity only).

At Fenton Creek, not all samples were analysed for TSS/VSS. A linear regression between TSS/VSS and turbidity for the site was established and missing TSS/VSS values were interpolated using this relationship (Figure 2, Table 4). Two outliers were excluded from the regression.

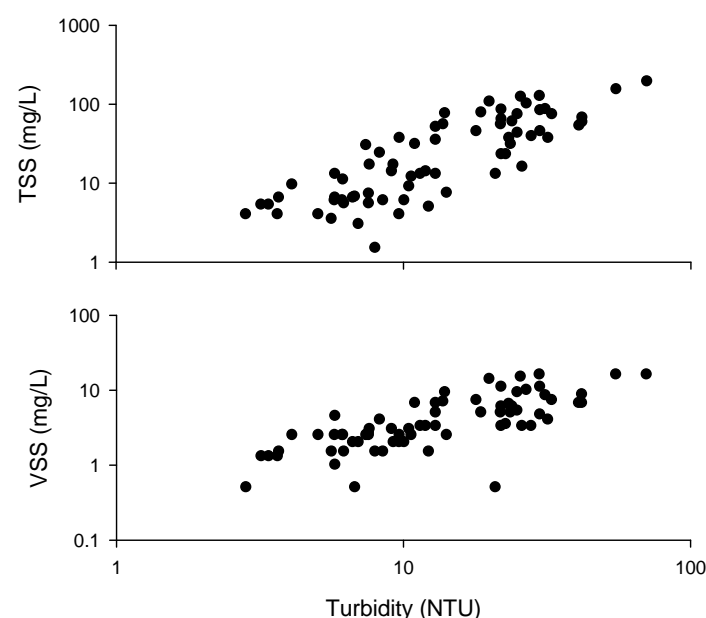


Figure 2. Turbidity vs. log-10 TSS/VSS at Fenton Creek

Table 4. Fenton Creek linear regression statistics for turbidity/TSS and turbidity/VSS

Coefficients				
	Intercept (SE)	a (SE)	R ²	n
TSS	-5.36 (4.61)	2.49 (0.22)	0.67	70
VSS	1.06 (0.53)	0.22 (0.02)	0.54	70

Calculation of Loads (Lower Daly River)

The lower Daly River loads were calculated for the period of 15 November 2007 to 30 April 2008. A plot of sample times on the hydrograph showed that there were no major gaps in the data, except for the first run-off event of the year in early November, which occurred before sampling commenced. No storm events occurred after 30 April 2008 (see Figure 7).

To calculate export loads, flow volumes were estimated by trapezoidal integration for integration periods defined by the mid-point between sample times.

$$V_x = f_1 * (t_2 - t_1) + (f_2 - f_1)/2 * (t_2 - t_1)$$

Where

V_x : flow volume of each integration period

t_1 : Date/time at midpoint between sample 1 and sample 2

t_2 : Date/time at midpoint between sample 2 and sample 3

f_1 : flow at t_1

f_2 : flow at t_2

Flow at the midpoint between sample times was calculated using a linear regression of the two nearest flow data points.

Wet season loads were calculated by multiplying concentrations by the flow volume for the corresponding period and summing these for the entire wet season.

Wet Season export coefficients were calculated by dividing loads by the catchment area (47,100 km²) and are expressed as mass per unit area.

Calculation of loads (Katherine/Douglas/Fenton)

To calculate nutrient and sediment loads for the three remaining sites, baseflow and storm runoff events were separated using the methodology described in Townsend & Douglas (2000). Volume-weighted mean concentrations of total nitrogen (TN), total phosphorus (TP), total suspended sediment (TSS), volatile suspended sediment (VSS), dissolved organic carbon (DOC) and particulate organic carbon (POC) were calculated for each storm event and each baseflow period.

The start of a storm event was defined by a steep rise of the hydrograph, while the end of the event was defined as the point where baseflow represented 80% or more of total

flow. The proportion of baseflow or stormflow was determined according to Nathan and McMahon (1990) as described in Townsend and Douglas (2000).

Sample numbers varied depending on the size and duration of the event and ranged from 1 to 10 per storm event and 1 to 13 for baseflow periods.

Not all storm events and baseflow periods were sampled. Six predictor variables were used to estimate volume-weighted mean concentrations of unsampled storms:

- (1) Time since flow commenced
- (2) Maximum discharge of the storm event
- (3) Duration of the storm
- (4) Maximum discharge of the previous storm
- (5) Time between max discharge of current and previous storm
- (6) Total flow volume of the storm

These variables were computed for each storm and the volume-weighted mean concentrations of unsampled storm events were estimated by multiple regression using backward stepwise deletion of variables based on Akaike's Information Criterion (AIC). The most parsimonious model was selected and tested for a significant reduction in deviance against other models and a null model by analysis of variance (Table 5). Where no significant regression was found, the mean volume-weighted concentration of all sampled storms was used to calculate the parameter.

Unsampled baseflow periods were estimated by using the mean of the two nearest sampled baseflow periods.

Table 5. Results of backward stepwise linear regressions to determine volume-weighted mean concentrations of water quality variables for unsampled storm events. Coefficients of determination and level of significance are shown for the most parsimonious models only. Explanatory variables included in maximal models were Time since First Flow (TsF), Duration, Maximum discharge of storm event (MaxFlow), maximum discharge of preceding storm (MaxPrec), time between maxima of current and preceding storms (TsP) and Total Flow of the storm event (Tflow). Null models are shown as “Dependent Variable” ~ 1.

	Dependent variable	Selected Model	R ²	p
Fenton Creek	TN	TN~1	N/A	
	TP	TP~TsF	0.17	p=0.02
	TSS	TSS~TsF+Duration	0.20	p=0.05
	VSS	VSS~TsF	0.20	p=0.014
Douglas River	TN	TN~TsP + Duration	0.49	p<0.05
	TP	TP~ TsP + Duration	0.60	p<0.01
	TSS	TSS~Total Flow	0.45	p<0.01
	VSS	VSS~TsF + MaxFlow	0.54	p<0.05
	DOC	DOC~TsF	0.54	p<0.01
	POC	POC~Tflow	0.53	p<0.01
Katherine River	TN	TN~TsF	0.25	p<0.01
	TP	TP~ 1	N/A	
	TSS	TSS~1	N/A	
	VSS	VSS~1	N/A	
	DOC	DOC~TsF+TsP	0.58	p<0.001
	POC	POC ~Duration+MaxFlow	0.36	P<0.01

2.2.2. Dry Season Sampling

In July and September 2008, more spatially extensive sampling was undertaken at 16 sites throughout the Daly River catchment. Sites were chosen to represent the whole catchment and incorporate areas of major groundwater and surface water inflows. A list of sites is given in Table 6 and their locations are shown in Figure 1.

Table 6. Details of Sampling sites in the Daly River catchment.

No.	Site	Easting	Northing	NTG Hydstra database code
1	Katherine R. @ BlueMetal Xing.	207970	8403584	G8140029
2	Katherine Hot Springs	204027	8397152	G8140312
3	Katherine R. @ Galloping Jacks	190683	8389743	G8140301
4	Katherine R. @ King R.	820953	8373326	G8145747
5	King R. @ Katherine R.	820973	8373294	G8145746
6	Katherine R. @ Limestone Ck.	806600	8371034	G8145126
7	Flora R. @ Kathleen Falls	779330	8366854	G8145021
8	Daly R @ u/s Florina	791738	8385560	G8145748
9	Daly R @ d/s Florina	787728	8402581	G8140347
10	Daly R. @ Dorisvale Xing.	775769	8410498	G8140067
11	Stray Ck @ road xing.	763573	8438009	G8145749
12	Daly River @ Theyona Station	752137	8433624	G8140098
13	Daly R. @ Oolloo Xing.	743162	8443266	G8140038
14	Douglas River @ Lower Crossing	733132	8469137	G8140325
15	Daly R. @ Beeboomb Xing.	721334	8466964	G8140042
16	Daly R. @ Mt Nancar	687113	8470677	G8140040
17	Daly R. @ Police station	685210	8477179	G8140003

At each site, flow was determined from the product of current velocity measured either with an Acoustic Doppler Current Profiler (ADCP) or a propeller-type current meter and cross-section area. Water samples were taken for nitrite, nitrate, ammonia, filterable reactive phosphorus, total nitrogen, total phosphorus, dissolved organic carbon and particulate carbon. Physico-chemical parameters (temperature, pH, dissolved oxygen and electrical conductivity) were measured *in situ* with a Hydrolab multi-parameter probe and turbidity was measured with a portable Hach turbidity meter.

2.2.3. Calculation of approximate whole-system budgets

To calculate wet-season and dry-season water, sediment, nitrogen and phosphorus budgets for the Daly River as a whole, daily loads were calculated for each of the four regular water-quality sampling sites to give loads for the Katherine River, Douglas River, Hayes Creek tributary, and Daly River at Mount Nancar. In addition, approximate daily loads were estimated for the Fergusson River, Flora River and the seasonal headwaters of the Daly River (“Dry Daly”), Daly River at Beeboom (downstream of the confluence of the Douglas River), and Daly River at Dorisvale (downstream of the confluence of the Fergusson River) and Daly River at the Police Station. To make these approximations, it was assumed that:

- Given high flow rates, sediment and nutrient concentrations at all Daly River sites during the wet season was the same as observed at Mount Nancar.
- Sediment and nutrient concentrations in Flora River, the seasonal headwaters of the Daly River, and Fergusson River were the same as those observed in the Katherine River.
- Dry-season water quality varied linearly in time between sampling occasions, and remained constant after the last sample for each site.

Obviously, these are significant assumptions, and will limit the accuracy of the resulting sediment and nutrient budgets.

By subtracting from the flow (or load) at a given point on the Daly River from the total flow (or load) contributed by tributaries upstream of that point, the amount contributed by unknown sources and sinks between any two sites on the Daly River can be calculated. These sources and sinks include direct catchment runoff to the Daly River, smaller, unmonitored tributaries, evaporation and precipitation, groundwater inflows and outflows. For sediments, additional sources and sinks include sedimentation and resuspension from the river bed. For nutrients, biogeochemical processes such as nitrification and denitrification and uptake and release by river plants and animals also affect downstream loads.

2.3. Results and Discussion

2.3.1. Flow

Flow in the Daly River during the 2007/2008 hydrological year followed a typical seasonal pattern, based on records from 1960-2008 (Figure 3). Total discharge for the 2007/08 study year was 11th highest at Dorisvale and 4th highest at Mt. Nancar observed during the 50-year period to 2009-2010.

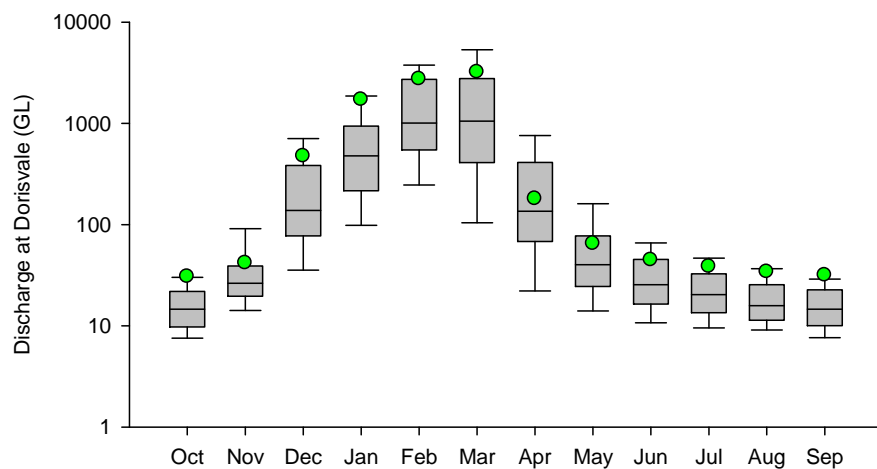


Figure 3 Box plot showing median monthly discharge, 25th/75th and 10th/90th percentile at Dorisvale gauge station (G8140067) for the period 1960-2008. Green circles are monthly discharge for the 2007/08 hydrological year.

2.3.2. Wet Season loads

During the wet season between 40 and 146 samples were collected at the four intensive sampling sites for nutrient and sediment analysis. Sample numbers for each site are given in Table 7. Figure 4 to Figure 7 show the raw sample data and temporal distribution of samples in relation to river flows.

Table 7. Sample numbers for intensive sampling of TN, TP, TSS, VSS, POC, DOC, electrical conductivity and turbidity at the Katherine, Douglas and Daly Rivers and Fenton Creek

Site	TN	TP	TSS	VSS	POC	DOC	EC	Turb.
Katherine	61	61	61	61	58	61	4	57
Fenton	120	120	150	150	52	57	102	102
Douglas	42	42	42	42	40	42	15	14
Daly	146	146	146	146	43	49	146	146

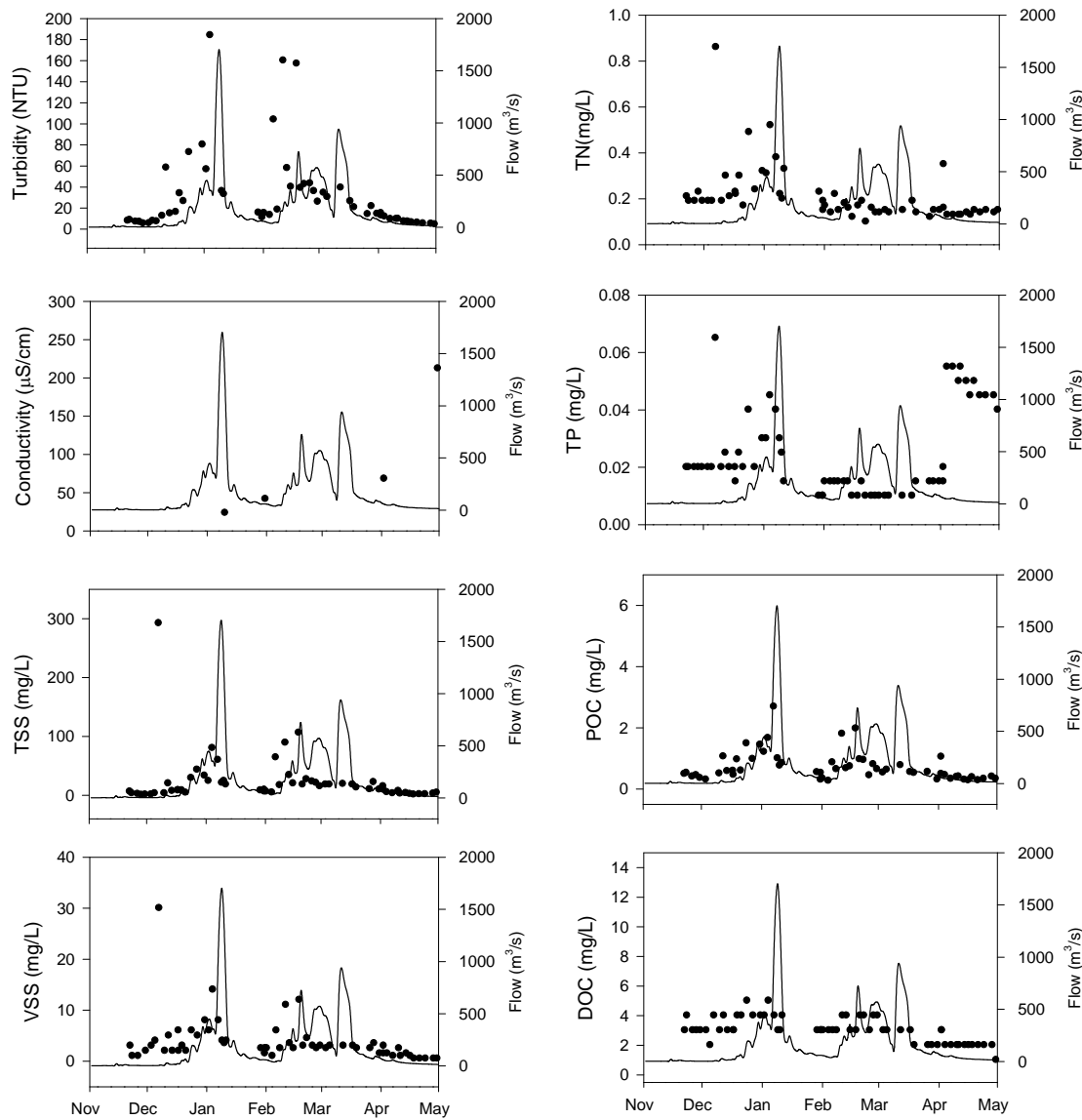


Figure 4. Katherine River hydrograph and sample concentrations for parameters measured at the Katherine River Bridge. Parameters measured are turbidity, conductivity, TSS, VSS, TN, TP, DOC, POC.

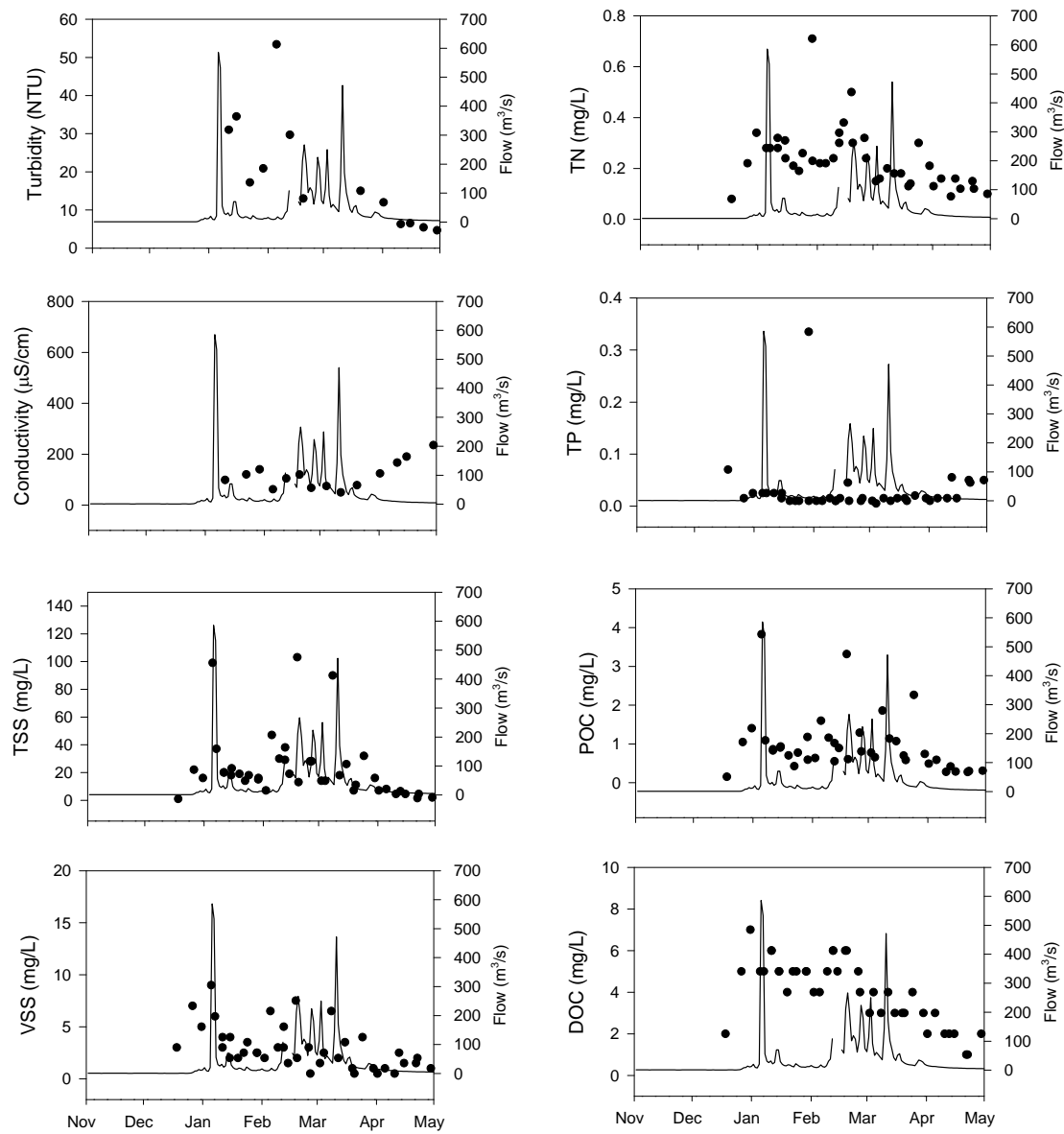


Figure 5. Douglas River hydrograph and sample concentrations for parameters measured at the Douglas River Bridge. Parameters measures are turbidity, conductivity, TSS, VSS, TN, TP, DOC, POC.

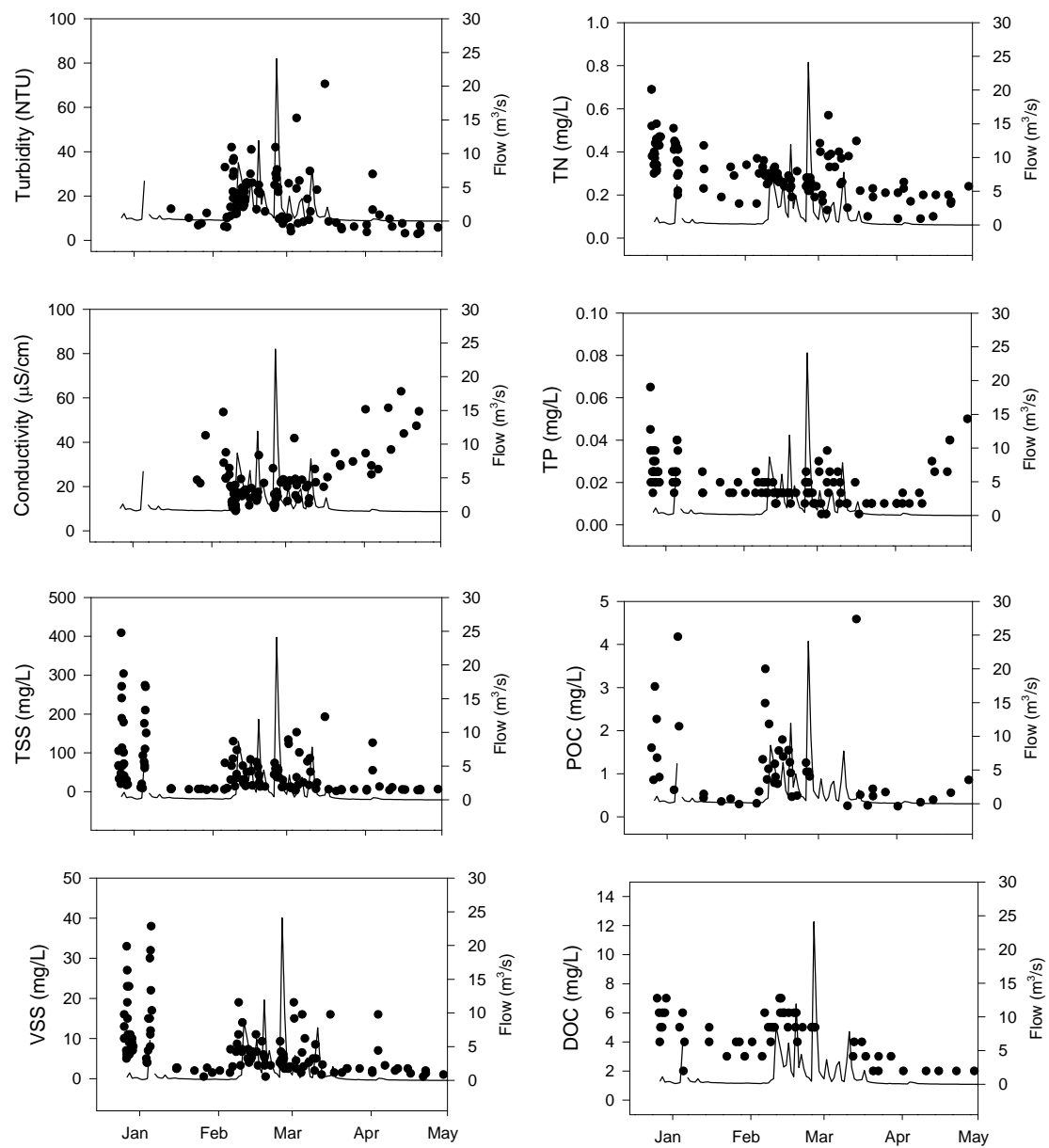


Figure 6. Fenton Creek hydrograph and sample concentrations at Fenton Creek Gauge station (G8140169). Parameters measures are turbidity, conductivity, TSS, VSS, TN, TP, DOC, POC.

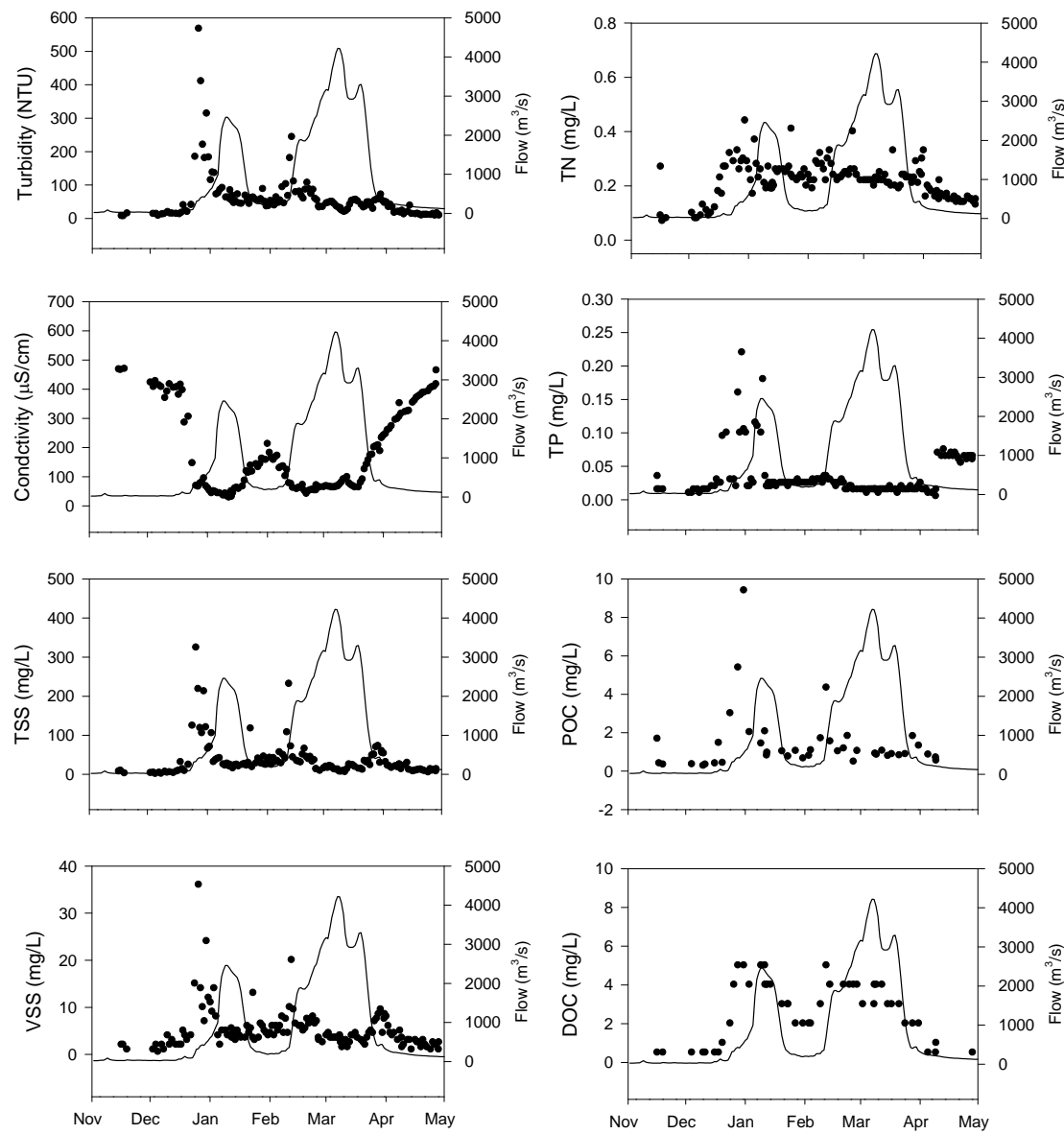


Figure 7. Lower Daly River hydrograph and sample concentrations (G8140040). Parameters measured are turbidity, conductivity, TSS, VSS, TN, TP, DOC, POC.

Volume-weighted mean concentrations of TP, TN, TSS, VSS, DOC and POC are shown in Figure 8.

Total nitrogen concentrations during baseflow ranged from 0.16 mg/L at the Katherine and Douglas Rivers to 0.17 mg/L at Fenton Creek and the lower Daly with stormflow concentrations between 0.24 and 0.30 mg/L, 1.5 to 1.8 times higher than baseflow (Figure 8).

Total phosphorus concentrations were similar during baseflow and stormflow at the Katherine River (22 µg/L) but increased from 16 to 39 µg/L and 10 to 17 µg/L during stormflow at the Douglas River and Fenton Creek sites, respectively. At the lower Daly TP increased from 28 to 39 µg/L.

Differences between storm and baseflow concentrations were most pronounced for total and volatile suspended solids. Total suspended solids increased by a factor of 9 at Fenton Creek from 7.9 to 74 mg/L during stormflow. At the Katherine River, stormflow concentrations were 3.8 times higher than baseflow with 9.7 and 37 mg/l while mean TSS concentrations increased from 12 to 28 mg/L at the Douglas River and 19 to 34 mg/L at the lower Daly. During storm events, the mean concentration of VSS reached 11 mg/L at Fenton Creek, compared to 2.1 during baseflow. Again, the difference was less pronounced at the Douglas River (2.1 vs. 3.5 mg/L), Katherine River sites (2.3 vs. 5.4 mg/L) and lower Daly (3.4 vs. 5.1 mg/L).

Organic carbon concentrations increased from 2.8 and 2.9 mg/L of DOC during baseflow to 3.4 mg/L and 4.8 mg/L during stormflow in the Katherine and Douglas Rivers, while particulate organic carbon concentrations rose from 0.5 and 0.8 mg/L to 0.9 and 1.1 mg/L respectively. At the lower Daly River average DOC and POC concentrations were 1.3 and 0.8 mg/L during baseflow and rose to 3.9 mg/L DOC and 1.4 mg/L of POC during storm flow.

The comparison of bank and mid-channel samples at the lower Daly River in 2008/09 showed no significant differences for total nitrogen concentrations on any of the five sampling occasions while total phosphorus concentrations were significantly different on one of the five occasions (Table 8). At the time of writing, data for total and volatile suspended solids were only available for one sampling occasion. Differences were significant for mean TSS, with 61 mg/L in mid-channel samples compared to 45 mg/L in bank samples. This suggests a possible underestimate of about 25% of the total suspended solids load for the lower Daly River.

Regional scale sediment and nutrient budgets for the Daly River developed through another TRaCK project indicate that most of the sediment and nutrient mass in the Daly River is derived from subsoil bank erosion in the Daly River channel and some of its tributaries (Caitcheon, *pers. comm.*)

Table 8. Results of t-tests for comparison of samples collected from the bank and mid-channel of the Daly River in the 2008/09 wet season (t-test).

Date	Flow (m ³ /s) at G8140040 (Mt Nancar)	WQ Variable	Bank			Mid-channel			p
			Mean	SE	n	Mean	SE	n	
23/01/09	630	TN	0.51	0.08	4	0.35	0.06	4	0.17
		TP	0.02	0.001	4	0.01	0.003	4	0.22
		TSS	61	2.3	5	45	4.8	5	<0.05*
		VSS	7.8	1.4	5	6.4	1.3	5	0.49
4/03/09	1960	TN	0.38	0.07	4	0.39	0.07	4	0.9
		TP	0.01	0.002	4	0.01	0.002	4	1
17/03/09	340	TN	0.29	0.003	4	0.29	0.01	4	1
		TP	0.03	0.001	4	0.03	0.004	4	0.79
31/03/09	180	TN	0.16	0.01	4	0.15	0.003	4	0.32
		TP	0.02	0.000	4	0.02	0.000	4	<0.001*
21/04/09	100	TN	0.12	0.003	4	0.12	0.006	4	0.48
		TP	0.02	0.001	4	0.02	0.001	4	0.21

Between November 2007 and April 2008 the lower Daly River carried a load of 3350 tonnes of nitrogen, 410 t of phosphorus, 420 kt of total suspended solids, 67 kt of which were volatile, 17 kt of particulate organic carbon and 52 kt of dissolved organic carbon. Total nutrient and sediment loads for each of the four sites and export coefficients are given in Table 9. The proportion of nutrients and sediments carried in stormflow was higher relative to the contribution of storm flow to total flow at all sites (Table 10).

Export coefficients were highest in the smaller catchments and decreased with increasing catchment size. Nitrogen export coefficients ranged from 2.2 kg/ha at Fenton Creek to 0.71 kg/ha at the lower Daly River. Phosphorus exports ranged from 0.21 kg/ha from the Douglas River catchment to 0.07 kg/ha at the Katherine. The Fenton Creek catchment exported 610 and 92 kg/ha of total suspended and volatile solids, compared to only 88 and 14 kg/ha in the lower Daly. Carbon exports from the Douglas River catchment were 0.9 and 2.7 kg/ha for particulate and dissolved organic carbon, respectively, compared to only 3.5 and 11 kg/ha at the lower Daly.

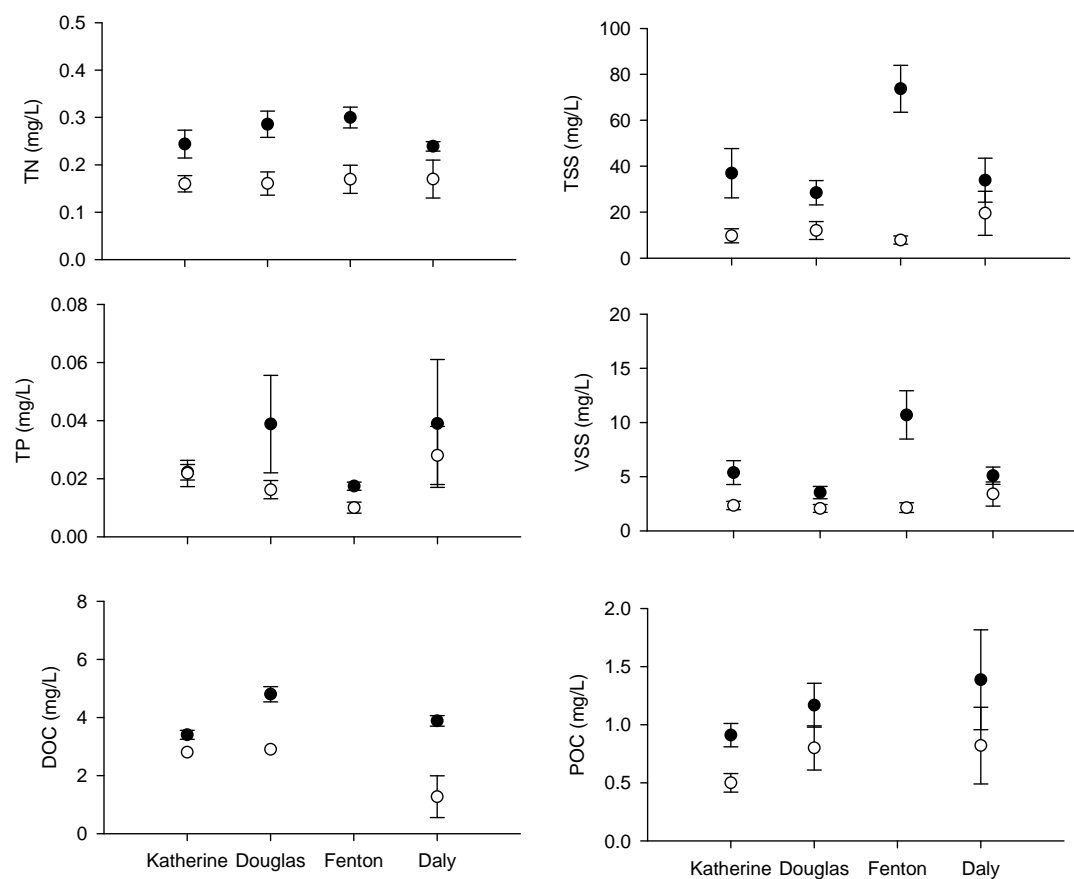


Figure 8. Volume-weighted mean concentrations and standard errors of TN, TP, TSS, VSS, DOC and POC for sampled storm events (filled circles) and baseflow periods (open circles) at Katherine, Douglas River and Fenton Creek over the 2007/08 wet season.

Table 9. Wet season loads and export coefficients of total nitrogen (TN), total phosphorus (TP), total suspended sediment (TSS), volatile suspended sediment (VSS), particulate (POC) and dissolved organic carbon (DOC) for four sites in the Daly River catchment.

	Catchment Size (km ²)	Wet season load (Nov 07-April 08)					
		TN (t)	TP (t)	TSS (kt)	VSS (kt)	POC (t)	DOC (t)
Fenton Creek	20	4.4	0.31	1.2	0.18	25	73
Douglas River	830	170	18	22	2.1	900	2700
Katherine River	8600	610	58	84	13	3500	9400
Daly River	47000	3350	410	420	67	17000	52000
Catchment Size (km ²)		Export Coefficients (kg/ha)					
Fenton Creek	20	TN	TP	TSS	VSS	POC	DOC
Douglas River	830	2.0	0.21	260	25	11	32
Katherine River	8600	0.70	0.07	97	15	3.5	11
Daly River	47000	0.71	0.09	88	14	3.5	11

Table 10. Percentage of total wet season load carried in storm flow vs. baseflow

	Daly		Katherine		Douglas		Fenton	
	%Storm	%Base	%Storm	%Base	%Storm	%Base	%Storm	%Base
Flow	94	6	93	7	86	14	92	8
TN	95	5	95	5	92	8	94	6
TP	92	8	93	7	92	8	94	6
TSS	95	5	97	3	95	5	99	1
VSS	95	5	96	4	92	8	98	2
POC	95	5	98	2	93	7	98	2
DOC	98	2	94	6	91	9	94	6

Flows in the Daly River can vary dramatically between years (Figure 9). The 2007/08 wet season was an above average year with more than twice the average flow recorded at the Mt Nancar gauge station. Assuming that sediment loads are proportional to flow, the annual wet season TSS load could range from as little as 27 kt in the driest year on record to 616 kt with an average of 208 kt.

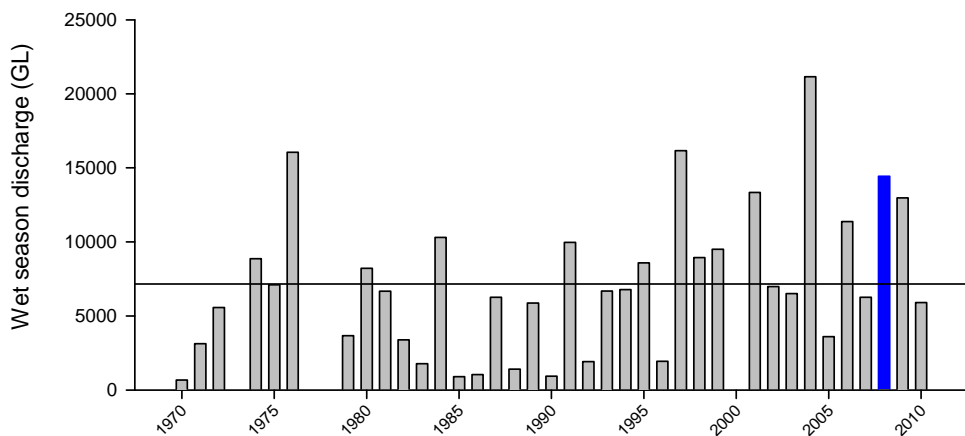


Figure 9 Total wet season discharge at Mt. Nancar gauge station (G8140040) between 1970 and 2010. The horizontal line indicates the mean wet season discharge over that period and the sampling year (2007/08) is highlighted in blue.

2.3.3. Dry Season Loads

Dry season flow decreased between July and September between 22-30% for Daly River sites and 25-70% for its tributaries (Table 11). Detailed results for the dry season gaugings are provided in a separate report (Tickell 2008).

Total nitrogen concentrations ranged from 30 µg/L to 150 µg/L in July and from 60-180 µg/L in September with increased concentrations at all but two sites (sites 4 and 9). Total phosphorus concentrations were between 10 and 25 µg/L throughout the dry season increasing at 4 sites in September compared to July.

These increases in concentrations led to higher daily nitrogen and phosphorus export loads later in the dry season at some sites, despite lower flows later in the season. Increases in nitrogen loads were particularly marked in the lower and middle reaches of the Daly River. While phosphorus loads were mostly closely associated with flows, at the four sites with increased concentrations (Sites 1, 5, 9 and 10) phosphorus loads remained higher compared to the reduction in flow.

Nitrite concentrations were below the detection limit in 11 of 15 samples in July and 6 out of 16 samples in September. Nitrate decreased at all but two sites (sites 12 and 13) and ranged from <1 to 95 µg/L in July to <1 to 77 µg/L in September.

FRP concentrations ranged from 2-11 µg/L in July and were higher at all sites in September (8-18 µg/L), resulting in a relatively high soluble phosphorus load later in the dry season.

Dissolved organic carbon was below the detection limit of 1 µg/L in all samples except for one sample in September at site 1 (2 µg/L).

Due to a laboratory error, a higher detection limit of 5 µg/L was used for ammonia in July. Ammonia concentrations were below the detection limit of 5 µg/L for 12 out of 15 sites in July and below the limit of 1 µg/L for 10 of 16 sites in September. Where sample concentrations were below the detection limit, a value equivalent to half the detection limit was used to compute nutrient loads and display data in graphs. Therefore, ammonia loads may appear unusually high in July.

Dry season nutrient loads were closely linked to flows at most sites, with the exception of nitrogen in the middle and lower Daly River.

Table 11. Dry season nutrient and sediment concentrations and loads at 16 sites in the Daly River catchment. Asterisks indicate concentrations below detection limit (DL). Where concentrations were below the detection limit, half the DL is given in this table and used to calculate loads

Site	Discharge				Concentration (ug/L)											
	m ³ /s		NO ₂ _N		NO ₃ _N		FRP		NH ₃ _N		TN		TP		DOC (mg/L)	
	Jul	Sep	Jul	Sep	Jul	Sep	Jul	Sep	Jul	Sep	Jul	Sep	Jul	Sep	Jul	Sep
1	2.3	0.7	0.5*	1	3	0.5*	2	8	2.5*	1	70	120	10	15	0.5*	2
3	5.6	3.3	1	2	95	67	6	10	2.5*	6	150	180	15	15	0.5*	0.5*
4	5.7	3.4	1	2	78	34	5	13	5	5	130	110	15	15	0.5*	0.5*
5	0.5	0.2	0.5*	2	4	1	6	14	2.5*	0.5*	80	70	15	20	0.5*	0.5*
6	6.6	3.3	0.5*	1	55	11	5	13	2.5*	3	100	100	15	15	0.5*	0.5*
7	3.3	0.5*	2	7	1	11	18	25	0.5*	40	60	25	20	0.5*	0.5*	
8	13	8.7	1	0.5*	25	3	9	16	15	0.5*	70	70	20	20	0.5*	0.5*
9	13	8.9	0.5*	0.5*	20	2	8	15	2.5*	0.5*	70	60	15	20	0.5*	0.5*
10	14	9.8	0.5*	0.5*	10	2	8	17	2.5*	0.5*	50	70	15	20	0.5*	0.5*
11	1.6	0.8	0.5*	1	4	2	7	14	2.5*	0.5*	60	80	15	15	0.5*	0.5*
12	25	17	0.5*	0.5*	1	3	9	17	2.5*	0.5*	30	90	20	20	0.5*	0.5*
13	27	21	0.5*	0.5*	0.5*	2	8	17	2.5*	1	30	120	20	20	0.5*	0.5*
14	3.5	2.6	0.5*	3	85	77	6	12	2.5*	3	140	150	15	15	0.5*	0.5*
15	39	29	0.5*	2	15	3	8	15	2.5*	0.5*	50	150	15	15	0.5*	0.5*
16		31		2		2		16		0.5*		70	0	15		0.5*
17	42	31	1	0.5*	10	3	8	15	2.5*	0.5*	70	100	20	20	0.5*	0.5*

Site	Discharge m³/s		NO2_N		NO3_N		FRP		NH3_N		TN		TP		DOC	
	Jul	Sep	Jul	Sep	Jul	Sep	Jul	Sep	Jul	Sep	Jul	Sep	Jul	Sep	Jul	Sep
1	2.3	0.7	0.1	0.1	0.6	0.0	0.4	0.5	0.5	0.1	14	7.1	2.0	0.9	99	118
3	5.6	3.3	0.5	0.6	46	19	2.9	2.8	1.2	1.7	73	51	7.3	4.3	244	142
4	5.7	3.4	0.5	0.6	39	10	2.5	3.9	2.5	1.5	64	33	7.4	4.5	248	149
5	0.5	0.2	0.0	0.0	0.2	0.0	0.2	0.2	0.1	0.0	3.3	1.0	0.6	0.3	21	7
6	6.6	3.3	0.3	0.3	32	3.1	2.9	3.7	1.4	0.8	57	28	8.6	4.2	287	141
7		3.3		0.6		0.3		5.1		0.1		17		5.7		142
8	13	8.7	1.1	0.4	27	2.3	9.7	12	16	0.4	76	53	22	15	540	376
9	13	8.9	0.5	0.4	22	1.5	8.7	12	2.7	0.4	76	46	16	15	541	385
10	14	9.8	0.6	0.4	12	1.7	9.7	14	3.0	0.4	60	59	18	17	604	423
11	1.6	0.8	0.1	0.1	0.5	0.1	0.9	1.0	0.3	0.0	8.1	5.7	2.0	1.1	67	36
12	25	17	1.1	0.7	2.1	4.4	19	25	5.4	0.7	64	133	43	30	1073	741
13	27	21	1.2	0.9	1.2	3.6	19	31	5.8	1.8	70	218	46	36	1159	909
14	3.5	2.6	0.2	0.7	26	17	1.8	2.7	0.8	0.7	42	34	4.5	3.4	151	113
15	39	29	1.7	4.9	51	7.4	27	37	8.5	1.2	171	371	51	37	1706	1237
16		31		5.3		5.3		43		1.3		187		40		1336
17	42	31	3.6	1.3	36	7.9	29	40	9.0	1.3	253	264	72	53	1809	1321

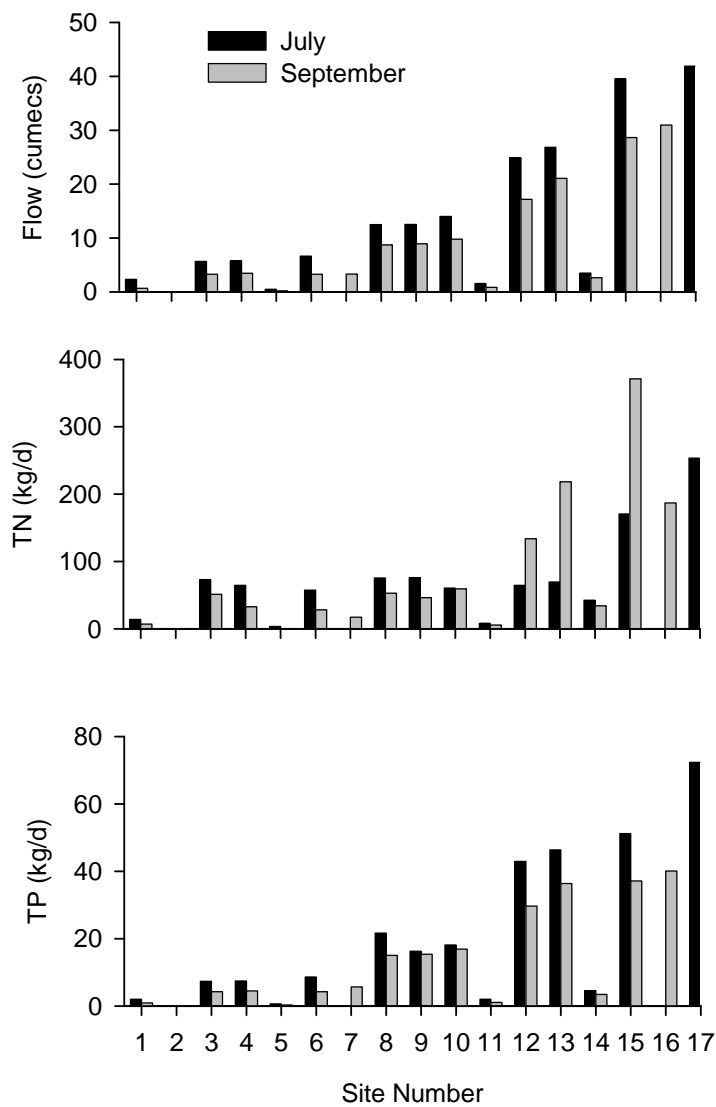


Figure 10. Total N and P loads for 17 sites in the Daly River catchment in July and September 2008.

2.3.4. Approximate Total Nitrogen, Phosphorus and Total Suspended Sediments budgets

Although accurate wet-season nitrogen, phosphorus and sediment loads could be calculated only for the few sites at which these constituents were regularly monitored, some effort has been made here to calculate approximate sediment and nutrient budgets for the system as a whole. Some components of these budgets have been found to be sensitive to the assumptions made and the method used to interpolate between water quality and flow observations, so these results should be interpreted with caution.

Total nitrogen load time-series for the lower Daly River (near Mt Nancar) and contributions from three tributaries are shown in Figure 11, while the same information is given for total phosphorus (TP) in Figure 12, and for total suspended sediments (TSS) in Figure 13.

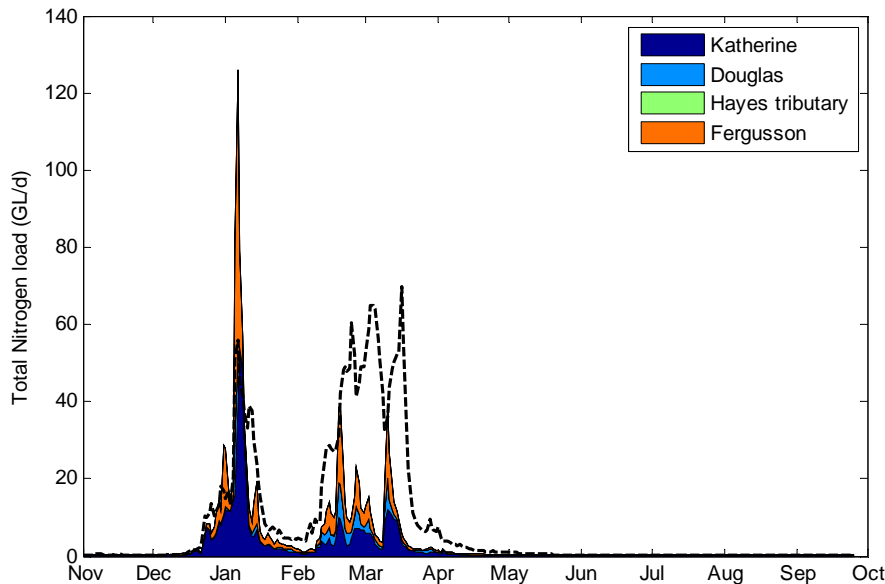


Figure 11 Total nitrogen load passing the Daly River near Mt Nancar (dashed line), and contributions from tributaries for which water quality measurements were taken. Contributions from Hayes tributary are minimal.

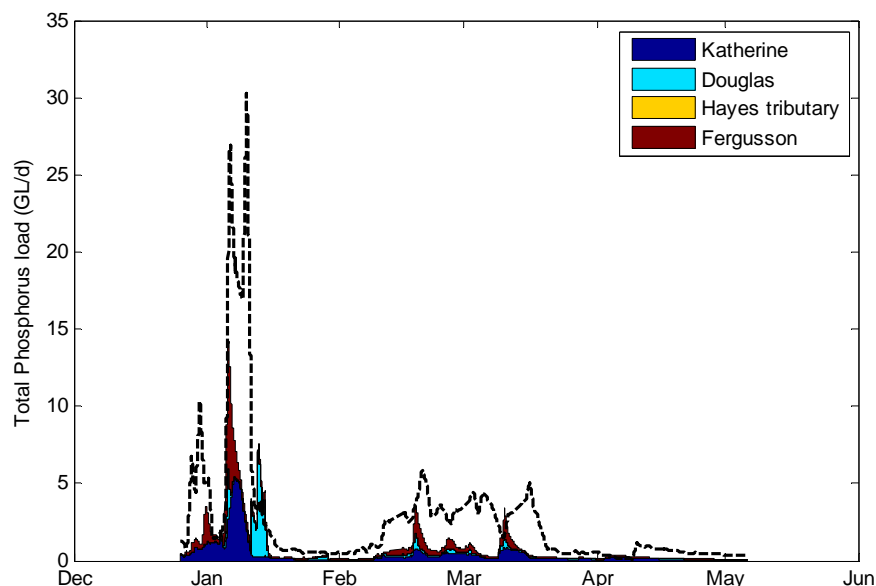


Figure 12 Total phosphorus load passing the Daly River near Mt Nancar (dashed line), and estimated contributions from tributaries for which water quality measurements were taken. Contributions from Hayes tributary are minimal.

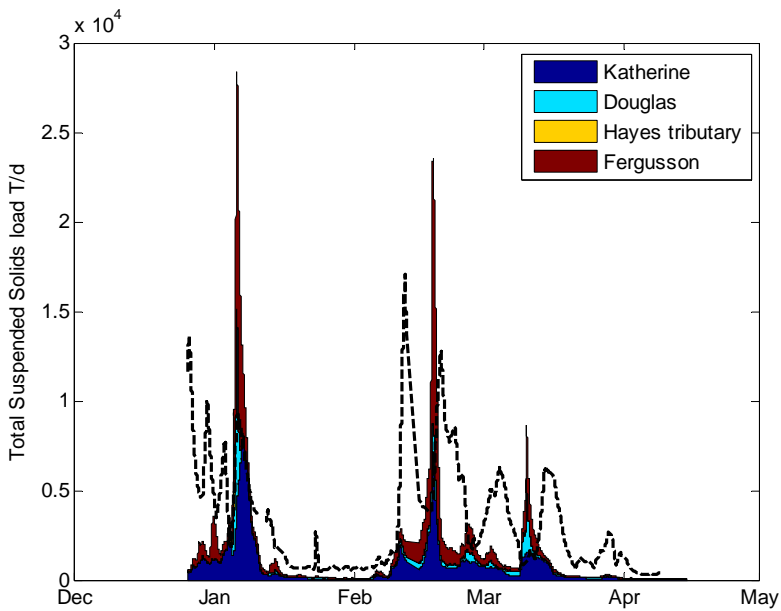


Figure 13 Total Suspended Solid load passing the Daly River near Mt Nancar (dashed line), and contributions from tributaries for which water quality measurements were taken. Contributions from Hayes tributary are minimal.

Estimated wet-season and dry-season nitrogen budgets for the Daly River catchment are presented in Figure 14 and Figure 15 respectively. Estimated wet-season and dry-season phosphorus budgets are presented in Figure 16 and Figure 17 respectively. Wet-season and dry-season TSS budgets for the Daly River catchment are presented in Figure 18 and Figure 19.

Most of the dry-season flow in the Daly River is ultimately derived from groundwater. TSS loads in the dry season are very much lower than in the wet season. Unaccounted sources account for 78% of this small dry-season TSS load: it is likely that this source is predominantly resuspension and downstream transport of material deposited in the river at the end of the wet season. Unlike wet-season surface flows, groundwater does not contribute particulate material (i.e. suspended solids) from the catchment, and appears to carry low concentrations of nitrogen and phosphorus. The main channel of the Daly River is a net sink of nitrogen in the dry season and approximately neutral with respect to phosphorus.

There is a similar unaccounted source of nutrients in the dry season. This will include some nitrogen and phosphorus from minor tributaries such as Green Ant Creek, groundwater and local runoff, and will also include some quantity of nutrients released from sediments and dry atmospheric deposition. By September, the majority of nitrogen and phosphorus in the system are in organic form, suggesting that most of the available nutrients have been taken up by plants and subjected to biological processing.

The unaccounted phosphorus source is larger (in relative terms) than that of nitrogen: this might indicate some removal by denitrification.

Further upstream, the Katherine River and Fergusson River are consistent sources of nitrogen and phosphorus to the main channel of the Daly River in both the wet season and dry season.

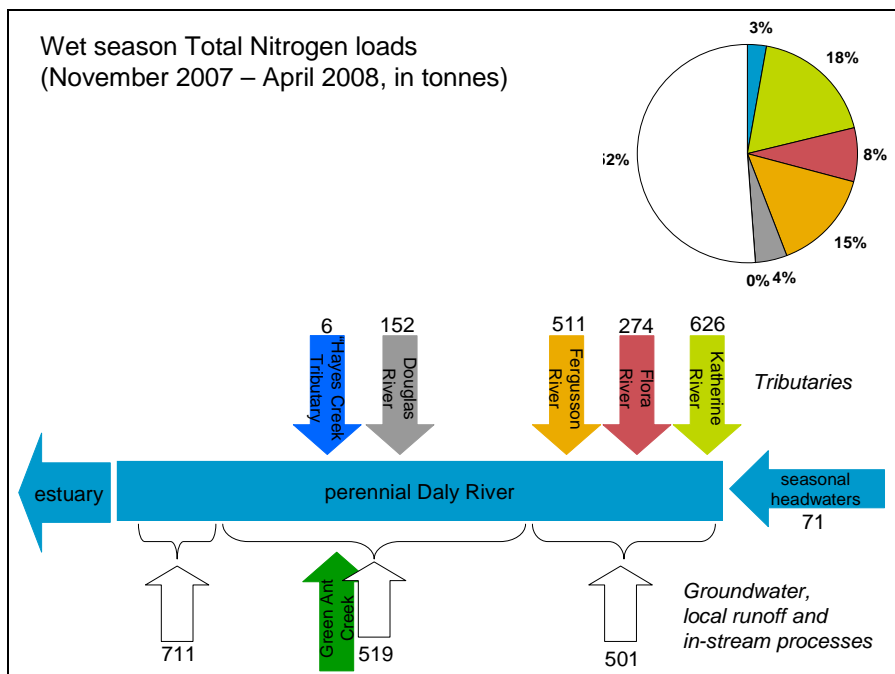


Figure 14 Contributions to total nitrogen loads in the Daly River during the 2007-2008 wet season. White arrows indicate unknown sources such as groundwater, local runoff and in-stream processes.

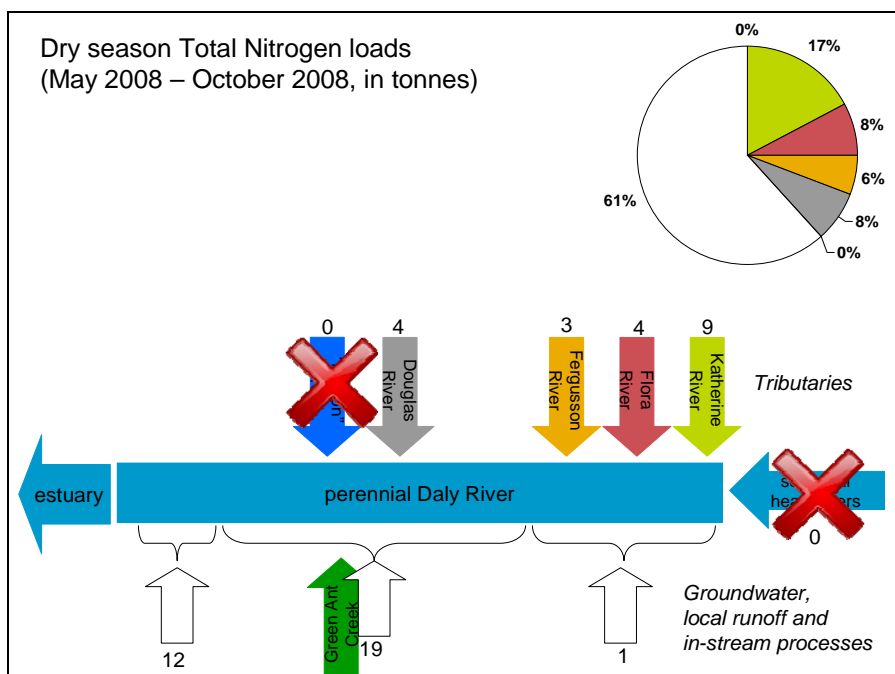


Figure 15 Contributions to total nitrogen load during the 2008 dry season. White arrows indicate unknown sources such as groundwater, local runoff and in-stream processes.

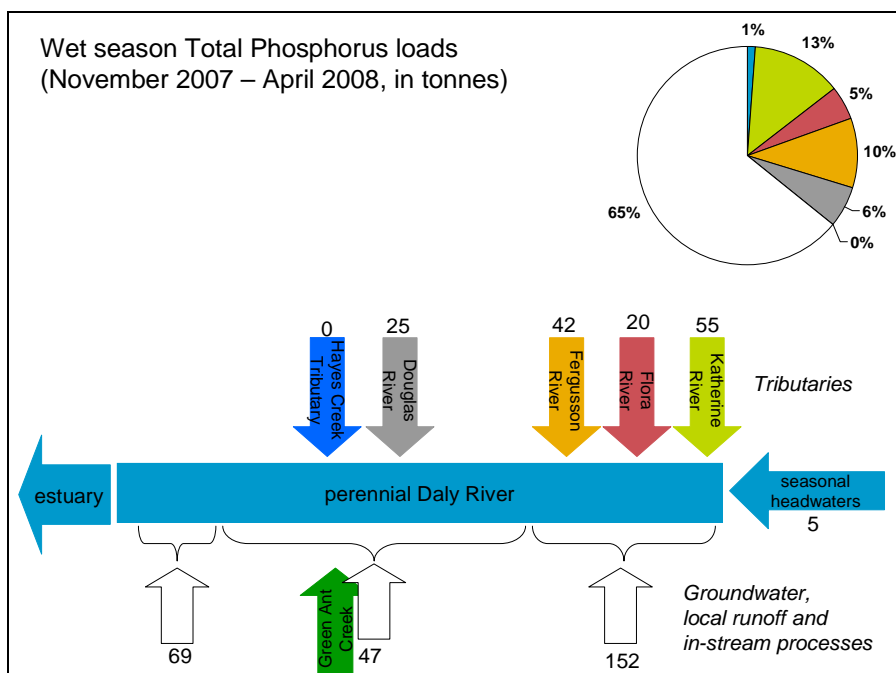


Figure 16 Contributions to Total Phosphorus in the Daly River during the 2007-2008 wet season.
White arrows indicate unknown sources such as groundwater, local runoff and in-stream processes.

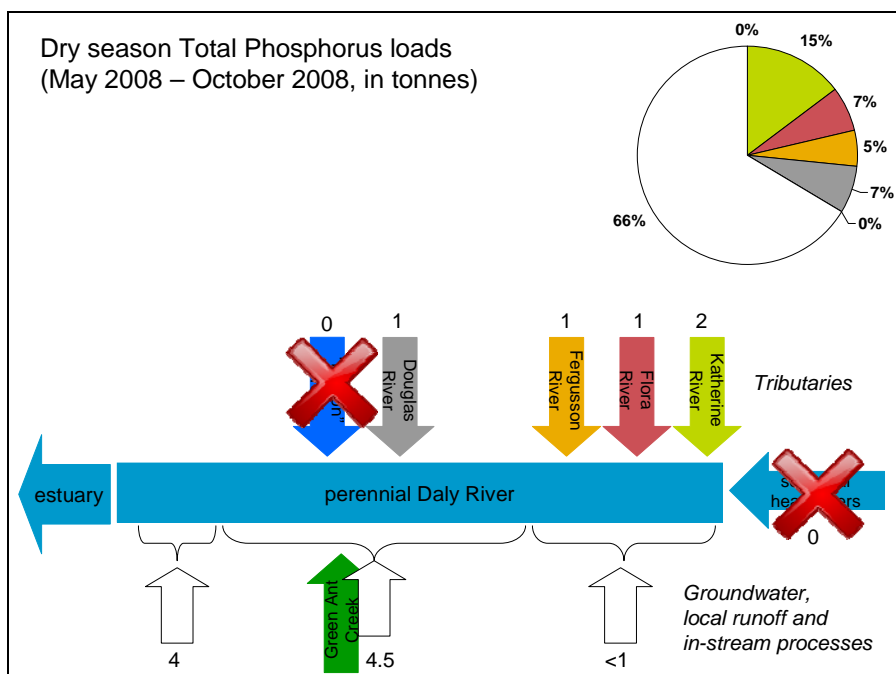


Figure 17 Contributions to Total Phosphorus in the Daly River during the 2008 dry season.
White arrows indicate unknown sources such as groundwater, local runoff and in-stream processes.

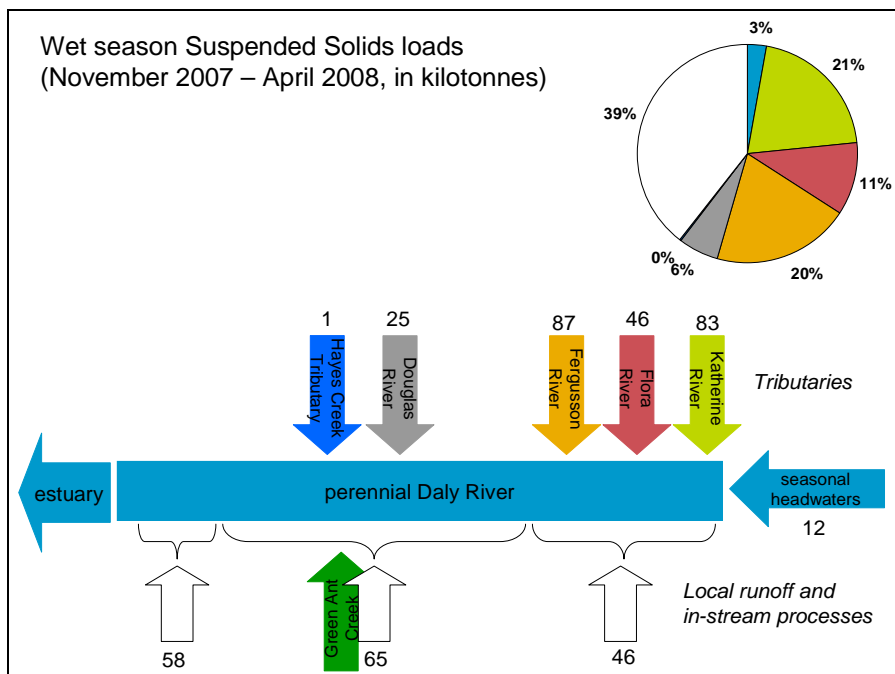


Figure 18 Contributions to total suspended solids loads to the Daly River during the 2007-2008 wet season. White arrows indicate unknown sources such as groundwater, local runoff and in-stream processes.

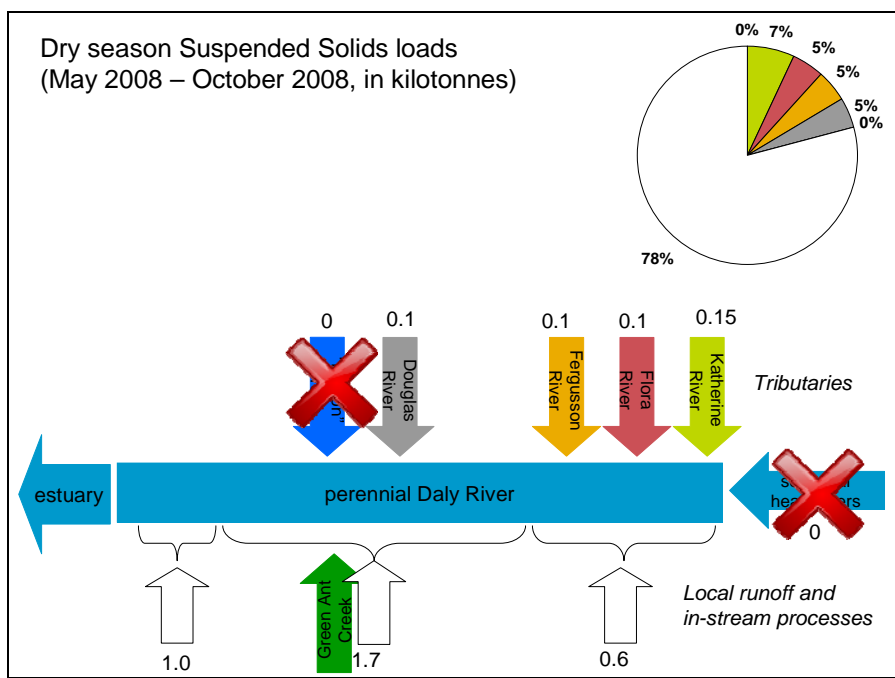


Figure 19 Contributions to the total suspended sediment load to the Daly River during the 2008 dry season. White arrows indicate unknown sources such as groundwater, local runoff and in-stream processes.

2.4. Conclusion

The Daly River exported 3350 tonnes of N, 410 t of P, 420 kt of TSS, of which 67 kt were volatile, 17 kt of particulate organic carbon and 52 kt of dissolved organic

carbon during the 2007/08 wet season. Nutrient and sediment exports were closely linked to flow conditions. Higher export coefficients in the upper catchment result from processes within the river such as uptake of nutrients by plants and settling of sediment in slower flowing waters.

Dry season nutrient and sediment loads were mostly closely related to flow. Further investigation is required to identify the source of increased nitrogen loads in the late dry season at some sites in the Daly River catchment.

3. Composition of sediments and organic matter

3.1. Introduction

Understanding the composition of sediments and associated organic matter in a river helps to create a picture of the physical and biogeochemical function of the river. Sediments play an important role in determining the physical habitat of the river and can be a key component of nutrient cycles. Analysis of the composition of organic matter also provides clues about the sources of carbon and nutrients that underpin the aquatic ecosystem.

River bed and suspended sediments in the Daly River were examined to determine the occurrence and characteristics of fine sediments and the organic matter associated with sediments. A small reach within the main channel of the Daly River (Figure 20) was studied in detail. This reach was chosen because it was accessible by road and was judged to be representative of the river in terms of habitat and sediment types.

3.1.1. Physical properties and geochemical composition

The bulk physical characteristics of sediments from a range of habitats along the river were examined. The fine sediment fraction of these sediments was separated and the geochemical composition determined in order to obtain an understanding of their potential role in nutrient dynamics, including the transport and fate of carbon and nutrients associated with fine sediments.

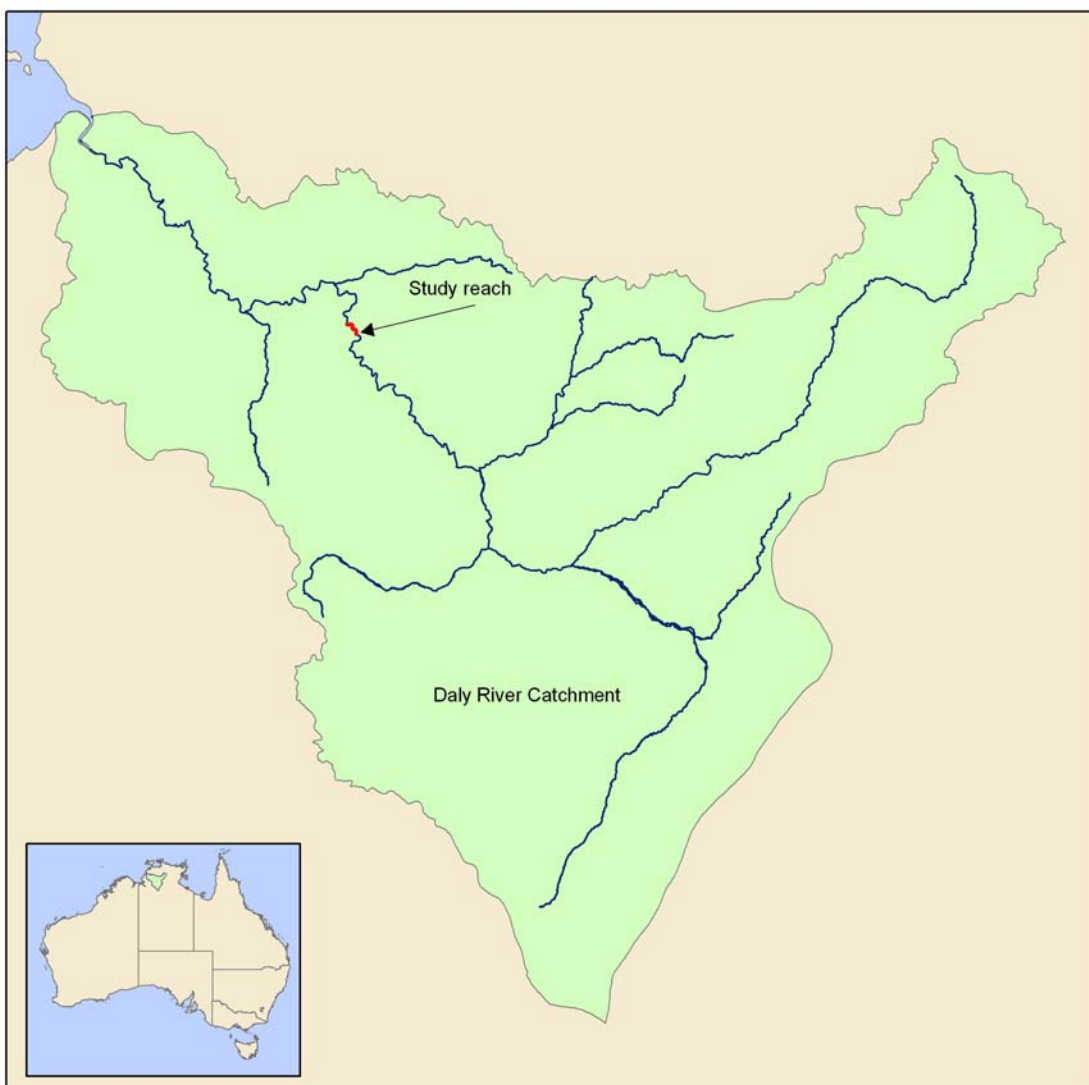


Figure 20: The Daly River catchment and the location of the study reach.

3.1.2. Sources of organic matter

There are a variety of potential sources of organic matter to Daly River sediments. Freshwater entering via river and drainage channel flows will bring with it suspended material with organic matter characteristic of the catchment and in-situ production and will also reflect any subsequent re-working during transportation. Local run-off will carry material representative of the local surroundings and there is likely to be significant in-situ primary production either within the water column from phytoplankton and in the shallow sediments by microphytobenthos and macrophytes.

Identifying and quantifying different sources is the goal of many organic geochemical studies, and a variety of techniques have been utilised.

3.1.3. Lipid biomarkers

A great variety of different lipids can be found in marine sediments and the water column attesting to the diversity of biosynthetic pathways employed by aquatic organisms. Many of these compounds have distinctive chemical structures allowing them to be used as biomarkers for particular sources of organic matter in marine ecosystems. Many of these compounds are sufficiently stable in sediments that they survive over geologically important time scales (in some cases millions of years) so their presence in ancient sediments can be used to infer changes in ecosystems over time.

All eukaryotes contain sterols, some of which have distinctive structures and limited distribution, the most commonly cited example being dinosterol which is found in certain dinoflagellates. Fatty acids are also ubiquitous and the presence of polyunsaturated fatty acids is usually indicative of living cells since these compounds are rapidly degraded in sediments.

The input of terrestrial organic matter to marine environments can be recognised from lipids of higher plant origin such as long-chain (C_{22} - C_{30}) *n*-alcohols and fatty acids showing a strong predominance of even chain-lengths, long-chain (C_{21} - C_{35}) *n*-alkanes showing strong odd-chain predominance and C_{29} sterols such as 24-ethylcholesterol (sitosterol) and 24-ethylcholesta-5,22E-dien-3 β -ol (stigmasterol).

Bacteria synthesize a diverse range of compounds such as *iso*-, *anteiso*- and mid-chain branched fatty acids, hopanoids such as the C_{32} β,β -hopanol and isoprenoids, many of which are particularly stable such as those that contain an ether bond.

Aquatic animals almost always contain a high content of cholesterol and C_{20} and C_{22} polyunsaturated fatty acids and, as end consumers in aquatic food webs, they can be important sources of organic matter and as agents for its transformation.

The qualitative assignment of organic matter sources using biomarkers is thus reasonably straightforward, although even today lipids can be found in sediments for which no source is known.

However, the quantitative aspects of this approach can be constrained by various limitations: Unique biomarkers may not be known for each potential source. Some markers may only be produced by a few species as already noted while some compounds appear to be almost ubiquitous (e.g. cholesterol which is found in most animals and some phytoplankton; the sterol sitosterol which occurs in all terrestrial plants).

The ratio of the lipid or pigment biomarker to C_{org} can vary as can the C and N content in plants, algae, animals or bacteria due to inter-species differences or seasonal and environmental conditions.

Like all organic compounds, biomarkers degrade and the rates vary depending on the chemical structure and the environment. This can be used to advantage for example, in that the presence of labile compounds such as polyunsaturated fatty acids (PUFA) clearly indicates the presence of “fresh” organic matter, which may represent living cells. However, this can be a disadvantage when trying to compare the two different

compound classes since as already mentioned, fatty acids may degrade quicker than sterols from the same source.

3.2. Methods

3.2.1. Sample Collection

A total of 13 sites, approx. 500 m apart, were sampled along a 6.5 km reach of the Daly River during two field trips in July and September 2008 (Figure 21). At each site, 3 samples were collected in a transect across the river (A, B and C representing bank, middle, bank), giving a total of 39 sample sites. At each sample site, surface sediments for bulk physical property and geochemical analysis were collected using a small Van Veen grab, stored in zip-lock bags and frozen until analysis.

For organic matter analyses, samples were collected using push corer where possible. A small hand grab was used where coring was unsuccessful. Samples were transferred to pre-cleaned glass jars, stored on ice and frozen as soon as possible for transport to Hobart for analysis.

During the July survey, 4 sample sites were rocky and no sediment was collected. In addition, one site (8B) was in a fast flowing channel and it was not possible to collect a sample of the gravelly sediment. During the September survey, an additional sample site was rocky and no sample collected. In total, 34 samples were collected in the July survey and 33 in the September survey.

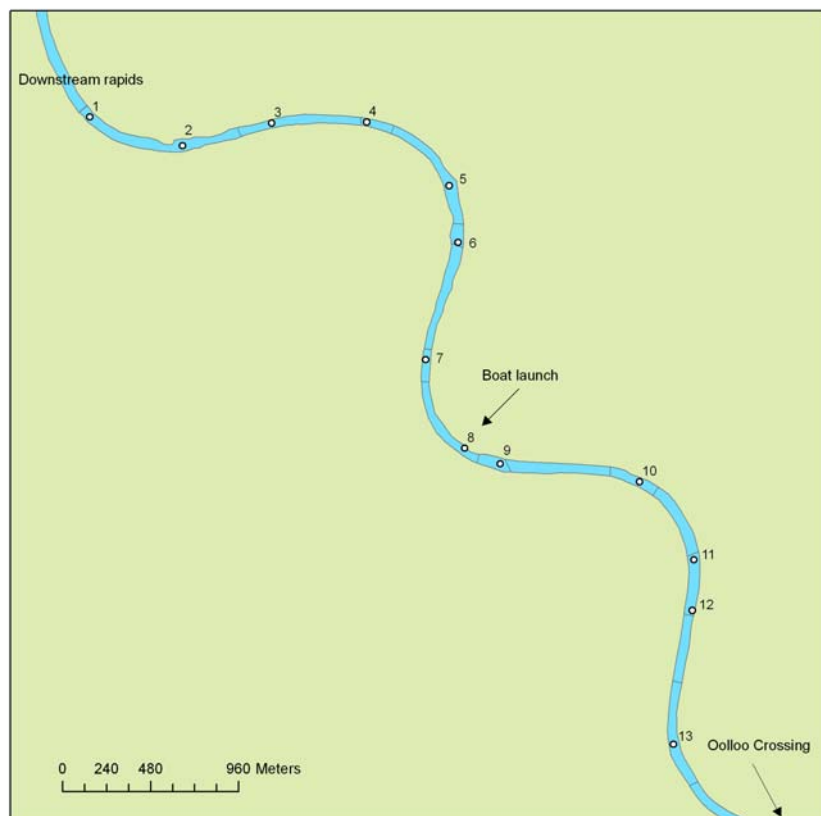


Figure 21: Location of surface sediment sampling sites

Additional sediment cores (0.79 m dia.) were collected from two pools (sites 6 and 9) in the study reach (Figure 21) during the July field survey using a push corer. The cores were used for grain size and porewater analysis. During the September field survey, cores were collected from the same two pools. An additional two cores were also collected from a sand riffle zone between sites 9 and 10 (Figure 21), with one core collected from the crest and another from the valley of a riffle. These cores were used for porewater analysis only.

Sediment traps were deployed in two pools (sites 6 and 9) at the end of the July field trip and were retrieved at the beginning of the September field trip. The traps were interfered with by crocodiles and the trap at site 9 had been dragged to the side of the pool and left on its side. The samples from this trap were discarded. The Schott bottles inside the traps at site 6 were full of sediment but it was unclear if this was a result of the traps being dragged or from sediment settling out of the water column. Additionally, it was unknown when the traps were moved. Because of these uncertainties, the sediment traps were redeployed for one week during the September field trip. The traps were retrieved and the sediment collected in the Schott bottles was retained for analysis.

3.2.2. Physical properties

The surface sediment samples and the sediment trap samples were analysed for bulk grain size by wet sieving. Following removal of the gravel section, laser grain size was measured to determine the grain composition. Particles were divided into three categories: gravel (>2 mm), sand (63 µm to 2 mm) and mud (<63 µm).

3.2.3. Geochemical analysis

Chemical analysis was performed on the fine sediments only (<63 µm fraction). There was not enough fine sediment collected from each sample for all the analysis so there is limited data available.

Of the 34 samples collected during the July survey, only 24 contained fine sediments. XRF and P-fractionation was measured on these 24 samples. Only 17 of these had enough material to perform all chemical analysis (including CaCO₃, TOC, TN, and isotopes). Of the 33 samples collected during the September survey, only 19 contained fine sediments and 18 had sufficient material for all chemical analysis. There were no fine sediments extracted from the sand ripple samples from the September survey.

The fine (<63 µm) sediments were freeze dried and ground with a mortar and pestle prior to analysis. Carbonate content (CaCO₃ %) was determined using the carbonate bomb method (Muller and Gastner 1971).

Total organic carbon (TOC) and total nitrogen (TN) concentrations, and the respective stable isotopic compositions δ¹³C and δ¹⁵N, were analysed at ANU after the samples were pre-treated with acid and washed with demineralised water to remove carbonate and residual acid. Results are presented in standard δ notation:

$$R (\%) = \left[\frac{R_{sample}}{R_{standard}} - 1 \right]$$

where $R = ^{15}\text{N}/^{14}\text{N}$ or $^{13}\text{C}/^{12}\text{C}$.

There were problems with the isotope analysis for the September samples so this data is not available.

Selective sequential fractionation of phosphorus was performed on the fine sediment using a 4-step process outlined in Anderson and Delaney (2000). The fractions extracted were adsorbed and oxide-associated P (CDB extract), authigenic P (Na-acetate extract), detrital P (HCl extract) and organic P (HCl extract after combustion). Dissolved P in the extract solution was determined by automated colorimetry. An additional sub-sample was analysed for total P (TP) to test the efficiency of the extraction method. TP, along with other major elements, was determined by X-ray fluorescence (XRF) according to a modified version of Norrish and Hutton's (1969) method and using a Philips PW2404 4kW sequential spectrometer.

Within a few hours after core retrieval, sediment from distinct depth intervals was extruded. Pore water was extracted by centrifugation (5250 g, 10 min), and supernatant water was filtered (0.45 µm) and subsampled for DIC and dissolved inorganic nutrient (NH_4 , NO_x , PO_4 and SiO_4) analysis. DIC samples were poisoned with HgCl_2 and were kept gas-tight without headspace (Exetainer 3mL), while nutrient samples were kept frozen before analysis. Bulk grainsize was determined by wet sieving.

3.2.4. Biomarker analysis

Sediment samples for sterol and fatty acid analysis were extracted quantitatively by a modified one-phase CH_2Cl_2 -MeOH Bligh and Dyer method (Bligh and Dyer, 1959). After phase separation, the lipids were recovered in the lower CH_2Cl_2 layer (solvents were removed in *vacuo*) and were made up to a known volume and stored sealed under nitrogen at -20 °C. The total sterol fraction was obtained following alkaline saponification of an aliquot of the total lipids. Fatty acids were recovered from the aqueous fraction of the saponified mixture after the addition of 1 ml of HCl. Sterols were converted to their corresponding O-TMSi ethers by treatment with bis(trimethylsilyl)trifluoroacetamide (BSTFA, 100 µl, 60 °C, 60 minutes). Fatty acids were converted to their methyl esters prior to analysis by treatment with acidified methanol.

Gas chromatography (GC) was performed using a Varian 3800, controlled by Galaxy chromatography software. The gas chromatograph was equipped with a 50 m x 0.32 mm i.d. cross-linked 5% phenyl-methyl silicone (HP5) fused-silica capillary column; hydrogen was the carrier gas. Sterol and fatty acid fractions were analysed using a flame ionisation detector, with $5\beta(\text{H})$ -cholan-24-ol (Chiron AS, Norway) as the internal standard for sterols and the C_{23} fatty acid methyl ester (FAME) as the injection standard for fatty acid analysis. Peak identifications were based on retention times relative to authentic and laboratory standards and subsequent GC-MS analysis.

Verification of the identity of individual sterols by GC-MS analyses was performed on a Thermoquest GCQ-Plus bench top mass spectrometer fitted with a direct capillary inlet and a split/splitless injector. Data were acquired in scan acquisition or selective ion monitoring and processed using Xcalibur software supplied with the instrument. The nonpolar column (HP5) and operating conditions were similar to that described above for GC-FID analyses, but helium was used as the carrier gas.

In order to assess primary sources of organic matter to the sediments a suite of common biomarkers was used to determine an estimate of relative contributions. Peak areas were measured for all markers detected and then percentage contribution to the total calculated for each one. Selected markers for each category (Algal, bacterial and terrestrial) were then summed to give an estimate of the overall relative contribution. Note that this method allows for comparison between field trips but not between categories. The selected markers are listed in Table 12.

Table 12 Biomarkers measured in sediment samples

Category	Markers
Fatty Acid algal markers	16:0, 18:1 ω 9, EPA, DHA
Sterol Algal markers	Phytol, Brassicasterol, Ergosterol, Stigmasterol, Dinosterol
Fatty Acid Bacterial markers	<i>Iso</i> -15:0, <i>anteiso</i> -15:0, <i>iso</i> -16:0, 10-methyl-16:0, 18:1 ω 7c
Fatty Acid Terrestrial markers	22:0, 24:0
Sterol terrestrial markers	Taraxerol, β -amyrin, α -amyrin, Lupeol

3.3. Results and Discussion

3.3.1. Bulk Grainsize Composition

Surface Sediments

The section of the river studied contained three dominant habitat types: deep pools, gravel beds and sandy ripples. There were also rocky outcrops along some sections of the river bank but sediment was not collected from these areas. The bulk grainsize data was used to classify each sample into one of the three habitat types. Two samples did not easily fall into the defined habitats so a fourth habitat, i.e. muddy banks, was included. The average grainsize data for each habitat was calculated for both field surveys and is shown in Figure 22.

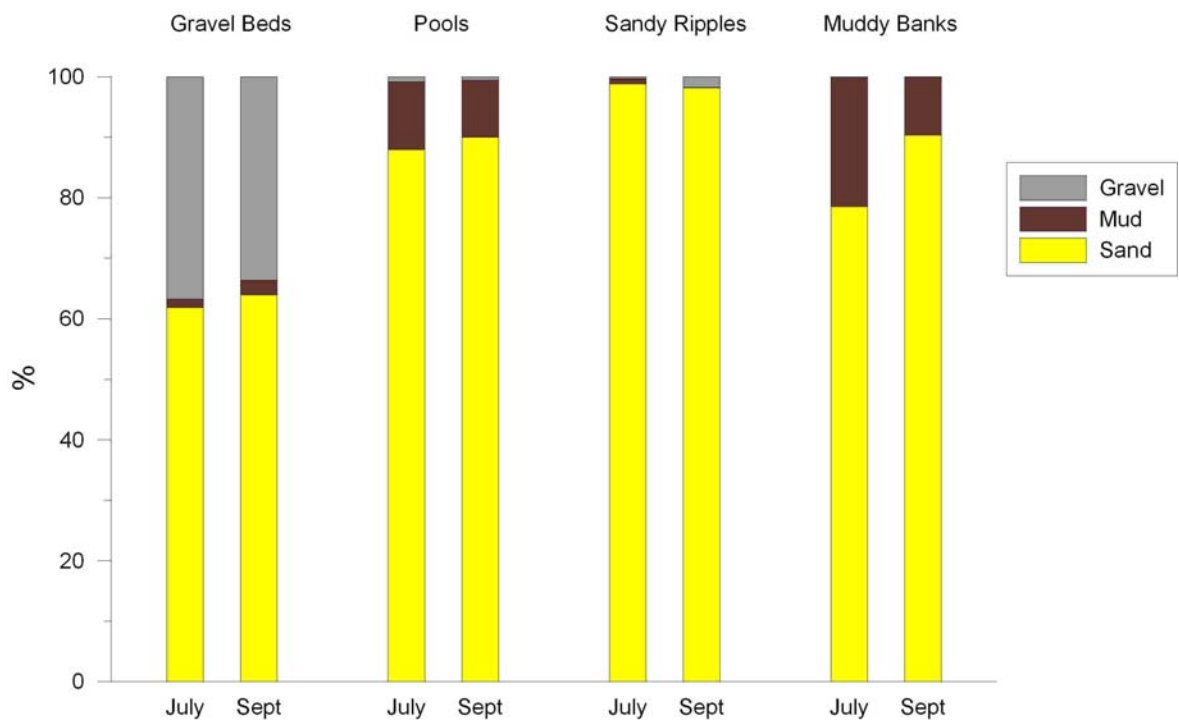


Figure 22: Average grain size characteristics in the Daly River habitat types

Large sections of the river reach were characterised by gravel beds. The sediments collected in the gravel beds were very diverse in their grain size composition (Figure 23), with the gravel content varying from 5 to 92%. Many of the gravel bed samples contained fine material and mud contents up to 10% were measured in some samples. Algal growth was commonly found in the gravel beds (Photo 1), either growing on individual pebbles or in the fine material in between the gravel. Excluding the gravel, the gravel beds were classified as coarse and medium sands although some were classified as fine sands.

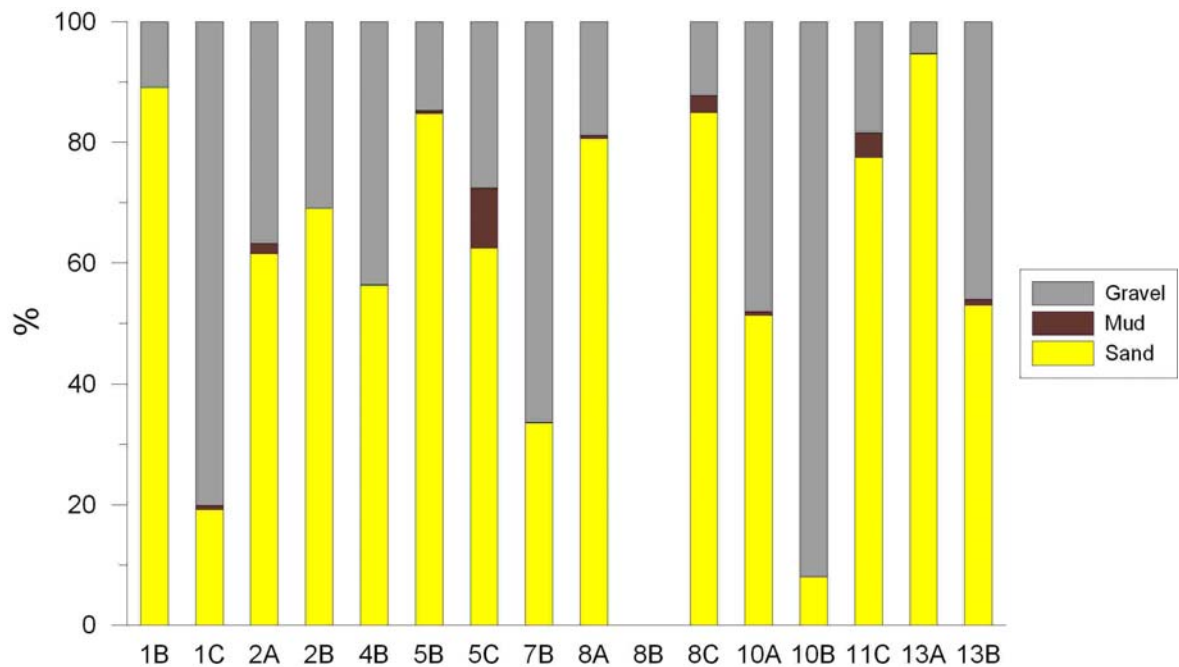


Figure 23: Bulk grainsize composition of gravel bed samples - July survey



Photo 1: Typical gravel bed showing coarse sediments and algal growth

There were three pools in the river reach studied (sites 6, 9 and 12). The sediment in the pools consisted of muddy sands (Figure 22). The mud content ranged from 0 to 33 % and was 10% on average. Some samples collected from the pools contained black leaf litter and algal material. The sediment in the pools was mostly characterised as fine sand, but ranged from very coarse silt and very fine sand to medium sand.

The grainsize composition of the muddy bank samples was similar to the average pool composition including high mud contents (Figure 22). However, the habitats of the pools and muddy banks were distinctly different. The muddy bank samples were adjacent to shallow (~1m depth) gravel beds (at sites 2 and 5) where the banks had collapsed into the river depositing fine sediment and therefore could not be classified as pools.

The sand ripples consisted of almost entirely sand (average 98-99% sand). Some samples contained finer material (up to 2.8% mud) and most samples contained <1% gravel.

The average grainsize in each habitat type did not vary much between the July and September field surveys (Figure 22). However, there were some subtle differences worth noting in some habitat types and at particular sites.

In the sand ripple zones, the mud content in the July survey samples ranged from 0 to 2.8%. The samples consisted of fine, medium and coarse sands and ranged from moderately sorted to well sorted. However, in the September survey, the mud content of all sand ripple samples was negligible (<0.04%). The sands were all characterised as coarse sands and moderately well sorted. In addition, the gravel content in the July survey samples was mostly 0% except for 2 samples (0.8% and 1.2%). However, in the September survey, the gravel content of all but one sample had increased. The gravel content at site 3B had increased from 1.2% in July to 9.2% in September. This site was in a distinct sandy ripple zone in the July survey but the sand ripples were gone in the September survey and the site contained coarse sands and gravels. However, sand ripples were still present at the adjacent river bank sample (3C).

While the average grainsize composition of the pools was similar during the two surveys with a small decline in the average mud content (Figure 22), the individual pools displayed different trends in grainsize composition throughout the dry season with mud contents increasing in some pools and decreasing in others as shown in Table 13. In the downstream pool (site 6) there was an increase in the mud content and concurrent decrease in the sand content of approximately 2%. However, in the pool at site 9 there was a large decrease in the mud content (approx. 7%) and a concurrent increase in the sand content. At the upstream pool (site 12) there was little difference between the two field surveys. It was observed that the sand ripples immediately upstream of the pools had migrated downstream during the two field surveys and movement of sand into the pools was clearly seen.

Table 13: Average grainsize composition in the three pools during the two field surveys

Site	Survey	%Mud		%Sand		%Gravel	
		Mean	Range	Mean	Range	Mean	Range
6	July	4.4	1.9 - 6.9	95.6	93.1 - 98.1	0.0	0.0 - 0.7
	Sept	6.5	0.4 - 12.0	93.5	87.9 - 99.6	0.0	0.0 - 0.8
9	July	12.7	3.2 - 19.5	86.9	80.2 - 96.6	0.4	0.2 - 0.6
	Sept	5.2	1.0 - 8.4	94.7	91.4 - 99.0	0.1	0.0 - 0.2

12	July	14.4	1.3 - 33.5	83.9	66.2 - 97.1	1.6	0.0 - 6.8
	Sept	13.7	0.1 - 29.9	85.0	70.0 - 99.3	1.3	0.1 - 5.0

There was also a decrease in the mud content of the muddy bank samples (Figure 22) and the sediments changed from being very fine sand to fine and medium sand.

In the gravel bed sections, there was large variation but overall, there was a slight increase in mud and sand content and a decrease in gravel content between the two field surveys.

Suspended Sediments

The suspended sediment collected in the sediment traps consisted of mud and very fine sand with little gravel (<1%). The composition was similar for the two deployments but the mud content was higher in the second sediment trap (Table 14).

Table 14: Grainsize composition of sediment trap samples

Sediment Trap #	Days deployed	% Mud	% Sand	% Gravel
1	55	26.6	72.8	0.6
2	7	33.0	66.2	0.7

Core Profiles

The grainsize composition of the sediment cores from 2 pools show the accumulation of fine material at the sediment surface (Figure 24). At site 6, the maximum mud content (10.6%) occurred at a depth of approx. 2 cm and the surface sediments had a lower mud content (approx. 5%). At site 9, the mud content was a lot higher and was highest at the surface (approx. 20%). The pool at site 9 had a large gravel content (approx 20-30%) below 2 cm.

The location where the cores were collected in the pools is likely to have influenced the grainsize composition. The core from site 6 was collected at the upstream end near the sandy ripple zone whereas the core from site 9 was collected further back from the sand bank in the deepest part of the pool. The proximity to the sand bank at the upstream end of the pool may affect the grainsize distribution, i.e. a higher sand content. Indeed, the surface sediment sample collected from site 6 in the middle of the pool had a mud content of 12%.

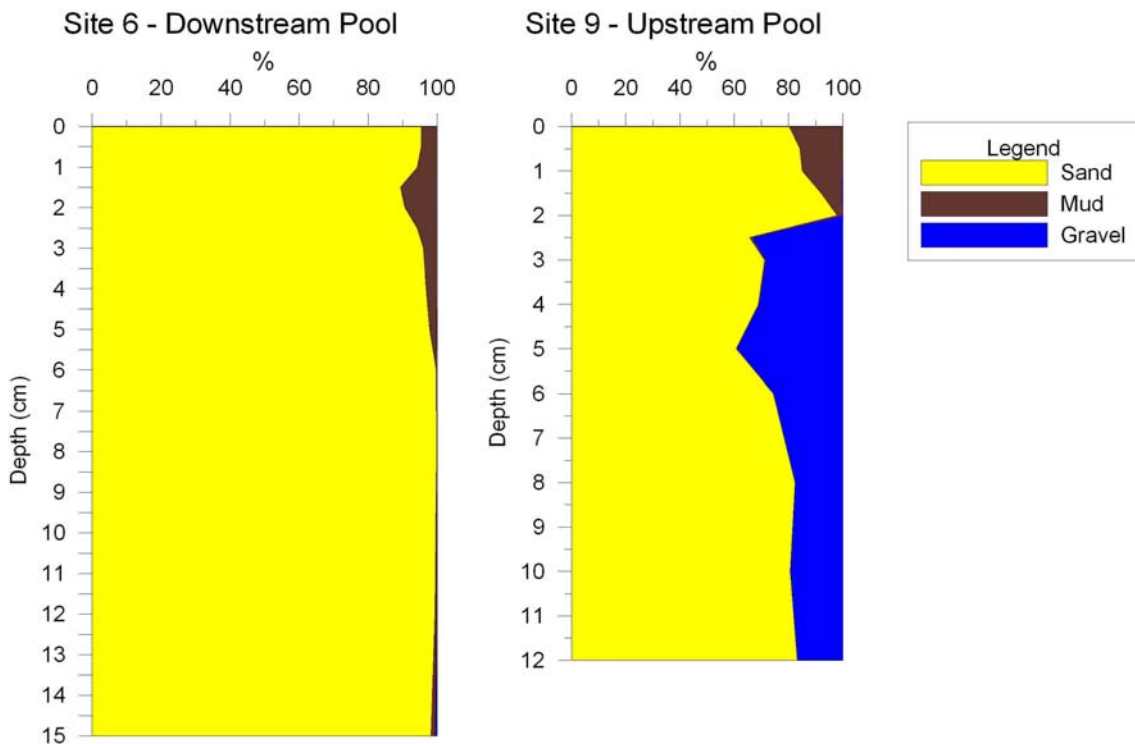


Figure 24: Grainsize composition of sediment cores collected in pools

Sedimentation Rates

The sedimentation rate was calculated for the two sediment trap deployments in the pool at site 6 (Table 15). The average sedimentation rates for the two sediment traps decreased from 205 to 129 g/m²/day.

Table 15: Sedimentation rates and grainsize composition of sediment trap samples

Sediment Trap #	Days deployed	Sedimentation rate g/m ² /day
1	55	205
2	7	129

3.3.2. Habitat Extents

The extent of each habitat type in the river reach was estimated based on field observations, satellite imagery (Google Earth) and the grainsize data. The pools always occurred at the downstream end of the sand ripple zone and were characterised by a sharp increase in water depth at the end of the sand bank. The pools were typically 3-4 m deep. The pools became shallower downstream and transitioned into gravel beds. The gravel beds were very diverse and were found in both shallow water and deeper, faster flowing channels. The gravel beds gradually transitioned into sandy ripple zones. At some sites, different habitat types were observed across the river transects and these were considered to be transition zones where one habitat type gradually merged into another.

The estimated habitat extents were mapped (Figure 25) and the average length of each section calculated. Note: these are only estimates as we did not record the actual start and end of each section in the field. The river reach was predominantly characterised by gravel beds which covered over 55% of the reach. The gravel beds varied in length and ranged from 580 to 920 m. Sandy ripple zones occurred in approximately one-third of the reach and ranged in length from 360 to 670 m. There were three pools in the study reach and they ranged in length from 120 to 340 m.

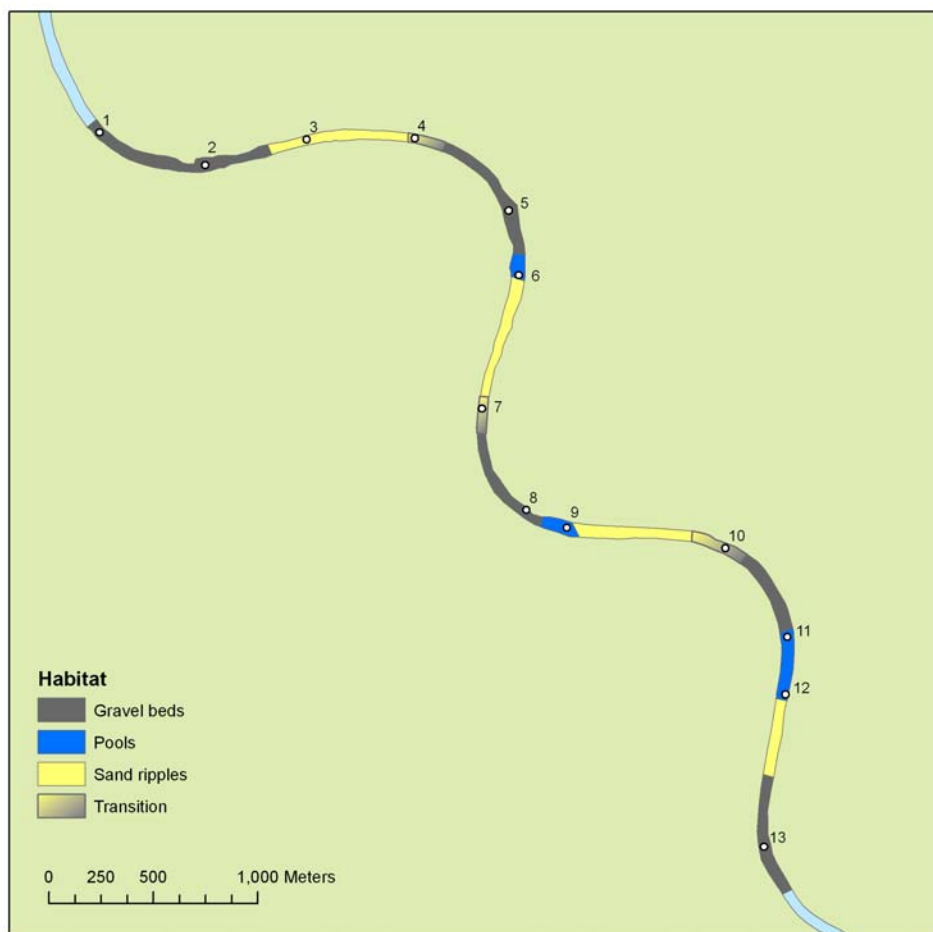


Figure 25: Estimated habitat extents in the river reach studied

3.3.3. Fine Sediment Deposition Over the Dry Season

Several lines of evidence suggest the river bed is scoured of fine sediment during the high flows in the wet season and the majority of fine sediment is deposited at the end of the wet season. Throughout the dry season there appears to be continual transport of the bed sediments, with accumulation of fine sediments in pools and gravel beds.

The decrease in mud content and increase in gravel content in the sandy ripple zones suggests there has been considerable movement of the sands in the sandy ripples during the dry season with the finer material (mud and fine to medium sands) being transported downstream. The fine sediment is most likely deposited in the pools where the water velocity slows, as was found with the increased mud content in pool

6. Additionally, the fine sediment may be trapped by aquatic vegetation and gravel in the gravel beds. It is likely that the growth of algae enhances the trapping of fine material. Indeed there were increases in the mud content of some gravel bed samples where algal growth was observed. The decrease in mud contents in the muddy bank samples further suggests the transport of finer material downstream.

It was also noted during the September field survey that the sand bars at the end of the sandy ripple zones, just upstream of the pools at sites 6 and 9, had migrated downstream. The decrease in mud content and increase in sand content in pool 9 is likely due to the deposition of sand from the upstream sand ripple during the dry season.

The sediment profile at site 9 suggests the pool was previously scoured and the mud found in the upper 2 cm has been deposited since the end of the wet season. The decline in mud content in the upper centimetres of the core from site 6 suggests that deposition of fine sediment has slowed following a peak at the start of the dry season. This is also supported by the sedimentation rates in the two sediment traps which shows a decline in fine sediment deposition.

The decrease in sedimentation rate and increase in mud content of suspended sediments is to be expected. The majority of sediment would settle out at the start of the dry season and the suspended sediment settling out at the end of the dry season (September) is likely to be very fine material or material that has been resuspended and reworked and is finding its way to the pools.

3.3.4. Fine Sediment Composition

C and N concentrations, stable isotopes and C:N ratios

The CaCO₃ content of the fine sediments increased during the dry season from an average of 0.5 to 1.7% (Table 16). The greatest increase and the highest values were measured in the gravel beds.

There was also a slight increase in the total organic carbon (TOC) concentration in the fine sediments in all habitats (Table 16). The largest increase occurred in the gravel beds. During the September survey, the majority of the gravel bed samples were noted to contain obvious algal growth. These samples all had higher mud contents.

There was an increase in the total nitrogen (TN) concentration in the fine sediments in the gravel beds and pools (Table 16) but the variation between sites was large.

The TOC and TN data for the September samples is questionable as there were technical problems during sample analysis.

Due to technical problems, only isotope data from the July survey is reported here. The δ¹³C values ranged between -27.9 and -23.9 ‰ and the δ¹⁵N values ranged from -1.68 to 1.83 ‰ with both positive and negative values recorded in each habitat type. The C/N ratio of the sediments ranges from 14.1 to 21.2. These values are typical for terrigenous organic matter in freshwater aquatic systems, where the range of stable carbon isotopic ratios vary from -30‰ to -26‰ in runoff from terrigenous organic

carbon (C3 plants), the $\delta^{15}\text{N}$ signature is low and the C/N ratio is more than 12. There were no consistent trends found between the habitat types.

Table 16: C and N concentrations in the surface sediment samples

Site	Survey	n	CaCO ₃ %		%N		%TOC	
			Mean	Range	Mean	Range	Mean	Range
Gravel Beds	July	3	0.46	0.17 - 0.78	0.053	0.043 - 0.068	0.69	0.55 - 0.89
	Sept	7	1.82	0.52 - 2.78	0.086	0.048 - 0.116	1.15	0.65 - 1.43
Pools	July	10	0.49	0.26 - 0.69	0.049	0.036 - 0.060	0.70	0.62 - 0.83
	Sept	9	1.25	0.26 - 4.25	0.066	0.031 - 0.127	1.00	0.63 - 1.49
Sandy Ripples	July	2	0.52	0.35 - 0.69	0.053	0.048 - 0.058	0.64	0.59 - 0.70
	Sept	0	-	-	-	-	-	-
Muddy Banks	July	2	0.65	0.52 - 0.78	0.059	0.052 - 0.066	0.73	0.66 - 0.79
	Sept	2	1.22	1.78 - 1.65	0.051	0.038 - 0.063	0.77	0.66 - 0.87

There was little difference in the chemical composition of the fine sediments collected in the sediment traps (Table 17). The CaCO₃ content was higher than what was measured in the surface sediments and was higher at the end of the dry season, increased from 3.0 to 5.3%. The TOC and TN concentrations were also higher than in the surface sediments with TOC concentrations of 1.43 and 1.28% and TN concentrations of 0.109 and 0.097%. The concentrations were slightly lower at the end of the dry season.

Table 17: Chemical composition of fine sediments collected in the sediment traps

Sediment Trap #	CaCO ₃ %	TN%	TOC%	C:N
1	3.0	0.109	1.43	13.4
2	5.3	0.097	1.28	13.2

XRF

The fine surface sediments were composed predominantly of silica (SiO₂ ~ 70%) and were also rich in aluminium (Al₂O₃ ~ 10%) and iron (Fe₂O₃ ~ 6%) and potassium (K₂O ~ 2%) suggesting the sediments are comprised mostly of quartz and aluminosilicate clay minerals.

There were few discernible differences in elemental composition between the different habitat types. Overall fine sediments in the sandy ripple zones had the highest Si and Ti concentrations and lowest Al and K concentrations indicating a stronger quartz influence. The highest Al and K concentrations were found in the pool samples, an indication that this material is finer. This is supported by the grainsize analysis which showed higher mud contents and a greater proportion of finer (clay + silt) material. The highest Fe and Mn contents were found in the gravel bed samples.

Additionally, there were few discernible differences in elemental composition between the two field surveys. Most notable was the Ca concentration which increased from an average of 4306 (\pm 653) to 10047 (\pm 5539) mg/kg. The average S concentration also increased from 218 (\pm 61) to 374 (\pm 229) mg/kg. Both of these indicate the contribution to river flow from groundwater during the dry season. The average Si concentration decreased from 330,988 to 318,331 mg/kg but there was large variation.

Total P concentrations in the surface sediments ranged from 257 to 423 mg/kg during the July survey, and from 262 to 541 mg/kg in the September indicating an overall increase in total P during the dry season at some sites. Five sites showed an increase in P concentration from 8 to 30%, while 2 showed a decrease (of 13-15%), 2 sites showed no change, and 4 sites had no data. The increase in P was mostly in the pool samples which increased from an average of 303.5 to 345.7 mg/kg (Table 18). Overall, the highest P concentrations were measured in the gravel bed samples. However, there was significant variability in P concentrations within each habitat as indicated by the large error bars (Figure 26).

Table 18: P concentrations in the surface sediment samples

Site	Survey	n	P mg/kg	
			Mean	Range
Gravel Beds	July	8	354.0	261.8 - 423.3
	Sept	8	363.3	283.7 - 541.2
Pools	July	11	303.5	257.5 - 340.4
	Sept	9	345.7	261.8 - 501.9
Sandy Ripples	July	3	304.0	292.4 - 318.6
	Sept	0	-	
Muddy Banks	July	2	274.9	266.2 - 283.7
	Sept	2	270.6	261.8 - 279.3

P-fractions

Total P content obtained from the fractionation experiments were typically 15% lower than values obtained from XRF (Figure 26). However, the same trends between habitat types and surveys were observed. It is likely there were small losses of sample between each extraction step resulting in the lower overall total P.

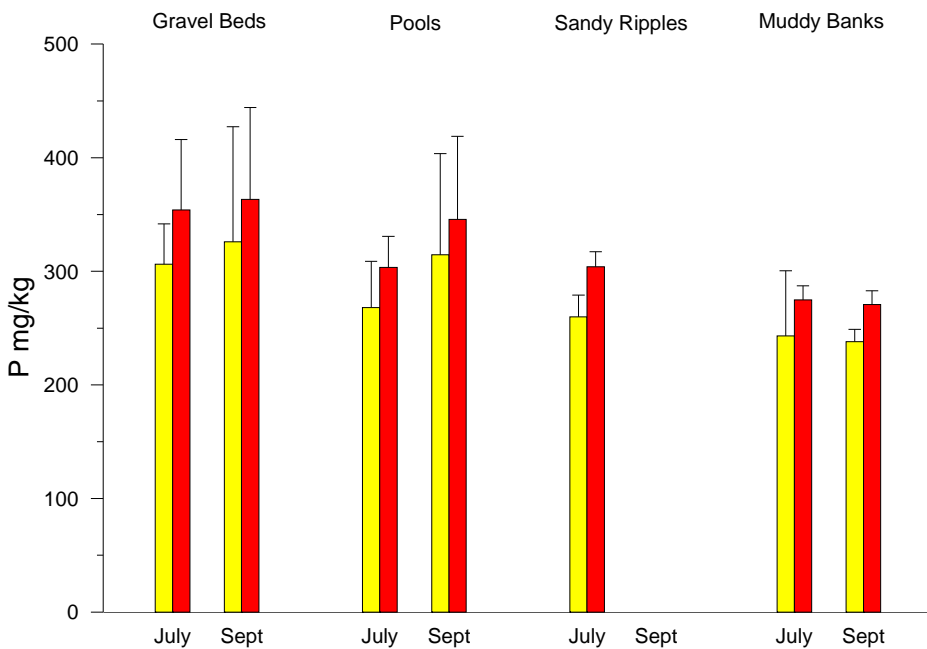


Figure 26: Comparison of total P concentration in the different habitat types determined by the sum of P-fractions (yellow bars) and XRF (red bars)

The average organic P concentration ranged from 156 to 207 mg/kg (Figure 27) but there was a large amount of error in each habitat type. Organic P was the predominant form, contributing 53 to 68% of the total P (Figure 28). Detrital P, including detrital apatite and other inorganic P, contributed 21 to 25% of total P while oxide-associated P contributed 10 to 23%. Authigenic P, including authigenic apatite, biogenic apatite and CaCO₃-bound P was not detectable in any samples during the July survey as well as most samples in the September survey. There was an increase in oxide-associated P between the July and September surveys, particularly in the gravel beds which increased from 12 to 23%.

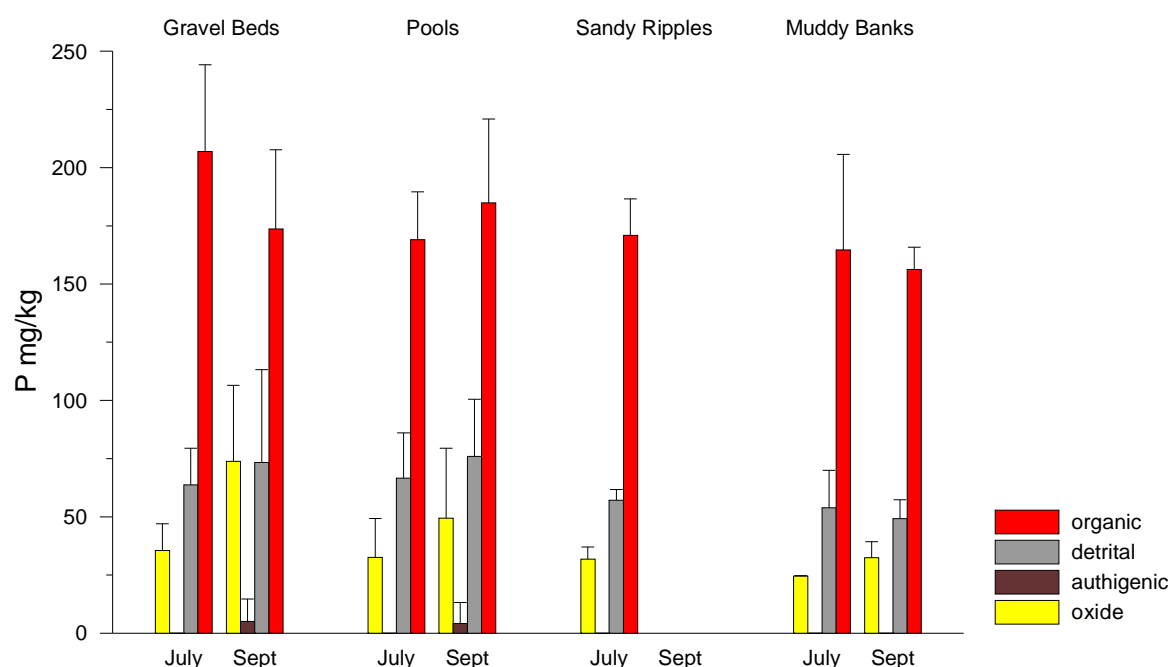


Figure 27: P concentration in the four fractions for the different habitat types and field surveys

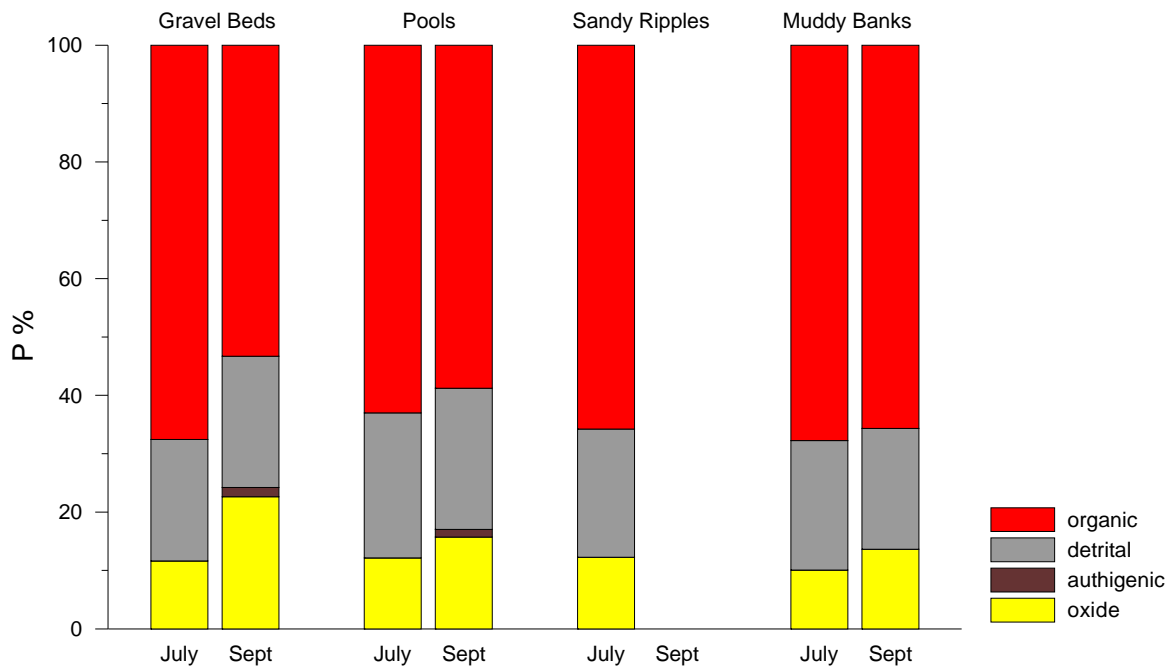


Figure 28: Proportion of P in each fraction for the different habitat types and field surveys

3.3.5. Porewater Nutrient Profiles

The porewater nutrient profiles for the two pools (sites 6 and 9) are shown in Figure 29 and Figure 30. In both pools, there was an increase in NH₄-N concentration in the porewaters at the end of the dry season (September). However, NO_x-N and PO₄-P concentrations were slightly lower at this time.

Site 6 - Downstream Pool

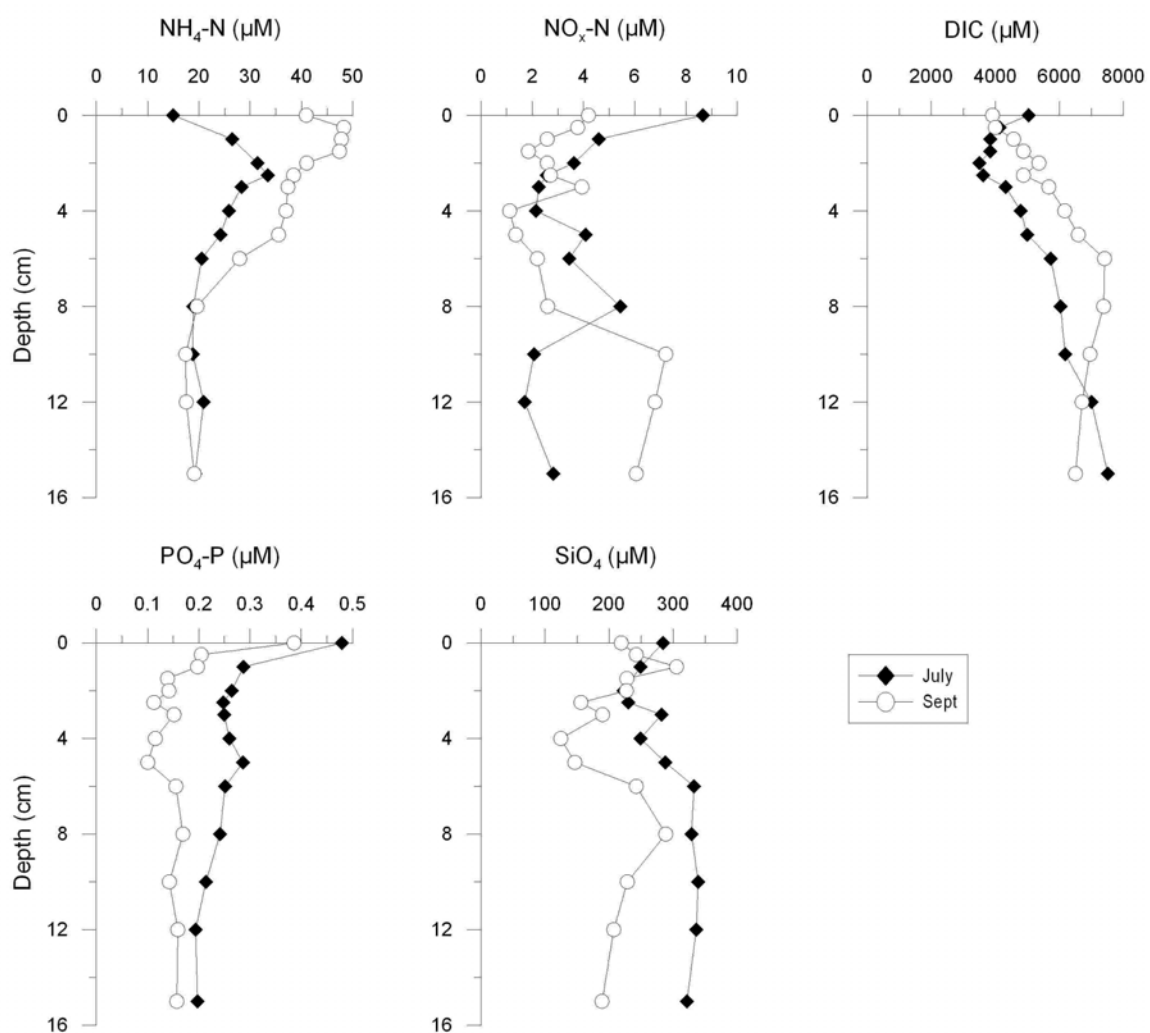


Figure 29: Porewater nutrient profiles at Site 6

Site 9 - Upstream Pool

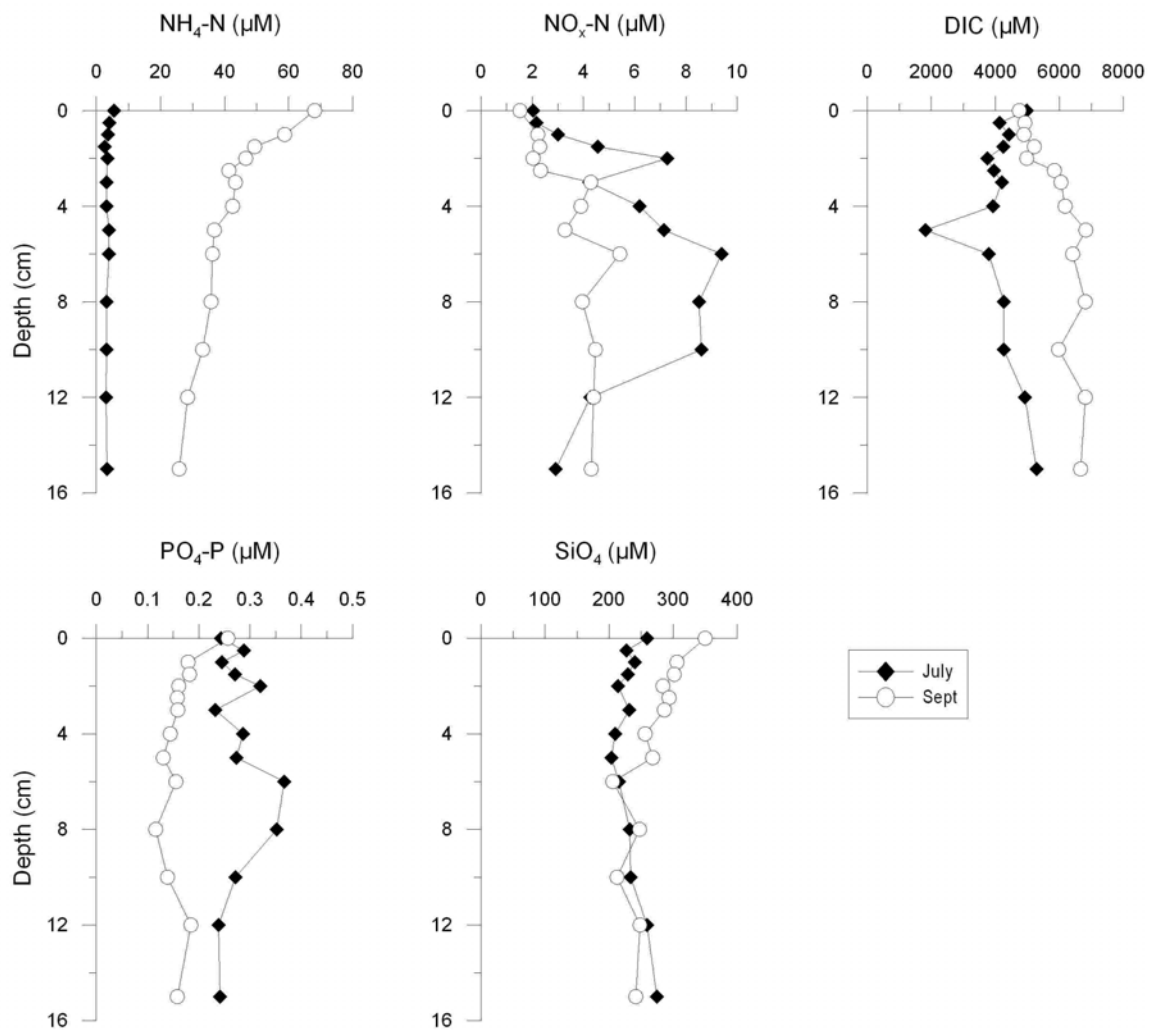


Figure 30: Porewater nutrient profiles at Site 9

There are small differences in the porewater profiles at the crest and in the valley of a sand ripple (Figure 31). However, given the difficulties in sampling and extracting the porewaters, it is difficult to draw any significant information from these profiles.

Site 14 - Sand Riffles - Upstream

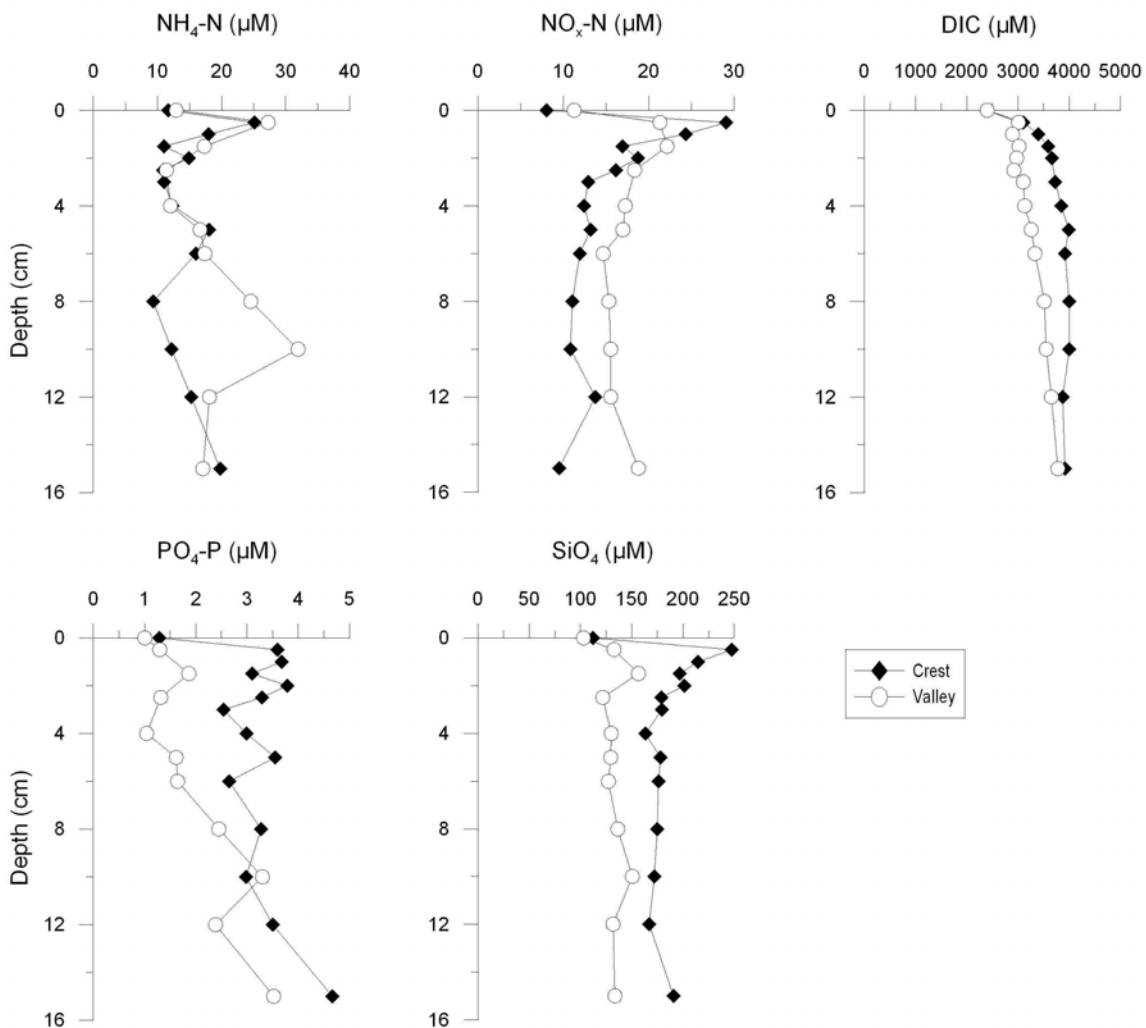


Figure 31: Porewater nutrient profiles at Site 14

3.3.6. Do fine sediments support algal growth?

Small increases in TOC, TN and TP over the dry season suggest the accumulation of nutrients in the fine sediments. It was initially hypothesised that fine sediments acted as a source of nutrients supporting algal growth. However, this does not appear to be the case in the Daly River. Results from reported in Chapter 4 suggest that rapidly growing algae (i.e. *Spirogyra*) utilise the abundant nutrients available at the end of the wet season. The nutrient concentrations in the water column rapidly decline and subsequent algal and macrophyte growth is supported by internal recycling of nutrients within the water column as algal material decomposes.

The decay of algal material on the sediment surface may be contributing some nutrients back into the sediments. The observed increase in TOC concentrations and the flux of PO₄-P from the overlying water into the sediments is likely due to the breakdown of organic matter at the sediment surface. Phosphorus is rapidly adsorbed onto iron-oxides and as organic matter decomposes in the surface sediments, it is likely the available phosphorus is bound by iron oxide as suggested by the

accumulation of oxide-associated P in the surface sediments throughout the dry season.

3.3.7. Biomarker analyses

Samples collected along the transect were categorised according to habitat type (i.e. gravel bed, sand ripple, pool or bank mud) and their biomarker profiles examined in an attempt to evaluate an average organic matter composition for each of the sediment types. Results of these assessments are shown in Figure 32 to Figure 36.

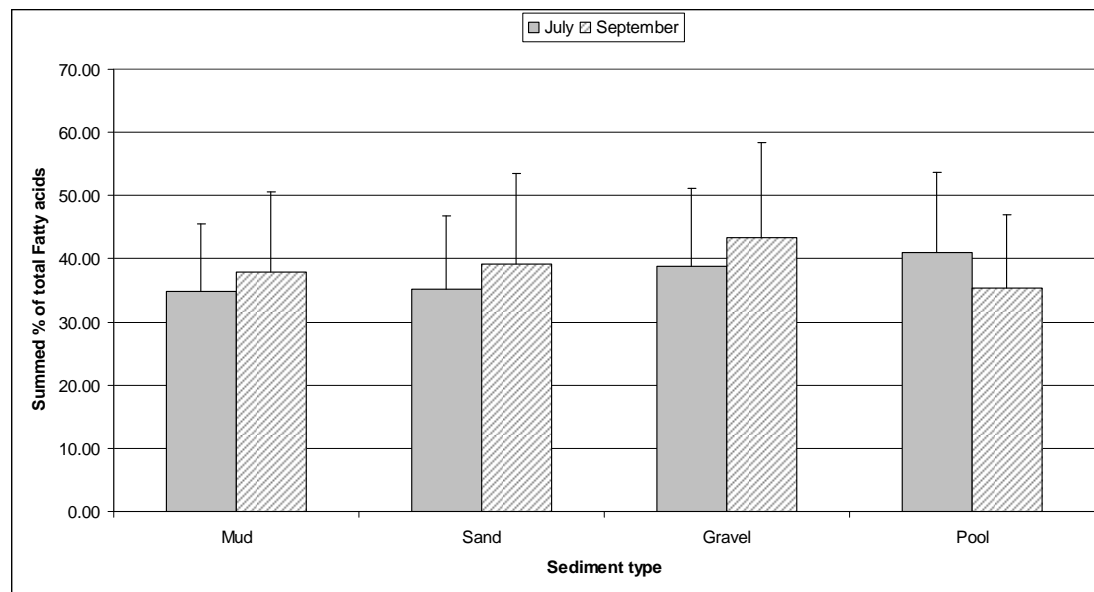


Figure 32 Selected algal fatty acids as a percentage of total fatty acids for samples collected in July and September

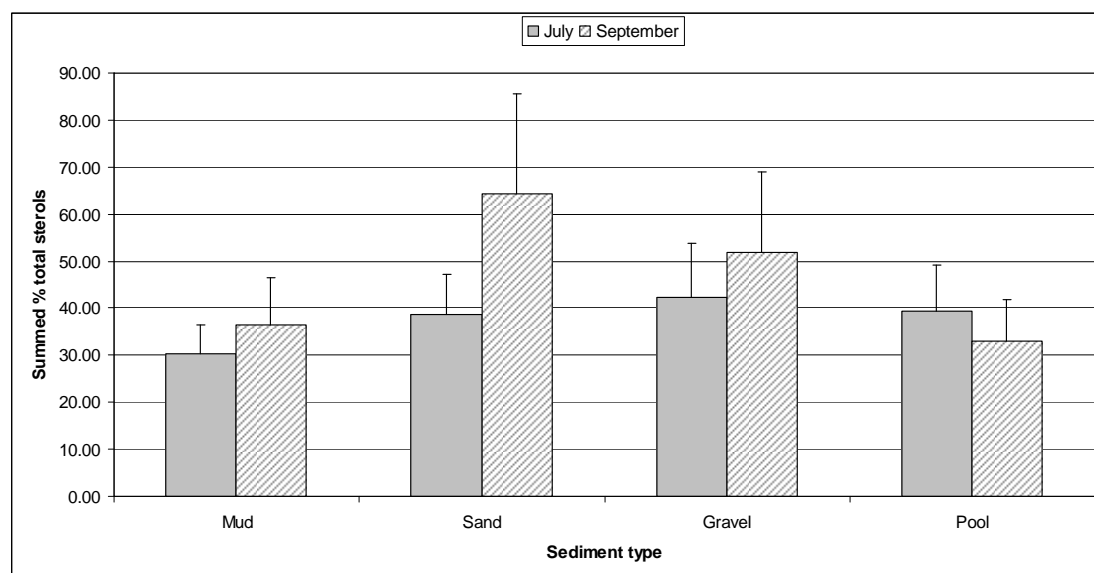


Figure 33 Selected algal sterols as a percentage of total sterols for samples collected in July and September.

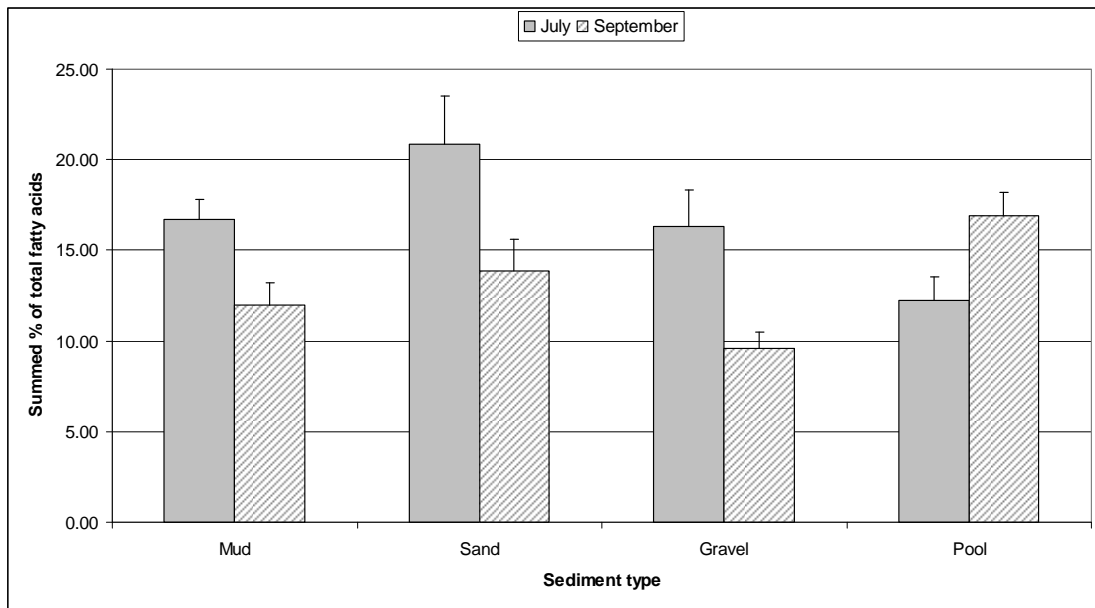


Figure 34 Selected bacterial fatty acids as a percentage of total fatty acids for samples collected in July and September.

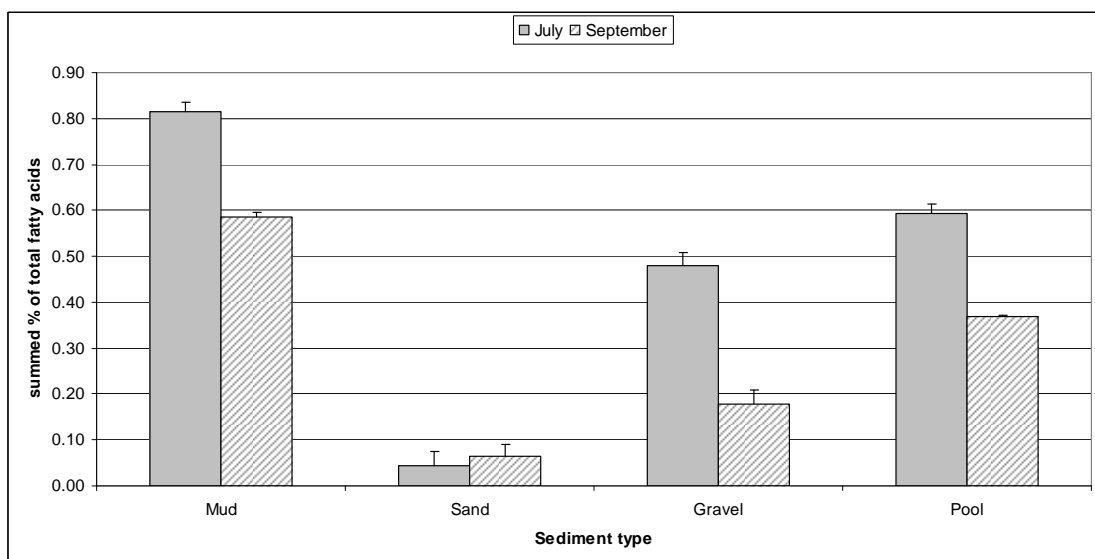


Figure 35 Selected terrestrial fatty acids as a percentage of total fatty acids for samples collected in July and September.

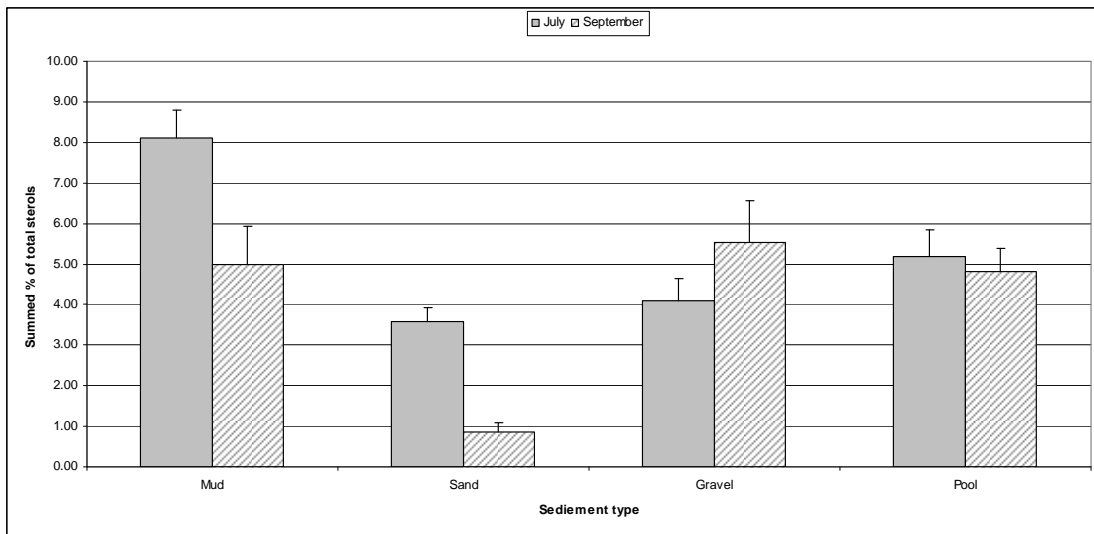


Figure 36 Selected terrestrial sterols as a percentage of total sterols for samples collected in July and September.

While it is theoretically possible to apportion some quantitative inputs using biomarker techniques this is really only feasible with a very comprehensive dataset. For example it would be necessary to know the carbon:marker value for all potential source materials, something which is clearly not possible in this case. Hence, in this study we have used a calculation of relative contribution by calculating the percent contribution of each marker to the total for that compound class. Several of these have then been summed to give an indication of contribution from that source. Clearly this is really only valid when comparing samples from two surveys or the relative contribution of that source material to each sediment type. It is also important to remember that fatty acid and sterol markers are very different in their chemical structure and will therefore exhibit different degrees of resistance to degradation. Each of these compound classes will be present in the different source materials at different concentrations, hence it is not valid to quantitatively apportion the contribution of each source relative to the other sources within a given sediment type.

Although only a relatively short period of time separated the two surveys, there were some significant changes in the organic matter composition in the different sediment types.

Gravel Beds

Samples from gravel beds are characterised by a relatively constant contribution from algal material between the two surveys (Figure 32 and Figure 33) but an overall decline in the contribution from bacteria (Figure 34) and terrestrial material as determined from fatty acid content (Figure 35). Terrestrially derived sterols appear to increase in contribution (Figure 36) but this may be a reflection of the relative stability of these compounds compared with fatty acids along with the decrease of other sterol inputs, increasing the relative contribution of these particular compounds.

Gravel beds make up the majority of the sediment in the reach studied and to this end the changes observed tend to mirror those seen in the other sediment types. Between July and September there appears to be a decrease in some material of terrestrial

origin. Terrestrially derived fatty acids decrease in their relative contribution to the overall fatty acid content. However, terrestrially derived sterols exhibited an increase. This may reflect removal of a particular type of terrestrial material or a different source for these compounds. In this instance, the particular fatty acids used as a terrestrial marker have a source within some of the macroalgae which grow within the Daly system. We have identified their presence in samples of *Chara*, *Vallisneria* and *Spyrogyra* but more work would be required to investigate the effects of degradation before more definite conclusions could be drawn. Thus, this decrease in fatty acid markers may reflect removal of dead/decayed remnants of these macroalgae, which would also be consistent with the observed decrease in bacterial markers, assuming these decaying remnants were the bacterial substrate. The sterol terrestrial markers are much more specific for terrestrially derived material and the fact that these increase between July and September may reflect the decrease in flow and settling out of more material. Algal markers increased slightly between the two surveys but both the fatty acid and sterol markers suggest this is a major contributor to the organic matter pool during both surveys. Given the sampling techniques and analyses, algal in this context refers to predominantly microalgae growing on the surface of the gravel. These zones are characterised by shallow water which maximises light availability while the gravel provides a stable structure for growth. Given the aerial extent of these zones this is likely an important area for production within the Daly River.

Sand ripples

The next most abundant sediment type is the sand ripples. Terrestrial markers appear to remain either relatively constant at low abundance (Figure 35) or show a marked decline (Figure 36). Bacterial derived markers show a decrease between the two surveys from over 20% of total fatty acids to 14% (Figure 30) while the algal fatty acids remain relatively constant and the algal sterols exhibit a marked increase from just under 40% to 65% of total sterols (Figure 33).

Sand ripples are characterised by a relatively low level of contribution from terrestrial material, which decreases between the two surveys, a relatively high bacterial content, which also declines, and an increase in algal material. The relatively high bacterial contribution suggests that the sand ripples are zones where more material is being remineralised compared with the other sediment types, particularly in July. The increase in algal sterol markers in September may well reflect an increase in benthic microalgae, possibly diatoms and this would be consistent with decreasing flows which in turn lead to increased water clarity and decreased movement of the sands, providing a more stable substrate for growth. It is worth pointing out that the increase in algal sterols is significantly greater than the decrease in terrestrial and bacterial markers, indicating that this is a real increase in algal material.

Pools

In samples from the pools, the relative contribution of most signature markers appears to remain relatively constant or exhibit a decline between the two surveys. The exception to this is the bacterial contribution which exhibits a significant increase from an average of 12% to 17% of total fatty acids (Figure 34).

The pools within the study reach appear to exhibit fewer relative changes between surveys than the other sediment types. Algal content remains relatively constant, with just a small decrease in September, reflecting the overall water clarity of the river (Pools are 3m deep). Bacterial contribution to these sediments increases and this probably reflects degradation of material which has accumulated in these zones. Interestingly the fatty acid terrestrial markers decrease over the study, while the sterol markers remain fairly constant. Again, as with the gravel beds, this probably reflects removal of more labile material which may not strictly be terrestrial in origin but more likely macroalgal remnants.

Bank muds

Mud, in the context of this study, refers to areas where exposed banks have slumped into the river.

Algal contribution appears to be relatively similar to the other sediment types, especially in July (Figure 30 and Figure 33) and remains relatively constant, whereas the contribution from bacterial and terrestrial material appears to decline. Terrestrial markers in particular exhibit a marked decrease in their overall contribution (Figure 35 and Figure 36).

Terrestrial and bacterial contributions appear to decrease between the two surveys and this may well reflect just physical “washing” of the sediment removing the terrestrial residues and therefore decreasing bacterial substrate. The algal content of these sediments appears to remain relatively constant, suggesting that these muds provide at least some substrate for benthic microalgae.

3.4. Conclusions

The Daly River contains three dominant habitat types: deep pools, gravel beds and sandy ripples. Sediment composition in each of these habitat types is highly heterogeneous. Throughout the dry season there appears to be continual transport of the bed sediments, with accumulation of fine sediments (<63µm) in pools and gravel beds.

The sediments contain organic matter compositions typical of terrigenous origin in freshwater aquatic systems. There is evidence of the increased contribution from groundwater to the river during the dry season with a marked increase in calcium concentration.

In general, it appears that within the reach studied:

- Benthic microalgae, as part of the periphyton, growing on gravel substrate make a significant contribution to production within the Daly river
- Sand ripples are potentially important zones for re-mineralisation
- There appears to be longer term accumulation and degradation of terrestrial material in the pools
- Areas of collapsed mud bank are able to support growth of benthic microalgae.

In terms of changes between July (the early dry-season field campaign) and September (late dry-season), the results suggest:

- Macroalgal detritus is removed from gravel beds and sand ripples
- Benthic microalgae within sand ripples increased significantly
- There was an increase in fine terrestrial material deposited in gravel beds as flows decreased
- Terrestrial detritus was removed from collapsed mud, possibly due to physical washing

Small increases in TOC, TN and TP suggest nutrients are accumulate in the fine sediments during the dry season and the sediments are not a net source of nutrients to the overlying water column or benthic algae. The majority of phosphorus is in organic form, however there is an increase in the oxide-associated fraction during the dry season, suggesting phosphorus released during organic matter decomposition is accumulating in the surface sediments.

4. Primary Producers: biomass, standing crop and nutrient limitation of aquatic plants and algae

4.1. Introduction

To develop an understanding of how altering nutrient and sediment inputs and river flows will affect ecosystem function, it is important to gain knowledge of the form and rate of primary production in the system. This knowledge will help develop an understanding of the interdependence of primary production and ecosystem health.

The objective of the work described in this chapter is to examine temporal patterns of primary producer biomass and standing crop in the middle reaches of the Daly River and insight into the factors that control biomass and primary production to inform modelling of the impacts of nutrient and sediment inputs on primary production.

4.2. Methods

4.2.1. Characteristics of study reach

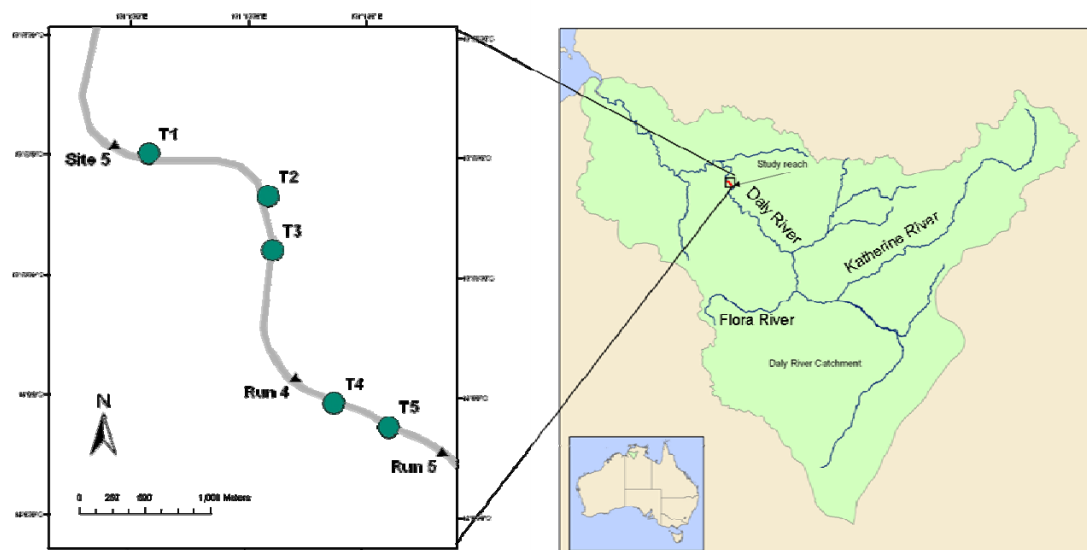


Figure 37. Map of the Daly River study reach and water quality sample sites.

Sampling was conducted in the same study reach used for sediment analyses (Chapter 3). The study reach is located in the middle reaches of the Daly River (Figure 37) and consists of two pool-riffle sequences (i.e. gravel run-pool-run-pool) totalling 3.3 km in length. The runs characteristically contain a gravel reach which is followed downstream by a sand bank of mobile sand that forms a wave pattern of ripples on the river bed. The sand banks are highly mobile and moved up to 60 m downstream during the study period. The transition from run to pool was readily identified by a sudden increase in depth where a sand bank drops off into deeper water. The transition from a pool to a run, however, was not as readily defined, and was selected based a decrease to about 1 m in depth and an increase in velocity.

Areas of the two sand banks were estimated using records of substrates at biomass survey points to calculate the length of the sand banks. To calculate the average width of each section, width measurements were taken at 10 randomly located points using high resolution satellite imagery (Google Earth).

Total flow volumes for the four sections were modelled from bathymetric data of the area (collected in 2001) and measured flows at gauge stations upstream and downstream of the study reach, at Claravale and Beeboom crossing respectively.

4.2.2. Water Quality

Water quality measurements were taken at five sites, one at the upstream end of the reach (Site T5), and one at the downstream end of each pool or run (T1-T4), in July, September and November (Figure 37). At each site, temperature, pH, conductivity and dissolved oxygen concentrations were measured with a Hydrolab multi-parameter probe. Turbidity was measured with a portable Hach turbidity meter and light penetration was assessed using a Licor light meter with a submersible scalar bulb. Water samples were taken and analysed for total nitrogen, total phosphorus, nitrite, nitrate, ammonia, filterable reactive phosphorus and chlorophyll *a*. All samples were stored on ice and frozen upon return to the laboratory until just prior to analysis.

Additional water quality measurements and samples were taken in May and June at Sites T1-T3 and two additional sites, one within Run 4 and one just upstream of Pool 4 (“Run 5”) (see Figure 37).

Where concentrations were below the detection limit (Table 19) half the detection limit was used in calculations of means and other representations of values.

Water level changes were measured at a site just downstream of the study reach (Site 5) on four occasions between June and November.

Table 19. Detection limits for water quality analyses

Detection limit	
TN	5 µg/L
TP	5 µg/L
NO3	1 µg/L
NO2	1 µg/L
NH3	1 µg/L
FRP	1 µg/L
Chl-a	0.5 µg/L

4.2.3. Biomass survey

For each of the two pools and runs, the biomass and standing crop of benthic microalgae, phytoplankton, suspended macroalgae, benthic macroalgae and macrophytes was determined three times during the dry season, in July, September and November 2008, to quantify seasonal changes. Prior to this, a different run, located approximately 3 km downstream, was sampled in June 2008 and the results of that study are presented here as a general reference only.

Along the river bed, sample sites were chosen at random on each occasion, 10 in pools and 20 in runs. At each point, depth, substrate and mean velocity were recorded

and biomass samples collected or observations were made for benthic microalgae, macroalgae and macrophytes as described below.

River banks were sampled separately. An additional 10 or 20 points respectively were sampled along the river banks. At these points, the substrate and observations of macroalgae and macrophyte cover were recorded.

Periphyton

Where the water depth allowed safe sample collection, sand and gravel substrates were sampled by pressing a petri dish or plastic sample jar into the substrate. A spatula was then slid under the dish, the sample lifted out from the river bed, allowing pore water to drain, and sealed with a lid and electrical tape. Sample diameters ranged from 48-68 mm.

In deeper areas a sediment corer (\varnothing 63 mm) was used to obtain undisturbed samples of the substrate. The core was removed from the sampler and the top 1 cm of the core was sliced off with a knife and collected for analysis. This technique was mainly suitable for finer sediments.

Where rock substrates were encountered in shallow areas, a rock was lifted out of the water and a 5 cm x 5 cm area was scraped with a chisel and the scrapings collected for analysis.

All samples were placed immediately on ice, and then frozen within 5 hours of collection. To extract chlorophyll *a*, the entire sample was ground in 90% acetone, and centrifuged to remove particulates. The chlorophyll *a* content of the extract was subsequently determined either by fluorometry (APHA 1998 standard method 10200-H3) for low levels of chlorophyll or spectrophotometry (10200-H2) for higher levels of chlorophyll *a*.

Some substrates in deep areas, mainly rock, coarse gravel and some coarse sand, could not be sampled due to the unsuitability of the coring equipment for such substrates and the presence of crocodiles in the river. This reduced the number of samples by up to 25%. Table 20 shows the numbers of samples that were missed for these reasons.

Table 20. Number of missing periphyton samples due to sampling difficulties

	Total sites	Missing samples		
		July	Sep	Nov
Pool 3	10	1	3 rock	3
Run 3	20	7 gravel	2 sand	2 rock
Pool 4	10	3 rock	3 (2 rock, 1 sand)	6 (3 rock)
Run 4	20	4	4 (2rock/2coarse sand)	4 coarse sand

Macroalgae

Surveys undertaken in 2005 in the study reach identified *Spirogyra sp.*, *Chara sp.* and *Nitella sp* as the most common macroalgal taxa in the reach (Schult, Townsend *et al.* 2007). For the purposes of this study, the biomass of *Chara* and *Nitella* (both

Characeae) was determined together. At each sampling point, a visual assessment of macroalgal cover was made for *Spirogyra* and *Characeae* respectively in a 1 m x 1 m quadrat.

Where the water clarity and depth did not allow visual assessments from the boat, a camera was lowered into the water and video images of the river bed were recorded. Cover scores were determined from these images.

Cover scores for *Spirogyra* were converted to biomass using the relationship established by Townsend and Padovan (2005) for a 17 km reach of the Daly River that overlapped with the current study reach (Table 21).

At a number of quadrats, *Characeae* were sampled destructively after recording a cover score and stored on ice. On return to the laboratory, samples were cleaned, blotted dry, and weighed and a sub-sample analysed for chlorophyll *a*. A linear regression was established to convert cover scores to biomass ($y=0.59 (\pm 0.1)x+0.43 (\pm 5.2)$, $r^2=0.47$, $p<0.001$, $n=37$). This regression was used to convert cover scores to chlorophyll *a* where direct measurements were not available.

Table 21. Conversion table for *Spirogyra* cover to biomass (from Townsend and Padovan 2005)

Cover (%)	Mean Chl-a (mg/m ²)	SE
0	0	0
1-10	14.7	6
11-30	18.8	2.4
31-60	28.2	4
61-80	42.7	8
>80	72.7	28

Macrophytes

The main macrophyte present in the Daly River is *Vallisneria nana*. Where *Vallisneria* was present in the sample quadrat, a cover score was recorded and the plants sampled destructively to determine biomass. Where destructive sampling was not possible because the water was too deep, cover scores were converted to biomass using a regression established from the other samples ($y=6.2e^{0.036x}$, $R^2=0.79$, $p<0.001$, $n=46$).

Two small stands of the macrophyte *Schoenoplectus sp.* occupying less than 0.001% of the total reach, were also present within Run 3. The area and biomass of this stand was also determined to provide data on the second ranked, albeit much less common, macrophyte.

Suspended Algae

Suspended algae in the river comprise of microalgae and infrequently occurring clumps of *Spirogyra* sloughed off from the riverbed and readily visible to the naked eye. Samples of both types of suspended algae were collected at a total of five sites, one at the upstream end of the reach and one at the downstream end of each run and pool (Site T1-T5, Figure 37).

For microalgae, one litre water samples were collected and analysed for chlorophyll *a*. For macroalgae, a framed net (0.5 mm mesh) was held into the stream flow for 30 to 60 seconds depending on current velocity; and any algae caught in the net were collected and stored on ice. Samples were analysed for chlorophyll *a*. The volume of samples was determined from the product of the cross-sectional area of the net, velocity and time, and approximated 5-12 m³.

4.2.4. Nutrient limitation

During the July and September field campaigns, additional work was conducted to determine the response of phytoplankton and benthic algae to nutrient additions. The objective of this work was to determine whether phytoplankton from the Daly River were nutrient-limited, and to what degree pelagic production is responsive to additional nitrogen or phosphorus.

A PHYTOPAM© phytoplankton analyser (Heinz Walz, Effeltich, Germany) was used to measure the photosynthetic yield response of benthic algae and phytoplankton to nutrient (nitrogen and phosphorus) additions. The instrument uses pulse-amplitude-modulation (PAM) fluorometry to measure the capacity of plant cells to respond to incident light.

Substrate cores or samples were collected from gravel, sand ripple and water samples, and adding ammonium, phosphate or a combination to excess, and incubating for 24 h. The photosynthetic yield response, in a saturating pulse of light, was compared with a control after 24 h.

4.2.5. Carbon fixation and photosynthesis-irradiance responses

During the July and September field campaigns, incubations were conducted to establish the response of phytoplankton and *Spirogyra* to variations in light. The primary productivity rates under a range of percentages of surface light were determined in order to develop a curve of primary productivity vs. irradiance, and hence to determine the depth-integrated primary productivity.

To measure primary productivity-irradiance responses of algae in the Daly River, ¹³C-uptake experiments were conducted. This involved measurements with *Spirogyra* (September 2008) and phytoplankton (July, September 2008). For the phytoplankton the light profile was measured *in situ* and a water sample was collected. The water was placed in triplicate water bottles at 6 light levels (100, 50, 25, 14, 5, 0% surface light) using shade bags around local apparent noon. ¹³C-bicarbonate was added to all bottles and incubations were conducted in flowing water at the field station with temperature logged throughout. After 2-3 h the incubations were concluded and water was filtered onto pre-combusted GF/F filters. Filters were then frozen for later analysis using a mass spectrometer.

4.3. Results and Discussion

4.3.1. Study reach characteristics and water quality

The pools of the study reach were 400 and 440 m long, with a mean width of 58 and 60 m (Table 22). Runs were approximately three times as long, Run 3 with 1070m and Run 4 with 1430 m. Runs were 51 and 53 m wide on average. Mean current velocities over the study period were 0.12 and 0.25 m/s in pools compared to 0.34 to 0.62 m/s in runs.

The main substrates encountered in pools were sand, silt and rock, while runs had a larger proportion of gravel and mobile sand substrates (Table 22). The total area of sand banks in Runs 3 and 4 was 31300 m² and 21,000 m² respectively.

Table 22. Mean depth, velocity and substrate types of sample points in pools and runs of the study reach in July, September and November 2008. Values exclude areas within 1m of the river bank.

	Pool 3			Pool 4			Run 3			Run 4		
	Jul	Sep	Nov	Jul	Sep	Nov	Jul	Sep	Nov	Jul	Sep	Nov
Length (m)		400			440			1070			1430	
Avg Width (m)		58			60			51			53	
Avg velocity (m/s)	0.25	0.19	0.12	0.21	0.12	0.17	0.62	0.53	0.51	0.48	0.37	0.34
SE	0.02	0.05	0.03	0.01	0.03	0.05	0.04	0.05	0.04	0.05	0.06	0.04
Avg Depth (cm)	224	191	190	247	178	139	95	75	80	119	95	84
SE	19	30	25	22	25	23	5	7	7	8	10	10
Max Depth	310	304	300	330	280	260	137	135	126	220	200	170
% rock and gravel	20				30			35			35	
% sand and silt	80				60			10			35	
% mobile sand	0				0			55			28	
% unknown	0				10			0			0	

Over the study period, the water level (measured at Site 5) dropped by 0.53 m between June and November 2008 (Figure 38).

Figure 39 summarises water quality measurements for eight sample sites in the study reach. The mean water temperature in the study reach rose from 25.5°C in May to 32.4°C in November. There was some variation in pH, with measurements ranging from 7.1 to 7.8. The waters of the study reach were well oxygenated throughout the study period with oxygen concentrations of 7.2 to 9.4 mg/L.

Turbidity decreased over the study period and ranged from 3.7-5.0 NTU in June to 2.0 to 3.0 NTU in November. The euphotic depth increased slightly from a mean of 8.5 m in July to 8.8 m in November, exceeding the river depth by at least a factor of two throughout the study period. Differences between sites were within the range of 2-3 m.

Electrical conductivity increased from 575 µS/cm in May to a mean of 636 µS/cm in November as the dry season progressed and the ground water influence increased. The high conductivity, water clarity and lower water levels indicate that baseflow conditions prevailed through to November. Continuous water level data recorded at Claravale hydrographic station, approximately 73 km upstream of the study reach, does not show any significant early wet season flushes until after the end of the study

period and local rainfall data from the Douglas-Daly area also indicate that local flushes were highly unlikely to have happened.

Nutrient concentrations from the eight sites are summarised in Figure 40. Concentrations of filterable reactive phosphorus ranged from 3 to 13 µg/L. Oxidised nitrogen (NO_x) concentrations ranged from 4-13 µg/L and appeared to increase over the dry season with a mean of 6 µg/L in July, 8 µg/L in September and 11 µg/L in November. However, variation between sites was high. There was some suggestion that sites downstream of pools (T2, T4) had lower NO_x concentrations than those downstream of runs but due to the small sample size this could not be tested.

Ammonia concentrations were below the detection limit of 1 µg/L for all November samples and reached a maximum of 2 µg/L in July at site T1. Ammonia and NO_x measurements are not available for May and June due to problems with the chemical analysis for those samples.

Total phosphorus concentrations ranged from 10 to 20 µg/L over the study period with little or no variation between sites at different sample times. Total nitrogen concentrations were variable between sites and months ranging from 26 -70 µg/L.

The total P and soluble P concentrations are higher than previous years, and also higher than the results of other nutrient analyses undertaken during the study period (2-4 ug/L soluble P). It is possible the results reported here are greater than actual values.

Chlorophyll *a* concentrations were between 0.5 and 1.4 µg/L (Figure 40).

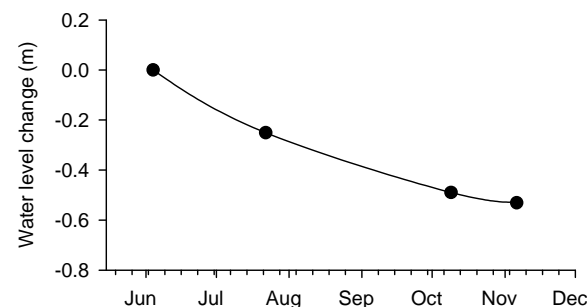


Figure 38. Water level changes at Site 5 between June and November 2008.

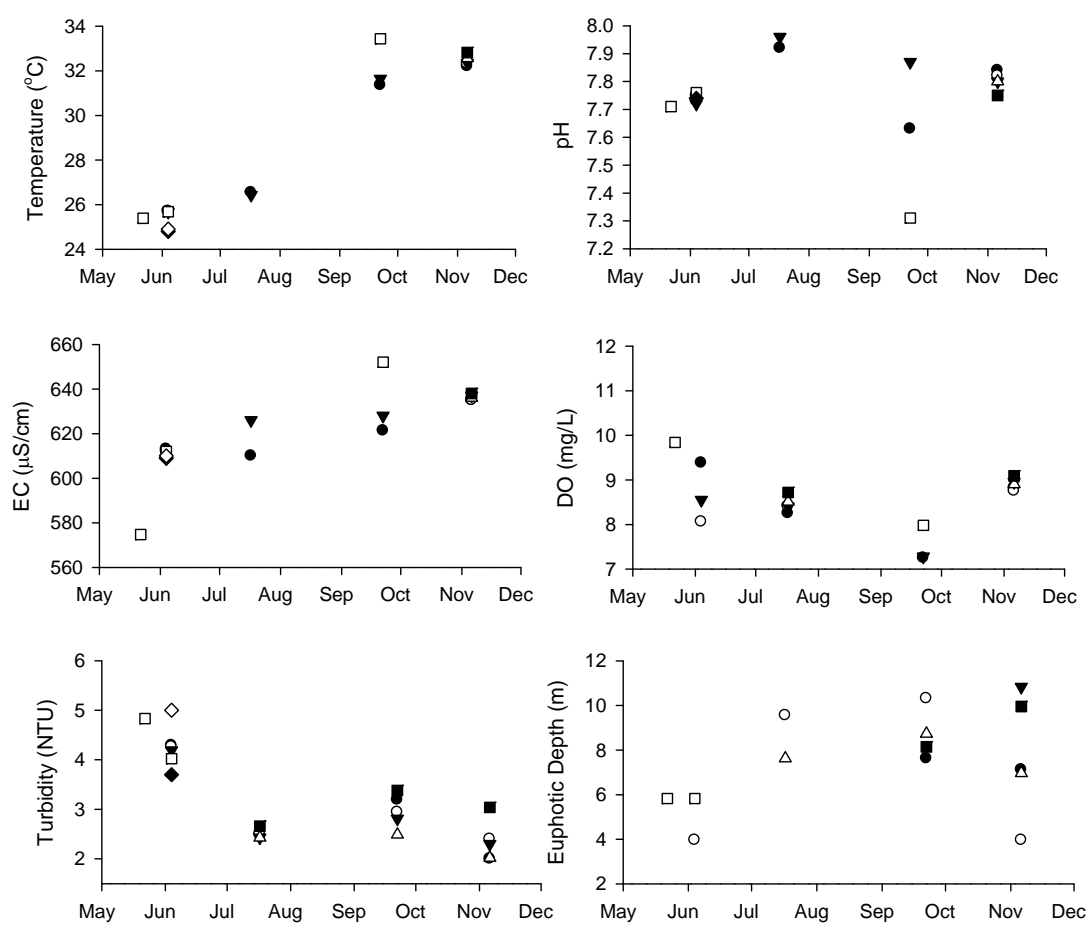


Figure 39. Summary of physico-chemical water quality measurements at eight sites in the study reach between June and November 2008. ● T1, ○ T2, ▼ T3, △ T4, ■ T5 □ Site 5, ♦ Run 4, ◇ Run 5

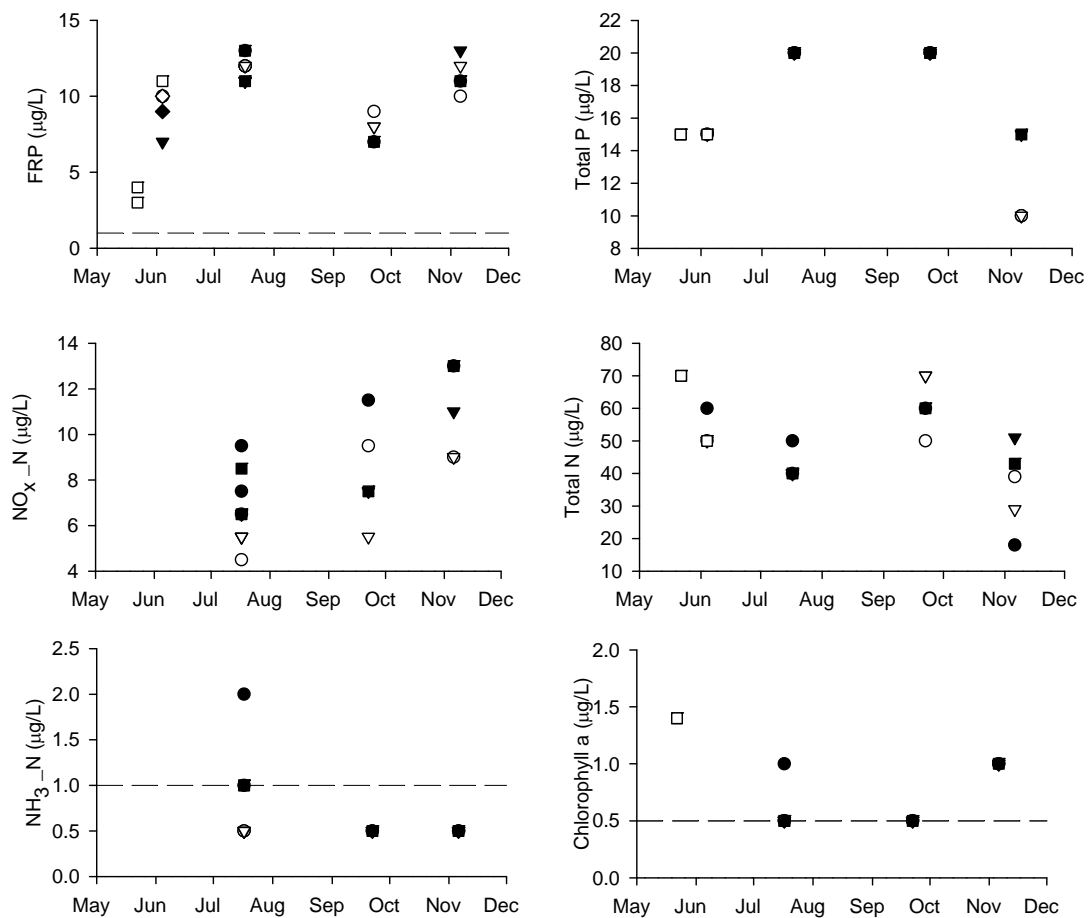


Figure 40. Summary of soluble and total nutrient measurements at eight sites in the study reach between May and September 2008. Dashed lines indicate detection limits. ● T1, ○ T2, ▼ T3, ▽ T4, ■ T5 □ Site 5, ◆ Run 4, ◇ Run 5.

4.3.2. Biomass of primary producers

The mean biomass of primary producers in pools of the study reach more than doubled over the dry season from 21 and 30 mg/m² in July to 59 and 57 mg/m² in November. In Run 3 average biomass was low (10-15 mg/m²) and changed little over the study period while Run 4 had a 5-fold increase from 8 mg/m² in July to 40 mg/m² in November (Table 23). A large proportion of Run 3 consisted of mobile sand substrate which had low periphyton chlorophyll a and was unsuitable as a substrate for macroalgae.

For the entire study reach, primary producer biomass more than doubled from 15 mg/m² in July to 37 mg/m² in November. In September, the total biomass was 24 mg/m².

Table 25 and Table 26 provide an overview of the biomass and standing crop of the different types of primary producers for each section of the reach.

Table 23. Average biomass of primary producers as chlorophyll *a* (mg/m²)

	Pool 3	Pool 4	Run 3	Run 4	Total reach
July	21	30	15	8	15
September	44	34	10	25	24
November	59	57	15	40	37

Table 24. Standing crop of primary producers as chlorophyll *a* (g)

	Pool 3	Pool 4	Run 3	Run 4	Total reach
July	480	800	790	630	2700
September	1020	890	530	1900	4350
November	1370	1500	840	3050	6760

Table 25. Summary of seasonal changes in primary producer biomass in the middle reaches of the Daly River. (ns= not sampled)

Month	Pool/Run	River bank/bed	Periphyton	Benthic chlorophyll <i>a</i> (mg/m²)					Suspended chl <i>a</i> (mg /m²)			
				<i>Spirogyra</i>	<i>Characeae</i>	<i>Vallisneria</i>	<i>Schoenoplectus</i>	Total benthic chl <i>a</i> (mg/m²)	Microalgae	Macroalgae	Total suspended chl <i>a</i> (mg/m²)	
June	Pools	River bank	ns	ns	ns	ns	ns	ns	ns	ns	ns	
		River bed	ns	ns	ns	ns	ns	ns	ns	ns	ns	
	Run 1	River bank	7	13	0	0	0	20	ns	ns	ns	
		River bed		6	0	0	0	13	ns	ns	ns	
July	Pool 3	River bank	5	2	2	0	0	9	1.1	0.06	1.21	
		River bed		2	11	0	0	18				
	Pool 4	River bank	7	0	10	0.2	0	17	0.8	0.04	0.89	
		River bed		6	15	0	0	28				
	Run 3	River bank	2	17	1	0	0.2	19	0.7	0.03	0.69	
		River bed		8	0.1	0	0	10				
	Run 4	River bank	3	5	0.2	0.5	0	9	0.9	0.05	1.00	
		River bed		4	0	0	0	7				
	September	Pool 3	River bank	8	0	14	1	0	23	1.0	0.05	1.03
		River bed		6	30	1	0	45				
		Pool 4	River bank	1	3	30	1	0	34	0.7	0.04	0.72
		River bed		9	23	1	0	34				
	Run 3	River bank	1	10	3	4	0.5	18	0.6	0.03	0.67	
		River bed		4	3	0	0	8				
	Run 4	River bank	6	8	7	4	0	25	0.7	0.04	0.76	
		River bed		5	8	6	0	24				
	November	Pool 3	River bank	7	6	21	9	0	43	1.9	0.16	2.02
		River bed		20	32	1	0	59				
		Pool 4	River bank	9	1	27	56	0	93	1.3	0.11	1.37

		River bed	9	22	16	0	56			
Run 3	River bank	9	11	10	22	0.5	53	1.2	0.10	1.28
	River bed	3	0	0	0	0	12			
Run 4	River bank	8	12	14	46	0	80	1.3	0.11	1.45
	River bed	10	5	13	0	0	37			

Table 26. Standing crop of primary producers in pools and runs of the study reach as chlorophyll *a* (g).

Month	Pool/Run	River bank/bed	<i>Periphyton</i>	<i>Spirogyra</i>	<i>Characeae</i>	<i>Vallisneria</i>	<i>Schoenoplectus</i>	total benthic (g)	Total benthic (g)	Phytoplankton (g)	Macroalgae (g)	Total suspended
July	Pool 3	River bank	4	2	2	0	0	8	446	27	1	29
		River bed	115	58	266	0	0	438				
	Pool 4	River bank	6	0	9	0	0	16	766	22	1	23
		River bed	185	166	399	0	0	750				
	Run 3	River bank	5	47	2	0	0	55	758	45	2	48
		River bed	131	569	3	0	0	704				
September	Run 4	River bank	9	15	1	1	0	26	557	69	4	73
		River bed	219	313	0	0	0	532				
	Pool 3	River bank	6	0	11	1	0	18	999	21	1	23
		River bed	181	125	656	19	0	981				
	Pool 4	River bank	1	3	26	1	0	30	868	17	1	18
		River bed	25	234	564	16	0	838				
November	Run 3	River bank	2	21	6	10	1	41	498	35	2	36
		River bed	54	239	164	0	0	457				
	Run 4	River bank	17	24	20	13	0	73	1851	53	3	56
		River bed	429	341	568	439	0	1777				
	Pool 3	River bank	5	4	17	7	0	33	1326	41	3	44
		River bed	142	442	691	18	0	1293				
	Pool 4	River bank	7	1	23	48	0	80	1465	31	3	34
		River bed	214	213	549	409	0	1385				
December	Run 3	River bank	20	25	23	49	1	117	767	64	5	70
		River bed	483	168	0	0	0	650				
	Run 4	River bank	23	34	40	135	0	231	2946	99	8	107
		River bed	584	761	380	990	0	2715				

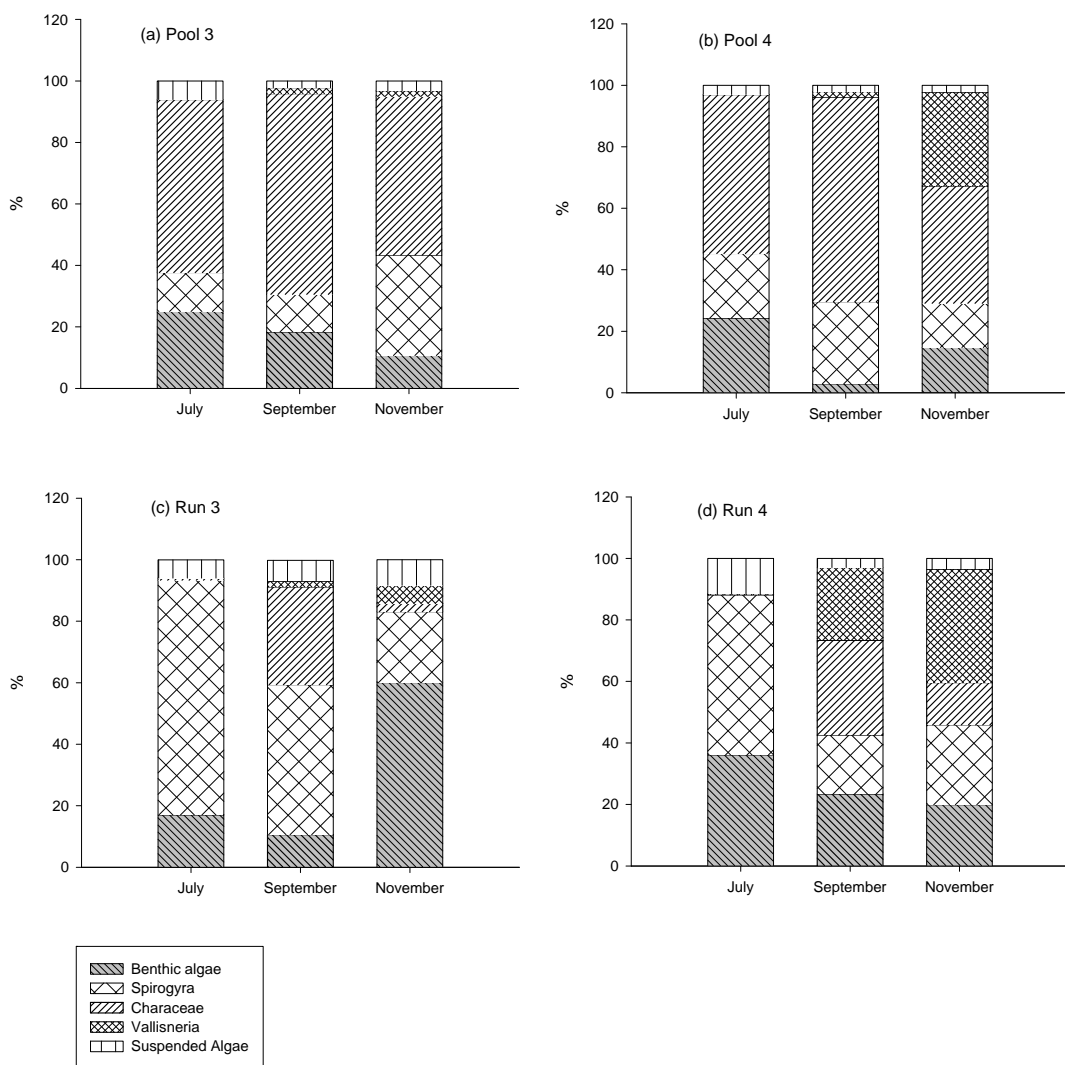


Figure 41. Contribution of different types of primary producers to total standing crop.

Periphyton

Variability in periphyton biomass was high within and between habitats throughout the study period. Mean periphyton biomass in Run 1 was $6.7 (\pm 2.4)$ mg chl $a\ m^{-2}$ in June. In Runs 3 and 4 periphyton biomass was similar in July (2.5 ± 0.9 mg chl $a\ m^{-2}$) and September (3.4 ± 0.9 mg chl $a\ m^{-2}$) and highest in November (8.4 ± 2.0 mg chl $a\ m^{-2}$). In pools, the change in periphyton biomass was less pronounced. Mean periphyton biomass was similar throughout the dry season (Figure 42).

Mean periphyton chlorophyll a was $23.8 (\pm 4.4)$ mg chl $a\ m^{-2}$ on rock substrates, approximately 10-fold the amount found on mobile sand ($2.3 (\pm 0.6)$ mg chl $a\ m^{-2}$) while sand, gravel and silt substrates had similar amounts with $6.7 (\pm 1.9) - 7.1 (\pm 1.8)$ mg chl $a\ m^{-2}$ (Table 27). This differed greatly from measurements made for gravel in 2005 where the mean biomass of periphyton on gravel was 32.8 mg chl $a\ m^{-2}$ in shallow areas (Schult, Townsend *et al.* 2007), but is similar to Webster *et al.* (2005) who reported 12 ± 2 mg chl $a\ m^{-2}$ for gravel substrate.

Periphyton contributed 3-25% to the total standing crop of primary producers in pools and 11-60% in runs (Figure 41).

Table 27. Mean periphyton chlorophyll *a*/m² for different substrates in the study reach

	Gravel	Rock	Mobile sand	Sand	Silt
mean	6.7	23.8	2.3	6.9	7.1
SE	1.85	4.42	0.64	1.37	1.78
n	22	22	37	33	11

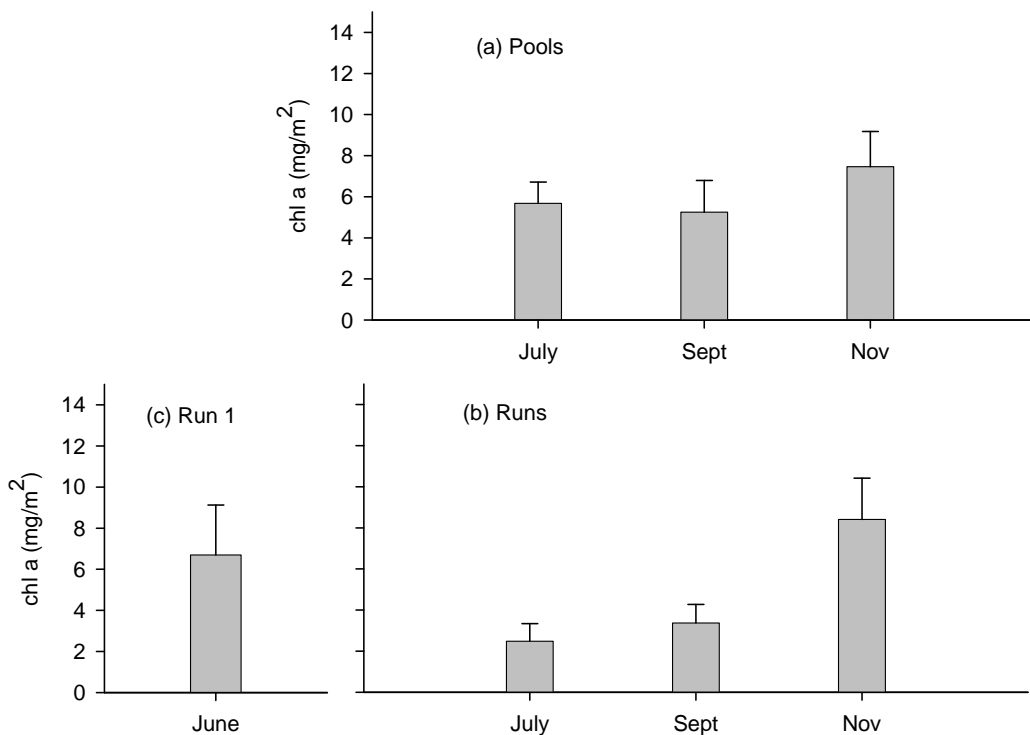


Figure 42. Periphyton biomass changes between June and November 2008 in pools (a) and runs (b, c). (Error bars indicate + 1 SE).

Macroalgae (Spirogyra sp.)

Spirogyra biomass in pools increased on the riverbed, though river bank biomass was similar throughout the dry season (Figure 43).

In runs *Spirogyra* biomass was higher on the river banks than the riverbed but there was no marked difference in biomass between the July, September and November sample dates. In June, the biomass was similar to the later part of the year.

Spirogyra contributed 13-33 % to the total standing crop in pools and 19-76 % in runs (Figure 41).

Macroalgae (Characeae)

Characeae were mainly present in the slow flowing waters of pools and along the banks of runs where flow was relatively slow. Only two observations of *Characeae*

were made at current velocities of more than 0.34 m s^{-1} . The biomass of *Characeae* almost doubled between July and September and then remained much the same. Biomass was highest at the bottom of pools where it reached $27 \text{ mg chl } a \text{ m}^{-2}$ in November (Figure 44). Runs had substantially lower biomass of *Characeae* with a maximum of $\text{mg chl } a \text{ m}^{-2}$ along the banks in November. During the survey of the downstream run (Run 1) in June, no *Characeae* were observed. Personal observations from 2008 and previous years indicate that this was likely to be the case in upstream runs as well. *Characeae* made up 31 -67 % of the total standing crop in pools but only 0-32 % in runs.

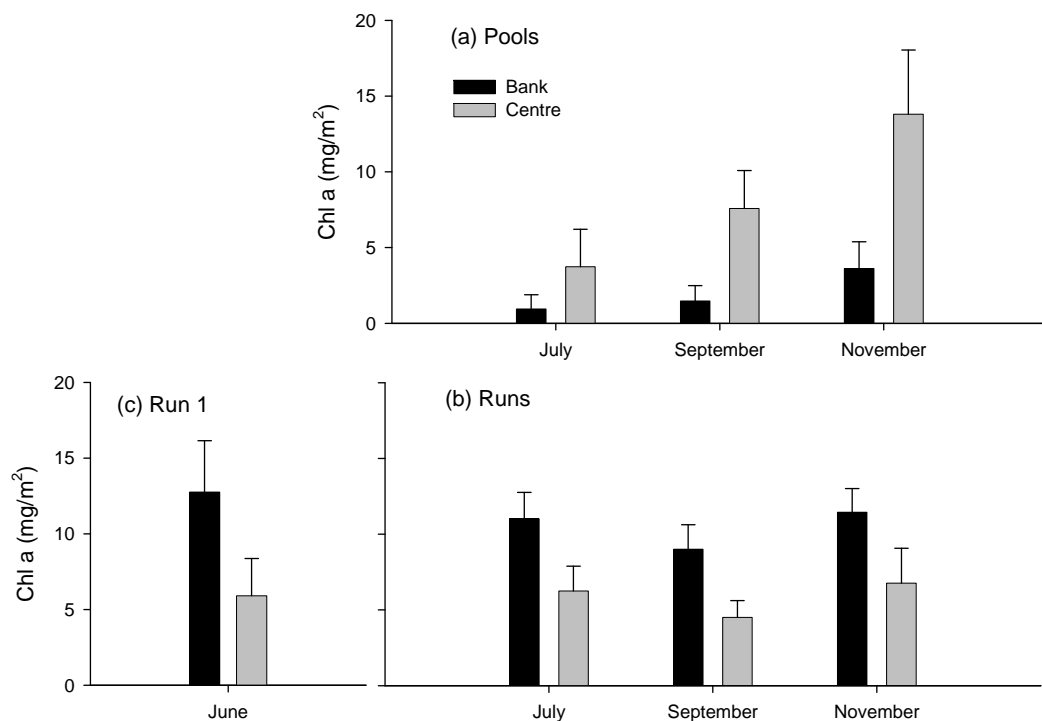


Figure 43. Changes in biomass ($\text{mg chl } a \text{ m}^{-2}$) of *Spirogyra* sp. in pools (a) and runs (b, c) of the study reach. Data are presented separately for centre (river bed) and bank habitats. (Error bars indicate $\pm 1 \text{ SE}$).

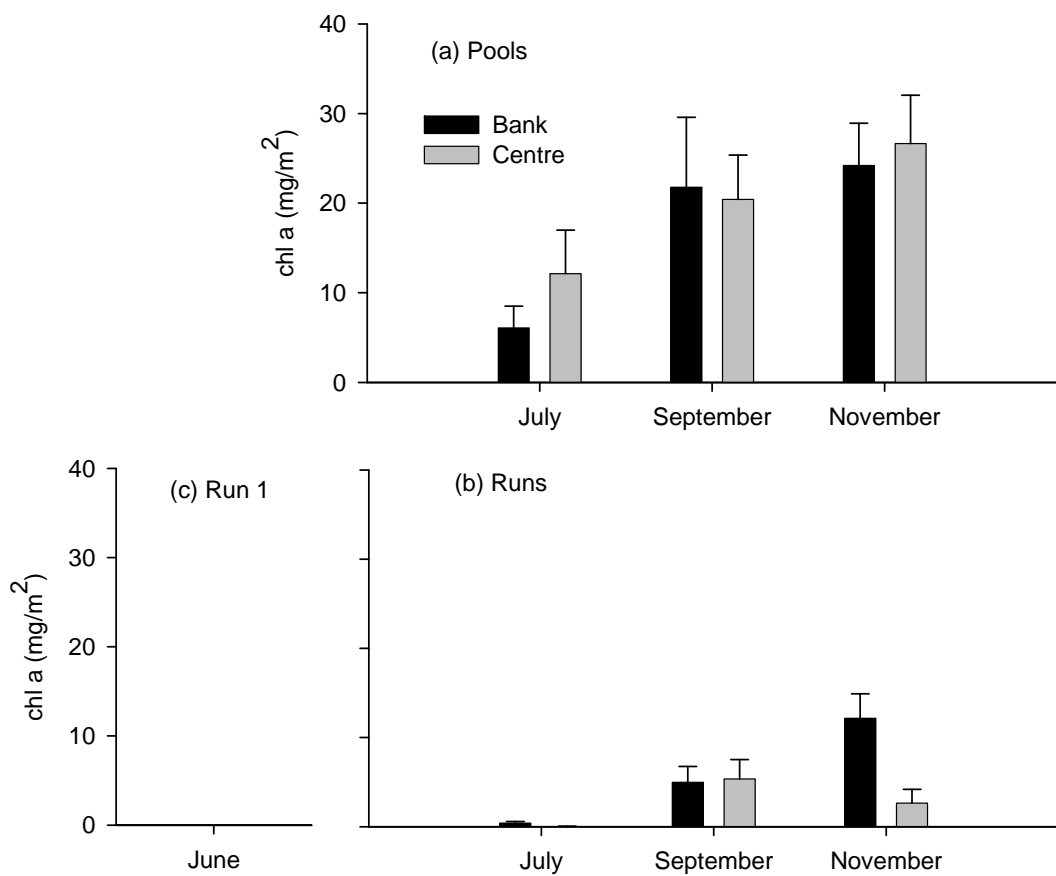


Figure 44. Changes in biomass ($\text{mg chl } a \text{ m}^{-2}$) of *Characeae* in (a) pools and (b) runs of the study reach. Data are presented separately for centre (river bed) and bank habitats. Note; pools were not sampled in June (Error bars indicate $+ 1 \text{ SE}$). *Characeae* was absent in June along Run 1.

Macrophytes

Vallisneria nana contributed little to the total plant biomass during the early part of the dry season but increased markedly in the late dry season (Figure 45). In June, *Vallisneria nana* was not observed at all in Run 1, downstream of the study area. In July very small amounts ($< 1 \text{ mg chl } a \text{ m}^{-2}$) were found along the banks of both pools and runs in the study reach. *Vallisneria* biomass then increased by at least two orders of magnitude to $>30 \text{ mg chl } a \text{ m}^{-2}$ along the banks of pools and runs in November. The overall increase was mainly attributed to an increase in Pool 4 and Run 4 where *Vallisneria* made up 30% and 37%, respectively, of the total standing crop in November.

The total amount of chlorophyll *a* in the stand of *Schoenoplectus* was 8.7 g in July and 25.5 g in September. This is the equivalent of 0.07 and 0.20 mg chl *a* m⁻² for the two runs and is $<1\%$ of the total standing crop.

Suspended Algae

The amount of microalgae present in the water column was low throughout the study period with a mean of 0.7-1.1 mg chl *a* m⁻² in July, 0.6-1.0 mg chl *a* m⁻² in September and 1.2-1.9 mg chl *a* m⁻² in November (Figure 40).

The biomass of suspended macroalgae was similar during the earlier part of the dry season, ranging from 0.03 to 0.06 mg chl *a* m⁻² in July and 0.03 to 0.05 mg chl *a* m⁻² in September, but increased in November to 0.10 to 0.16 mg chl *a* m⁻².

Both micro- and macroalgae combined contributed 2-12% to the total standing crop of pools and runs (Figure 41).

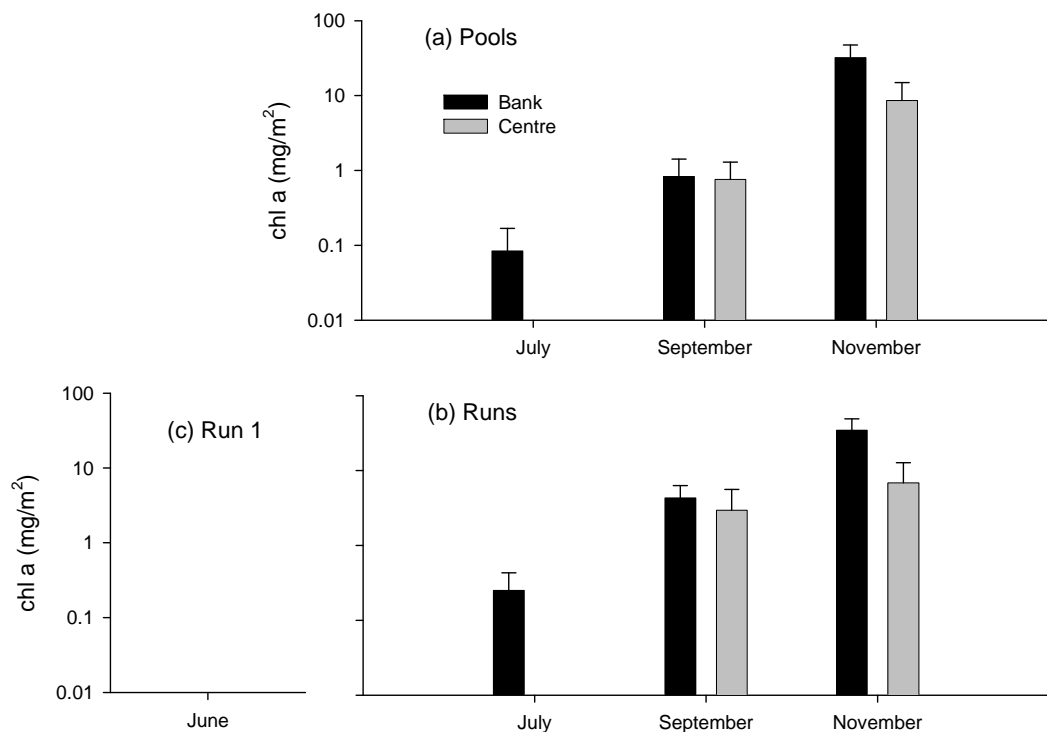


Figure 45. Changes in biomass (mg chl *a* m⁻²) of *Vallisneria nana* in (a) pools and (b) runs of the study reach. (c) shows data for a separate run (Run 1) which was sampled in June. Data are presented separately for centre (river bed) and bank habitats. Note logarithmic scale for y-axis. (Error bars indicate + 1 SE).

4.3.3. Nutrient limitation of benthic algae and phytoplankton

Insufficient algae were present for a detectable response at the sand ripples site. At the gravel site, algae responded to N+P but not to either N or P alone (Figure 46). Phytoplankton similarly responded to a combination of nitrogen and phosphorus, but neither alone (Figure 47). This suggests that the addition of nitrogen and phosphorus to the Daly River will result in increased phytoplankton and benthic algal growth. A dose-response experiment was conducted which showed that the maximum photosynthetic response for phytoplankton was at approximately 1.6 µM N and 0.1 µM P (Figure 48). This suggests that the phytoplankton are highly adapted to low

nutrient concentrations and that even the addition of low levels of N and P will result in an algal growth response.

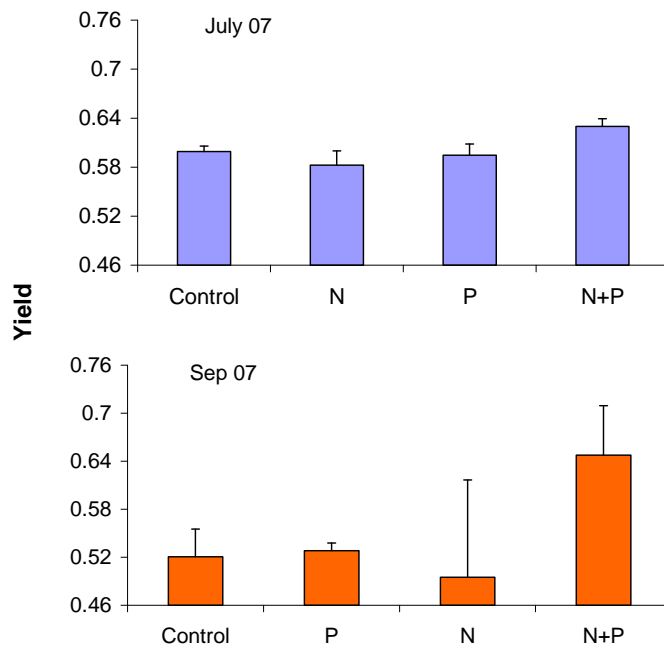


Figure 46 Photosynthetic yield response to nutrient addition in rocky substrate samples in July and September 2008

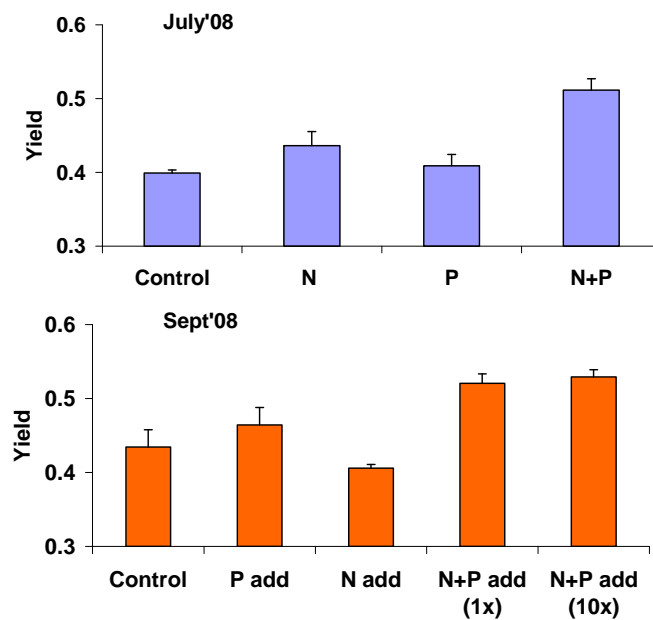


Figure 47 Photosynthetic yield response to nutrient addition in water samples in July and September 2008

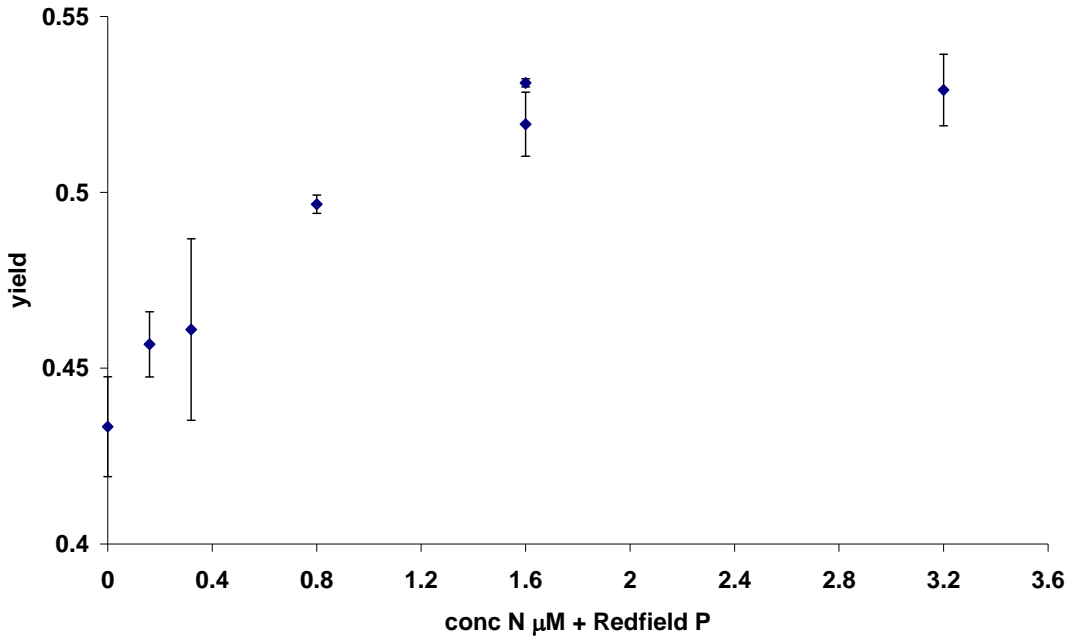


Figure 48 Photosynthetic yield response to increasing nutrient additions in water samples in July 2008.

These results echo the findings of Ganf and Rea (2007), who found that Australian tropical rivers including the Daly River are nutrient limited and are likely to experience algal blooms if nutrient enrichment occurs. Whereas Ganf and Rea (2007), reporting results from similar incubations conducted in June 2005, found that phosphorus is most likely to limit algal growth in the Daly River, the results presented here indicate that both nitrogen and phosphorus limited production during the 2008 dry season.

4.3.4. Carbon fixation and photosynthesis–irradiance response

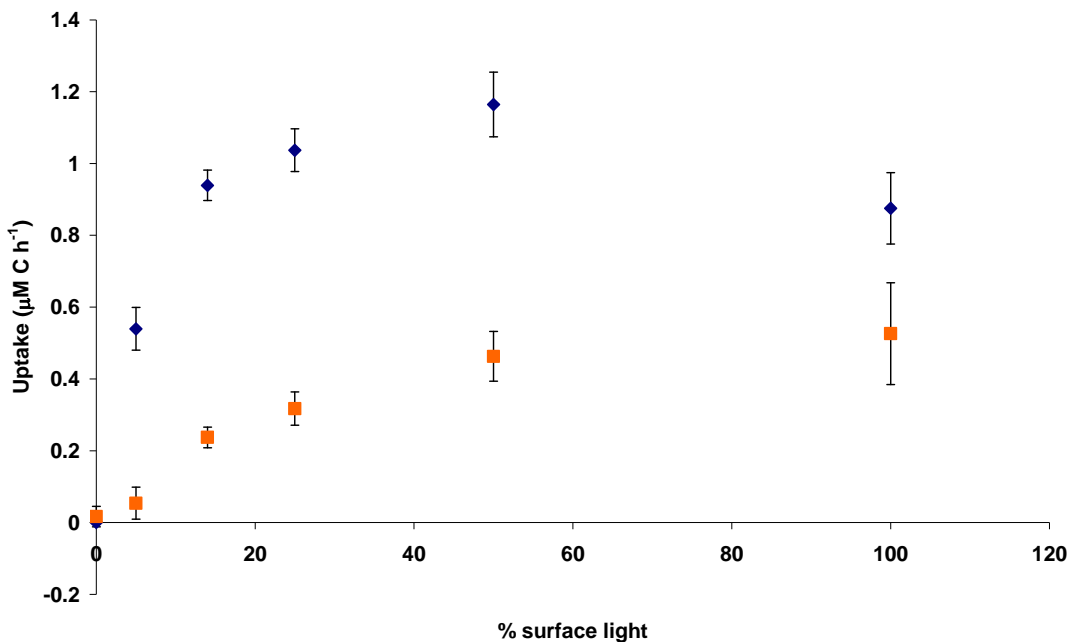


Figure 49 Photosynthesis-irradiance curves for phytoplankton in July and September 2008.

Primary productivity (carbon fixation) rates were higher in September than July 2008 (Figure 49). Maximum primary production occurred at 50% of surface light, and in September there was also evidence of photoinhibition (or photosynthetic damage due to excessive light) above 50% light.

Primary productivity (carbon fixation) rates were also measured for *Spirogyra*. Maximum primary production occurred at 25 and 50% of surface light with photoinhibition at 100% of surface light.

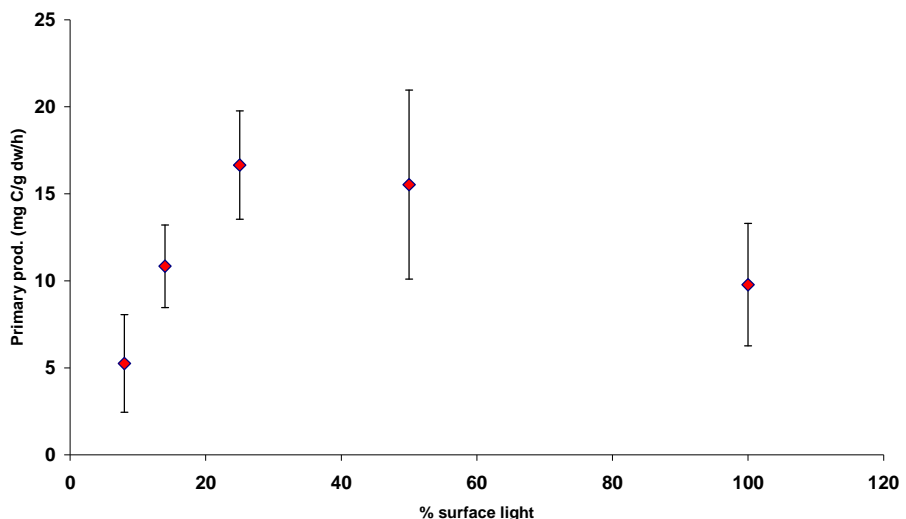


Figure 50 Photosynthesis-irradiance curve for *Spirogyra* in September 2008.

Table 28 Mean (\pm SD) chlorophyll a concentrations in the water column, rocky substrate and *Spirogyra* mats in July and September 2008.

	July 2008	September 2008
Water column ($\mu\text{g L}^{-1}$)	0.5	2.1
Rocky substrate/gravel (mg m^{-2})	132 (81)	-
<i>Spirogyra</i> ($\mu\text{g (g d.w.)}^{-1}$)	6713 (1596)	7851 (2644)

An attempt was made to measure primary productivity in the sand and gravel but the ^{13}C -uptake method used was not sensitive enough to determine rates.

4.4. Conclusion

The average benthic primary producer biomass in the study reach almost tripled from $13 \text{ mg chl } a \text{ m}^{-2}$ to $36 \text{ mg chl } a \text{ m}^{-2}$ between July and November (Table 29). Biomass was substantially higher in pools than in runs throughout the study period, ranging from $23\text{-}58 \text{ mg chl } a \text{ m}^{-2}$ compared to $9\text{-}28 \text{ mg chl } a \text{ m}^{-2}$.

As a result of the high biomass of benthic primary producers in pools, the contribution of pools to the total standing crop was almost equal to that of runs in the study reach, despite their considerably smaller size (Table 30). Suspended algae constituted only 1-4% of the total throughout the dry season.

Table 29. Average primary producer biomass (as chlorophyll *a*) for benthic algae in pools and runs (mg/m^2) and for suspended algae (mg/m^3).

	Pools	Benthic Runs	Total	Suspended
July	23	9	13	0.63
September	39	18	23	0.53
November	58	28	36	1.09

Table 30. Summary of temporal trends in standing crop (as chlorophyll *a*) for benthic primary producers of pools and runs and suspended algae

	Pools, benthic (g)	Pools suspended (g)	Runs benthic (g)	Runs suspended (g)	Total (g)	Pools, benthic (%)	Pools suspended (%)	Runs benthic (%)	Runs suspended (%)
July	1300	52	1400	120	2700	45	2	49	4
September	1900	41	2400	92	4300	43	1	54	2
November	2900	78	3900	177	6800	41	1	55	3

There was a distinct difference in the contribution of different primary producers in the two habitats. While *Characeae* made the biggest contribution to the total standing crop in pools throughout the dry season, *Spirogyra* dominated in runs in July but decreased in importance later in the year, when *Characeae*, *Vallisneria* and benthic microalgae increased their relative influence.

Phytoplankton and benthic algae in the Daly River are highly adapted to low nutrient concentrations and maximal production occurs at around 50% of surface irradiance, with some evidence of photoinhibition at higher light intensities. This implies that the addition of even low levels of nitrogen and phosphorus will result in an algal growth response, changing the biomass and potentially the species balance of primary producers in the river.

High rates of photosynthesis/carbon fixation do not necessarily imply high rates of algal biomass production in a low-nutrient system (Webster, Rea *et al.* 2005), however they suggest a potential for rapid algal growth in the presence of sufficient nitrogen and phosphorus.

5. Whole-system photosynthesis and respiration

5.1. Introduction

Measurement of diurnal oxygen curves in a river system can be used to calculate whole-system photosynthesis and respiration, which includes oxygen production due to photosynthesis by phytoplankton, benthic algae and other aquatic plants, as well as oxygen consumption due to respiration by plants, animals and bacterial degradation of organic matter in the river. Such measurements have frequently been used in the past to estimate of gross and net primary production and system consumption (Chapra and Ditoro 1991; Iwata, Takahashi *et al.* 2007; Portielje, Kersting *et al.* 1996).

Photosynthesis rates can also be modelled from the observed biomass and growth rates of algae and other plants. By comparing measured photosynthesis from dissolved oxygen curves with modelled photosynthesis, we can form a clearer picture of the fate of carbon fixed by primary producers.

5.2. Methods

5.2.1. Deployment of Hydrolab dataloggers

Four hydrolab dataloggers (Hach Hydromet, USA) were deployed during June, July, September and November 2008 in the study reach indicated in Figure 20. These devices were set to record dissolved oxygen concentrations, pH and conductivity at three to four sites within the study reach, at 5-minute intervals. A few records (data from one instrument in each of the first three study periods) were identified as dubious (e.g. due to failure of the oxygen metre), and omitted from subsequent analyses.

5.2.2. Analysis of diurnal oxygen curves

The diurnal oxygen analysis was applied to the oxygen time series as per the method outlined in Webster *et al.* (2005). The comparison between the measured oxygen concentrations and those modelled using the fitted photosynthesis, respiration and gas exchange are shown in Figure 51 to Figure 54. Fitting the measurements with a model that included daily variation in total solar radiation as estimated by the Bureau of Meteorology resulted in little change to the goodness of fit in all cases.

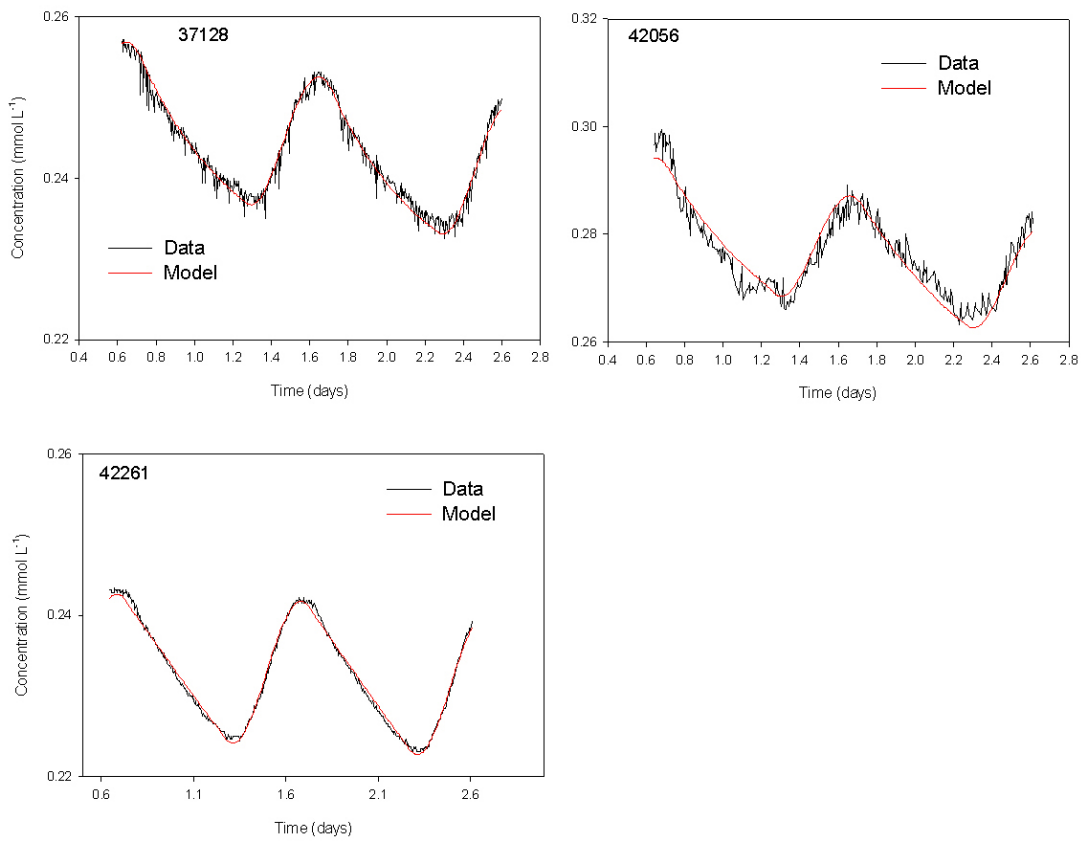


Figure 51 Comparison between measured and modelled oxygen for deployments during June 2008.

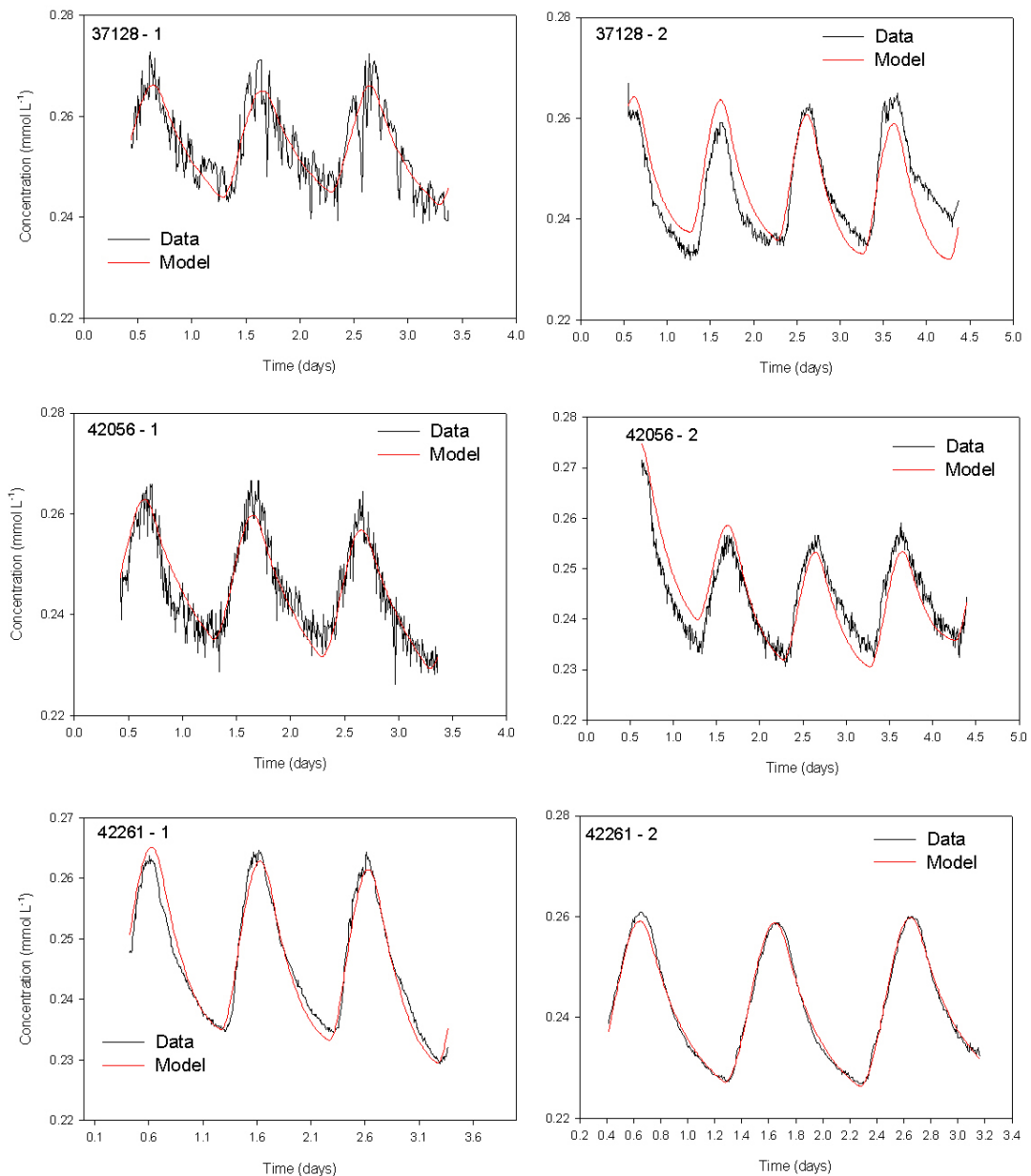


Figure 52 Comparison between measured and modelled oxygen for deployments during July 2008.

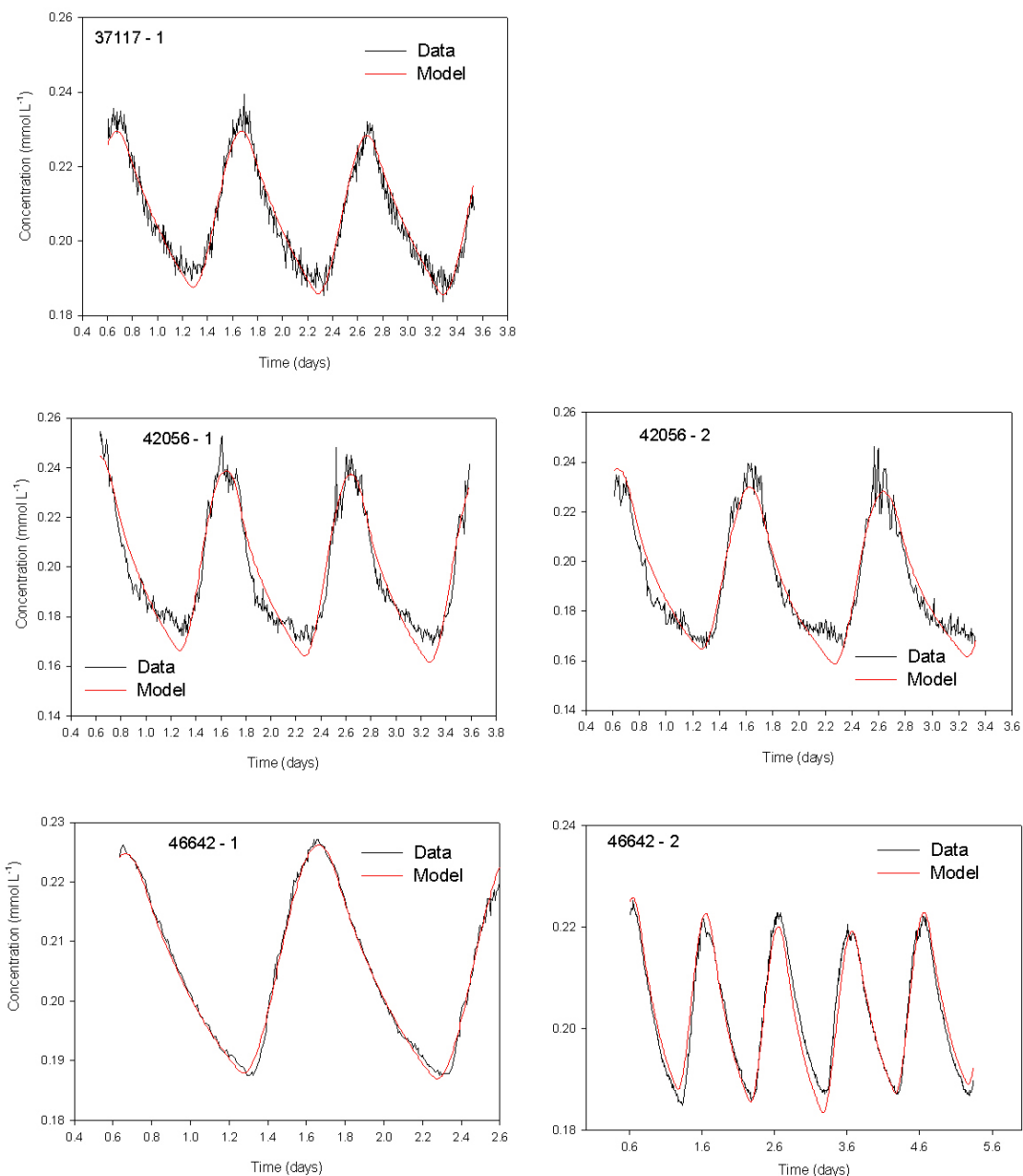


Figure 53 Comparison between measured and modelled oxygen for deployments during September 2008.

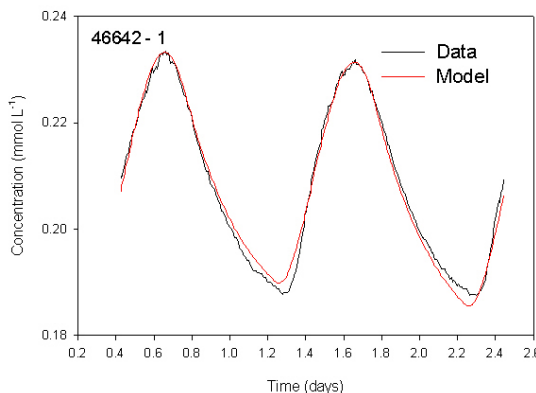


Figure 54 Comparison between measured and modelled oxygen for deployment during November 2008.

5.2.3. Photosynthesis modelling

Here, we determine the expected rate of photosynthesis given the measured standing crop and growth rates of benthic plants. Conceptually, the approach is similar to that described by Webster et al. (2005). The rate of photosynthesis production is assumed to take the form:

$$P = Chl P_{\max} \tanh(\alpha I / P_{\max}) \quad (1)$$

where P is the photosynthesis rate ($\text{mmol C m}^{-3} \text{s}^{-1}$), Chl is chlorophyll concentration (g m^{-3}), P_{\max} is light-saturated photosynthesis rate ($\text{mmol C (g chl } \alpha)^{-1} \text{s}^{-1}$), α is the photosynthesis coefficient ($\text{g C m}^{-2} (\text{g chl } \alpha)^{-1} \text{E}^{-1}$), and I is incident light at the depth of photosynthesis ($\mu\text{E m}^{-2} \text{s}^{-1}$). Note that Equation 1 pertains to volumetric concentrations.

Measurements of the biomass of the dominant macroalgae, macrophytes, and of phytoplankton were obtained during field surveys over pool and run sections within the middle reach of the Daly River in June, July, September and November 2008. The descriptions of these surveys and their results are reported in Chapter 4.

If the chlorophyll concentration is expressed as the areal concentration g m^{-2} (as are all the macrophyte measurements), then the volumetric photosynthesis rate is expressed as:

$$P = Chl P_{\max} \tanh(\alpha I / P_{\max}) / H \quad (2)$$

where H is the water depth. Note that we shall also assume that the photosynthesis ratio is unity so that for every mmol of carbon that is sequestered by photosynthesis, 1 mmol of oxygen gas is released.

During July, September and November, the study reach consisted of two pool-riffle sequences totalling 3.3 km length. Only one gravel run was sampled in June and these results will be excluded from the analysis. Suppose that a river section (pool or run) has volume V_i and area A_i . The time taken for a parcel of water to traverse the study section will be:

$$T = \frac{\sum_{i=1}^4 V_i}{Q} \quad (3)$$

where Q is the river discharge. For all three study periods, T is ~ 0.1 days. The adjustment time scale for dissolved oxygen concentrations in the river is $\sim H/E$ where E is the piston speed for gas exchange across the water surface. This time is calculated as part of the analysis of the Hydrolab measurements to vary between 0.45 and 0.61 days for the three survey periods. If the time taken for a parcel of water to traverse the study region is ~ 0.1 days, then the distance travelled by a parcel during the adjustment time period will be about 5 times as long or $\sim 16\text{km}$. That is, the distance upstream that has a large effect on the Hydrolab measurements of photosynthesis will be about 5 times longer than the study reach itself. We will make the implicit assumption that the sequence of pools and runs over this adjustment distance has the same distribution of depths and biomass as does the study reach and that photosynthesis over the study reach is characteristic of photosynthesis through the whole of the adjustment distance.

Within a river section i (pool or run), the rate of addition of oxygen as mass (mmol) to the total oxygen mass due to photosynthesis by a particular primary producer (m) in the section will be:

$$\frac{dO_i^m}{dt} = V_i P_i^m \quad (4)$$

Over 24 hours, the mass change within the section will be:

$$\Delta O_i^m = \int_0^{24h} V_i P_i^m dt \quad (5)$$

In our analysis, we consider the measurements of the abundances for the five primary producer groups phytoplankton, periphyton, *Spirogyra*, *Characeae*, and *Vallisneria*. Measurements are available for *Schoenoplectus* (bulrush) also, but its biomass was small compared to the other groups and this plant will photosynthesise into the air rather than the water column. Over 24 hours, the total addition of oxygen mass across 4 primary producer groups and the 4 river sections will be:

$$\Delta O = \sum_{i=1}^4 \sum_{m=1}^5 V_i \Delta O_i^m \quad (6)$$

and the total oxygen addition per volume of water (the daily photosynthesis rate) becomes:

$$\bar{P} = \frac{\Delta O}{\sum_{i=1}^4 V_i} \quad (7)$$

For each primary producer group, measurements were obtained near the bank ($\sim 1\text{m}$ from shore) and near the centre of the river. Suppose the proportion of the area of the river channel that could be represented as near the bank as R , then the centre part of

the channel would represent the fraction $1 - R$ of the channel area. The average rate of photosynthesis in river section i due to benthic primary producer m would then be:

$$P_i^m = \frac{RP_{ib}^m + (1-R)P_{ic}^m}{H_i} \quad (8)$$

Here P_{ib}^m and P_{ic}^m refer to the rate of photosynthesis production per unit area of river bed for bank and centre channel, and H_i refers to the average depth of the river section. For each primary producer group and for each bed and centre channel section, photosynthesis rate is calculated using Equations 1 or 2 depending on whether chlorophyll concentration is calculated on a volumetric basis (phytoplankton) or on an areal basis (periphyton, macroalgae and macrophytes). Photosynthesis rate for each primary producer group and each channel section are calculated using Equation 8 and then these are summed over all groups and averaged over the 4 river sections using Equations 5-7 to obtain an estimate of Daly River photosynthesis rate for each study period. A key task is the estimation of the parameters used in the calculations including the photosynthesis parameters (α and P_{max}), and the irradiance (I).

Estimation of photosynthesis parameters

Photosynthesis parameters are well known to vary significantly over primary producers of different species and even within a single species responding to factors such as illumination history. Reynolds (1984) notes that α , which is the photosynthesis efficiency, has been observed to fall within the range

$2 - 37 \text{ mg C}(\text{mg chla})^{-1}\text{E}^{-1}\text{m}^2$ for phytoplankton, with the peak falling in the range $6 - 18 \text{ mg C}(\text{mg chla})^{-1}\text{E}^{-1}\text{m}^2$. Nielsen and Sand-Jensen (1989) examined the relationship between photosynthesis rate and light for 14 species of submerged rooted macrophytes in the laboratory. They determined that the rates were related to chlorophyll content with all measurements falling in the range $0.3 - 2.8 \text{ mg O}(\text{mg chla})^{-1}\text{E}^{-1}\text{m}^2$ (corrected to 25°C). The lower efficiency of macrophytes compared to phytoplankton is likely due to the significantly greater ‘thickness’ of the former compared to the latter. Light attenuation within thick tissues and internal gas and solute exchange limitations diminish the photosynthesis capability for a given chlorophyll content (Enriquez, Duarte *et al.* 1996). Another factor that is certain to impact on the apparent photosynthesis parameters is shelf shading which starts to occur when algal mats thicken or macroalgae foliage becomes denser (Krause-Jensen and Sand-Jensen 1998).

Phytoplankton and Spirogyra

Photosynthesis parameters were determined for phytoplankton from photosynthesis-irradiance (P-I) experiments undertaken in July and September 2008 on collected Daly River samples. P-I measurements were also undertaken for Spirogyra during September 2008, and are described in Chapter 4.

In the experiments, irradiance was expressed as a proportion of surface light. From the height of the sun, we can calculate the incident light for solar noon which is about the time when the experiments were conducted. At solar noon on 16 July and 17 September, the incident PAR irradiance was calculated to be 1912 and $2259 \mu\text{Em}^{-2}\text{s}^{-1}$,

respectively. Hutley and others (*pers. comm.*) measured PAR on these two days to have maxima of 2073 and 2402 $\mu\text{Em}^{-2}\text{s}^{-1}$ which are 8 and 6% larger than the calculated values. What does seem likely is that both the 16 July and 17 September had clear skies.

Figure 55 shows the results of the experiments. It is apparent that for all three sets of experiments (2 phytoplankton, 1 *Spirogyra*) photosynthesis becomes light-saturated before full sunlight is achieved. Also, for the September measurements for phytoplankton and *Spirogyra*, there is evidence of photo-inhibition at the highest irradiances. A photosynthesis model is fitted to each set of measurements excluding the points that clearly demonstrate photoinhibition. Rather than fit Equation 1 directly, we express the equation as

$$P = Chl \alpha I_k \tanh(I/I_k) \quad (9)$$

where $I_k = P_{\max}/\alpha$ is a measure of the irradiance at which light saturation sets in. The results of the fitting procedure are presented in Table 1. Note that for comparison with measurements by others, α is expressed here in terms of mg of C rather than mmol.

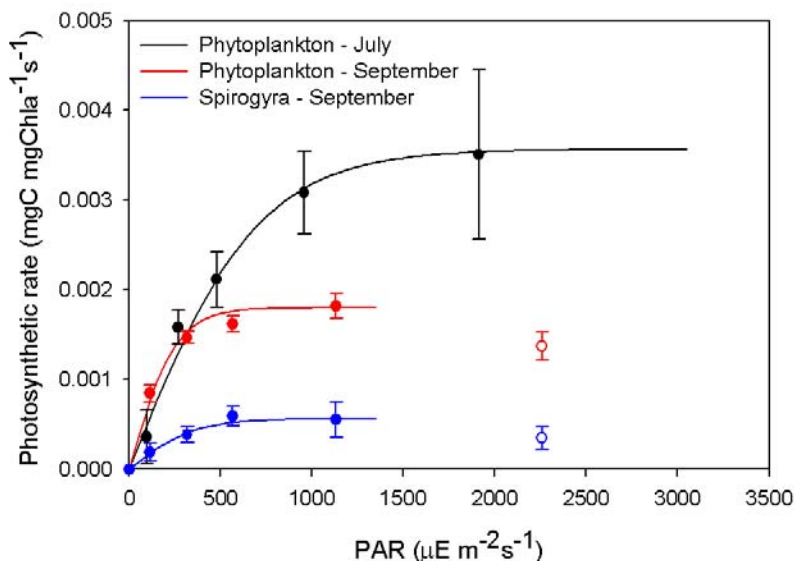


Figure 55 Comparison between measured photosynthesis rate and rates modelled using Equation 1. Points represent measurements and lines are the optimal model fits. The solid points are used in the fitting procedure, whereas the open points are not.

Table 31 Best fit values of α and I_k for the P-I experiments in July and September 2008.

	α ($\text{mgC (mgChla)}^{-1}\text{E}^{-1}\text{m}^2$)	I_k ($\mu\text{Em}^{-2}\text{s}^{-1}$)
Phytoplankton (July)	5.1	700
Phytoplankton (Sept.)	7.2	250
Spirogyra	1.6	350

The values of α for phytoplankton fall towards the bottom end of the range reported by Reynolds (1984) as being most common. Light saturation occurs at a significantly

lower irradiance in September than it does for July, but this could reflect a change of species composition. *Spirogyra* has a significantly lower α than does the phytoplankton. This is consistent with the expectation that macrophytes should have lower values of their photosynthesis coefficients than phytoplankton.

Characeae, Vallisneria, and periphyton

No experiments were undertaken to determine the P-I characteristics of *Characeae*, *Vallisneria*, and periphyton. Rather, we resort to the scientific literature to provide an estimate of what their photosynthesis parameters might be. Libbert and Walter (1985) measured photosynthesis parameters for *Chara tomentosa* a species that lives in brackish water in northern Europe. Conversion of the units used in their paper shows $\alpha = \sim 6.8 \text{ mg C}(\text{mg chla})^{-1}\text{E}^{-1}\text{m}^2$ and $I_k \sim 60 \mu\text{Em}^{-2}\text{s}^{-1}$. Pentecost (1984) studied the growth characteristics of *Chara globularis* in a shallow UK lake. He observed a maximum growth rate of $P_{\max} \sim 6 \times 10^{-5} \text{ mg C}(\text{mg chla})^{-1}\text{s}^{-1}$ and this maximum to occur at an irradiance of $I_{\max} \sim 170 \mu\text{Em}^{-2}\text{s}^{-1}$. If we suppose $I_k \sim I_{\max}/2$ (see Figure 55 and Table 31), then $I_k \sim 90 \mu\text{Em}^{-2}\text{s}^{-1}$ and so $\alpha = P_{\max}/I_k \sim 0.7 \text{ mg C}(\text{mg chl a})^{-1}\text{E}^{-1}\text{m}^2$. For our application, we will assume that α and I_k are the geometric means of the values determined in these two studies; that is, $\alpha = \sim 2.2 \text{ mg C}(\text{mg chla})^{-1}\text{E}^{-1}\text{m}^2$ and $I_k \sim 70 \mu\text{Em}^{-2}\text{s}^{-1}$.

There does not seem to be information on the photosynthesis parameters on *Vallisneria nana* which is the species found in the Daly River. Harly and Findlay (1994) measured growth of *Vallisneria americana* in the Hudson River and estimated a growth rate of $\alpha = 1.5 \text{ mg C}(\text{mg chla})^{-1}\text{E}^{-1}\text{m}^2$ and $I_k = 179 \mu\text{Em}^{-2}\text{s}^{-1}$. We will use these values.

For a periphyton community comprised mainly of algae, one might expect similar photosynthesis responses to those of phytoplankton. However, for sufficiently thick algal mats self shading can limit photosynthesis and the position of individual cells within the matrix of the periphyton layer can affect their nutrient dynamics (Boston and Hill 1991). Boston and Hill determined the P-I relationships for 10 intact periphyton communities in the laboratory and found α to vary over the range $0.8 - 6.4 \text{ mg C}(\text{mg chla})^{-1}\text{E}^{-1}\text{m}^2$. Krause-Jensen and Sand-Jensen (1998) compiled the results of 414 studies of the photosynthesis responses of phytoplankton, benthic microalgae and macrophytes and determined that there is a convergence of these properties when normalised against chlorophyll concentration when chlorophyll concentration was low. A large part of the divergence at high chlorophyll concentrations occurs due to shelf shading. The concentrations of periphyton measured in the Daly study were a maximum of $\sim 10 \text{ mg m}^{-2}$. At this concentration, the results of Krause-Jensen and Sand-Jensen (1998) would suggest that self-shading would be minimal and that the P-I characteristics of benthic microalgae would be similar to those of phytoplankton. Accordingly, we shall assume that the P-I characteristics of periphyton for the Daly study to be the geometric means of those measured for phytoplankton in July and September; that is, $\alpha = 6.1 \text{ mg C}(\text{mg chla})^{-1}\text{E}^{-1}\text{m}^2$ and $I_k = 420 \mu\text{Em}^{-2}\text{s}^{-1}$.

The photosynthesis parameters that are used in further analysis are listed in Table 32.

Table 32 Values of α and I_k used in further photosynthesis analysis.

	α (mgC (mgChla) $^{-1}$ E $^{-1}$ m 2)	I_k (μ Em $^{-2}$ s $^{-1}$)
Phytoplankton (July)	5.1	700
Phytoplankton (Sept. & Nov.)	7.2	250
<i>Spirogyra</i>	1.6	350
<i>Characeae</i>	2.2	70
<i>Vallisneria</i>	1.5	179
Periphyton	6.1	420

Underwater light

Our analysis of the dissolved oxygen measurements for the estimation of photosynthesis rates assumes that the incoming PAR radiation can be calculated from the height of the sun only; that is, clear sky conditions prevail. For fitting optimal time series of photosynthesis, respiration, and gas exchange rates, it is the shape of the hourly irradiances that needs to be well represented and not their absolute magnitude. The analysis is insensitive to the degree of cloudiness provided that the cloudiness remains uniform during the day and variations do not significantly distort the shape of the irradiance curve.

Figure 55 compares the clear-sky PAR irradiance (expressed as W m $^{-2}$) calculated from the sun height with irradiance measured at a site adjacent to the river by Hutley and others (*pers. comm.*). The period shown is when the Hydrolab was installed in the river. The sun heights are calculated using an algorithm that uses day of year, time of day, and latitude. The two irradiance curves follow one another well even though the Hutley et al. measurements show a degree of raggedness presumably due to the passage of clouds. Similar comparisons were undertaken for the July and September measurement periods. For the July period, there was virtually no evidence of any reduction in irradiance by cloud, whereas the September period showed similar behaviour to that shown in Figure 56 on some days. For all three periods, the shapes of the measured irradiance time series are good approximations of the clear-sky time series so we would expect that photosynthesis rates calculated from the Hydrolab measurements would be negligibly affected by clouds.

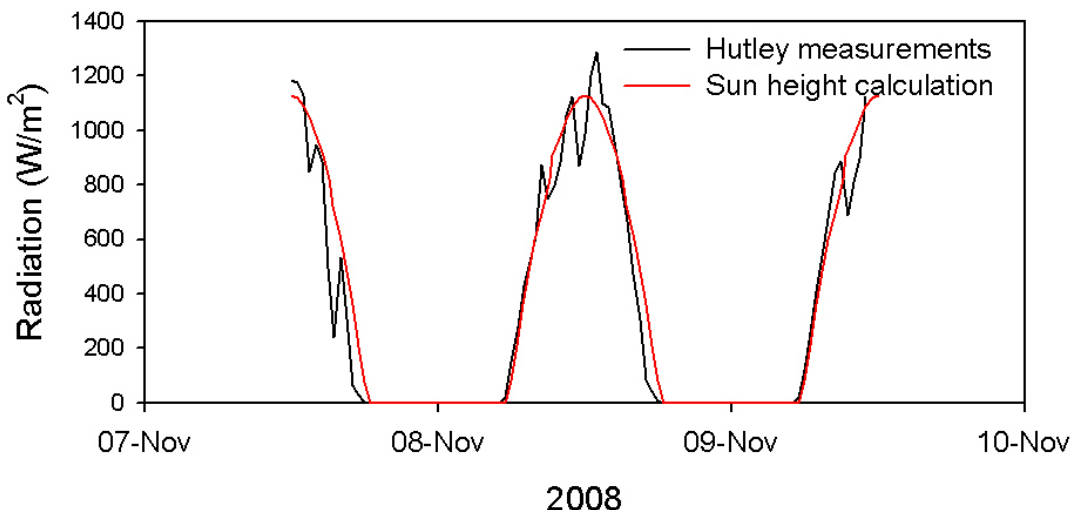


Figure 56 Comparison between irradiances calculated from sun height and measured irradiances (Hutley et al.).

We shall assume that the PAR irradiance at distance z (depth) from the water surface is given by Beer's Law:

$$I = I_0 e^{-Kz} \quad (10)$$

where I_0 is the instantaneous irradiance at the water surface and K is the PAR extinction coefficient. For benthic organisms including periphyton, *Characeae*, and *Spirogyra*, the irradiance required in Equation 5 to calculate photosynthesis rate is:

$$I = I_0 e^{-KH} \quad (11)$$

whereas phytoplankton would experience the average light irradiance in the water column. Averaging of Equation 10 from the surface to the bottom yields:

$$\bar{I} = \frac{I_0}{KH} [1 - e^{-KH}] \quad (12)$$

Vallisneria is a plant that grows towards the water surface so its leaves are more likely to receive an irradiance that is more representative of the water column than for the other benthic primary producers considered here. Accordingly, we will use Equation 12 to represent the irradiance experienced by both *Vallisneria* and phytoplankton in Equation 5.

Equations 11 and 12 require the specification of K . Measurements of K were obtained during each survey period. The extinction coefficients are listed in Table 33. It happens that the average extinction coefficient for each of the three surveys is the same; that is,

$\bar{K} = 0.54 \text{ m}^{-1}$. This is the value that will be used in further analysis.

Table 33 Measured extinction coefficients during the July, September and November surveys.

Date	Station	K (m ⁻¹)
7 July 2008	T2	0.48
“	T4	0.6
22 September 2008	T1	0.6
“	T2	0.45
“	T4	0.53
“	T5	0.56
6 November 2008	T5	0.46
“	T4	0.66
“	T3	0.43
“	T2	0.49
“	T1	0.65

In our analysis of irradiance, we have noted that measured irradiances are affected by cloud on some days. We account for this by considering the ratio of the average measured irradiance estimated across the periods of the Hydrolab installations (Hutley et al.) to the clear sky irradiance. Suppose this ratio is R . The average irradiances and the values of R are listed in Table 34.

Table 34 Average daily irradiance calculated for periods of Hydrolab installation. Measured irradiance (Hutley et al.) and irradiance calculated from the sun height are shown. Also, shown are their ratios.

	Irrad. Hutley et al. (Mw/m ² -d)	Irrad. – sun height (Mw/m ² -d)	R
July	24.4	24.2	0.99
September	27.7	30.1	0.92
November	30.5	32.4	0.94

In evaluating Equations 11 and 12, we correct I_0 for the possible effect of cloud cover as $I_0^C = RI_0$. In all calculations of irradiance used to estimate photosynthesis production from primary producer biomass, we will use I_0^C .

5.3. Results

5.3.1. Diurnal oxygen analysis

Figure 57 and Figure 58 show the results of the diurnal curve analysis for photosynthesis and respiration rates. Note that these rates represent averages for each deployment period and are adjusted to encompass an integral number of 24-hour periods. The error bars represent the expected error in the curve fitting. Inaccuracies in hydrolab calibration would not be reflected in these error bars. Mostly, photosynthesis and respiration rates show a gradual increase between June and September. Instrument 42056 shows significantly higher photosynthesis and respiration rates than the other instruments. As has been noted, there are some irregularities in the shapes of the temperature and oxygen time series compared to

those of the other instruments that need to be resolved. Table 35 provides a summary table of the results. The calculated gas exchange rate is expressed as the piston velocity (m d^{-1}).

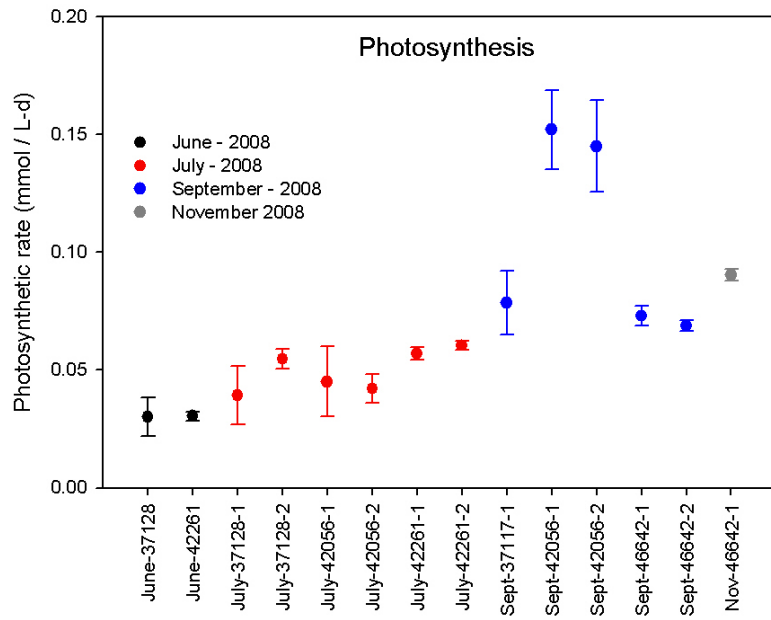


Figure 57 Modelled photosynthesis rates for the June, July, September, and November deployments.

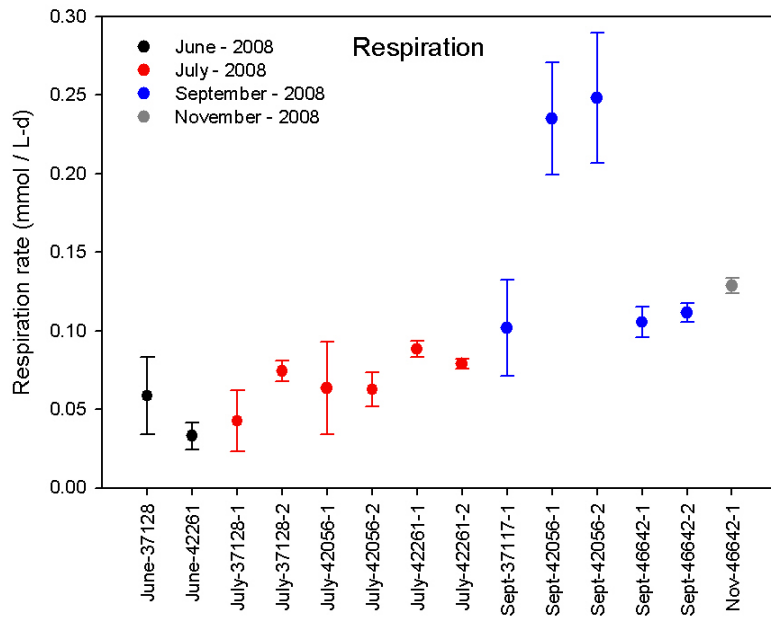


Figure 58 Modelled respiration rates for the June, July and September deployments.

Table 35 Calculated photosynthesis rate, respiration rate, and gas exchange piston velocity from diurnal oxygen analysis.

Station	Photosynthesis rate (mmol L ⁻¹ d ⁻¹)	Respiration rate (mmol L ⁻¹ d ⁻¹)	Gas exchange (m d ⁻¹)
June-37128	0.030	0.059	1.6
June-42261	0.031	0.033	0.1
July-37128-1	0.039	0.043	2.0
July-37128-2	0.055	0.074	3.9
July-42056-1	0.045	0.064	1.5
July-42056-2	0.042	0.063	2.7
July-42261-1	0.057	0.088	3.3
July-42261-2	0.060	0.079	2.3
Sept-37117-1	0.079	0.102	1.0
Sept-42056-1	0.152	0.235	2.6
Sept-42056-2	0.145	0.248	2.8
Sept-46642-1	0.073	0.106	1.3
Sept-46642-2	0.069	0.112	1.6
Nov-46642-1	0.090	0.129	2.3

5.3.2. Temporal trends

The ‘theoretical’ photosynthesis rates are calculated from measured primary producer biomass using the analysis procedure described above. These will be referred to as P_B . The results are summarised in Figure 59, which shows the estimated contribution of each primary producer group to the total photosynthesis rate in each sampling period. P_B for each primary producer generally increases between July and November and this is mostly attributable to the increase in measured biomass, and to a less extent to increases in radiance as summer is approached and as the water depth decreases. During all three surveys, periphyton is estimated to contribute to more than 50% of the total photosynthesis, but it contributes to less than 30% of the biomass in most pools and runs. A full analysis of the changes in the biomass over the survey period is presented in Section 3.

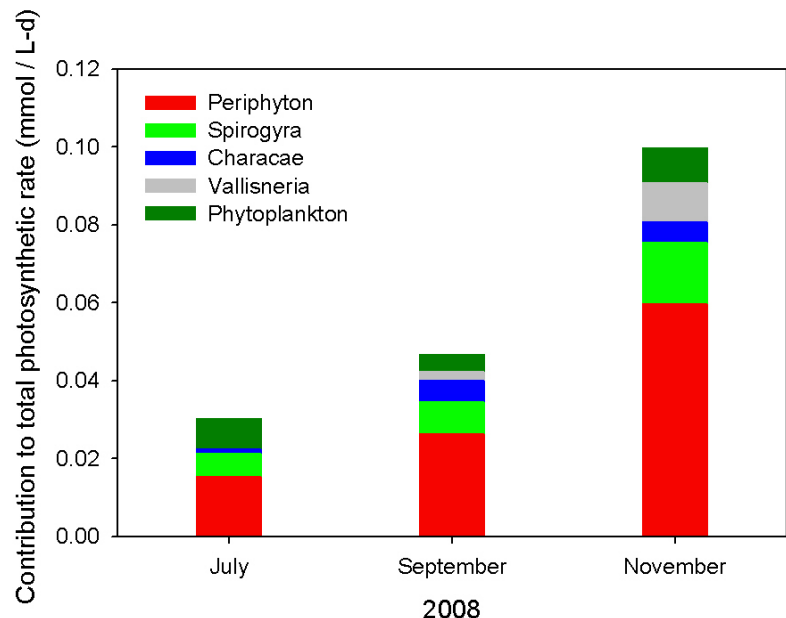


Figure 59 The estimated contribution of each primary producer group to the total photosynthesis rate in the July, September and November surveys.

The sum of the rates across all 5 primary producer types are compared to the rates estimated from the deployed Hydrolabs (P_H) in Figure 60. Table 36 provides a comparison between P_B and P_H averaged for each deployment period ($\overline{P_H}$). It is apparent that the P_B are significantly below P_H for all Hydrolab deployments for July and September, but are a ~10% higher than the single P_H obtained in November. We conclude that the biomass analysis is capable of accounting for the majority of the measured photosynthesis rates.

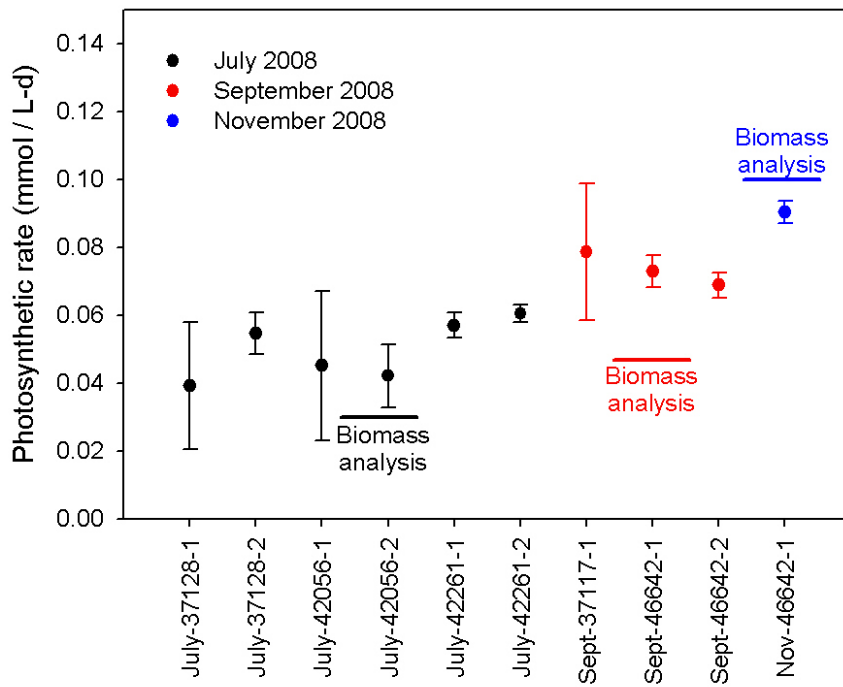


Figure 60 Comparisons between photosynthesis rates estimated from biomass analysis with those estimated from the analysis of Hydrolab measurements. The standard error bars are estimated from the fitting procedure.

Table 36 Comparison of photosynthesis rates determined from biomass analysis (P_B) and from Hydrolab measurements (\bar{P}_H). Note that the Hydrolab rates have been averaged over all instruments deployed during a survey period.

	P_B ($\text{mmol L}^{-1}\text{d}^{-1}$)	\bar{P}_H ($\text{mmol L}^{-1}\text{d}^{-1}$)
July	0.030	0.050
September	0.047	0.074
November	0.100	0.090

It is useful to consider possible reasons for the discrepancies between P_B and \bar{P}_H . There are a number of uncertainties including specification of the photosynthesis parameters and biomass estimates and these are considered in turn.

5.3.3. Error estimates

Error in calculation of P_H from Hydrolab measurements.

Here, there are several sources of uncertainty or error. For the specification of the function to represent irradiance when fitting photosynthesis, respiration and gas exchange rates to the Hydrolab measurements of dissolved oxygen we assume that $I = I_k \tanh(I/I_k)$. For the results presented so far we have specified that

$I_k = 5000 \mu\text{Em}^{-2}\text{s}^{-1}$ which effectively assumes that photosynthesis is light limited and

that its rate is directly proportional to irradiance. However, Table 32 shows that our estimated range of I_k to vary between $70 - 700 \mu\text{Em}^{-2}\text{s}^{-1}$ which would result in significant curtailment of P_H when the sun is high. In Figure 61, we show the calculated photosynthesis rates that result from assuming a range of values of I_k . When averaged across all Hydrolab deployments, the computed P_H varies between $0.059-0.063 \text{ mmol L}^{-1}\text{d}^{-1}$ when I_k is increased from 300 to $5000 \mu\text{Em}^{-2}\text{s}^{-1}$.

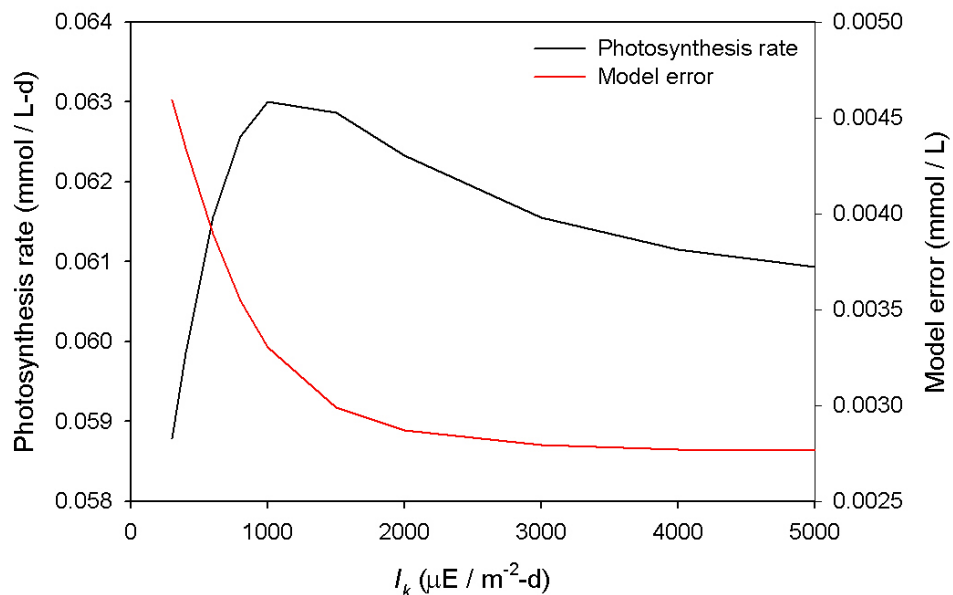


Figure 61 Effect of variation in I_k on computed photosynthesis rates averaged across all Hydrolab deployments. Also, shown is the average RMS difference between modelled and measured oxygen concentrations.

A measure of the goodness of fit for the photosynthesis model fitted to the measurements is the RMS difference between measured and modelled oxygen concentrations. This difference is shown averaged across all deployments in Figure 61. It is apparent that the best fit by the model to measurements occurs for the largest value of $I_k = 5000 \mu\text{Em}^{-2}\text{s}^{-1}$ and the difference steadily increases as I_k is reduced. It would seem that the photosynthesising biomass within the Daly River is behaving as if it is light limited. The difference in modelled oxygen time series for three values of I_k is exemplified in Figure 7, which shows results for the deployment of Hydrolab #42261-1 in July. Clearly, the assumption of smaller values of I_k results in a significant truncation of peak oxygen concentrations.

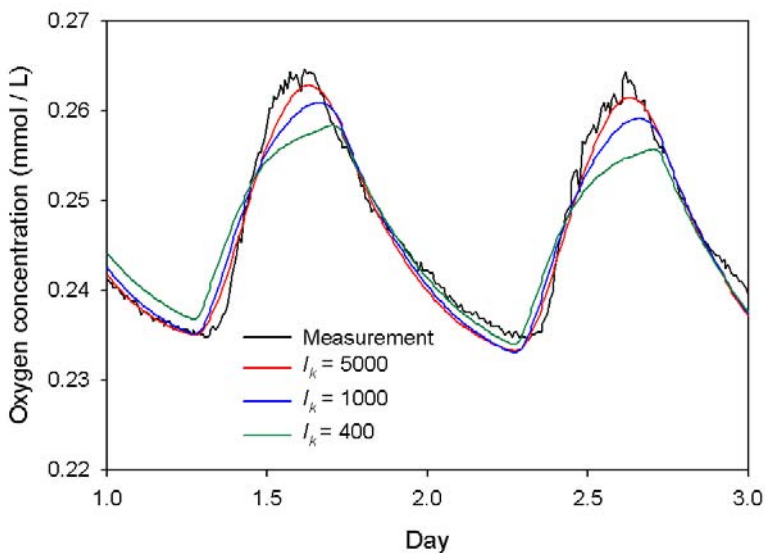


Figure 62 Time series of measured oxygen concentration for Hydrolab #42261-1 in July. These measurements are compared to the best fit modelled time series of oxygen concentrations for $I_k = 400, 1000$, and $5000 \mu\text{Em}^{-2}\text{s}^{-1}$.

From these analyses, we suggest that the assumption that photosynthesis is light limited is most valid for calculating P_H . In any event, P_H calculated using

$I_k = 5000 \mu\text{Em}^{-2}\text{s}^{-1}$ is within 4% of the rates calculated using other values of I_k . The apparent lack of light saturation on photosynthesis rates in the Daly was noted by Webster et al. (2005) and possible explanations presented.

The Hydrolabs deployed during the July survey were located within a section of river ~ 1.5 km long, yet P_H varied between 0.039 - $0.060 \text{ mmol L}^{-1}\text{d}^{-1}$ (see Figure 60). We have noted that the distance scale that is important for determining measured photosynthesis rates is ~ 16 km during the study periods which is about ten times longer than the maximum separation between Hydrolabs. Consequently, one might expect that the Hydrolab estimates of P_H should be closer to one another than they are. It is possible that the Hydrolabs are affected by local effects such as the presence or absence of oxygen sources or sinks. Also, it is certain that ventilation of the oxygen sensors will differ between deployments and that there is some degree of calibration error in the instruments. We suggest that a measure of the variation in estimated P_H due to all these factors is the standard deviation of the July measurements from their mean; that is $0.009 \text{ mmol L}^{-1}\text{d}^{-1}$.

Error in estimation of photosynthesising biomass

For each sampling period, the standing crop of benthic microalgae, phytoplankton, macroalgae and macrophytes was determined on the river bed at 10 randomly selected locations in the pools and at 20 locations in the runs. Additional samples were taken in the pools and runs ~ 1 m from shore at the same numbers of locations. Error can occur in estimating biomass in the pools and runs from a limited number of samples, but also from the assumption that the measured biomass concentrations along the

study reach are representative of the whole of the 16 km section of river which is responsible for the measured P_H . We shall assume that the observed variation between biomass concentrations in the two pools (or two runs) is representative of the variation in biomass concentrations along the 16 km reach.

Consider the two measurements of the areal concentration of a particular primary producer in pools during a particular survey period, C_{1p} and C_{2p} . Suppose that average concentrations of this primary producer across all pools in the river section have a normal distribution. Then, integration of the normal probability function shows that the expected difference in the concentration is 0.95σ where σ is the standard deviation of the normal distribution. Thus, for the pool sections, $\sigma_p \sim |C_{1p} - C_{2p}|$. The equivalent for the run sections is $\sigma_r \sim |C_{1r} - C_{2r}|$ and equivalent considerations apply for the bank measurements. In the section describing photosynthesis modelling, we note that photosynthesis production for each primary producer and for each river section is directly proportional to biomass. Thus, we can ascribe a standard error in photosynthesis production associated with the error in biomass for each primary producer group and river section by solving the equations. Suppose this error is σ_P^{im} , then the estimated total standard error in average photosynthesis rate over all river sections and primary producer groups is:

$$\Delta_P = \sqrt{\sum_{i=1}^4 \sum_{m=1}^5 (\sigma_P^{im})^2} \quad (13)$$

The estimated standard errors in the photosynthesis rate calculated for July, September, and November are 0.007, 0.035, and 0.020 mmol L⁻¹d⁻¹, respectively. The S.E. for September seems unusually high and this was investigated further. It seems that both the pools and the runs had very different measured periphyton biomass from one another during this survey resulting in large values of σ_P^{im} for this primary producer in pools and runs. With about 56% of the photosynthesis production being due to periphyton during this survey, the uncertainty statistics were dominated by the large uncertainty in periphyton biomass. The ratio of Δ_P to total primary production for the July and November surveys is ~25% and we suggest that the ratio of uncertainty for the September survey may be similar to this value also giving an estimated S.E. for the September survey of ~0.012 mmol L⁻¹d⁻¹.

Error in estimation of photosynthesis parameters

Direct measurements of α and of I_k are available only for phytoplankton in July and September and for *Spirogyra* in September. All other values of photosynthesis parameters used in the analysis are either inferred from these limited measurements or from literature values obtained in all cases for different species in different locations. Since periphyton appears to provide the largest contribution to primary production, we focus on examining how modifying its parameters affects estimated photosynthesis.

Figure 63 shows the P-I curve obtained for $\alpha = 6.1 \text{ mg C}(\text{mg chla})^{-1}\text{E}^{-1}\text{m}^2$ and $I_k = 420 \mu\text{Em}^{-2}\text{s}^{-1}$ which are the parameters assumed for periphyton. Also shown are the curves for $P = \alpha I$ and for $P = P_{\max} = \alpha I_k$ which are the limiting forms of the P-I curve for $I \ll I_k$ and for $I \gg I_k$, respectively and the proportion of daylight time that the irradiance is greater than a particular value (in mid-September).

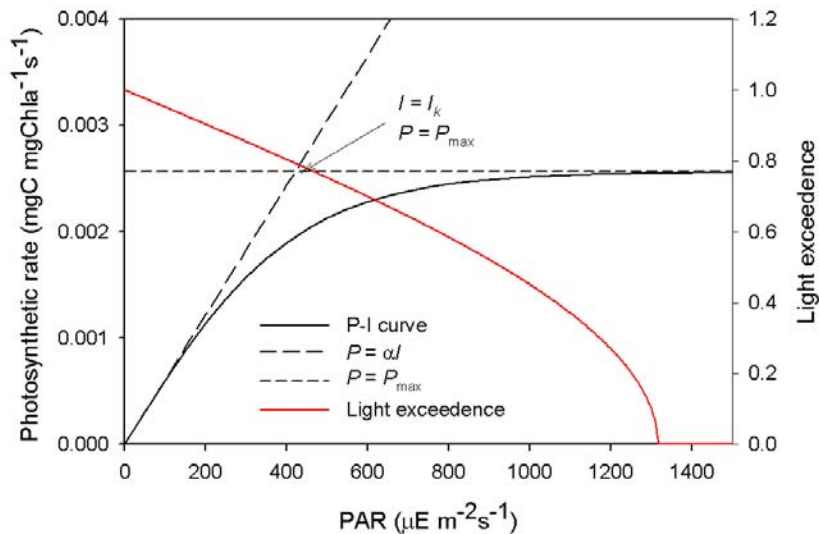


Figure 63 Fitted P-I curve for phytoplankton estimated from measurements in September. Also shown are the limiting forms for $I \ll I_k$ and for $I \gg I_k$ and the proportion of daylight time that clear-sky irradiance is estimated to be greater than a particular level.

It is apparent that the irradiance experienced by the periphyton is greater than I_k for 79% of the daylight time; that is, the modelled rate of photosynthesis is mostly determined by the chosen value of P_{\max} for this primary producer. It is likely that this value of P_{\max} is too low. Even though this value was based on measurements for phytoplankton, algae adapted to lower light levels are likely to have higher values of P_{\max} . It is certain that periphyton would generally receive lower irradiance than phytoplankton in part because they live on the bottom, but also because they are likely to be found on all sides of bottom objects including some that are not facing directly upwards. A 50% increase in the assumed value of I_k from 420 to $630 \mu\text{Em}^{-2}\text{s}^{-1}$ would cause a 50% increase in P_{\max} and raise the modelled periphyton photosynthesis rate from 0.026 to $0.035 \text{ mmol L}^{-1}\text{d}^{-1}$, an increase of 35%. An error in α with I_k fixed can be readily shown to cause a proportional error in photosynthesis rate at all irradiances; that is, a 50% increase would cause a 50% increase in total photosynthesis production. This last result applies to all primary producers, but changes in I_k will cause less than a proportional change in production.

5.4. Discussion

This analysis endeavours to reconcile measured photosynthesis rates inferred from Hydrolab measurements of oxygen concentrations with rates inferred from measured

biomass in a section of the Daly River in July, September and November 2008. In all cases, the rates P_H and P_B are of the same order of size and showed the same increasing trend from July to November. The maximum relative difference occurred in July when P_B was calculated to be 60% of P_H . The relative difference was only 10% in November. We have undertaken an analysis of the uncertainties and errors that might have lead to the discrepancies.

In September, $P_B = 0.047 \text{ mmol L}^{-1}\text{d}^{-1}$ and $P_H = 0.074 \text{ mmol L}^{-1}\text{d}^{-1}$, which is a ratio of 64%. However, this survey had the largest absolute difference of 0.027 $\text{mmol L}^{-1}\text{d}^{-1}$. We suggest that the standard error in a Hydrolab estimate of photosynthesis rate is $\sim 0.009 \text{ mmol L}^{-1}\text{d}^{-1}$. For an estimate based on the average of three such measurements, the standard error of the mean would be $\sim 0.009/\sqrt{3}$ $\sim 0.005 \text{ mmol L}^{-1}\text{d}^{-1}$. We have estimated the uncertainty in P_B due to uncertainty in the biomass measurement to be $\sim 0.01 \text{ mmol L}^{-1}\text{d}^{-1}$. This estimate is based on statistics determined over $\sim 20\%$ of the river reach that affects P_H , but it also assumes that the remaining 80% of the reach has biomass concentrations in the reaches and runs that are statistically similar to the one in which measurements were obtained. A source of uncertainty that is difficult to quantify is uncertainty in the assumed photosynthesis parameters. Variations in the assumed values of α will cause a proportional changes in P_B . Variation in I_k will cause a less than proportional change, but it will still be large. The choice of these parameters is based on some limited measurements, but mostly it is based on literature values for other species in aquatic systems in different climates from the Daly River. Overall, considering the uncertainty, it would seem that the P_H and P_B are not inconsistent with one another.

A feature of the photosynthesis dynamics that still needs to be resolved is the apparent lack of light saturation in the photosynthesis rates. The modelled oxygen evolution due to photosynthesis compares best with oxygen measurements if photosynthesis is light limited. Fortunately, the calculation of daily photosynthesis rate from the Hydrolab measurements is little affected by the assumption of light-limitation or not.

5.5. Conclusions

Net system photosynthesis calculated from diurnal oxygen curves consistently exceeded photosynthesis estimates from biomass observations. Photosynthesis calculated by either method rose over the course of the dry season, but net respiration consistently exceeded photosynthesis.

Periphyton is estimated to contribute to more than 50% of the total photosynthesis throughout the dry season, though it contributes to less than 30% of total biomass. This accords with our findings from the biomarker study (Section 3.2.4) that periphyton was a major source of organic matter to the system.

Spirogyra makes the second greatest contribution to system photosynthesis, while phytoplankton, despite low measured chlorophyll *a* concentrations, also contributes to oxygen production.

While results reported in Section 4.3.4 indicate a potential for photoinhibition of individual algae, this analysis suggests that photoinhibition did not occur at a system scale.

6. Hydraulic modelling

6.1. Introduction

In order to improve our ability to assess how changes in flow are likely to affect the river in terms of the physical habitat that it provides, one aspect of this study was the development of a one-dimensional hydraulic model of the main channel of the Daly River. This model complements the more complex two-dimensional hydrodynamic models developed through TRaCK project 4.1, providing an efficient means to simulate flow, depth and current in the river, including the impact of hydraulic breaks (such as small waterfalls) on flow. The model may also be used as the basis for a transport model for nutrients and sediments.

Here, we apply the hydraulic model HEC-RAS (Haestad Methods Inc., Dyhouse *et al.* 2003) to the middle section of the Daly River. HEC-RAS was developed by the US Army Corps of Engineers to simulate one-dimensional steady and unsteady flow analysis in river networks.

The steps in the application of the model include the definition of the channel shape and dimensions, the application of the model with prescribed flows, and ideally a calibration and validation step.

6.2. Channel shape and dimensions

The hydraulic model requires the prescription of the river channel cross-sections at suitable spatial separations along the application reach. Georges *et al.* (2002) describe how the thalweg along the 130 km section of the Daly River between Dorisvale gauging station (site G8140067) and Beeboom gauging station (site G8140042) was measured during high flow conditions ($\sim 1000 \text{ m}^3\text{s}^{-1}$) in March 2001. The depths were measured using a broad band RDI Acoustic Doppler Current Profiler (ADCP). The water surface elevation between Dorisvale and Beeboom gauging stations was assumed to be linear because all river controls were assumed to be well submerged during the measurement period. The elevation of the thalweg in AHD was calculated from measured depth and from the assumed water surface. These data are shown plotted in Figure 64.

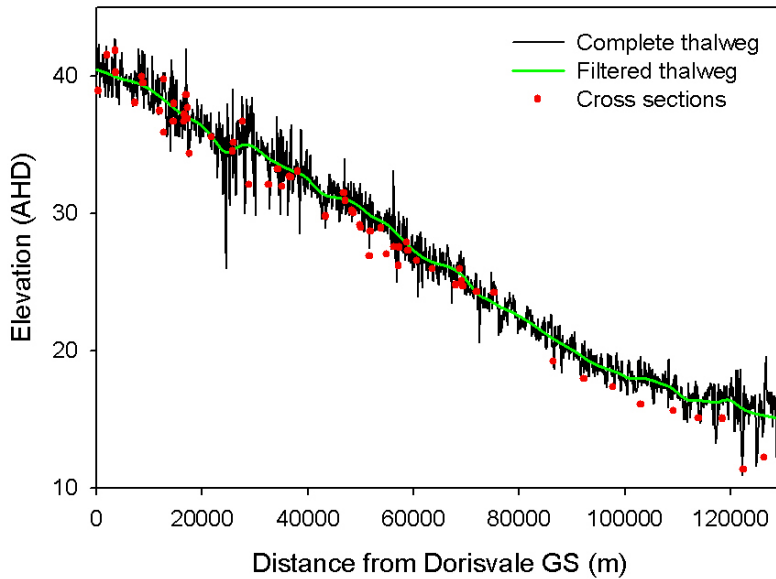


Figure 64 Thalweg of Daly River between Dorisvale GS and Beeboom GS measured during March 2001 (Georges et al., 2002).

Cross sections were measured at 19 control points during this survey and an additional 46 cross sections have since been measured within this river section (Valentine *pers. com.*). The locations of the cross sections in the river reach are also shown in Figure 64. It is apparent that the numbers of cross sections are inadequate to resolve the variations in channel depth between Dorisvale and Beeboom.

To address this issue, a strategy of grouping the cross sections according to a measure of the local water depth was tried initially. In this first scheme, the thalweg was first smoothed by filtering (Figure 64). A measure of the local depth was taken to be the difference in height between the filtered and unfiltered thalwegs ($= \Delta$). Subsequently, the measured cross sections were binned in 0.5m intervals and then averaged first across the left and right hand sides of the channel and then across the profiles in each bin. Thus, an averaged cross section was constructed for each 0.5m interval in Δ between $\Delta = -3.0$ to $+2.0$ m. Subsequently, cross sections for each of the 7220 measured thalweg depths along the river reach were constructed by selecting the averaged measured cross sections with matching Δ s in turn.

The resulting set of cross sections was used to run HEC-RAS. HEC-RAS simulated water level at each cross section and its output included the width of the water surface at each location. From Google Earth, the width of the water surface of the Daly River was measured at 339 locations. The comparison between measured and modelled widths is shown in Figure 65.

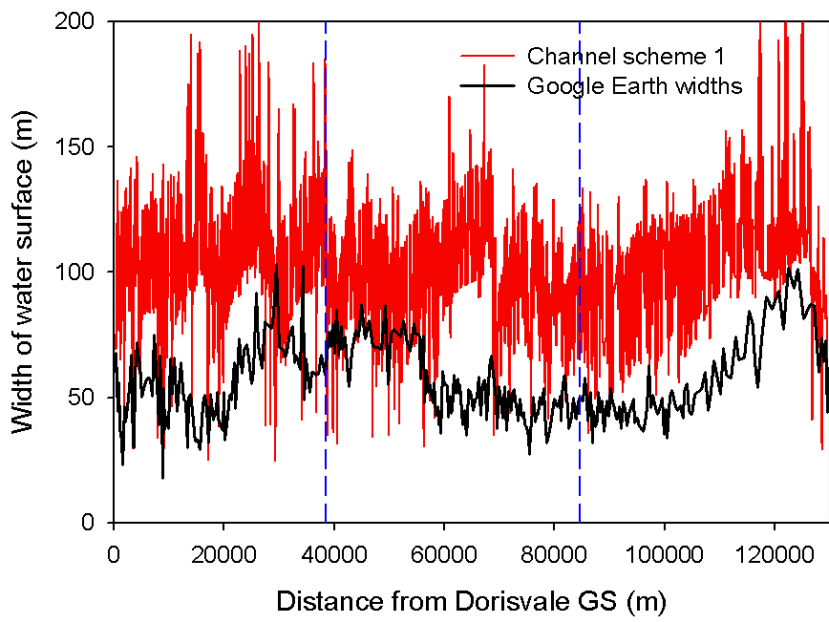


Figure 65 Comparison of channel widths obtained from Google Earth with those modelled using the first scheme for estimating channel cross sections. The vertical blue lines indicate the extent of the Google imagery of high resolution.

The Google Earth image of the Daly River section is a composite of images taken on several occasions. None of the dates of these images is known so flow conditions for the river could not be determined. The central section of the Google image has the highest resolution and clearly shows the river to be clear and well below its bank top. This image was certainly taken during a time of low flow during the dry season so for comparison purposes, the HEC-RAS model was run using low-flow conditions. These conditions were assumed to be $5\text{ m}^3\text{s}^{-1}$ at Dorisvale GS, increasing to $10\text{ m}^3\text{s}^{-1}$ at Stray Creek, and increasing by another $5\text{ m}^3\text{s}^{-1}$ at Oolloo crossing. These discharges are indicative of low flow conditions only. As will be shown later, discharges would need to be significantly greater than these to appreciably alter modelled channel depths and widths.

It is clear from Figure 65 that the widths of the river calculated using the first scheme for inferring cross sections are in poor agreement with the measured widths from one end of the river section to the other. Further, the small scale variation of the widths is much greater than observed. Making other assumptions about the river discharge rate or the bottom friction used in the model does not improve the degree of agreement significantly.

A second scheme for estimating cross sections was tested. Many of the measured cross sections showed the river channel to be characterised as having an approximately flat bottom with steeper banks (Figure 66). Accordingly, we shall assume that each cross section takes the form of having a flat bottom and uniformly sloping sides (Figure 67).

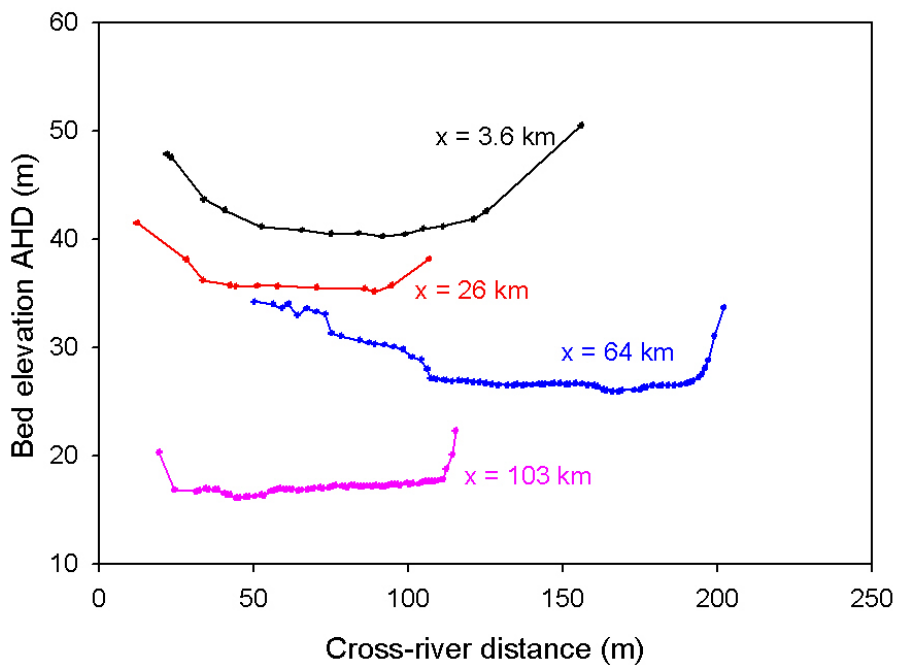


Figure 66 Selection of measured cross sections of the Daly River at the indicated distances downstream from Dorisvale GS.

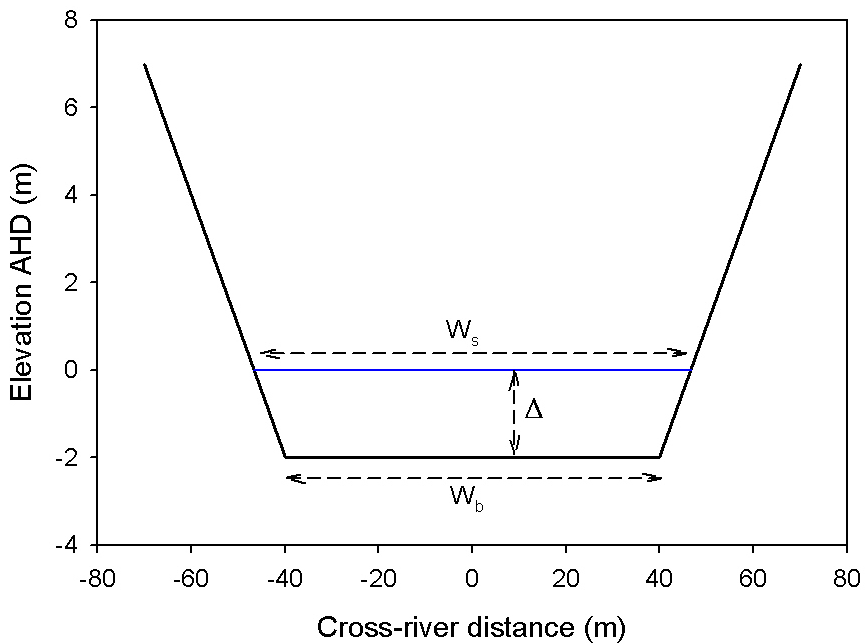


Figure 67 Trapezoidal river cross section assumed by the second scheme for representing cross sections.

The sides of the channel are assumed to have a uniform slope of 0.3. This slope was the median bank slope derived from an analysis of the measured channel cross sections. The position of the channel bottom is taken to be the elevation of the unfiltered thalweg (Figure 64) and the elevation of the water surface as a first

approximation is the elevation of the filtered thalweg (Figure 64). The width of the water surface (W_s) is estimated as its width as measured from the Google Earth images. Thus when $\Delta > 0$ as shown, the width of the channel bottom (W_b) is less than that of the water surface. However, when $\Delta < 0$, we set the width of channel bottom as being equal to that of the measured water surface.

HEC-RAS was run using the channel cross sections as specified by the above procedure. The model provides a modelled water surface elevation. Using this revised water surface profile along the river, we recalculate the water depths at each cross section and determine the width of the channel bottom (W_b) by matching the width of the water surface (W_s) to that in the Google images. Figure 68 compares the modelled widths of the water surface determined using the filtered thalweg as the reference elevation and using model simulated elevation profile. It can be seen that estimating the modelled channel widths as a two-step process results in modelled widths which are close to those measured. Further convergence on measured widths with more model iterations would occur, but we consider two iterations to be adequate considering the variability in measured widths.

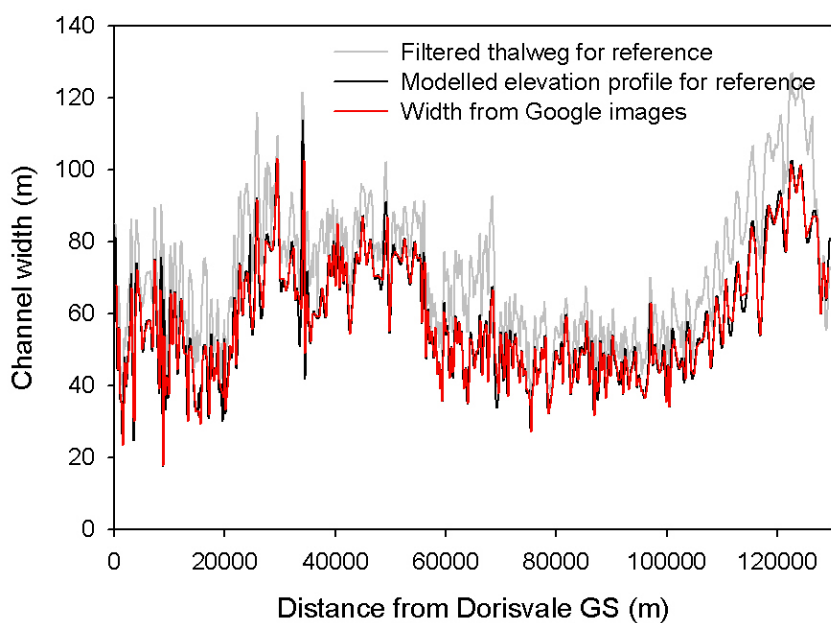


Figure 68 Comparison of modelled water surface widths using the filtered thalweg as the reference elevation and using simulated water surface elevation as the reference. Also shown are the widths measured using Google Earth images.

6.3. Application of hydraulic model

6.3.1. Specification of bed roughness

Besides the specification of channel geometry and discharge, HEC-RAS requires that values of the Manning's roughness coefficient along the channel be specified. This coefficient (n) depends on a number of factors including the roughness of the bottom (i.e. sand, pebbles, rock), the frequency and sizes of obstructions such as fallen trees or macrophytes along the banks, as well as some factors relating to channel shape

including whether the channel meanders and whether it changes depth or width frequently (Arcement and Schneider 1984). For sand channels, resistance to flow can arise from the roughness of the sand grains themselves, but also from form drag due to bed forms that develop or disperse according to the energy of the flow. Consequently, values of n are not only grain size dependent, but are flow dependent also (Figure 69). Table 37 provides ranges of n for bedforms that form as flow energy increases.

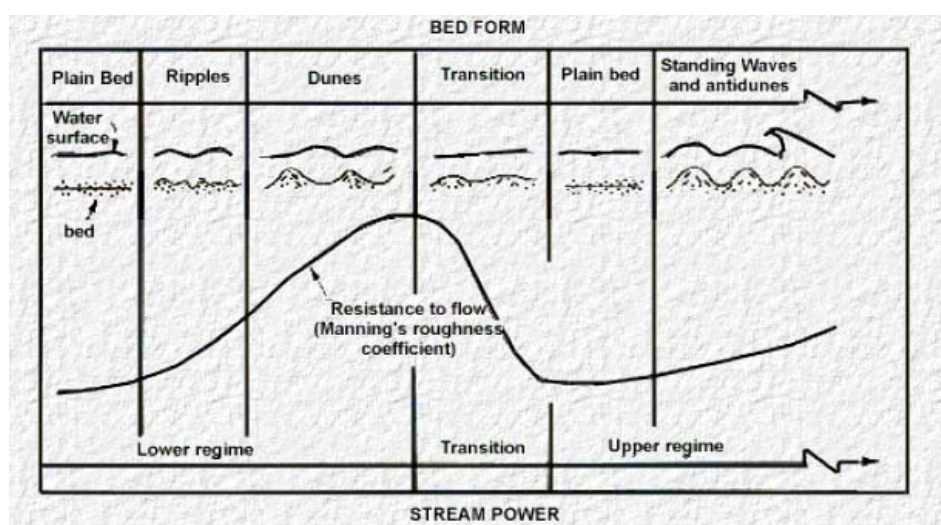


Figure 69 Bed forms and roughness in sand channels (Reproduced from Arcement and Schneider 1984)

Table 37 Roughness variations for alluvial streams (Reproduced from Simons 1985)

Bed Form	Range of Manning's n
Ripples	0.018 - 0.030
Dunes	0.020 - 0.035
Washed-out dunes	0.014 - 0.025
Plane bed	0.012 - 0.022
Standing waves	0.014 - 0.025
Antidunes	0.015 - 0.031

For the Daly River, during the July and August 2008 field trips, actively migrating dune structures were observed across relatively shallow sand areas between deeper pools. It seems that the deeper pools had smoother less active beds with a higher proportion of mud. Roughness for these pools would likely be closer to the $n = 0.012$ for the plane bed than to the roughness of other bed forms. Considering the range of bed forms encountered in the Daly during low flow conditions, we consider a representative value is likely to be ~ 0.025 .

The thalweg measurements obtained during 2001 (Georges, Webster *et al.* 2002) showed a water depth at Dorisvale GS of 10.42m and at Beeboom GS of 8.00m. Discharge at Dorisdale on the day this measurement was taken was $1050 \text{ m}^3 \text{s}^{-1}$, whereas at Beeboom it was $980 \text{ m}^3 \text{s}^{-1}$. Specifying these flows in HEC-RAS suggested that the best agreement between water depths at both sites taken together was obtained with $n = 0.035$. This value is somewhat higher than our assumed value for

low-flow times, but during high flows it is possible that channel obstructions such as trees growing on the banks would contribute significantly to channel roughness.

6.3.2. Low flow simulations

Stream gauging in the Daly River during September 2001 described by Tickell (2002) showed the river discharge at Dorisvale to be $\sim 11 \text{ m}^3 \text{s}^{-1}$. Springs near Stray Creek ($x \sim 35 \text{ km}$) increased the flow to $\sim 25 \text{ m}^3 \text{s}^{-1}$, and further discharges into the river increased the flow to $\sim 33 \text{ m}^3 \text{s}^{-1}$ downstream of the Daly's confluence with the Douglas River ($x \sim 117 \text{ km}$). Flows described by Jolly (2002) as 'average' for October 1982 are somewhat less than these. In October 1982, flows were $\sim 5 \text{ m}^3 \text{s}^{-1}$ at Dorisvale increasing to $\sim 19 \text{ m}^3 \text{s}^{-1}$ at Nancar which is $\sim 50 \text{ km}$ further downstream from Beeboom. Jolly suggested that the volumes of the spring flows into the Daly River during the dry season are determined by groundwater levels established during the previous wet season.

A representative flow in the Daly River between Dorisvale and Beeboom during the late dry season could be taken to be $Q = 20 \text{ m}^3 \text{s}^{-1}$. Here, we investigate properties of the hydraulic simulation for low flows of similar size. Figure 70 shows the thalweg and water level profile along the river channel for $Q = 20 \text{ m}^3 \text{s}^{-1}$ and $n = 0.025$. The water surface profile shows that most of the drop in elevation along the river section occurs in association with hydraulic break points occurring at high points in the river bed. The most pronounced of these occur at Oolloo Crossing and just upstream of Beeboom GS. In large part, the river at these low flows is characterised by a series of pools with a relatively low water surface slope that are backed up behind the break points. At hydraulic break points, the flow becomes supercritical. A consequence of supercriticality is that the elevation of the water surface downstream of the break point becomes independent of the water surface elevation above the break point. At the downstream end of the pools, the water elevation is set by the elevation of the bed at the break point and by the hydraulics in its vicinity. Within a pool upstream of a break point, the slope of the water surface is controlled by bottom friction. At low flows, friction is relatively weak within the pools so the water surface slope tends to be small.

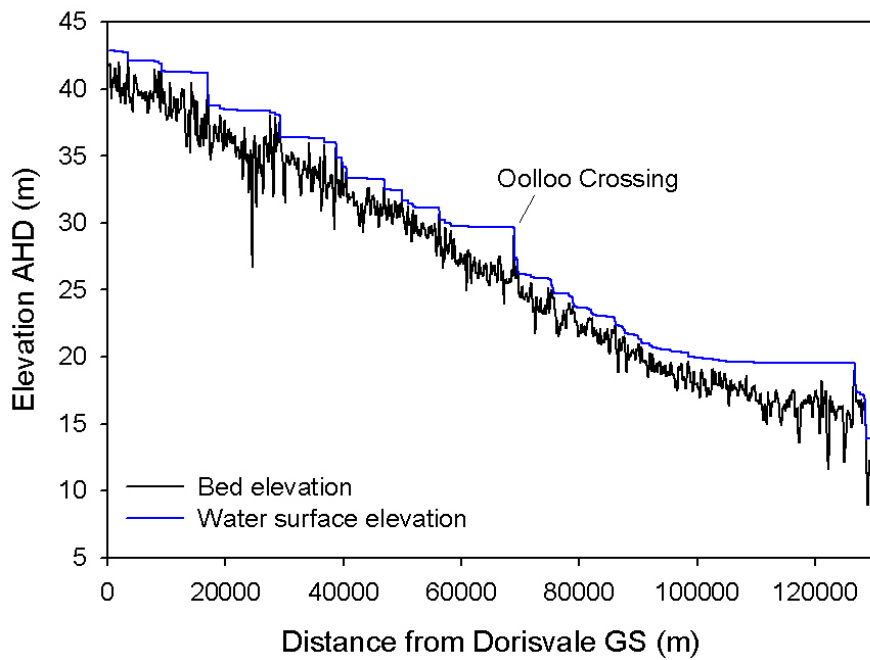


Figure 70 Model simulated water surface elevation for $n = 0.025$ and $Q = 20 \text{ m}^3\text{s}^{-1}$.

To demonstrate the sensitivity of the flow characteristics to the assumption of the friction parameter and to discharge volume, we compare hydraulic simulations for three values of Manning's friction coefficient (0.015, 0.025, and 0.035) which encompass the likely range of coefficients for the real channel. Three discharge rates are also considered, namely 10, 20, and $40 \text{ m}^3\text{s}^{-1}$. Figure 71 shows the effect of the selection of Manning's coefficient on average water depth along the 130-km river section.

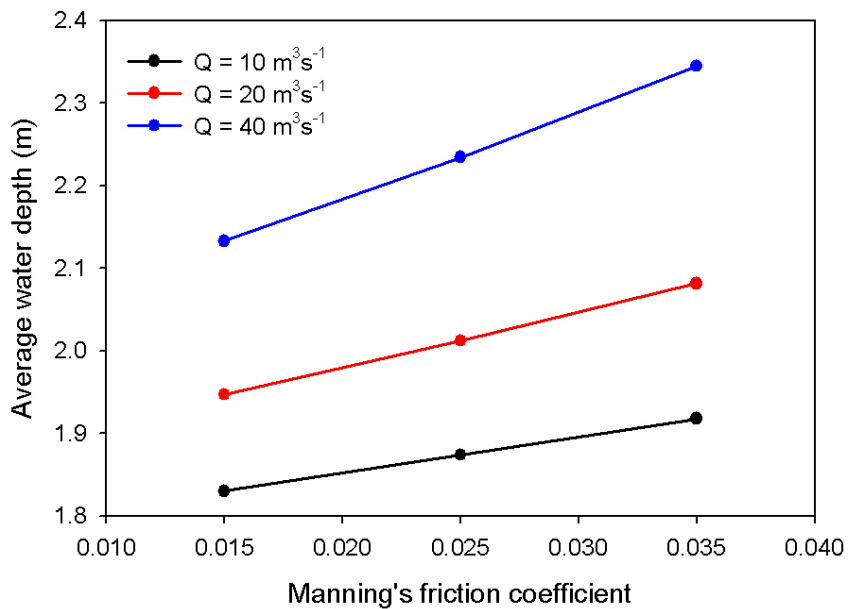


Figure 71 Effect of the selection of Manning's coefficient and of river discharge an average water levels between Dorisvale GS and Beeboom GS.

River depth increases with n for all flow volumes as one would expect. In effect, the greater the bottom friction the greater the slope in the water surface between the downstream end of each pool and its upstream end. For the smallest discharge of $10 \text{ m}^3 \text{s}^{-1}$, the change in average water depth when n is increased from 0.015 to 0.035 is less than 5% increasing to a change of 10% for $Q = 40 \text{ m}^3 \text{s}^{-1}$. Higher discharges both increase the water level near the hydraulic break points near the downstream end of each pool, but they also increase the water surface slope within the pools. For $n = 0.025$, average water level increases from 1.87m to 2.23m when discharges increases from 10 to $40 \text{ m}^3 \text{s}^{-1}$. We conclude from these results that for the dry-season low flows in the Daly River, the exact specification of the Manning's coefficient is not of major importance for determining water levels. Even for the highest discharge tested here, water depths within the river channel are dominantly determined by the positions and heights of the bed forms causing the hydraulic break points.

The submerged volume of the river channel increases as the average water depth increases. With $n = 0.025$, the modelled channel volume for $Q = 10 \text{ m}^3 \text{s}^{-1}$ is $1.42 \times 10^7 \text{ m}^3$ which increases by $\sim 24\%$ to $1.79 \times 10^7 \text{ m}^3$ when $Q = 40 \text{ m}^3 \text{s}^{-1}$. Thus, even though water depths increase by 0.36m with this discharge change, channel residence times, which are calculated as channel volume divided by discharge, decrease from 16.4 days to 5.2 days, a factor of more than 3.

6.4. Conclusions

A one-dimensional hydraulic model has been developed and applied to a 120 km reach of the Daly River. The model is suitable for prediction of water depth and current as it varies along the length of the river, and takes into account the impact of hydraulic breaks. Although the available hydraulic data were not sufficient to allow a full calibration of the model, a sensitivity analysis indicates that the results are not

very sensitive to the choice of Manning's roughness coefficient for the low flows typical of dry-season conditions.

Depth in the river is primarily determined by the influence of hydraulic breaks, and varies much less than would be predicted by a model that did not consider the influence of such breaks. A river bathymetry derived by interpolation between the available, widely spaced cross-sections, with no attempt to identify hydraulic breaks between these cross-sections, would not allow accurate hydrodynamic modelling

Current speed and residence time vary more strongly as a function of flow. In dry-season conditions, a four-fold increase in flow increased channel volume by only 24%, while residence time dropped by a factor of three.

Changes in dry-season flows are thus likely to affect the habitat of aquatic plants and animals more by altering current strength and shear stress than by altering the available habitat area and depth.

7. A dynamic model of primary production and plant coverage in the Daly River

7.1. Introduction

Plants, including algae, form the basis of the food web as well as being an important component of the habitat of aquatic animals and the aesthetic value of the Daly River. Changes in primary production (photosynthesis and subsequent growth and accumulation of plant biomass) and the relative abundance of different plants would lead to flow-on effects for the entire ecosystem as well as for the biogeochemical functioning of the river.

Previous work in the Daly River (Rea, Postine *et al.* 2002; Townsend and Padovan 2005; Townsend and Padovan 2009) has demonstrated that the Daly River is a low-nutrient system in which the velocity of water and shear stresses play a key role in determining the coverage and biomass of plants, particularly *Spirogyra* and *Vallisneria*. Process studies, monitoring and analyses described in earlier sections of this report have filled in many of the key knowledge gaps to allow development of more comprehensive models.

Here we build on previous work to develop a dynamic simulation model of plant coverage and biomass in the Daly River, which we will then use to explore possible scenarios for the future of the River.

The purpose of this model is three-fold:

- 1) To integrate knowledge derived from the process studies and monitoring described in previous chapters of this report and test our conceptual understanding of key processes affecting the succession of aquatic plants in the river;
- 2) To provide a tool to allow us to predict quantitatively the likely impact of changes in flow or nutrient concentrations on plants and algae in the Daly River.

Because of the number of assumptions that have been made in the development of the model, the results of scenario predictions must be considered speculative rather than conclusive; they do, however provide hypotheses that can be tested with further well-targeted process studies.

7.2. Methods

7.2.1. Model overview

Five benthic plant groups are represented in the model: *Spirogyra* (a benthic macroalgae), *Chara/Nitella* (benthic algae of more complex structure), *Vallisneria* (a flowering aquatic plant), *Schoenoplectus* (an emergent sedge), and periphyton (a mix of microalgae and bacteria that grows on submerged surfaces).

The rate of change in biomass of each plant group is a result of the balance between growth and loss. Growth is controlled by light, nutrient availability and availability of suitable substrate. Losses are due to physical sloughing (enhanced at higher flows), grazing, and mortality due to other causes such as viruses (often higher when plant density is high). Our numerical model uses the following formulation:

$$\begin{aligned}\frac{dC_i}{dt} &= C_i \mu_i - S_i - G_i \\ &= C_i \mu_{\max,i} f_{1,i}(I) \cdot f_{2,i}(N, P) \cdot f_3(C_1 \dots C_5) - S_i(u_*, C_i) - G_i(C_i)\end{aligned}\quad (1)$$

where t is time in days, C_i is the areal biomass ($\text{mg chl } a \text{ m}^{-2}$) of plant group i , μ_i is the current growth rate of plant group i (d^{-1}), S_i is the rate of sloughing under current flow conditions, G_i is the loss rate due to grazing and mortality other than through sloughing, $\mu_{\max,i}$ is the maximum growth rate of group i under optimal conditions, $f_{1,i}(I)$ is a function of light reading the bottom of the water column (I), $f_{2,i}(N, P)$ is the nutrient limitation function, a function of the dissolved inorganic phosphorus concentration in the water, P , the dissolved inorganic nitrogen concentration in the water, N , and the shear velocity at the bottom of the water column, u_* . $f_3(C_1 \dots C_5)$ is a function of the current areal coverage of all plants, representing limitation by self-shading and limited substrate as biomass approaches the maximum. S_i represents the rate of loss due to physical sloughing (breaking away of algal biomass, especially at higher flows), which is a function of u_* and C_i . The rate of loss due to grazing and other mortality, G_i , is a function only of C_i , as grazers and viruses are not explicitly represented in the model.

The rate of change of plant biomass with time, $\frac{dC_i}{dt}$, and hence a time-series of C_i , is calculated for each plant group for each physical habitat type (defined in section 7.2.6) in the model.

Growth rates for each plant group were derived from our own observational data or results from previous literature.

The model does not simulate stocks of other system components, such as nutrient concentrations in the water column or the fate of detrital plant material: where required, these are taken as time-varying inputs from observational data.

7.2.2. Growth rates

For *Spirogyra*, our observations show a maximum productivity of $16.65 \text{ mg C (g D.W.)}^{-1} \text{ h}^{-1}$, which occurred when *Spirogyra* was incubated at 25% of full surface light (Section 4.3.4). This productivity was observed in ambient nutrient-limited conditions and may represent fixation of carbon without a corresponding uptake of nitrogen and phosphorus and production of plant biomass, however we will take it as indicative of the maximum growth rate that might be achieved if sufficient nitrogen and phosphorus were available within the *Spirogyra* cells.

Spirogyra in the Daly River was found to have a carbon content corresponding to 33.5% of dry weight (Section 4). Earlier results (Townsend, Schult *et al.* 2008) found a similar value, with carbon accounting for 30% of total dry weight. Using the 33.5% figure and the observed maximum productivity, we arrive at a maximum growth rate of 0.05 h^{-1} . Assuming that growth occurs over eight hours of sunlight, this translates to maximum potential daily growth rate of 0.47 d^{-1} : significantly higher than the maximum growth rate of 0.224 d^{-1} reported by O’Neal and Lemby (1995). It is possible that this difference is due to a limited rate of nutrient uptake across the cell wall and incorporation of nutrients into plant biomass.

For *Vallisneria nana*, we had no growth rate data and were not able to find literature values. Hence we refer to the literature for a close relative, *Vallisneria spiralis*. Hutorowicz *et al.* (2008), observed a maximum rate of increase in leaf length over a one-month period corresponding to a maximum net daily growth rate of 0.057 , while Li and Xie (2009) observed a net growth rate of 0.046 d^{-1} in a greenhouse experiment involving the same species. These measurements were taken under natural environmental conditions with grazers present and other conditions not optimised. We apply a maximum gross growth rate of 0.1 d^{-1} , which provides a reasonable fit to our data. Measurements specific to *V. nana* in the Daly River are needed.

Similarly, we were unable to find literature data for *Schoenoplectus literalis*, so we must rely on results for other *Schoenoplectus* species. Zhang *et al.* (2009) report a relative shoot growth rate of $0.068 \text{ mm cm}^{-1} \text{ d}^{-1}$ for *S. validus*, while Tanner (1994) found that *S. validus* in piggery effluent doubled in approximately 85 days, suggesting a growth rate of 0.0082 d^{-1} in the absence of grazing pressure. Deegan *et al.* (2005), studying the estuarine species *S. triquetus*, reported maximum frond growth from 10 cm to 100 cm after 12 weeks, which translates to an almost identical net growth rate of approximately 0.0083 d^{-1} . Again, this is an observed net growth rate – after grazing and other losses – so the actual growth rate must have been higher if loss terms were significant. We use a value of 0.03 d^{-1} for the gross growth rate of *S. literalis* in our model.

Kufel and Kufel (2002) estimate a maximum growth rate of 8.1 mg C d^{-1} for *Nitella*. Our observations (Section 4) suggest that *Nitella* dry biomass contains $0.16 \text{ g C (g D.W.)}^{-1} \text{ d}^{-1}$. From this, we obtain a maximum daily growth rate of 0.051 d^{-1} . A slightly higher maximum daily growth rate of 0.06 m^{-1} is used in the calibrated model.

For periphyton, we have simply adopted a growth rate typically observed for phytoplankton: 0.3 d^{-1} . We note that this is much lower than the maximum carbon fixation rate assumed by Webster (Section 5.2.3) and there is a large degree of uncertainty in this figure. Again, data specific to the populations observed in the Daly River are required.

Table 38 Doubling rates used in the model.

Parameter	Value adopted	Subjective <i>a priori</i> estimate of uncertainty (i.e. calibration range)
$\mu_{\text{Spirogyra},\text{max}}$	1.47 d^{-1}	15%
$\mu_{\text{Schoenoplectus},\text{max}}$	1.03 d^{-1}	70%

$\mu_{Vallisneria,max}$	1.1 d ⁻¹	50%
$\mu_{Nitella,max}$	1.06 d ⁻¹	20%
$\mu_{periphyton,max}$	1.3d ⁻¹	70%

7.2.3. 2D hydrodynamic model

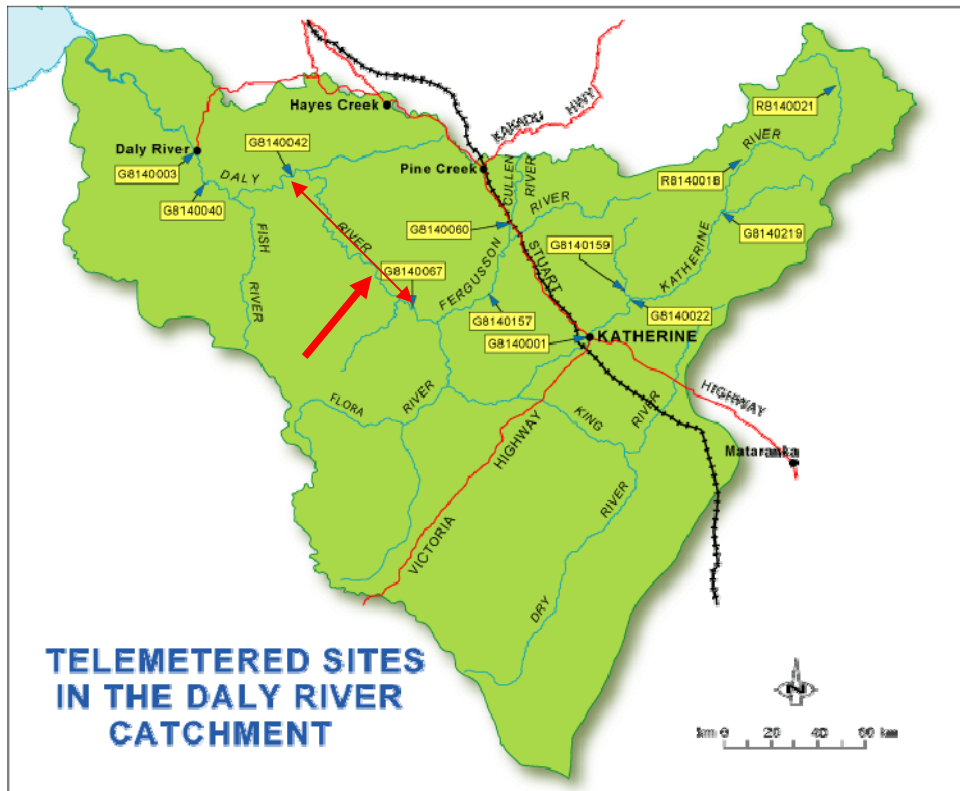


Figure 72 Model domain (indicated with red arrows).

Although we did not develop a hydrodynamic model as part of the model presented here, we use input from an existing hydrodynamic model developed as part of TRaCK project 4.1. Steady-state output of water depth and velocity from the reach-scale, two-dimensional, finite-element hydrodynamic model developed by Patil (*pers. comm.*) was obtained for a range of flows. This hydrodynamic model covers a reach of approximately 130 km length and provides velocities and depth for each of 42,030 nodes, representing approximately 8400 cross-sections within this reach (derived by interpolating between 50 measured cross-sections). It is assumed that there are no sources or losses of water within the domain (i.e. water flowing in at the upstream end is matched by outflow at the downstream end – any other sources and sinks such as groundwater exchanges and evaporation are ignored).

The model takes as input the stage height at the upstream end of the model domain. Steady-state results were obtained for stage-heights of 0.98, 1.33, 1.68, 2.01, 3.33, 4.58 and 5.74 m, corresponding approximately to flows of 25, 50, 75, 100, 200, 300 and 400 m³s⁻¹ at a telemetry station (G8140067) at the upstream end of the modelled reach (Figure 72).

The Patil model has not been verified, and has now superseded by an improved two-dimensional hydrodynamic model developed by Miloshis and Valentine (also as part of TRaCK 4.1). At the time of writing, results from the new hydrodynamic model have not been incorporated into the biomass model presented here; however this should be done as a matter of priority.

7.2.4. Depth and velocity as a function of flow

For each of the 42,030 nodes in the hydrodynamic model, 3rd-order polynomial fits were calculated between flow and depth, and between flow and velocity. Error estimates for these fits were obtained using the Matlab “polyfit” and “polyval” functions. These estimates were converted to relative errors and used to generate Figure 73. 50% of velocity estimates generated with these fitting functions have an estimated error (versus the estimated velocity obtained from the full hydrodynamic model) of less than 21%. Depth fits were less accurate: Fifty percent of results were returned with an estimated error of less than 43% of the fitted value.

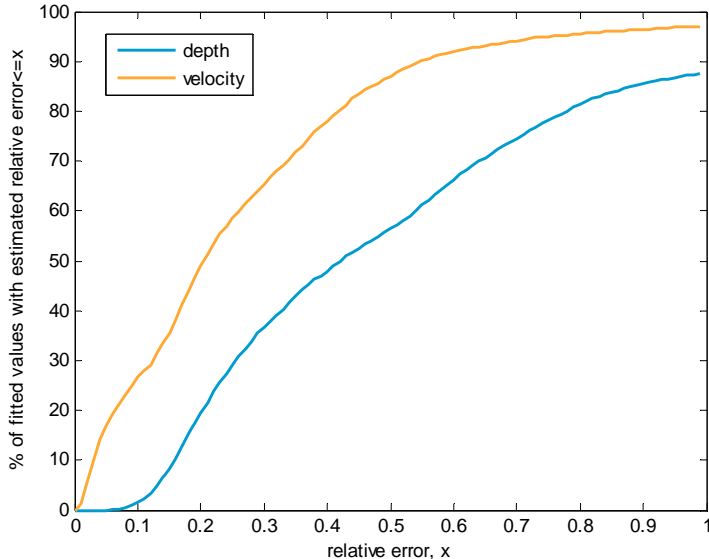


Figure 73 Error in predicting velocities and depths as a function of flow.

7.2.5. Friction velocity as a function of flow

Flow time-series were obtained from NRETAS records at station G8140067. Time-series of depth and velocity at each node in the model domain were obtained from flow using the polynomial functions described above. Minimum values of 0.01 m and 0.01 ms⁻¹ were applied in subsequent calculations.

The friction velocity, u_* , is given by Kays and Crawford (1993) as:

$$u_* = \frac{\tau_w}{\rho} = u \sqrt{\frac{c_f}{2}} \quad (2)$$

where τ_w is the wall shear stress, ρ the density of water (995.65 kg m⁻³ for pure water at 30°C), u is the bulk velocity (i.e. the velocity outside the influence of the bottom

boundary layer, in this case, the velocity from the two-dimensional hydrodynamic model) (ms^{-1}) and the friction coefficient, c_f , is obtained from:

$$c_f = 2g \frac{h}{u^2} \frac{\partial h}{\partial x} \quad (3)$$

where g is acceleration due to gravity (9.81 m s^{-2}), h is the depth of water (m), and $\frac{\partial h}{\partial x}$ is the slope of the surface (obtained for each node from the bathymetric grid of the hydrodynamic model).

This formulation produces friction velocities comparable (Figure 74) with those calculated by Townsend and Padovan (2009) (who used the formulation presented by Chow (1981)) when shear-stresses are moderate ($r^2=0.84$ when u^* by both methods $<0.1 \text{ ms}^{-1}$), but produces less extreme values at high velocities and takes into account the effect of slope. A comparison of the two methods for the depths, velocities and slopes used in the model is given as Figure 74.

Friction velocities were calculated for each node at each daily time-step.

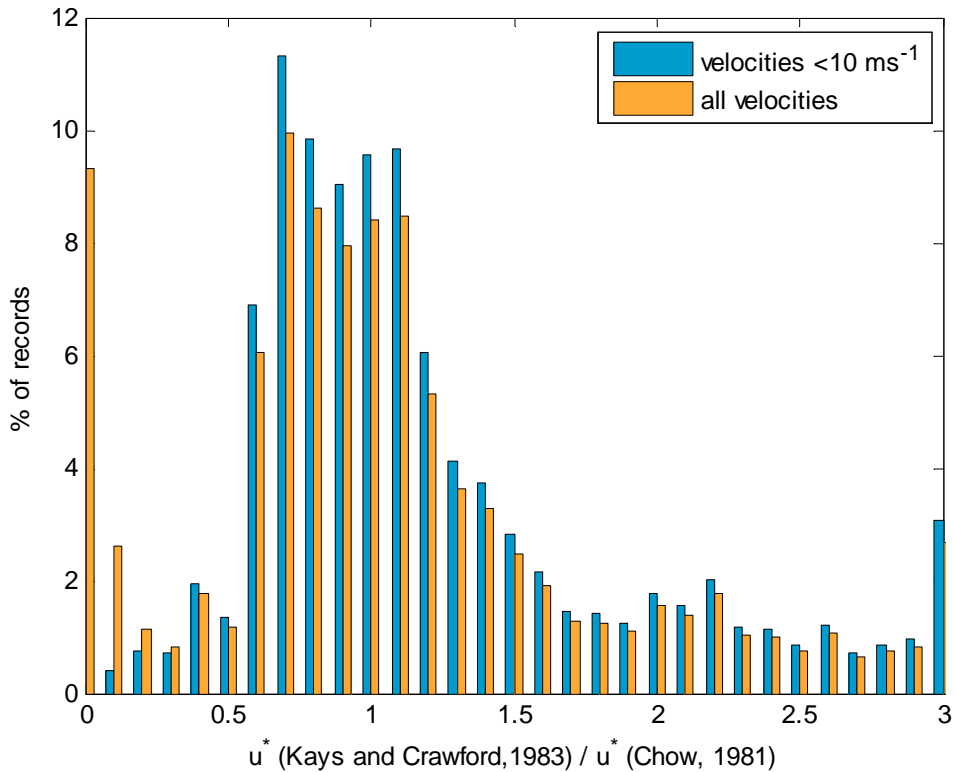


Figure 74 A comparison of shear velocities calculated using the formulation of Kays and Crawford (1993) with those calculated using that of Chow (1981).

7.2.6. Physical habitat categories

To simplify the model, the 42,030 nodes were grouped into 57 categories, hereafter referred to as “habitat categories”, each consisting of nodes that were functionally similar with respect to depth and shear velocity.

The 57 habitat types were generated by a set-up script that compared the flow-depth and flow-shear stress polynomials for each node described in Section 7.2.4, and grouped together those that were similar.

Cycling through each of the 42,030 nodes, if a node had not already been assigned to a previous category, a new category was created, with this node as its representative (for example, node 1 is the representative node for the first category). Each of the remaining unclassified nodes is then compared with this representative node. All nodes that match the representative node for both shear velocity and depth time-series with a root mean square error (r.m.s.e.) less than 0.05 are assigned to that category. The script then finds the next unclassified node, creates a new category, and repeats the process until >90% of nodes have been assigned to habitat categories. The remaining nodes are then categorised using the same procedure, but with a higher cutoff value for the r.m.s.e. match to prevent too many single-node categories from being created.

The distribution of the resulting categories was inspected visually to verify that the resultant groupings were reasonable in terms of their geographical distribution. For example, the nodal centres of a short section of river are plotted in Figure 75. Habitat category 1 is predominantly found along the outer edges of sharply curved sections of river, habitat category 2, in the centre of the channel, and so on.

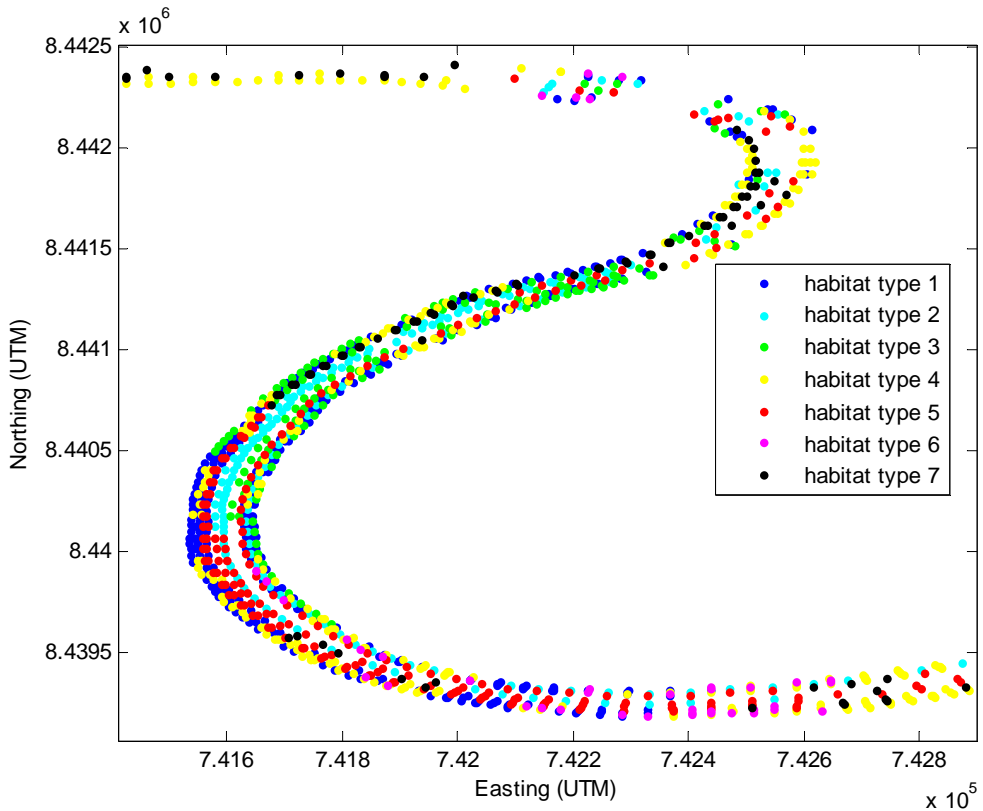


Figure 75 Location of nodes assigned to each of the first 7 habitat categories along a short section of river (colour-coded). Some nodes are not shown as they belong to none of the first 7 categories.

For each of the 57 habitat categories, the total area was calculated. Shear-velocity and depth time-series from the representative node were used in subsequent calculations to represent shear-velocity and depth variations for the habitat category as a whole.

Rea et al. (2002) observed that *Vallisneria* grow mainly in areas along the outer edge of curves in the Daly River, where velocities are lower and gravel substrates are more likely (though this species was occasionally observed in pools in the late dry season). In our model, we reflect this by limiting *Vallisneria* growth to the eight habitat categories identified as occurring mainly in such locations.

7.2.7. Light

Daily incident solar radiation, $I_0(\mu\text{E m}^{-2})$, was obtained from the SILO data drill (Jeffrey, Carter *et al.* 2001). These values were then converted to estimated daily average photosynthetically active radiation (PAR). Light incident at the bottom of the water column (i.e. at the sediment surface) in the absence of benthic plants was calculated from the light at the surface and the observed turbidity (Robson, Schult *et al.* 2010).

From data obtained during 2000 (Townsend *pers. comm.*), we obtain the following empirical relationship ($r^2=0.55$) for the relationship between turbidity (NTU) and the attenuation coefficient (k_d, m^{-1}) for photosynthetically active radiation (PAR) in the Daly River during the dry season:

$$k_d = 0.4677 \cdot turbidity^{0.5351} \quad (4)$$

Turbidity is derived from observed turbidity during the 2008 study period, as reported by Robson et al. (2010) (measurements were made at daily intervals for most of 2008).

PAR at depth z (m), I_z ($\mu\text{E m}^{-2}$), is then estimated from:

$$I_z = I_0 \exp(-k_d z) \quad (5)$$

For light limitation of production, we use:

$$f_{1,i}(I) = \tanh(I/I_{k,i}) \quad (6)$$

(Murray and Parslow 1997) where I_k a measure of the PAR at which saturation sets in (both in $\mu\text{Em}^{-2}\text{s}^{-1}$). As discussed in Chapter 5, there is no evidence that photoinhibition occurs in the system as a whole, though individual plants might be affected if exposed to full sunlight.

Values for I_k use in the model are given in Table 39. I_k for *Spirogyra* is derived from our own observations (Section 4.3.4) while values for other plants are derived from the literature (as described in Section 5.2.3), except for *Schoenoplectus*, which was not considered in Section 5.2.3. We were unable to find literature data relevant to *Schoenoplectus literalis*, so we resort to studies of other *Schoenoplectus* spp. Smith and Houpis (2004) found maximum carbon assimilation for *Schoenoplectus habitat* occurred at $1200 \mu\text{Em}^{-2}\text{s}^{-1}$. We have set $I_k, \text{Schoenoplectus}$ in our model to half this saturating value, i.e. $600 \mu\text{Em}^{-2}\text{s}^{-1}$.

Figure 76 shows time series of the strength of light-limitation for each plants during the simulation. At the start of the dry season, plant growth is light-limited where it is not more strongly limited by nutrient availability. By the end of the dry-season, however, there is little light limitation of most plants apart from that due to self-shading, as the water of the Daly River is clear and shallow. For *Schoenoplectus* with its high I_k , and low maximum growth rate, light-limitation remains substantial. For periphyton, light limitation continues to play a role (Figure 72). Overall, however, photosynthesis exceeds net carbon fixation (Reynolds 1997; Webster, Rea et al. 2005) and nutrient availability limits growth.

Table 39 Parameter values for light limitation of production

Parameter	Value adopted ($\mu\text{Em}^{-2}\text{s}^{-1}$)	a priori estimate of uncertainty
$I_{k,Spirogyra}$	350	50% (only one set of measurements available)
$I_{k,Schoenoplectus}$	600	50% (literature value for another species)
$I_{k,Vallisneria}$	179	30%
$I_{k,Nitella}$	70	30% (range of literature values for <i>Chara</i>)

$I_{k,periphyton}$

420

80% (varies with species composition)

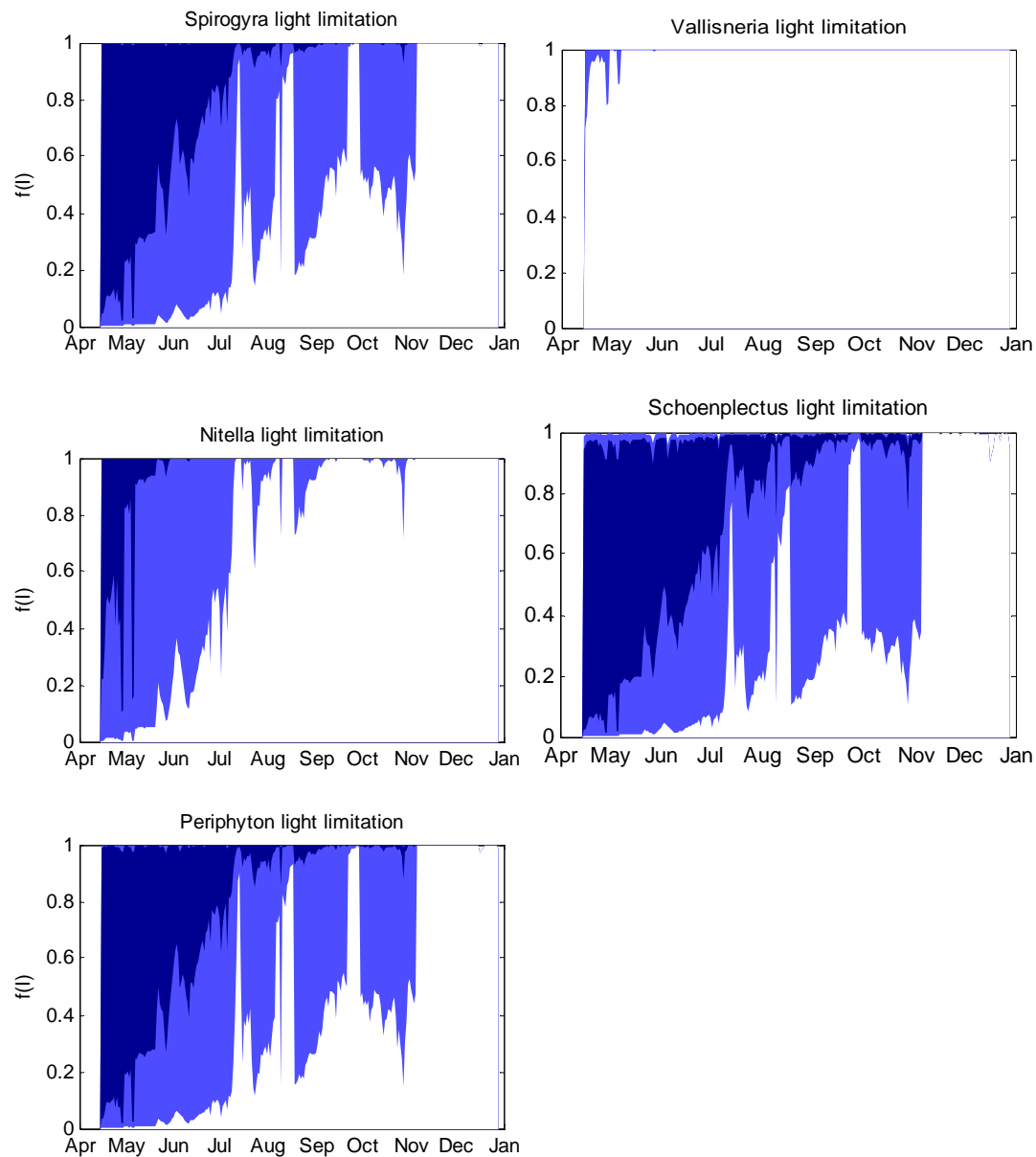


Figure 76 $f(I)$ for each plant group during the primary simulation period (April to December 2008). Dark blue areas span the 25-50 percentiles (weighted by geographical area), lighter blue areas show the full range of results (i.e. the bottom and top 25%). $f(I)=0$ means that no growth can occur due to strong light limitation, $f(I)=1$ means that light is such that the plant can grow at its maximum rate if other factors are optimal.

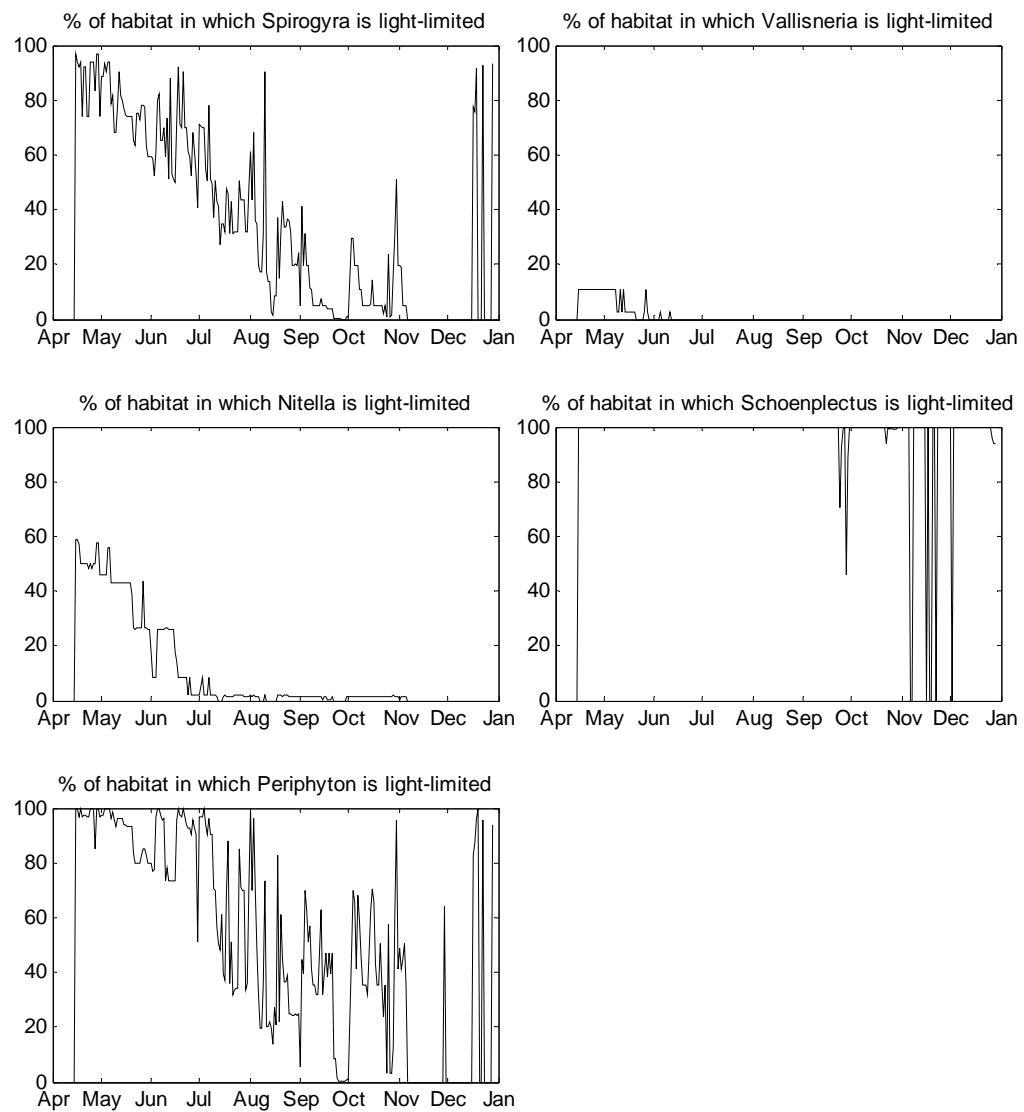


Figure 77 Percent of available habitat area in which light-limitation exceeds nutrient-limitation (i.e. $f(I) < f(N,P) < 1$) for each plant group.

7.2.8. Nitrogen and phosphorus requirements of plants

In the model, we will assume that chlorophyll *a*:N:P ratios of all plants remain constant at the average ratios measured during our 2008 field work and previous work in the Daly River. In reality, these ratios vary, however we do not have enough data regarding the variability of chla *a*:N:P ratios to constrain a more detailed model of plant nutrient stores.

The rate at which nitrogen must be supplied to a plant if it is to achieve its maximum growth rate, M_N ($\text{mg N m}^{-2}\text{d}^{-1}$), is then given by:

$$M_N = C_i \mu_{i\max} b_{i,N} \quad (5.7)$$

where $\mu_{i\max}$ is the maximum doubling rate $b_{i,N}$ is the amount of nitrogen stored in plant biomass per unit chlorophyll *a* ($\text{mg N/mg chl } a$). A corresponding formulation

applies for phosphorus. When the rate at which plants can take up nitrogen or phosphorus falls below M_N or the corresponding maximum phosphorus uptake rate, M_P , the growth rate is limited accordingly. Hence:

$$f_i(N, P) = \min\left(\frac{A_N}{M_N}, \frac{A_P}{M_P}, 1\right) \quad (5.8)$$

where A_N is the actual supply rate of nitrogen ($\text{mg N m}^{-2}\text{d}^{-1}$) and A_P is the actual supply rate of phosphorus ($\text{mg P m}^{-2}\text{d}^{-1}$).

It should be noted that *Vallisneria* and *Schoenoplectus* are rooted plants that may take up nutrients from sediments as well as water – indeed, it is possible that sediment nutrient stores are the primary nutrient source for these plants. In the absence of data from this study or the literature, however, the simple model applied here considers only uptake through the leaves of these plants and the fronds of benthic macroalgae. In the case of *Schoenoplectus*, this should make little difference, as the model suggests that this emergent plant is more often light- than nutrient-limited (Figure 77). In the case of *Vallisneria*, the importance of uptake through the roots warrants further investigation.

Nitrogen and phosphorus to chlorophyll *a* ratios

We base our N:P:chl *a* ratios on direct observations of plants in the Daly River (Section 4 and previous work by Townsend and Padovan, (2008)). Note that we use ratios by mass rather than molar ratios in this model.

Townsend and Padovan (2009) report that *Spirogyra* sampled in the Daly River in August 2002 was (by mass) 31% C, 2.6% N, 0.058% P and 0.27% chl *a*. This gives $b_{Spirogyra,N} = 9.6$ and $b_{Spirogyra,P} = 0.21$. Results from our biomass survey (Section 4.3.2) found $b_{Spirogyra,N} = 5.6$ and $b_{Spirogyra,P} = 0.12$. It is likely that these values vary considerably over the course of the dry season, depending on nutrient availability and carbon fixation rates.

For periphyton, we assume that the Redfield ratio applies, giving $b_{periphyton,N} = 7$ and $b_{periphyton,P} = 0.97$.

For other plant groups, the values used are based on the results of Schult and Townsend (Section 4, this report) and are given in Table 40.

Table 40 Nitrogen and phosphorus to chlorophyll *a* ratios used in the model

Parameter	Value adopted	Subjective <i>a priori</i> estimate of uncertainty (i.e. calibration range)
$b_{Spirogyra,N}$	9.6	50%
$b_{Schoenoplectus,N}$	3.2	50%
$b_{Vallisneria,N}$	4.0	50%
$b_{Nitella,N}$	2.8	50%

$b_{periphyton,N}$	7.0	50%
$b_{Spirogyra,P}$	0.12	60%
$b_{Schoenoplectus,P}$	0.30	60%
$b_{Vallisneria,P}$	0.51	60%
$b_{Nitella,P}$	0.22	60%
$b_{periphyton,P}$	0.97	60%

7.2.9. Nitrogen and phosphorus transfer and uptake rates

The rate at which an aquatic plant can take up nitrogen or phosphorus from the surrounding water is controlled by two factors: the flux rate of nutrients across the boundary layer surrounding the plant surface, and the rate of transfer of nutrients across the cell wall. In environments with higher nutrient concentrations, the rate of nutrient transfer across the cell wall is often the most important control. In the oligotrophic (low nutrient) Daly River, however, the flux rate across the boundary layer dominates.

In a flowing fluid, velocity gradates from the free-flowing “bulk velocity” at some distance from a solid surface to zero at the surface itself. The thin layer of water between the surface and the height above the surface at which velocity approaches the bulk velocity (often, arbitrarily, 99% of the bulk velocity) is known as the boundary layer. The thickness of the boundary layer depends on the characteristics of the flow and surface, including whether the flow is turbulent or laminar. Uptake of nutrients through the leaves or fronds of plants and algae combine with low velocities at the surface to produce a layer within which nutrients are depleted and can only be replenished by diffusion across the boundary layer.

The flux rate of nitrogen across the boundary layer, F_N ($\text{mg N m}^{-2} \text{ s}^{-1}$) is given by:

$$F_N = \frac{(N - N_0)D_N}{\partial_N} \quad (9)$$

where N (mg m^{-3}) is the concentration of dissolved inorganic nitrogen in the bulk flow of water (i.e. the concentration as determined from our monitoring programme), N_0 is the concentration at the leaf surface (set to zero to arrive at the maximum theoretic flux-rate if uptake is not limited by transfer across the cell wall), D_N is the diffusivity of dissolved nitrogen ($\text{m}^2 \text{s}^{-1}$) and ∂ is the thickness of the boundary layer in metres (Fram, Stewart *et al.* 2008; Stevens, Hurd *et al.* 2003). A corresponding formulation applies for phosphorus.

7.2.10. Nitrogen and phosphorus concentrations

In the absence of continuous records of nutrient concentrations, it was necessary in the model to make some assumptions regarding the variations in available nitrogen and phosphorus concentrations over time. Nutrient concentrations also vary along the length of the river (Chapter 2). For the sake of simplicity, spatial variability in nutrient concentrations is not taken into account in this model.

In this analysis, ammonium concentrations were considered negligible, as measured dry-season ammonium concentrations were generally below the laboratory detection limit (Section 0).

Water samples for nutrient measurements in the main channel of the Daly River were taken at irregular intervals throughout 2008. Measured nutrient concentrations were also available from previous studies conducted during 2000, 2001 and 2005. The available data were sufficient to establish an approximate relationship between flow and N (Figure 78), but not between flow and P (Figure 79).

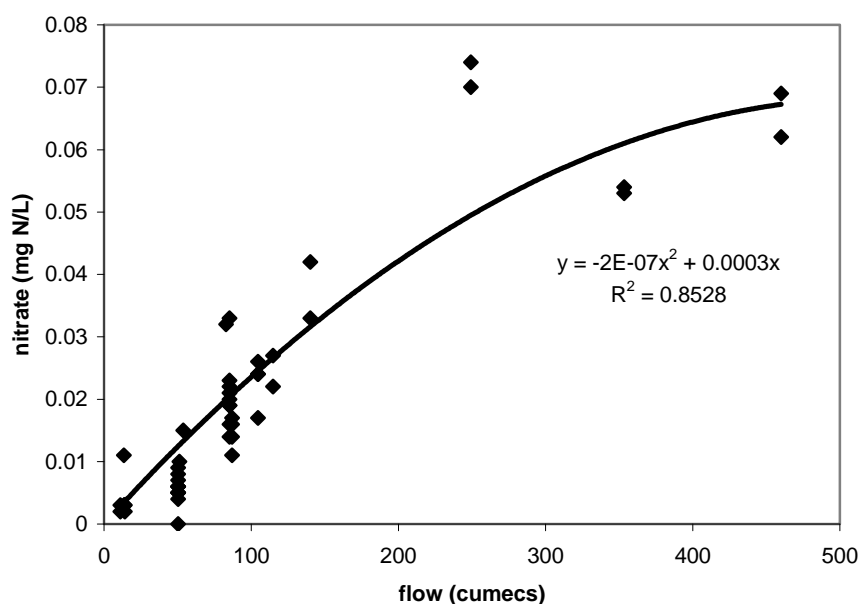


Figure 78 Flow versus measured nitrate concentration and a fitted curve excluding an outlier at $>1700 \text{ m}^3\text{s}^{-1}$. The fitted curve was applied in the model, restricting the calculated nitrate concentration to a maximum of $0.096 \text{ mg N L}^{-1}$ (the maximum observed value, which occurred during 2000) when flow exceeded $462 \text{ m}^3\text{s}^{-1}$.

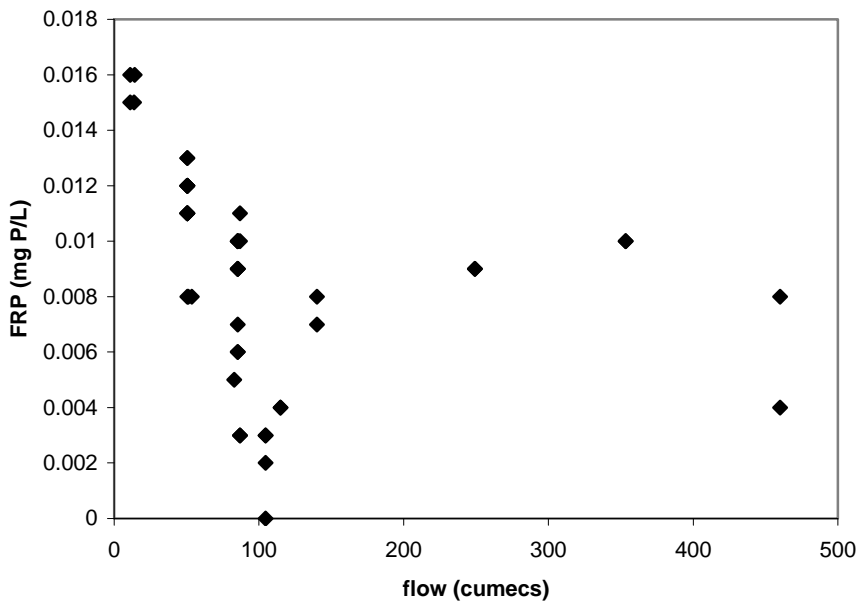


Figure 79 Flow and measured filterable reactive phosphorus.

To obtain daily values for P during the period of the simulation and beyond the 2008 observation period, the following idiosyncratic procedure was followed:

- 1) Where a measured filterable reactive phosphorus (hereafter, P) concentration were available for the date in question, P in the model was set to that values.
- 2) Where more than one data point for P was available on a given day, the mean of the data points for that day was taken.
- 3) Where two consecutive data points were taken within 28 days, concentrations for all days between these two points were obtained by simple linear interpolation.
- 4) For all other dates, it was assumed that P concentrations varied as a function of flow and month of the year:
 - a) If data points were available from other times during the same month of the year (even if in a different year) when flow was within 5% of the observed flow on the date in question, then the observed concentration at that time was applied (or the median, if more than one such data point was available). E.g. if there were no nutrient measurements within 2 weeks of 15 July 2008 but data were available from a period in July 2005 with very similar flows, P concentrations from July 2005 were applied to 15 July 2008.
 - b) If no such data points were available from the same month of the year, but data points existed for other times when the flow was within 5% of the flow on the date in question, the median of the observed P concentrations in these data were applied. E.g. if flows in July 2005 did not match flows in July 2008 but flows at some other observation time (say 5 August 2008 and 20 June 2005) were within 5% of July 2008 flows, the median P concentrations from those observation times were applied.

c) If there are no nutrient concentration data points for days with flows within 5% of the flow observed on the day in question, (a) and (b) are repeated using a weaker standard for matching flows that includes all flows within 50% of the flow on the day in question.

d) For the few remaining data points, nutrient concentrations from whatever observation time had the closest flow to the flow on the day in question were applied. This occurred only during wet-season conditions when nutrient limitation was unlikely to be the key factor limiting production.

The resulting time-series of N and P used in the model for the 2008 simulations are shown in Figure 80. There is, unfortunately, a high degree of error in P throughout the year and in both N and P at higher flows. The use of a Generalised Additive Model (GAM) to predict nutrient concentrations may be considered in future work. This approach would have the advantage of providing a quantitative estimate of error.

Investment in continuously logging optical instruments to measure nutrient concentrations may be advisable if these instruments can be shown to be accurate at the low nutrient concentrations typical of the Daly River. Better nutrient observations would improve both modelling results and monitoring of any changes in conditions.

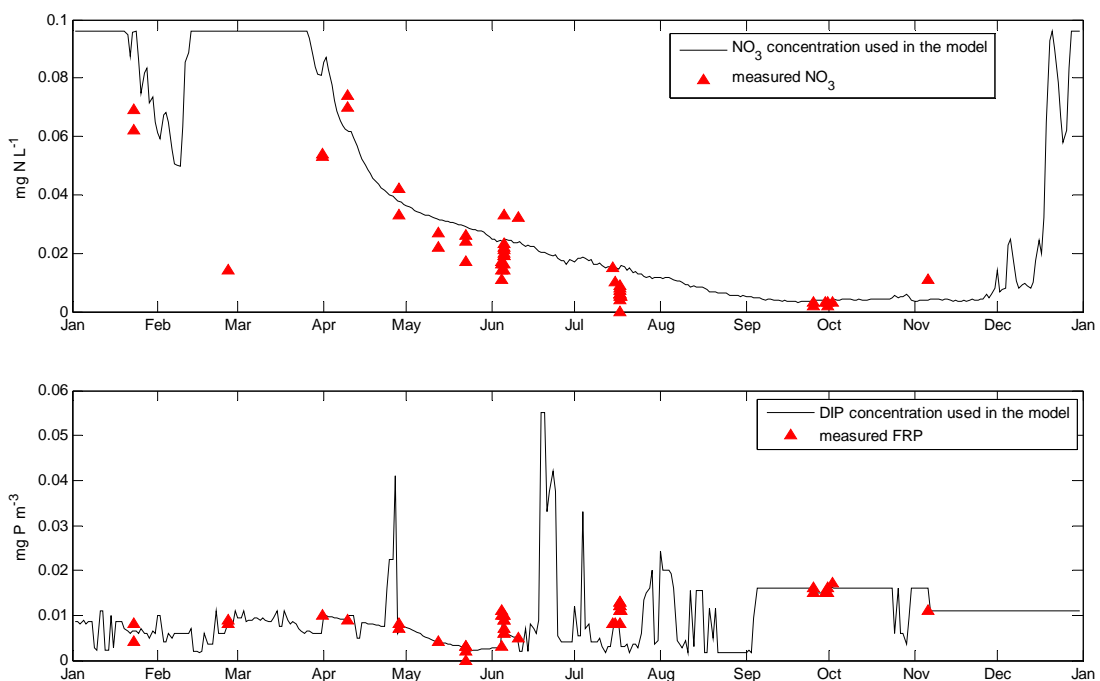


Figure 80 Nitrate (top) and dissolved inorganic phosphorus (bottom), showing both measurements in the main channel of the Daly River (red triangles) and time-series used in the model (black lines).

7.2.11. Boundary layer transfers

The diffusivities of nitrogen and phosphorus in water are functions of both temperature and salinity. The diffusivity of nitrogen in fresh water at the prevailing temperature, T ($^{\circ}\text{C}$), is given by:

$$D_N = \frac{(T + 273.15) \mu_{w25sea}}{(25 + 273.15) \mu_{wTfresh}} D_{N25sea} \quad (10)$$

($\pm 2\%$, $20 < T < 35^\circ\text{C}$) where μ_{w25sea} is the dynamic viscosity of seawater at 25°C (approximately $1.08 \times 10^{-3} \text{ Pa s}^{-1}$), $\mu_{wTfresh}$ is the dynamic viscosity of pure water at temperature T , and D_{N25sea} is the diffusivity of nitrogen in seawater at 25°C ($1.9 \times 10^{-9} \text{ m}^2\text{s}^{-1}$ for NO_x according to Li and Gregory 1974). A corresponding formulation applies to phosphorus, with D_{P25sea} approximately $7.43 \times 10^{-10} \text{ m}^2\text{s}^{-1}$ for HPO_4 (Li and Gregory 1974). For simplicity, we set T to a constant 30°C , which gives a $\mu_{wTfresh}$ of approximately $1.003 \times 10^{-3} \text{ Pa s}^{-1}$.

Following Hearn et al. (2001), we use the length scale of Batchelor (1967) as the boundary layer thickness applicable to nitrogen, δ_N :

$$\delta_N = \left(\frac{\nu D_N^2}{\varepsilon} \right)^{0.25} \quad (11)$$

where ν is the molecular viscosity of water (approximately 7.978 Pa s^{-1} at 30°C , Hearn et al., 2001) and ε is the rate of turbulent energy dissipation in the bottom layer, given as:

$$\varepsilon = \frac{\mu_*^3}{\kappa z_0} \quad (12)$$

where κ is the von Karman constant (0.4), z_0 is a roughness length scale (m) and μ_* is shear velocity.

z_0 for gravel (the primary substrate for benthic primary production in the Daly River, according to our observations) is approximately 3 mm, according to Soulsby (1997), however Clifford et al. (1992) state that "in natural gravel-bed channels, an empirical constant (6.8 or 3.5) has to be introduced to scale up the characteristic grainsize to represent the effective roughness length," and explain the reasons for this. Following this advice, we have adopted $z_0 = 0.0204 \text{ m}$. Note that this does not allow for the effect of plant coverage altering the roughness length as biomass accumulates over the gravel surface.

Table 41 Physical parameters. A 50% change in the value of z_0 would lead to a 16-19% change in the value of flux rates across the boundary (F_N and F_P).

Parameter	value adopted	estimated uncertainty
z_0	0.0204 m	50%

Initially, we set $A_N = F_N$ and $A_P = F_P$ (i.e. the flux-limited nutrient uptake rate equal to the boundary-layer transfer limited uptake rate) to explore the frequency with which nutrient uptake is limited by flux through the boundary layer.

The results of this initial analysis (not reported in detail here) indicated that the growth of all the plant groups considered, apart from *Schoenoplectus*, is constrained by transfer across the boundary layer during the dry season. Growth of *Schoenoplectus* was light-limited. Hence, we did not further consider the effects of delays in transfer across the cell walls of plants.

Given observed concentrations of available nitrogen and phosphorus, we can also calculate a minimum shear velocity for optimal growth, i.e. the lowest shear velocity at which $f_i(N, P)=1$. This value varies as a function of nitrogen and phosphorus concentration and biomass, however the median value over the duration of the simulation is 0.028 ms^{-1} . This is very close to the observed minimum optimum shear velocity of 0.025 ms^{-1} for *Spirogyra* accrual in the Daly River reported by Townsend and Padovan (2009). The close match gives us confidence that our model is adequately representing the physical dynamics involved, while the use of a dynamic model rather than simply directly applying the optimal shear velocity range reported by Townsend and Padovan (2009) allows us to extend the model to other plant species and simulate how the system might respond to variations in nutrient concentrations as well as flow.

7.2.12. Sloughing

Townsend and Padovan (2009) reported a maximum shear velocity for optimal *Spirogyra* accrual of 0.055 ms^{-1} . Above this shear velocity, physical stress breaks the algae, leaving fronds floating downstream. Although results from our dissolved oxygen logger that became entangled in such floating *Spirogyra* mass during the June 2008 field campaign suggest that such masses do continue to photosynthesise and respire, the relative effectiveness and the effective residence time of such damaged *Spirogyra* may be greatly reduced.

Other plants and algae are also subject to disruption at higher shear-stresses. In normal (moderate-flow) conditions, *Vallisneria* in the Daly River are believed to spread mainly through vegetative reproduction, as successful reproduction through fruit-setting occurs only at low flows ($<0.3 \text{ m}^3 \text{s}^{-1}$). *Vallisneria* beds may persist from year to year, but are intermittently scoured by large flow events that occur in some wet seasons (Rea, Postine *et al.* 2002). Following such an event, it is hypothesised that the plant must grow from seed, rather than through vegetative reproduction, so occasional periods of lower than usual flow may be necessary to the long-term success of *Vallisneria* (Rea, Postine *et al.* 2002). Recovery of previous *Vallisneria* coverage following a scouring event may take years.

Biggs *et al.* (1996) and Bouletreau *et al.* (2006) describe a model for flow-mediated loss, using the following formulation:

$$S_i = c_{\text{det}} Q(C_i - C_{i0}) \quad (5.13)$$

where c_{det} is a constant, C_{i0} is a “base” areal biomass of plant i and Q is the flow rate ($\text{m}^3 \text{s}^{-1}$). We adapt this formulation to reflect sloughing as a function of shear stress rather than flow, hence:

$$S_i = c_i \cdot u^{*2} (C_i - C_{i0}) \quad (5.14)$$

Where c is a constant. The relationship between S_i and Q will be system-dependent, and we do not have data for the Daly River. However, we arrive at a starting value for calibration of c for *Spirogyra* by multiplying the c_{det} applied by Bouletreau et al. (2006) by the mean Q/u^{*2} for the Daly River. Bouletreau et al. (2006) give c_{det} in the range 0.0016 to 0.0024 m⁻³. This gives us c_i in the range 86-129 m⁻²s². We use a value of 300 m⁻²s² in our model, which provides a better fit to our data. This value for c results in 80% sloughing of *Spirogyra* biomass per day at a friction velocity of 0.055 ms⁻¹, the upper limit for *Spirogyra* habitat defined by Townsend and Padovan (2009).

For periphyton, with its lower form and lower maximum coverage, we apply a slightly lower (calibrated) c_i of 200 m⁻²s².

For *Nitella/Chara*, we have no observational evidence, but apply a calibrated c_i of 30 m⁻²s⁻¹. *Schoenoplectus*, once established, may be more resistant to sloughing, so we apply a lower c_i , 20 m⁻²s².

For *Vallisneria*, we apply the same formulation, using a calibrated c_i of 100 m⁻²s². This plant, with its stronger leaves, may be less prone to sloughing than *Spirogyra* when mature, but more prone to disruption during establishment, however this simple model does not account for different life-stages. It has been observed anecdotally that *Vallisneria* beds are extensively scoured during some wet seasons (such as 2001), but not every year (Rea, Postine *et al.* 2002). After scouring, *Vallisneria* may take several years to re-establish from seed.

Table 42 Parameter values controlling sloughing.

Parameter	Value adopted (m ⁻² s ²)	Subjective <i>a priori</i> estimate of uncertainty
$c_{\text{Spirogyra}}$	300	50%
$c_{\text{Schoenoplectus}}$	20	500%
$c_{\text{Vallisneria}}$	100	50%
c_{Nitella}	30	50%
$c_{\text{periphyton}}$	200	50%

7.2.13. Substrate

Substrate in the Daly River varies. Stretches of sand alternate with gravel runs and deeper pools that have gravel or silty sand at the bottom. The sand ripples are highly mobile and do not provide suitable anchorage for plants. We found only a small chlorophyll *a* content and no larger plants in these ripples (Chapter 4). Gravel runs, by contrast, were extensively covered by macroalgae such as *Spirogyra* with some *Vallisneria*, while the edges of the river supported small *Schoenoplectus* beds in a few places. The deeper pools – generally only 2-3m deep – also supported macroalgae.

In the 10 km stretch of river used as a focus study site for the present study, approximately 40% of the substrate was covered by sand ripples (Figure 25). Estimates of sand extent from aerial photography for a 100 km stretch of the river

downstream of our model (Figure 81) domain suggest that this percentage is spatially variable and likely to be lower downstream of our focus stretch.

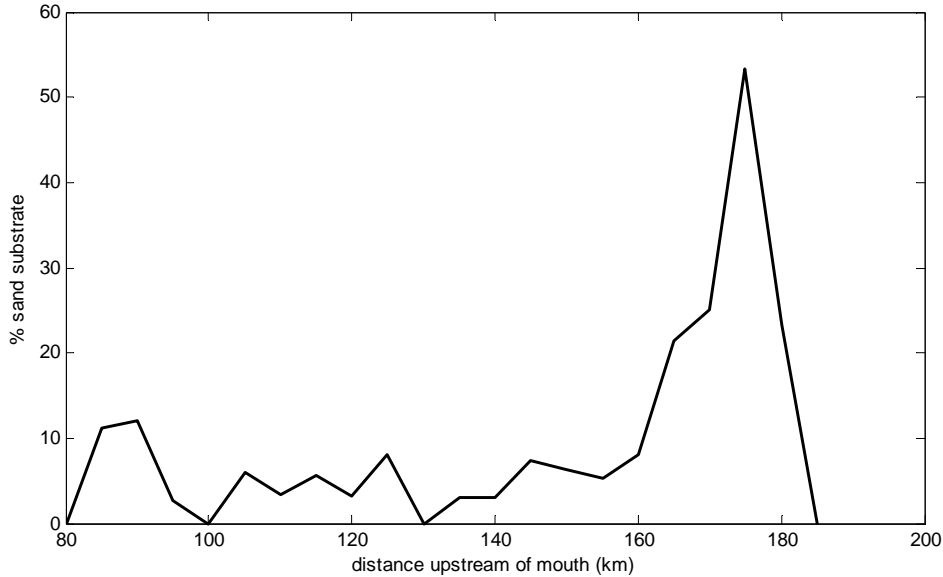


Figure 81 Estimated % sand substrate further down-river, from analysis of aerial photography (from data provided by Knight and Brookes, *pers. comm.*)

In our model, we do not specify the substrate for each node or each depth- and velocity-defined “habitat category”. It is assumed that the calculated biomasses apply to those stretches with a gravel substrate, while sandy stretches do not support benthic production.

7.2.14. Self-shading and competition for substrate

An area of gravel substrate can support a finite quantity of plants. This limit is determined by a combination of the amount of substrate available and the degree of shading (or self-shading) by existing plants. Rather than modelling the morphology and shading dynamics of each plant, we apply the following simplified formulation for limitation due to shading and limited substrate to all plant groups:

$$f(C_1 \dots C_5) = \max \left(0, \left(1 - \sum_{i=1}^5 \frac{C_i}{C_{\max,i}} \right) \right) \quad (5.15)$$

As coverage rises towards the maximum aerial coverage ($C_{\max,i}$) for any plant, growth of all plants declines towards zero. Parameter values defining the maximum aerial coverage of each plant are given in Table 43.

For *Spirogyra*, the maximum was set to the maximum value observed during 2008, 72.7 mg chl a m^{-2} , at which it was noted that there was “100% coverage” (Townsend and Padovan 2005).

For *Vallisneria*, the observed maximum reach average of 56 mg chl *a* m⁻² (Section 4.3.2) did not correspond to 100% coverage. Among individual samples, a maximum of 470 mg chl *a* m⁻² was measured. Studies of other systems have reported *Nitella* dry weights up to 500 g m⁻² (Kufel and Kufel 2002), though maximum values of 300g m⁻² are more commonly reported (Kufel and Kufel 2002; e.g. Schwarz and Hawes 1997). *Vallisneria* samples from the Daly River were found to be about 0.14% chlorophyll *a*, by dry weight (Section 4.3.2). Hence, a dry weight of 300g m⁻² equates to approximately 420 mg chl *a* m⁻².

For *Schoepplectus*, we have no data regarding maximum coverage, though the maximum observed during our 2008 study was only about 0.2 mg chl *a* m⁻² (Section 4.3.2). We set an arbitrary maximum of 60 mg chl *a* m⁻² through calibration of the model. *Schoenoplectus* was allowed to grow only in suitable habitat along outer curves of the river, as discussed under “habitat types”.

For periphyton, coverage up to 33 mg chl *a* m⁻² has been observed in the Daly River (Schult, Townsend *et al.* 2007) while coverage in other systems reaches nuisance levels up to 65 mg chl *a* m⁻²; the value we adopt as the maximum in this model.

Table 43 Maximum areal biomass for each plant (parameter values and uncertainty estimates).

Parameter	Value adopted (mg chla m ⁻²)	Subjective <i>a priori</i> estimate of uncertainty
$C_{max,Spirogyra}$	72.7	20%
$C_{max,Schoenoplectus}$	60	200%
$C_{max,Vallisneria}$	66	40%
$C_{max,Nitella}$	420	70%
$C_{max,periphyton}$	64	20%

Shallow areas of the river channel dry completely when flow is very low. When this occurs, *Schoenoplectus* is allowed to survive, but biomass of other plants is reset to the minimum.

7.2.15. Grazing and mortality

The final element included in the model is loss of plant biomass due to grazing by fish, turtles, invertebrates, birds and other animals or due to cell lysis (often a function of viral infection). Both of these pressures increase as plant biomass increases, as higher biomasses support larger grazer populations and enhance the spread of viruses. Since our model does not explicitly represent either grazers or viral infection, we employ a common quadratic loss term:

$$G_i = g_i C_i^2 \quad (5.16)$$

Values of g_i for each plant group were obtained by calibration of the model, and are given in Table 44.

Table 44 Parameter values controlling grazing and lysis.

Parameter	Value adopted (d ⁻¹)	Subjective <i>a priori</i> estimate of uncertainty
-----------	----------------------------------	---

$g_{Spirogyra}$	0.003	200%
$g_{Schoenoplectus}$	0.0001	200%
$g_{Vallisneria}$	0.0001	200%
$g_{Nitella}$	0.0001	200%
$g_{periphyton}$	0.005	200%

7.2.16. Time-steps and initialisation

The model was initialised with minimal plant biomass at the start of the 2008 dry season (1 April). Minimum values were set to 0.1 mg chl $a\ m^{-2}$ for periphyton, 0.01 mg chl $a\ m^{-2}$ for *Schoenoplectus*, and 0.02 mg chl $a\ m^{-2}$ for other plants. The model was then stepped forward with a daily time-step, forced with estimate N and P concentrations, flow and light.

7.3. Results

The simulated aerial biomass of each of the five plant groups included in the model is given in Figure 82 to Figure 86, with observational results overlain. Observations taken at the same station at different times are connected by dashed black lines. The low resolution of the bathymetric data mean that it is not practical to attempt a point-by point comparison of observations with model results. Instead, we present the model results in terms of statistical probability. In each of the figures below, the lighter blue area indicates the full range of model output (for areas with suitable substrate). The apricot-coloured line indicates the mean value. The darker blue area delineates the region between the 25th and 75th percentile, weighted by geographical area. In other words, if the model were perfectly correct and the sampling sites chosen at random (within areas of suitable substrate), we would expect around 50% of the observational data points to fall within the dark blue band, and all data points to fall within the lighter blue area.

The model successfully reproduces the general ranges and relative abundance of the five plant groups, and shows a transition from a *Spirogyra*-dominated system in the early dry season to an increased abundance of *Nitella/Chara* and macrophytes later in the dry season.

The model underestimates the degree of spatial variability in *Spirogyra* (Figure 82) in September and November and probably over-estimates *Spirogyra* biomass in the mid dry-season. The high spatial variability simulated in the early part of the dry season is due mainly to spatial variations in shear velocity as flows recede following the wet season. Later in the dry season, lower shear velocities limit nutrient uptake by this fast-growing alga, and biomass is reduced, increasing a little in December in response to early pre-wet-season increase in flow and nutrient concentrations. The lower spatial variability later in the dry season, relative to observational data, may indicate the simplified topography of our model system (which reduces the complex bathymetry to only 57 “habitat types”), or it may reflect the influence of grazing on *Spirogyra* in the real system. Our model does not take into account the feeding and habitat preferences of the animals that consumer *Spirogyra*.

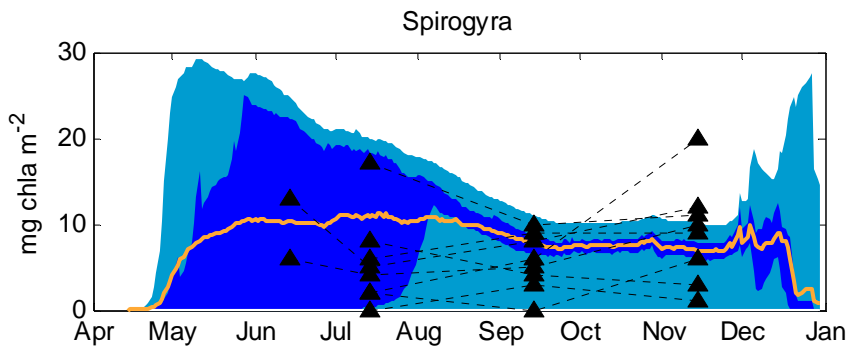


Figure 82 Simulated and observed *Spirogyra* biomass during 2008. The outer (light blue) areas indicate the full range of model results, the inner (dark blue) bands represent the 25th-75th percentile (by area). Solid lines indicate the mean, and black triangles, 2008 observations.

At the sampling sites in our study, both *Vallisneria* (Figure 83) and *Nitella/Chara* (Figure 84) increased gradually in the early part of the dry season, reaching a maximum in the mid-late dry season. The model reproduces this general pattern in both plants, but again, underestimates the degree of spatial variability. It may also underestimate the early growth of both species and over-estimate the late dry-season growth of *Nitella*. In the case of *Vallisneria*, it is possible that early growth is enhanced by remnant plants or roots that have survived through the wet-season: this possibility is not included in the model. In the case of *Nitella*, it is likely that we have not adequately specified the parameter values, given our reliance on literature values from other systems and complete lack of data regarding sloughing. Process studies of *Nitella* and/or *Chara* responses in the Daly River would improve our ability to model these species. Another possibility is that the model does not adequately represent changing grazing pressures over the course of the dry season.

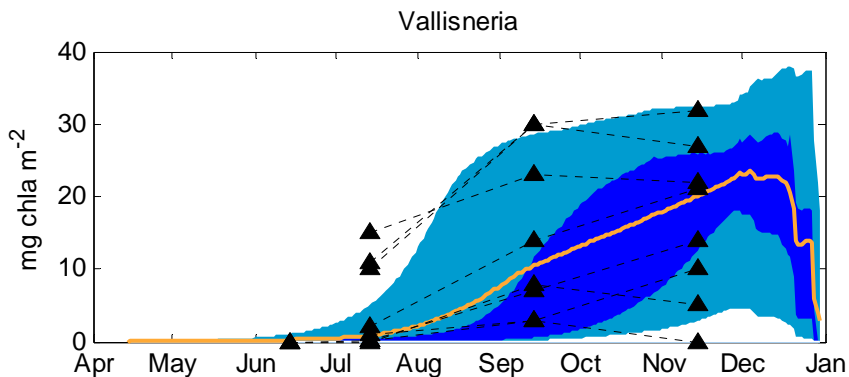


Figure 83 Simulated and observed *Vallisneria* biomass during 2008. The outer (light blue) areas indicate the full range of model results, the inner (dark blue) bands represent the 25th-75th percentile (by area). Solid lines indicate the mean, and black triangles, 2008 observations.

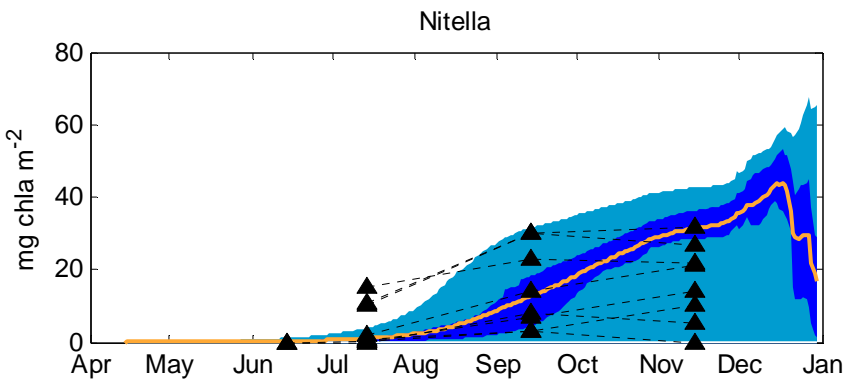


Figure 84 Simulated and observed *Nitella* biomass during 2008. The outer (light blue) areas indicate the full range of model results, the inner (dark blue) bands represent the 25th-75th percentile (by area). Solid lines indicate the mean, and black triangles, 2008 observations.

Schoenoplectus biomass (Figure 85) was low, and grew slowly, both in the model output and in the field observations. This plant often does well in eutrophic (high nutrient) systems, and is used in sewage treatment wetlands (e.g. Zhang, Rengel *et al.* 2009), so it might be expected to grow more strongly if nutrient concentrations were to increase. Given the low biomass and limited observational data, it is impossible to be confident that the model correctly simulates the dynamics of *Schoenoplectus*.

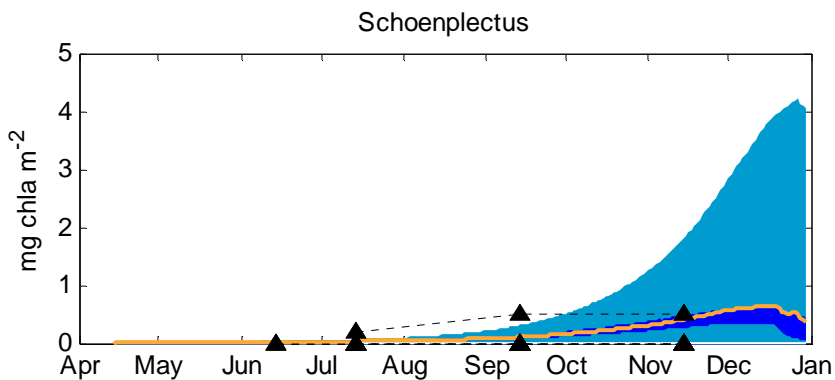


Figure 85 Simulated and observed *Schoenoplectus* biomass during 2008. The outer (light blue) areas indicate the full range of model results, the inner (dark blue) bands represent the 25th-75th percentile (by area). Solid lines indicate the mean, and black triangles, 2008 observations.

Periphyton biomass is relatively low and relatively consistent throughout the 2008 dry season in both the model and observational results (Figure 86), but shows more spatial variability than most of the other plants simulated.

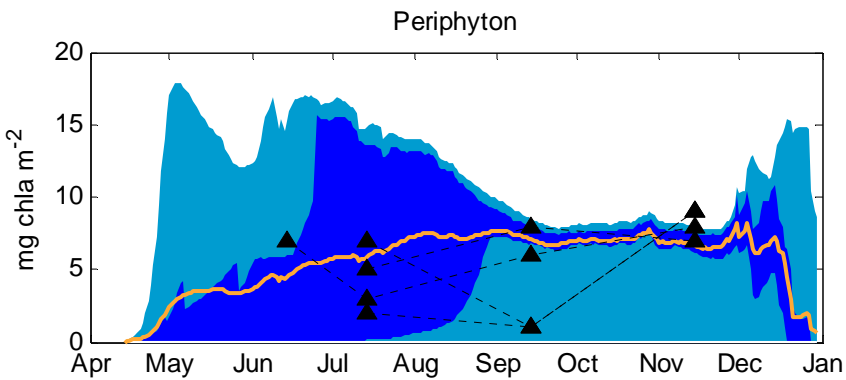


Figure 86 Simulated and observed periphyton biomass during 2008. The outer (light blue) areas indicate the full range of model results, the inner (dark blue) bands represent the 25th-75th percentile (by area). Solid lines indicate the mean, and black triangles, 2008 observations.

7.3.1. Photosynthesis and primary production

The model can also be used to calculate the rate of photosynthesis necessary to support the simulated growth of benthic plants if we assume a fixed C:chl *a* ratio for each plant group, a 1:1 ratio between carbon fixed and O₂ released, and also make some assumption regarding the proportion of benthic habitat within the 130 km stretch of river modelled that is suitable substrate for plant growth (i.e. not covered with sand ripples). We will assume that this figure is 40%.

Figure 87 shows the results of this calculation. The resulting figures are much lower than the actual photosynthesis rates calculated in Chapter 5: 0.050 mmol O₂ L⁻¹ in July, 0.074 mmol O₂ L⁻¹ in September and 0.090 mmol O₂ L⁻¹ in November. It has been noted previously (Webster, Rea *et al.* 2005) that much of the photosynthesis occurring in the Daly River is likely released as extracellular carbohydrates rather than being incorporated into plant biomass, due to the strong nutrient limitation of the system. The difference between the photosynthesis required to support plant growth calculated here and the actual photosynthesis calculated in Chapter 5 gives a measure of the amount of carbon that is fixed but does not contribute to the production of plant biomass.

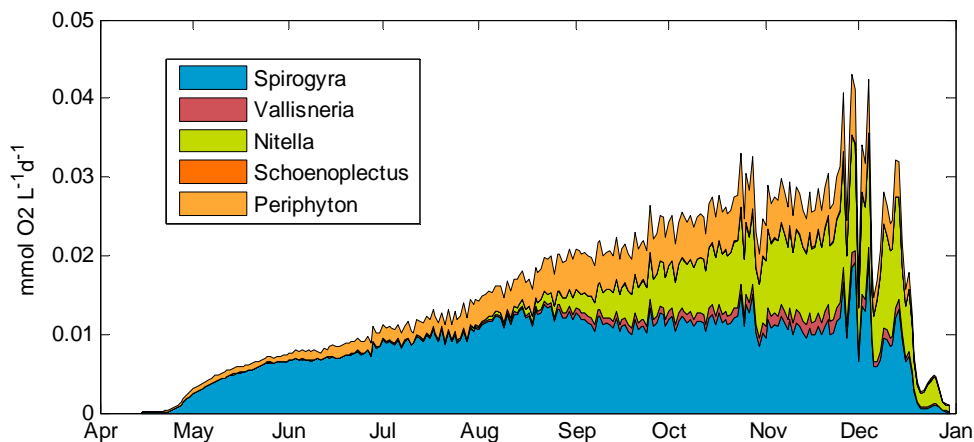


Figure 87 Photosynthesis required to support plant growth.

7.3.2. Nitrogen and phosphorus stores

Model outputs can be converted to nitrogen and phosphorus stores if we again assume fixed N:P:chl *a* ratios and that 40% of the river bed provides suitable substrate.

The total nitrogen and phosphorus stores in all five benthic plant groups gradually increase over the course of the dry season (Figure 88 and Figure 89). Water-column dissolved inorganic nitrogen (DIN) and dissolved inorganic phosphorus (DIP) gradually drop until DIN and DIP concentrations approach the detection limit in early September. Estimated total water column nitrogen and phosphorus stores (obtained by multiplying measured TN and TP concentrations in water samples from the main channel of the Daly River by the estimated volume of water in this section of river) decline faster than DIN and DIP stores in the first few months of the year, and continue to decline until the last measurement in November 2008, as simulated benthic plant stores continued to increase. The initial rapid decline in TN and TP stores in April to June may be associated with deposition of sediments on the river bed (Section 3.3.3), particularly in deeper pools, as water velocities decline in the early part of the dry season. Nutrients associated with these sediments may subsequently become available through gradual bacterial degradation.

Surface sediments along the muddy banks of the river were found to contain on average 590 mg N kg^{-1} and between 275 mg P kg^{-1} during our June survey (Section 3.3.4). The means for samples taken in September were lower: 510 mg N kg^{-1} and 271 mg P kg^{-1} . This suggests that sediment nutrient stores may indeed have acted as a source of nutrients to plants between the two surveys. Sediment nitrogen and phosphorus concentrations in samples from pools and gravel beds, however, showed an apparent increase over the same time period. This could be due to continued transfer of organic material to these sites, and subsequent deposition. It is likely that the growth of algae enhances the trapping of fine material. The strong spatial patchiness of sediment nutrient concentrations, however, makes overall sediment sources or sinks difficult to quantify from this information alone.

When dissolved inorganic nutrient concentrations in the water column drop to very low levels in the mid dry season, benthic plant biomass must be sustained by recycling of nutrients within the plant beds, degradation of organic detrital material in the water column or deposited sediment stores, or by new inputs (e.g. from atmospheric deposition or leaf litter). Understanding the transfer of nutrients from the water column to plant stores is complicated by the open nature of a river: nutrients are introduced to this stretch of the river with water flowing from upstream, and nutrients that are not taken up in the time taken for water to traverse this stretch of river are lost downstream. Nonetheless, water column nutrient stores and deposited organic stores are sufficient to account for the increase in plant biomass over the dry season.

The maximum benthic plant nitrogen store of approximately 2.6 t of nitrogen in this stretch of the river represents only a tiny fraction of the total nitrogen load carried by the river during the wet season (approximately 3350 t, see Chapter 2).

Simulated plant nutrient stores drop and water column stores rise at the start of the next wet season, when plant beds are disrupted by higher flows.

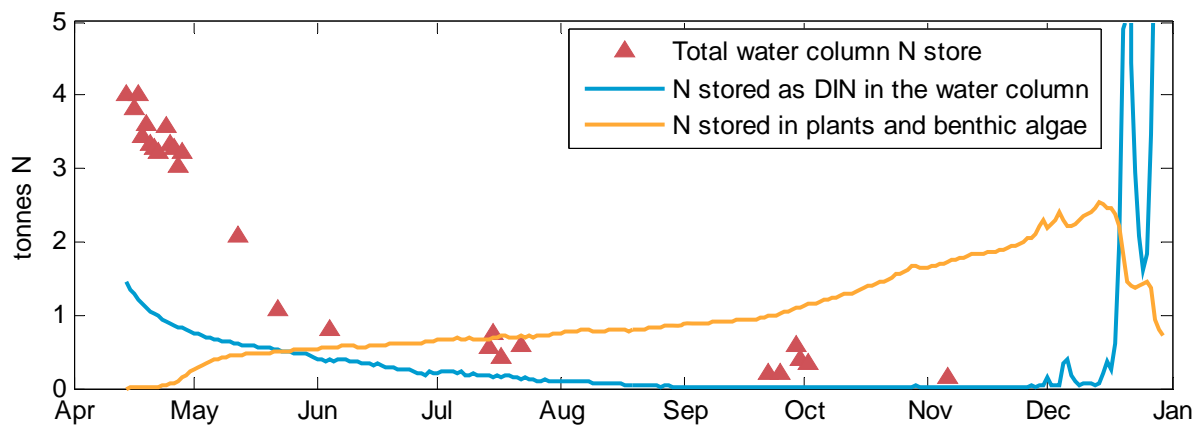


Figure 88 Changes in estimated water column and benthic plant nitrogen stores over the course of the 2008 simulation.

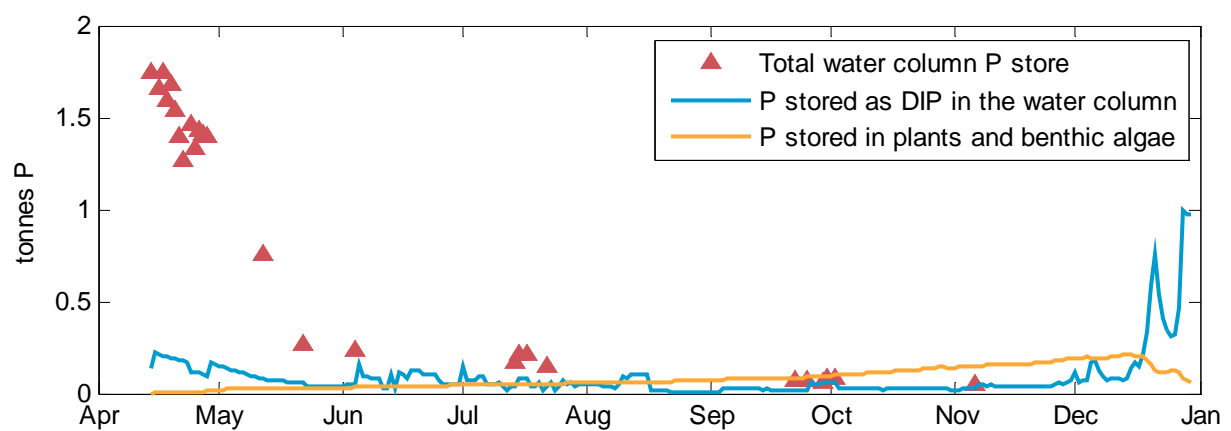


Figure 89 Changes in estimated water column and benthic plant phosphorus stores over the course of the 2008 simulation.

7.4. Scenarios

7.4.1. Scenario descriptions

The Daly River is a relatively unimpacted tropical river with oligotrophic (low nutrient) waters throughout the dry season. Its year-round flows make it an attractive proposition for further development (McJannet, Wallace *et al.* 2009). Climate change and climate variability are also likely to result in changes in flow, sediment and nutrient loads.

Current dissolved inorganic nitrogen (DIN) concentrations in the Daly River during the dry season are half to one-fifth of those observed in the Ord River at Tarrara Bar; (Robson, Burford *et al.* 2008). Dissolved inorganic phosphorus (DIP) concentrations and chlorophyll *a* are typically near detection limits in both rivers. To explore the possible implications of future agricultural development in the Daly River, we repeated the 2008 simulation with two changes:

Scenario 1: DIN concentrations increased to five times current concentrations (no change in turbidity or chlorophyll *a*).

Scenario 2: DIN and DIP concentrations increased to five times current concentrations (no change in turbidity or chlorophyll *a*).

Flows are also likely to change in the future: a result of natural climate variability, long-term climate change, and development of water resources. It is estimated that runoff in recent years (1996-2007) has been, on average, 66% higher than historical runoff (1930-2007, CSIRO, 2009), and it is possible that we will see a return to previous conditions in years to come. In the longer-term, global climate and local rainfall-runoff models suggest that runoff in the Daly River may either increase or decrease by up to 34% (with an increase predicted by the majority of global climate models considered) (CSIRO 2009).

With most primary production in the Daly River occurring in the dry season, changes in dry-season flows from groundwater are likely to be more significant than changes in wet-season flows, except with respect to the impact of wet-season flows on the shape of the river channel (which our model does not consider). Climate change and increased groundwater extraction may combine to either increase or decrease groundwater recharge and hence dry-season flows, however a slight decrease is considered more likely (CSIRO 2009).

At the time of writing the present report, we did not have access to the time-series of flows predicted for the various climate-change and development scenarios investigated by the Northern Australian Sustainable Yields (NASY) project (CSIRO 2009). Hence, we will consider only one simple flow change scenario: a 50% drop in wet-season and dry-season flows from 2008 levels. It is recommended that the model also be run for the full suite of NASY scenarios.

Scenario 3: 50% reduction in flows (with no change in nutrient concentrations, chlorophyll *a*, or turbidity)

All other aspects of model setup were as for the original, “current conditions” simulation.

7.4.2. Results

Under Scenario 1 (increased DIN concentrations), the model predicts an increase in algal production, with a substantial boost in *Spirogyra* and periphyton biomass (Figure 90). *Vallisneria* and *Nitella* production drops substantially as a consequence of competition for substrate (although the maximum simulated *Vallisneria* biomass is higher, the median, 25th and 75th percentiles, are substantially lower). The model does not simulate the growth of epiphytes on plant leaves: we would anticipate that increased epiphyte production resulting from an increase in DIN would further reduce *Vallisneria* biomass, and that this would have a flow-on effect throughout the foodchain. Increased algal production is sometimes associated with a simplification of the food-web (e.g. Carlier, Riera *et al.* 2008) and loss of diversity, but an increase in overall production.

Our experimental results (Chapter 4) indicate that *Spirogyra* from the Daly River is responsive to both nitrogen and phosphorus additions. Previous work (Schult, Townsend *et al.* 2007) has also found phosphorus limitation of *Spirogyra*, or suggested that N- or P-limitation may vary spatially (Townsend, Schult *et al.* 2008).

This being the case, we might expect Scenario 2 to show a further increase in algal production. In reality, the results of Scenario 2 (Figure 91) were very similar to those of Scenario 1, showing little additional increase in biomass. Our modelled system is nitrogen-limited but not phosphorus-limited. This may be a consequence of our handling of below-detection limit FRP samples (we set these values to half the detection limit) resulting in an over-estimation of the phosphorus supply, or it may be due to our assumption that ammonia and dissolved organic nitrogen are not significant resources for primary production in the Daly River, resulting in an under-estimation of nitrogen availability (again, additional ammonium measurements are required).

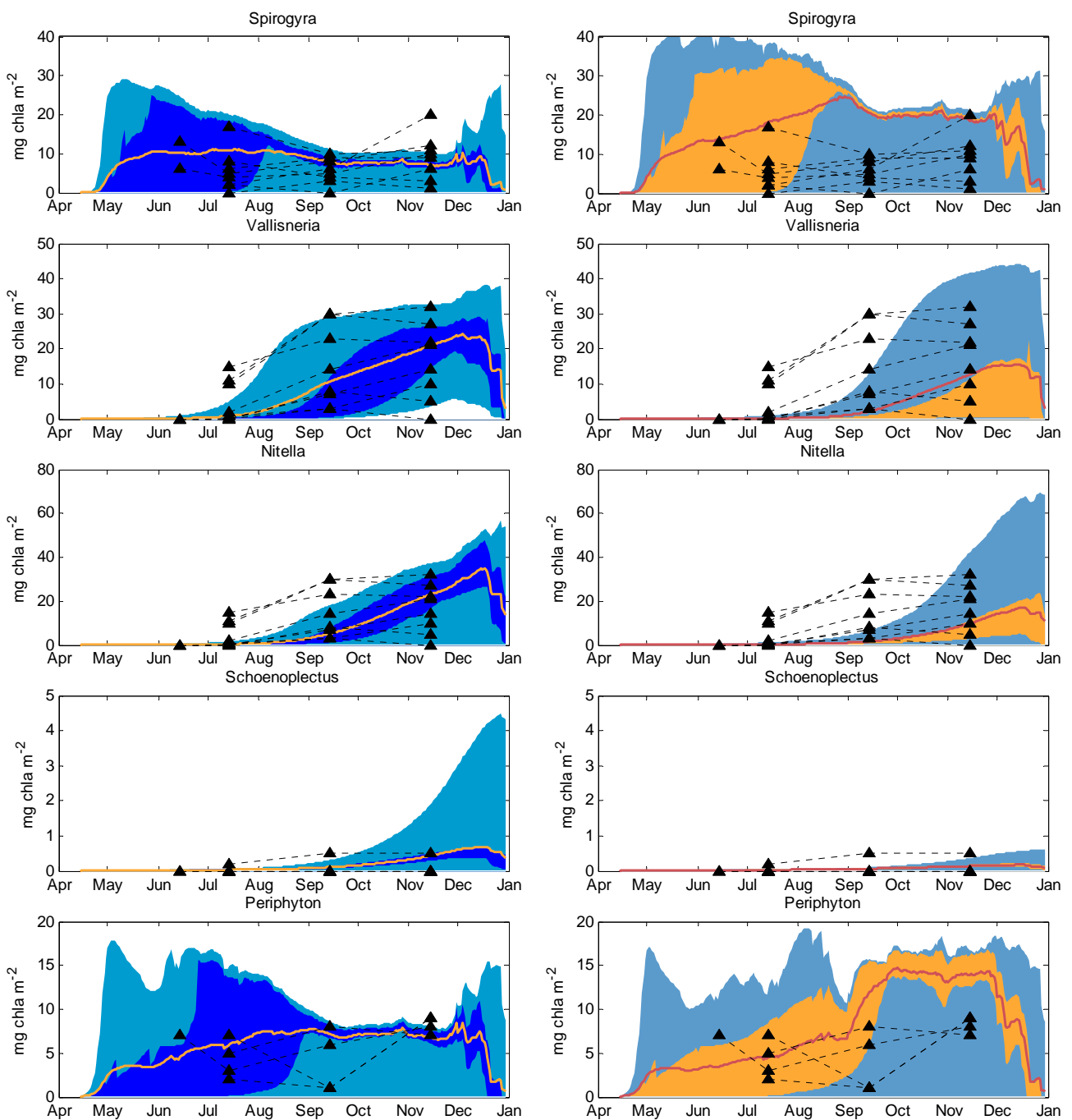


Figure 90 Model results for current conditions and Scenario 1. Left: current conditions. Right: Increased nitrogen. The outer (light blue) areas indicate the full range of model results, the inner (apricot or dark blue) bands represent the 25th-75th percentile (by area). Solid lines indicate the mean black triangles, 2008 observations.

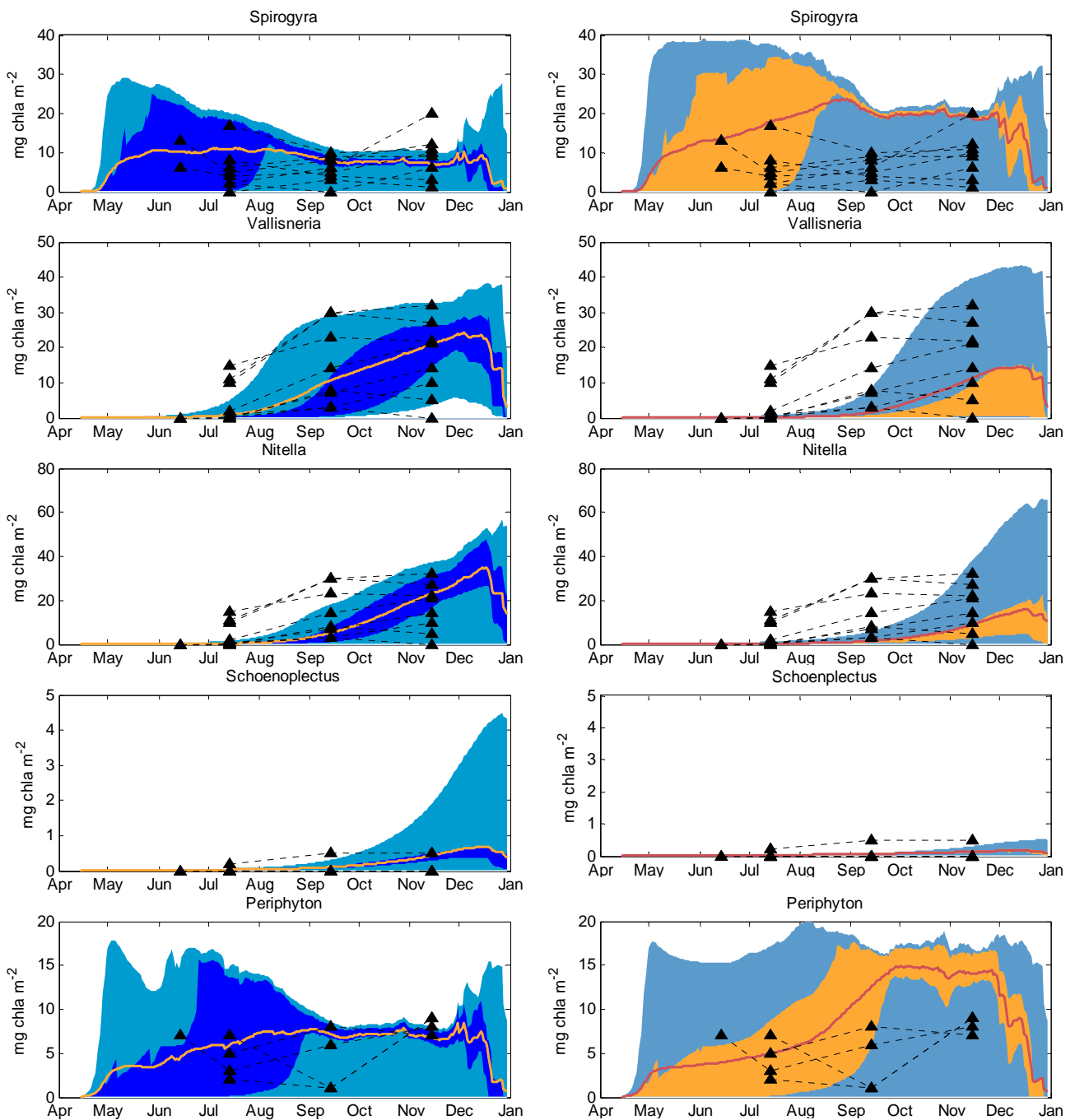


Figure 91 Model results for current conditions and Scenario 2. Left: current conditions. Right: Increased nitrogen and phosphorus. The outer (light blue) areas indicate the full range of model results, the inner (apricot or dark blue) bands represent the 25th-75th percentile (by area). Solid lines indicate the mean black triangles, 2008 observations.

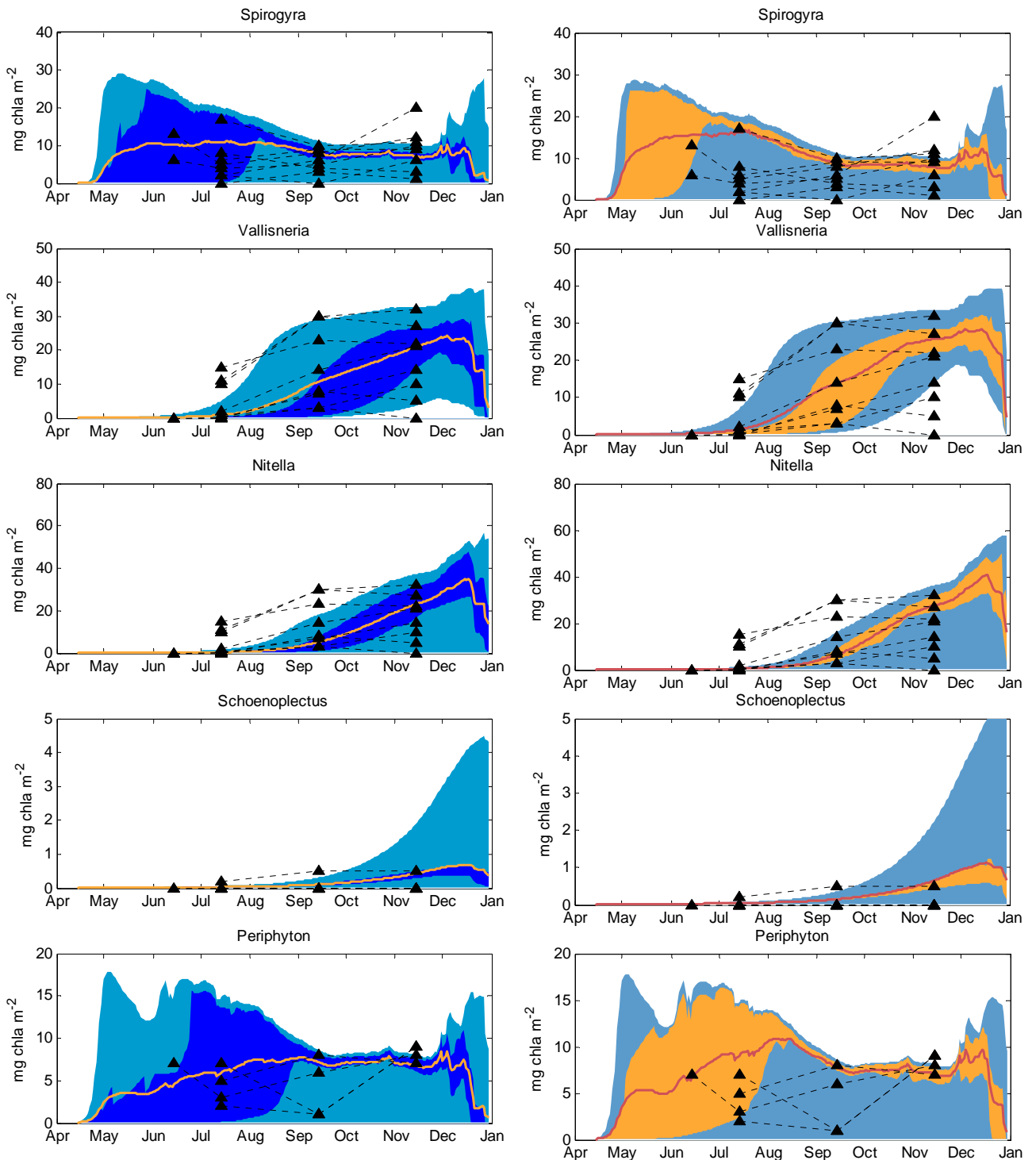


Figure 92 Model results for current conditions and Scenario 3. Left: current conditions. Right: Short-term reduction in flow. The outer (light blue) areas indicate the full range of model results, the inner (apricot or dark blue) bands represent the 25th-75th percentile (by area). Solid lines indicate the mean black triangles, 2008 observations.

The “reduced flow” scenario results (Figure 92) were at first surprising: the model predicts an increase in *Spirogyra* and *Vallisneria* and a small increase in *Nitella* and periphyton biomass (per unit area) under these conditions. The timing of peaks and the relative abundance of each plant group does not significantly change, and overall production is slightly reduced as a consequence of a reduction in wetted channel area.

Because water velocity is largely controlled by hydraulic breaks (small waterfalls) in the river, the simulated reduction in flow did not greatly change dry-season velocities, and hence did not significantly affect boundary layer flux rates of nutrients, but did reduce the depth of water. Reduced depth resulted in increased light availability at the bottom, which boosted production in the early part of the dry season when water was deeper and more turbid than later in the dry season.

7.4.3. Limitations

These scenarios do not consider the possible implications of changes in temperature (which may increase productivity and respiration), changes in dissolved inorganic carbon concentrations (which may boost carbon fixation), changes in community species composition (for example, through the introduction of invasive weeds), or changes in the physical use of the river (such as increases in cattle traffic or fishing), or changes in sediment loads that may also accompany climate change or development. They also do not consider the changes in river morphology and sand cover that occur from one year to the next and are which are likely to increase with changes in land use or flow. In addition, they are subject to all the limitations of the underlying model. These include: uncertain accuracy of the hydrodynamic model (which could be improved with better bathymetric data or a digital elevation model), simplification of the habitat model, greatly simplified plant life-cycles, uncertain parameter values (which could be improved with further targeted process studies), limited temporal resolution of nutrient measurements (which might be improved with newer monitoring technologies), omission of phytoplankton (a small component of production in the system as it currently is, but a component that may increase under some scenarios), omission of epiphytes, and omission of the biogeochemical cycles that control how nutrients may be taken up and recycled within the plant community, or removed from the system.

7.5. Conclusions

The model we have developed here is able to reproduce many of the observed features of plant dynamics in the Daly River and may form a basis for a range of scenario simulations. From the results of our simulations, in combination with the results of the process studies conducted during this project and previous work in the Daly River, we can conclude:

1. Primary production in the Daly River is strongly controlled by nutrient availability and the river is likely to be particularly sensitive to any change in nutrient loads.
2. Growth of plant biomass in the first half of the dry season is supported by uptake of water-column nutrients derived from loads at the end of the wet season. Towards the end of the dry season, plant biomass is supported by

recycling of nutrients within benthic communities and perhaps release of nutrients from sediment stores.

3. Plant biomass is strongly affected by seasonal changes in flows, with sloughing or scouring of benthic plant material at higher flows playing an important role in seasonal patterns and the distribution and relative abundance of different species.
4. Plants in the Daly River may be less sensitive to moderate changes in dry-season flow (if not accompanied by changes in sediment and nutrient loads), except in that the total habitat area and hence total production are affected. This conclusion is preliminary and needs to be tested.
5. In the course of generating this model, a number of knowledge gaps have been identified. Our ability to predict how the River will respond to changes would be greatly enhanced by process studies targeting the following questions:
 - a. How will land use and climate changes alter nutrient and sediment loads to the river?
 - b. How do grazers interact with the plants and algae in the river, and how strong are grazing pressures?
 - c. How do plants and algae other than *Spirogyra* respond to variations in shear velocity?
 - d. What proportion of the nutrients required by *Vallisneria nana* are taken up from the sediments rather than the water column?
 - e. How are nutrients recycled within algal and plant communities in the river?
 - f. What role does the Daly River estuary play in overall system function?

Meanwhile, there exists an opportunity to use our current knowledge and the model presented here in combination with results from other TRaCK projects and the CSIRO Northern Australia Sustainable Yields (NASY) project to explore in more detail the possible outcomes of a range of likely futures for the Daly River.

8. Summary and Concluding Remarks

The work presented in this report has, for the first time, developed an understanding of nutrient and sediment fluxes, primary production and organic matter in the Daly River, in Australia's Northern Territory.

Our results suggest the following conceptual picture for nutrients cycling, sediments and primary production in the Daly River:

Wet season (December to March)

High flow volumes during the wet season bring >95% of total annual sediment, nitrogen and phosphorus loads reaching the Daly River. High shear stresses associated with high flows scour the bed, removing most benthic plant biomass, though in lower-flow years, some *Vallisneria* beds survive. Turbidity is high during the wet season and water residence time is low, so primary production in the main channel is accordingly low.

Early Dry Season (April to June)

At the end of the wet season, sediments settle out of the water column and benthic substrate stabilises into alternating stretches of dynamic sand ripples, stable gravel beds and slightly deeper pools. The water clears and benthic microalgae (in periphyton) and fast-growing macroalgae (*Spirogyra*) establish rapidly, storing nutrients from the water column and keeping them within the system. Most benthic production occurs in gravel runs and along the edges of pools, with little production in sand ripples. Phytoplankton contribute little to total primary production in current conditions.

Total primary production is limited not by light, but by nitrogen and phosphorus concentrations and transfer of these nutrients across a benthic boundary layer.

Late Dry Season (July to November)

In the late dry season, flow is sustained entirely by groundwater inflows and hydrological breaks (i.e. small waterfalls) play an important role in controlling flow and water depth.

Primary production remains limited by nitrogen and phosphorus and much of the measured photosynthesis does not contribute to production of plant biomass.

With little additional nutrient input from the catchment, the system in the late dry season depends on nutrients recycled within the benthic community. *Spirogyra* biomass drops as lower flows cause a decline in transfer-limited nutrient uptake rates.

Release of nutrients from sediment muds does not appear to contribute significantly to the supply of nutrients in the system during the dry season: rather, nutrients released from decaying *Spirogyra* and periphyton or

otherwise recycled within the biotic community drive the growth of slower-growing benthic algae (*Chara* or *Nitella*) and aquatic plants (*Vallisneria*). Sand ripples may play an important role in remineralisation of detrital organic matter.

Outputs from this project include a one-dimensional hydraulic model, presented in Chapter 6 and a dynamic model to simulate changes in biomass of five key groups of plant and algae, presented in Chapter 7. The latter has been applied to two simple scenarios, exploring the possible effects of increased nutrient concentrations and reduced flows. The results are preliminary as significant knowledge gaps remain: key knowledge gaps affecting our ability to predict the impact of changes in nutrient loads and flows are discussed in Section 7.5.

This work identifies any future increase in nutrient loads as a threat to Daly River ecosystems. A regular water-quality monitoring program across multiple years would be required if there was a desire to establish a baseline with validity beyond the study year and to detect any future change to nutrient concentrations and primary production that may be associated with future land-use changes. Such a program would include, at minimum, monitoring of dry season total nitrogen and phosphorus, dissolved organic nitrogen and phosphorus, dissolved inorganic nitrogen (i.e. NH_4^+ NO_x) and dissolved inorganic phosphorus (i.e. FRP) as well as areal biomass of benthic algae (*Spirogyra*, periphyton and *Nitella* or *Chara*) and plants (esp. *Vallisneria*) and water column chlorophyll *a* at selected, representative sites. Because the system is not light-limited but strongly nutrient-limited, calculations based on diurnal oxygen curves are not sufficient to measure any change in algal production. Detailed recommendations for monitoring and management are beyond the scope of this report, but are being prepared as part of an NWC/TRaCK Synthesis and Adoption project.

Future work in the Daly River should include:

- Addressing the key knowledge gaps identified in Section 7.5 (among them: how will climate change affect the system, and what role does the estuary play?);
- Conducting field experiments to test the predictive power of the model presented in Chapter 7;
- Further developing the model to: a) include an estimate of uncertainty; and b) simulate the full nutrient cycle, including the role of sediments and the potential future role of phytoplankton;
- Applying the model to a series of more realistic scenarios, driven by such factors as predicted climate futures and planned or proposed land and water management practises;
- Incorporation of these results into an integrated model that also considers aquatic animals and socio-economic factors;

- Development of integrated conceptual models that consider sediments, nutrients and primary production in the context of overall ecosystem dynamics, catchment processes and socio-economic processes; and
- Design of a long-term water quality monitoring and data collection programme.

The last-three dot points above are already being considered through TRaCK and NWC transition-year projects.

Many of the results of the work presented here and future related work may be applicable to other perennial wet-dry tropical river systems in Australia.

References

- American Public Health Association (1998) Standard methods for the examination of water and wastewater. In ' 10th Edition edn. (American Public Health Association: New York)
- Anderson, L.D., and Delaney, M.L. (2000) Sequential extraction and analysis of phosphorus in marine sediments: Streamlining of the SEDEX procedure. *Limnology and Oceanography* **45**(2), 509-515.
- Arcement, G.J.J., and Schneider, G.R. (1984) Guide for Selecting Manning's Roughness Coefficients for Natural Channels and Flood Plains. US Department of Transportation, Federal Highways Administration.
- Australia, N. (2004) Australia's Tropical Rivers -- Data Audit. Land & Water Australia, No. Product Number PR040674, Canberra.
- Batchelor, G.K. (Ed.) (1967) 'The theory of homogeneous turbulence.' (Cambridge University Press: Cambridge)
- Biggs, B.J.F. (1996) Patterns in Benthic Algae of Streams. In 'Algal Ecology.' (Eds. RJ Stevenson, ML Bothwell and RL Lowe) pp. 31-56. (Academic Press: San Diego)
- Boston, H.L., and Hill, W.R. (1991) Photosynthesis Light Relations of Stream Periphyton Communities. *Limnology and Oceanography* **36**(4), 644-656.
- Bouletreau, S., Garabetian, F., Sauvage, S., and Sanchez-Perez, J.M. (2006) Assessing the Importance of a Self-Generated Detachment Process in River Biofilm Models. *Freshwater Biology* **51**(5), 901-912.
- Brodie, J.E., and Mitchell, A.W. (2005) Nutrients in Australian tropical rivers: changes with agricultural development and implications for receiving environments. *Marine and Freshwater Research* **56**(3), 279-302.
- Bunn, S.E., Thoms, M.C., Hamilton, S.K., and Capon, S.J. (2006) Flow variability in dryland rivers: Boom, bust and the bits in between. *River Research and Applications* **22**(2), 179-186.
- Carlier, A., Riera, P., Amouroux, J.-M., Bodiou, J.-Y., Desmalades, M., and Grθmare, A. (2008) Food web structure of two Mediterranean lagoons under varying degree of eutrophication. *Journal of Sea Research* **60**(4), 264-275.
- Chapra, S.C., and Ditoro, D.M. (1991) Delta Method for Estimating Primary Production, Respiration, and Reaeration in Streams. *Journal of Environmental Engineering-Asce* **117**(5), 640-655.
- Chow, V.D. (Ed.) (1981) 'Open Channel Hydraulics.' (McGraw-Hill: New York)

Clifford, N.J., Robert, A., and Richards, K.S. (1992) Estimation of flow resistance in gravel-bedded rivers: a physical explanation of the multiplier of roughness length. *Earth Surface Processes and Landforms* **17**, 111-126.

CSIRO (2009) Water in the Ord-Bonaparte Region. In 'Water in the Timor Sea Drainage Division. A report to the Australian Government from the CSIRO Northern Australia Sustainable Yields Project.' (Ed. CSIRO) pp. 183-272. (CSIRO Water for a Healthy Country Flagship: Australia)

Deegan, B., Harrington, T.J., and Dundon, P. (2005) Effects of Salinity and Inundation Regime on Growth and Distribution of *Schoenoplectus Triquetus*. *Aquatic Botany* **81**(3), 199-211.

Enriquez, S., Duarte, C.M., SandJensen, K., and Nielsen, S.L. (1996) Broad-scale comparison of photosynthetic rates across phototrophic organisms. *Oecologia* **108**(2), 197-206.

Fram, J.P., Stewart, H.L., Brzezinski, M.A., Gaylord, B., Reed, D.C., Williams, S.L., and MacIntyre, S. (2008) Physical pathways and utilization of nitrate supply to the giant kelp, *Macrocystis pyrifera*. *Limnology and Oceanography* **54**(4), 1589-1603.

Ganf, G.G., and Rea, N. (2007) Potential for algal blooms in tropical rivers of the Northern Territory, Australia. *Marine and Freshwater Research* **58**(4), 315-326.

Georges, A., Webster, I., Guarino, F., Jolly, P., Thoms, M., and Doody, S. (2002) Modelling Dry Season Flows and Predicting the Impact of Water Extraction on a Flagship Species – the Pig Nosed Turtle (*Carretocchelys insculpta*). Report prepared for the Northern Territory Department of Infrastructure Planning and Environment, Darwin.

Haestad Methods Inc., Dyhouse, G., Hatchett, J., and Benn, J. (2003) 'Floodplain modeling using HEC-RAS.' 1st edn. (Haestad Press: Waterbury, CT) xxiii, 696 p.

Hamilton, S.K., and Gehrke, P.C. (2005) Australia's tropical river systems: current scientific understanding and critical knowledge gaps for sustainable management. *Marine and Freshwater Research* **56**(3), 243-252.

Harley, M.T., and Findlay, S. (1994) Photosynthesis-Irradiance Relationships for 3 Species of Submersed Macrophytes in the Tidal Fresh-Water Hudson River. *Estuaries* **17**(1B), 200-205.

Hearn, C.J., Atkinson, M.J., and Falter, J.L. (2001) A physical derivation of nutrient-uptake rates in coral reefs: effects of roughness and waves. *Coral Reefs* **20**(4), 347-356.

Hutorowicz, A., and Hutorowicz, J. (2008) Seasonal development of *Vallisneria spiralis* L. in a heated lake. *9*(-1), 79-86.

Iwata, T., Takahashi, T., Kazama, F., Hiraga, Y., Fukuda, N., Honda, M., Kimura, Y., Kota, K., Kubota, D., Nakagawa, S., Nakamura, T., Shimura, M., Yanagida, S., Xeu,

L., Fukasawa, E., Hiratsuka, Y., Ikebe, T., Ikeno, N., Kohno, A., Kubota, K., Kuwata, K., Misonou, T., Osada, Y., Sato, Y., Shimizu, R., and Shindo, K. (2007) Metabolic balance of streams draining urban and agricultural watersheds in central Japan. *Limnology* **8**(3), 243-250.

Jeffrey, S.J., Carter, J.O., Moodie, K.B., and Beswick, A.R. (2001) Using spatial interpolation to construct a comprehensive archive of Australian climate data. *Environmental Modelling and Software* **16**(4), 309-330.

Jolly, P. (2002) Daly River Catchment Water Balance. Department of Infrastructure Planning and Environment, Natural Resources Division.

Kays, M.W., and Crawford, M.E. (Eds) (1993) 'Convective Heat and Mass Transfer (3rd Edition edn).' (McGraw-Hill: New York)

Krause-Jensen, D., and Sand-Jensen, K. (1998) Light attenuation and photosynthesis of aquatic plant communities. *Limnology and Oceanography* **43**(3), 396-407.

Kufel, L., and Kufel, I. (2002) Chara beds acting as nutrient sinks in shallow lakes--a review. *Aquatic Botany* **72**(3-4), 249-260.

Leigh, C., and Sheldon, F. (2008) Hydrological Changes and Ecological Impacts Associated with Water Resource Development in Large Floodplain Rivers in the Australian Tropics. *River Research and Applications* **24**(9), 1251-1270.

Li, F., and Xie, Y. (2009) Spacer elongation and plagiotropic growth are the primary clonal strategies used by *Vallisneria spiralis* to acclimate to sedimentation. *Aquatic Botany* **91**(3), 219-223.

Libbert, E., and Walter, T. (1985) Photosynthetic Production of a Brackish Water Community of Chara-Tomentosa L and Its Dependence on Environmental-Conditions. *Internationale Revue Der Gesamten Hydrobiologie* **70**(3), 359-368.

McJannet, D.L., Wallace, J.W., Henderson, A., and McMahon, J. (2009) High and low flow regime changes at environmental assets across northern Australia under future climate and development scenarios: A report to the Australian Government from the CSIRO Northern Australian Sustainable Yields Project. CSIRO Water for a Healthy Country National Research Flagship, Canberra.

Muller, G., and Gastner, M. (1971) The "karbonate bombe" a simple device for the determination of the carbonate content in sediments, soils and other materials. *Neues Jahrbuch Fur Mineralogie-Monatshefte* **10**, 466–469.

Murray, A., and Parslow, J. (1997) Port Phillip Bay Integrated Model: Final Report. CSIRO Division of Marine Research, No. Technical Report No. 44, Canberra, Australia.

Nathan, R.J., and McMahon, T.A. (1990) Evaluation of automated techniques for baseflow and recession analyses. *Water Resources Research* **26**, 1465-1473.

- Nielsen, S.L., and Sand-Jensen, K. (1989) Regulation of photosynthetic rates of submerged rooted macrophytes. *Oecologia* **81**, 364-368.
- Norrish, K., and Hutton, J.T. (1969) An Accurate X-Ray Spectrographic Method for Analysis of a Wide Range of Geological Samples. *Geochimica Et Cosmochimica Acta* **33**(4), 431-&.
- O'Neal, S.W., and Lemby, C.A. (1995) Temperature and irradiance effects on growth of *Pithophora oedogonia* (Chlorophyceae) and *Spirogyra* sp. (Charophaeceae). *Journal of phycology* **31**(5), 720-726.
- Pentecost, A. (1984) The growth of *Chara globularis* and its relationship to carbonate deposition in Malham Tarn. *Field Studies* **6**, 53-58.
- Portielje, R., Kersting, K., and Lijklema, L. (1996) Primary production estimation from continuous oxygen measurements in relation to external nutrient input. *Water Research* **30**(3), 625-643.
- Rea, N., Postine, P.L., Cook, S., Webster, I., and Williams, D. (2002) Environmental water requirements of *Vallisneria nana* in the Daly River, Northern Territory. Department of Infrastructure, Planning and Environment, No. Report No. 35.2002, Darwin, NT.
- Reynolds, C.S. (1984) 'The ecology of freshwater phytoplankton.' (Cambridge University Press: Cambridge ; New York) x, 384 p.
- Reynolds, C.S. (Ed.) (1997) 'Vegetation Processes in the Pelagic: a Model for Ecosystem Theory.' Excellence in Ecology No. 9 (Ecology Institute: D-21385 Oldendorf/Luhe, Germany)
- Robson, B.J., Burford, M.A., Gehrke, P.S., Revill, A.T., Webster, I.T., and palmer, D.W. (2008) Response of the lower Ord River and Estuary to changes in flows and sediment and nutrient loads. Water for a Healthy Country National research Flagship, CSIRO, Canberra, ACT.
- Robson, B.J., Schult, J., Smith, J., Webster, I., Burford, M., Haese, R., Townsend, S., and Revill, A. (2010) Toward understanding the impacts of land management on productivity in the Daly and Flinders Rivers: Final report for the Daly River, TRaCK Project 4.3. Darwin, N.T.
- Schult, J., Townsend, S.A., Douglas, M.M., Webster, I.T., Skinner, S., and Casanova, M. (2007) Recommendations for nutrient resource condition targets for the Daly River. Charles Darwin University, Darwin.
- Schwarz, A.-M., and Hawes, I. (1997) Effects of changing water clarity on characean biomass and species composition in a large oligotrophic lake. *Aquatic Botany* **56**(3-4), 169-181.
- Simons, L.A. (1985) Design Manual for Engineering Analysis of Fluvial Streams. Arizona Department of Water Resources, Arizona.

Smith, M., and Houpis, J.L.J. (2004) Gas exchange responses of the wetland plant *Schoenoplectus Hallii* to irradiance and vapor pressure deficit. *Aquatic Botany* **79**(3), 267-275.

Smith, V.H. (2003) Eutrophication of freshwater and coastal marine ecosystems - A global problem. *Environmental Science and Pollution Research* **10**(2), 126-139.

Soulsby, R. (Ed.) (1997) 'Dynamics of Marine Sands.' (Thomas Telford)

Stevens, C.L., Hurd, C.L., and Isachsen, P.E. (2003) Modelling of diffusion boundary-layers in subtidal macroalgal canopies: the response to waves and currents. *Aquatic Sciences* **65**(1), 81-91.

Tickell, S.J. (2008) Dry Season Stream Flows in the Katherine / Daly Rivers, 2008. Department of Natural Resources, Environment, the Arts and Sport, NT Government, Darwin.

Tickell, S.R. (2002) A Survey of Springs along the Daly River. Department of Infrastructure Planning and Environment, Natural Resources Division, Darwin.

Townsend, S.A., and Douglas, M.M. (2000) The effect of three fire regimes on stream water quality, water yield and export coefficients in a tropical savanna (northern Australia). *Journal of Hydrology* **229**(3-4), 118-137.

Townsend, S.A., and Padovan, A.V. (2005) The seasonal accrual and loss of benthic algae (*Spirogyra*) in the Daly River, an oligotrophic river in tropical Australia. *Marine and Freshwater Research* **56**, 317-327.

Townsend, S.A., and Padovan, A.V. (2009) A Model to Predict the Response of the Benthic Macroalga *Spirogyra* to Reduced Base Flow in the Tropical Australia. *River Research and Applications* **25**(9), 1193-1203.

Townsend, S.A., Schult, J.H., Douglas, M.M., and Skinner, S. (2008) Does the Redfield ratio infer nutrient limitation in the macroalga *Spirogyra fluviatilis*? *Freshwater Biology* **53**(3), 509-520.

Webster, I.T., Rea, N., Padovan, A.V., Dostine, P., Townsend, S.A., and Cook, S. (2005) An analysis of primary production in the Daly River, a relatively unimpacted tropical river in northern Australia. *Marine and Freshwater Research* **56**(3), 303-316.

Zhang, Z.H., Rengel, Z., and Meney, K. (2009) Kinetics of ammonium, nitrate and phosphorus uptake by *Canna indica* and *Schoenoplectus validus*. *Aquatic Botany* **91**(2), 71-74.

Appendix 1: Details of sediment sampling

Table 1: Sediment samples collected from the Daly River in July 2009

Site	Date	Time	Lat		Long		Depth (m)	Comments	Samples collected
			deg	min	deg	min			
DR01A	16/07/2008	09:50:00	-13	58.06	131	11.758	1.5	sand	core top 1cm
DR01B	16/07/2008	10:05:00	-13	58.065	131	11.756	1.1	sand	core top 1cm
DR01C	16/07/2008	10:15:00	-13	58.073	131	11.753	1.4	very coarse gravel	grab surface scrape
DR02A	16/07/2008	10:33:00	-13	58.121	131	12.023	0.5	fine material on top of coarse sand. Visible macroalgae and seeds/charcoal on surface	core top 1cm
DR02B	16/07/2008	10:43:00	-13	58.131	131	12.033	1.4	sand	core top 1cm
DR02C	16/07/2008	10:58:00	-13	58.145	131	12.034	2.5	mud - next to eroded bank with visible G/W input	core top 1cm
DR03A	16/07/2008							no sample - rock	
DR03B	16/07/2008	11:38:00	-13	58.051	131	12.29	1.5	sand	core top 1cm
DR03C	16/07/2008	11:45:00	-13	58.066	131	12.286	1.4	muddy sand	core top 1cm
DR04A	16/07/2008							no sample - rock	
DR04B	16/07/2008	11:57:00	-13	58.031	131	12.569	1.5	very coarse sand/gravel	grab surface scrape
DR04C	16/07/2008	12:08:00	-13	58.045	131	12.587	1.1	muddy sand	core top 1cm
DR05A	16/07/2008	12:25:00	-13	58.192	131	12.841	1.4	muddy sand	core top 1cm
DR05B	16/07/2008	12:35:00	-13	58.199	131	12.822	2.3	muddy gravel	grab surface scrape
DR05C	16/07/2008	12:50:00	-13	58.226	131	12.824	0.9	sand	core top 1cm
DR06A	16/07/2008	13:35:00	-13	58.37	131	12.868	3.3	fine sand	core top 1cm
DR06B	16/07/2008	13:48:00	-13	58.36	131	12.858	4.0	fine sand	core top 1cm
DR06C	16/07/2008	14:12:00	-13	58.355	131	12.84	3.0	sandy mud	core top 1cm
DR07A	16/07/2008	14:28:00	-13	58.714	131	12.793	1.3	sand	core top 1cm
DR07B	16/07/2008	14:45:00	-13	58.702	131	12.785	1.4	coarse gravel	grab surface scrape
DR07C	16/07/2008							no sample - rock	
DR08A	16/07/2008	15:08:00	-13	58.948	131	12.915	0.3	coarse sand	core top 1cm

Site	Date	Time	Lat		Long		Depth (m)	Comments	Samples collected
			deg	min	deg	min			
DR08B	16/07/2008							no sample - very coarse large gravel and fast flowing water, unable to anchor	
DR08C	16/07/2008	15:24:00	-13	58.962	131	12.902	1.7	mud - some obvious algal growth	core top 1cm
DR09A	16/07/2008	15:45:00	-13	58.976	131	13.018	2.3	sandy mud - obvious algae	core top 1cm
DR09B	16/07/2008	15:55:00	-13	58.987	131	13.022	3.6	sandy mud - obvious algae + abundant leaf litter	grab surface scrape
DR09C	16/07/2008	16:10:00	-13	59.003	131	13.052	2.6	sand	core top 1cm
DR10A	17/07/2008	9:37:00	-13	59.01	131	13.441	1.3	coarse gravel between rocky bottom	grab surface scrape
DR10B	17/07/2008	9:57:00	-13	59.013	131	13.434	1.2	very coarse gravel - obvious algae	grab surface scrape
DR10C	17/07/2008	10:11:00	-13	59.028	131	13.436	0.8	muddy sand - obvious growth	core top 1cm
DR11A	17/07/2008	10:27:00	-13	59.235	131	13.621	1.6	mixture of mud, algae and leaf litter. Obvious white "fluff" layer	"fluff" + core top 1cm
DR11B	17/07/2008	10:45:00	-13	59.228	131	13.607	2.6	muddy sand - obvious growth	core top 1cm
DR11C	17/07/2008	11:00:00	-13	59.241	131	13.594	1.4	coarse sand + obvious algae	core top 1cm
DR12A	17/07/2008	11:17:00	-13	59.378	131	13.617	3.2	coarse sand	core top 1cm
DR12B	17/07/2008	11:35:00	-13	59.372	131	13.612	2.7	coarse sand + obvious algae	core top 1cm
DR12C	17/07/2008	11:50:00	-13	59.369	131	13.593	1.6	mud over rock + algae	grab surface scrape
DR13A	17/07/2008	12:10:00	-13	59.756	131	13.593	1.2	coarse sand	core top 1cm
DR13B	17/07/2008	12:33:00	-13	59.76	131	13.58	1.4	coarse gravel	grab surface scrape
DR13C	17/07/2008							no sample - rock	

Table 2: Sediment samples collected from the Daly River in September 2009

Site	Date	Time	Lat		Long		Depth (m)	Comments	Samples collected
			deg	min	deg	min			
DR01A	20/09/2008	07:35:00	-13	58.06	131	11.758	1.2	sand	core top 1cm
DR01B	20/09/2008	07:47:00	-13	58.065	131	11.756	1.0	very coarse sand/gravel	grab surface scrape
DR01C	20/09/2008	07:57:00	-13	58.073	131	11.753	1.1	muddy gravel	grab surface scrape
DR02A	20/09/2008	08:10:00	-13	58.121	131	12.023	<0.5	muddy gravel	grab surface scrape
DR02B	20/09/2008	08:17:00	-13	58.131	131	12.033	1.5	coarse sand/gravel/mud mix	grab surface scrape
DR02C	20/09/2008	08:25:00	-13	58.145	131	12.034	1.1	mud - next to eroded bank with visible G/W input	core top 1cm
DR03A	20/09/2008							no sample - rock	
DR03B	20/09/2008	08:37:00	-13	58.051	131	12.29	1.3	sand	core top 1cm
DR03C	20/09/2008	08:47:00	-13	58.066	131	12.286	0.8	sand (waves)	core top 1cm
DR04A	20/09/2008							no sample - rock	
DR04B	20/09/2008	09:00:00	-13	58.031	131	12.569	1.3	sand with filamentous algae	grab surface scrape
DR04C	20/09/2008	09:08:00	-13	58.045	131	12.587	1.1	sand	core top 1cm
DR05A	20/09/2008	09:17:00	-13	58.192	131	12.841	1.3	gritty mud	core top 1cm
DR05B	20/09/2008	09:30:00	-13	58.199	131	12.822	2.0	sandy mud + obvious filamentous algae	grab surface scrape
DR05C	20/09/2008	09:40:00	-13	58.226	131	12.824	1.1	mud + obvious algae and surface "fluff"	core top 1cm
DR06A	20/09/2008	09:58:00	-13	58.353	131	12.869	3.0	fine muddy sand	core top 1cm
DR06B	20/09/2008	10:12:00	-13	58.36	131	12.858	3.4	mud	grab surface scrape
DR06C	20/09/2008	10:25:00	-13	58.355	131	12.84	2.9	silty mud	grab surface scrape
DR07A	20/09/2008	10:55:00	-13	58.714	131	12.793	1.2	sand	core top 1cm
DR07B	20/09/2008	11:05:00	-13	58.702	131	12.785	1.3	sandy gravel	grab surface scrape
DR07C	20/09/2008							no sample - rock	
DR08A	20/09/2008	11:18:00	-13	58.948	131	12.915	0.3	coarse sand	grab surface scrape
DR08B	20/09/2008							no sample - very coarse large gravel and fast flowing water, unable to anchor	
DR08C	20/09/2008	11:35:00	-13	58.962	131	12.902	1.9	mud - some obvious algal growth	grab surface scrape
DR09A	20/09/2008	11:50:00	-13	58.976	131	13.018	2.0	muddy sand	core top 1cm
DR09B	20/09/2008	12:00:00	-13	58.987	131	13.022	3.6	mud + dead vegetation + algae +	core top 1cm

Site	Date	Time	Lat		Long		Depth (m)	Comments	Samples collected
			deg	min	deg	min			
								surface "fluff"	
DR09C	20/09/2008	12:12:00	-13	59.006	131	13.035	2.5	sandy mud + obvious algae	core top 1cm
DR10A	20/09/2008	12:28:00	-13	59.01	131	13.441	0.9	no sample - rock	
DR10B	20/09/2008	12:35:00	-13	59.013	131	13.434	0.9	very coarse gravel	grab surface scrape
DR10C	20/09/2008	12:47:00	-13	59.028	131	13.436	0.8	coarse sand	grab surface scrape
DR11A	20/09/2008	13:35:00	-13	59.235	131	13.621	1.1	mud	core top 1cm
DR11B	20/09/2008	13:47:00	-13	59.228	131	13.607	2.2	muddy sand - obvious growth	grab surface scrape
DR11C	20/09/2008	14:00:00	-13	59.241	131	13.594	1.3	muddy sand/gravel + obvious algae	grab surface scrape
DR12A	20/09/2008	14:10:00	-13	59.378	131	13.617	2.4	sand	core top 1cm
DR12B	20/09/2008	14:22:00	-13	59.372	131	13.612	1.9	mud with dead vegetation + algae	core top 1cm
DR12C	20/09/2008	14:35:00	-13	59.369	131	13.593	1.5	mud + filamentous algae	grab surface scrape
DR13A	20/09/2008	14:47:00	-13	59.756	131	13.593	0.8	fine over coarse sand	core top 1cm
DR13B	20/09/2008	14:57:00	-13	59.76	131	13.58	1.1	muddy sand/gravel + obvious algae	grab surface scrape
DR13C	20/09/2008							no sample - rock	

